Sara Kurakin, BSc

Biocatalytic oxidative decarboxylation of Dioic acids

To yield terminal dienes

Masterarbeit

Zur Erlangung des akademischen Grades

Diplom-Ingenieurin

Masterstudium Biotechnologie

eingereicht an der

Technischen Universität Graz

Betreuer:

O. Univ.-Prof. Dr. phil. Kurt FABER

Institut für Chemie

Organische und Bioorganische Chemie

Universität Graz

Graz, 08.2016

EIDESSTATTLICHE ERKLÄRUNG

Ich erkläre an Eides statt, dass ich die vorliegende Arbeit selbstständig verfasst, andere als die angegebenen Quellen/Hilfsmittel nicht benutzt, und die den benutzten Quellen wörtlich und inhaltlich entnommenen Stellen als solche kenntlich gemacht habe. Das in TUGRAZonline hochgeladene Textdokument ist mit der vorliegenden Masterarbeit identisch.

…… ……

Datum Unterschrift

AFFIDAVIT

I declare that I have authored this thesis independently, that I have not used other than the declared sources/resources, and that I have explicitly indicated all material which has been quoted either literally or by content from the sources used. The text document uploaded to TUGRAZonline is identical to the present master‘s thesis dissertation.

…… ……

Date Signature

Zusammenfassung

Terminale Diene werden hauptsächlich zur Herstellung von Kunststoffen und bifunktionellen Verbindungen oder als Vernetzter verwendet. Diese Verbindungen werden üblicherweise über ROMP von Cycloalkanen mit niedrigeren Alkenen wie Ethen (Ethenolyse) hergestellt, wofür Grubbs oder Schrock Katalysatoren verwendet werden. Eine weitere Möglichkeit ist die Decarboxylierung von Disäuren mit Essigsäureanhydrid, Pd oder Rh Katalysatoren und Temperaturen von ca. 250 °C. Jedoch sind die Abhängigkeit von fossilen Rohstoffen, (schädlichen) Metallkatalysatoren und die hohen Reaktionstemperaturen große Nachteile dieser Prozesse.

Aus diesem Grund ist ein Syntheseweg zur Herstellung terminaler Diene ausgehend von erneuerbaren Rohstoffen unter milden Reaktionsbedingungen und ohne schädliche Katalysatoren sehr gefragt. Hierbei würde ein biokatalytischer Ansatz eine gute und umweltfreundliche Alternative zu den chemischen Prozessen darstellen. Das, in dieser Hinsicht, vielversprechendste System wurde von Dennig *et al.* beschrieben, wobei die Decarboxylierung von gesättigten Fettsäuren, zur Synthese von 1-Alkenen, mit der Monooxygenase OleT, O_2, Elektrontransferkomponenten von Spinat oder Putidaredoxin CamAB und NAD(P)H, in Verbindung mit einem effizienten NAD(P)H Recyclingsystem, erreicht wurde.

Das Ziel dieser Arbeit war es, mit dem etablierten System von Dennig *et al.*, durch Decarboxylierung von Disäuren, einen umweltfreundlichen und nachhaltigen Syntheseweg für terminale Diene zu generieren.
Die Produktion terminaler Diene mit Kettenlängen von C16 bis C5 wurde mit diesem System (OleT-CamAB-FDH Reaktionskaskade) gezeigt. Es wurde starke Abhängigkeit der erhaltenen Umsätze von dem verwendeten Substrat gefunden, wobei die höchste Produktivität mit der C14-Disäure erzielt wurde (0,49 $g.L^{-1}.d^{-1}$ terminales Dien). Des Weiteren wurde, über die erfolgreiche Decarboxylierung terminal ungesättigter Fettsäuren, gezeigt, dass die Decarboxylierung von Disäuren über jene als Zwischenprodukt passiert. Zudem wurden verzweigte Fettsäuren ebenfalls von OleT als Substrat akzeptiert. Schließlich wurde noch gezeigt, dass die Effizienz von OleT stark von der Reaktionstemperatur, der Enzym- und Substratkonzentration, dem Lösungsmittel und dessen Konzentration, der FDH Konzentration sowie dem verwendeten Elektronentransfersystem abhängt.

Abstract

Terminal dienes are mainly used for synthesis of synthetic rubbers, co-crosslinkers or for synthesis of bi-functional compounds. Usually, these compounds are obtained from ring opening metathesis polymerization (ROMP) of cycloalkenes with lower alkenes such as ethylene (ethenolysis), using Grubbs or Schrock catalysts. Further, chemical decarboxylation of dioic acids using acetic anhydride, a Pd or Rh catalyst and a reaction temperature of about 250 °C would be another option for terminal diene synthesis. However, the dependency from fossil fuels, the need of (harzardous) metal catalyst and high reaction temperatures are main drawbacks of these processes.

Therefore a synthesis route to terminal dienes starting from renewable resources under mild reaction conditions without hazardous catalyst would be highly desirable. To that end a biocatalytic approach would present an attractive and environmental friendly alternative compared to the chemical approaches. In this respect, the so far most promising system was described by Dennig *et al*., achieving decarboxylation of saturated fatty acids to yield 1-alkenes using the monooxygenase OleT, O_2, electron transfer components of spinach or putidaredoxin CamAB and NAD(P)H in combination with an efficient NAD(P)H recycling system.

The aim of this work is to achieve an environmentally friendly and sustainable access to terminal dienes using the reaction system established by Dennig *et al*. for decarboxylation of dioic acids.

Production of terminal dienes with a chain length from C16 to C5 was shown possible with the current reaction system (OleT-CamAB-FDH reaction cascade). A strong influence of the substrate on the conversion was observed, achieving the highest productivity with tetradecanedioic acid (0.49 $g.L^{-1}.d^{-1}$ terminal diene). Furthermore, it was shown that decarboxylation of dioic acids occurs via ω-enoic acids as reaction intermediates. Moreover, branched fatty acids were also accepted as substrates by OleT. Finally, it was shown that the performance of OleT strongly depends on the reaction temperature, enzyme- and substrate concentration, co-solvent and co-solvent concentration, FDH concentration and the used electron transfer system.

Acknowledgement

First and foremost I want to thank Prof. Kurt Faber for the opportunity to work on this interesting project and to write my Master thesis as a member of his group.

Special thanks I give to Dr. Alexander Dennig for his support and for his time and patience, when introducing me into the world of P450 monooxygenases and supporting me in writing my thesis.

Next, I would like to express my graditude to the whole ElkGroup for the great working atmosphere and the support I got during my work. I want to thank Mélanie Hall for proofreading, Nikolaus Turrini and Christoph Winkler for taking care about GC-MS, Anđela Dordic and Stefan Velikogne for the good company and for sharing all their buffers with me. I also want to thank Elisabeth Eger, Wolfgang Jud and Michaela Zechner for nice talks and making the time running fast. Thanks to all member of the ElkGroup for a fantastic time.

Last I want to thank my family and friends, who accompanied me on my way. Especially I want to thank my parents supporting me in all the decisions I made. I also want to thank Anna and Tobias, being the best sister and brother I can imagine and for a lot of fun during the years. Magdalena, thank you for the long and wonderful friendship, your understanding, the laughter and the weekly dinner. Manuel, thank you for your love, understanding, patience and the wonderful time we spend togheter. Last I want to thank Sarah and Silvia for the great years of study and friendship.

Content

1 Introduction

1.1 Application and synthesis of olefins and terminal dienes

Short chain 1-alkenes such as ethylene or propene are very valuable. They are important building blocks for the production of various polymers, additives and solvents as well as for fine chemical synthesis [1]. Terminal dienes are mainly used for synthesis of synthetic rubbers, co-crosslinkers or for synthesis of bi-functional compounds [2a].

So far, lower 1-alkenes (ethylene, propene) as well as 1,3-butadiene are mainly obtained from steam cracking of naphtha. To that end, naphtha, which is obtained from distillation of crude oil, is heated with steam in a Cr-Ni heater up to 1050 °C at increased pressure. The cracked products leave the heater at a temperature of about 850 °C and are immediately quenched to 300 °C to avoid side reactions. Afterwards the crude gas is separated from process water, compressed and washed to eliminate H_2S and CO_2. Finally the gas is dried and distilled to obtain the single fractions and subsequently the end products [1][2b][3] (Scheme 1).

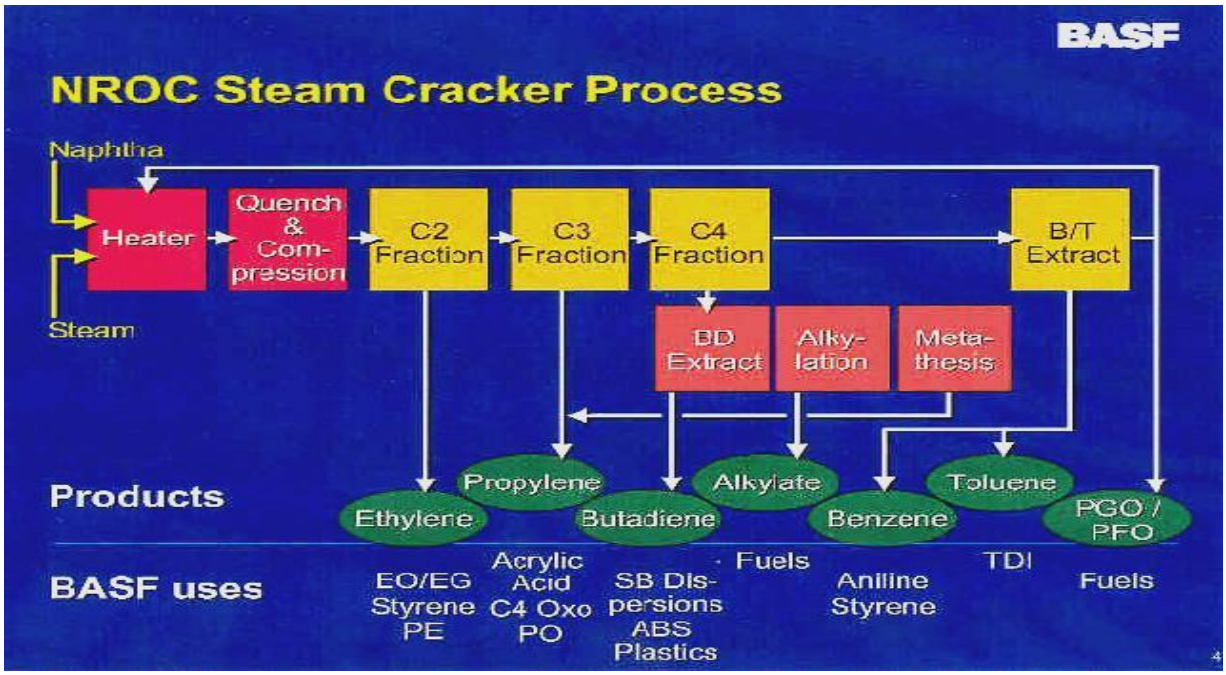

Scheme 1: Schematic steam cracking process for production of lower alkenes as well as aromatic compounds from naphtha (taken from [4]).

Production of higher olefins is achieved via SHOP (Shell higher olefin process), where α-olefins (> C4) are produced from ethylene. The process is performed at 80 - 120 °C and 70 - 140 bar and Ni-catalysts with phosphine ligands (e.g. Ph_2PCH_2COOK) are used. Due to the

Ni-catalyst, oligomerization of ethylene is achieved. After separation of the olefin phase from the catalyst, the directly marketable α-olefins (C11 - C14) were separated by distillation. Further olefin isomerization followed by olefin metathesis is done with those fractions that are not directly marketable [5][6a] (Scheme 2).

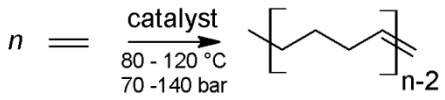

Scheme 2: SHOP - reaction scheme, for the reaction a Ni-catalyst with phosphine ligands is used [6a].

In contrast to the production of 1-alkenes, terminal dienes (> C4) cannot be obtained from steam cracking or SHOP. Instead, these compounds are obtained from ring opening metathesis polymerization (ROMP) of cycloalkenes with lower alkenes such as ethylene (ethenolysis) [6b][7][2a] (Scheme 3).

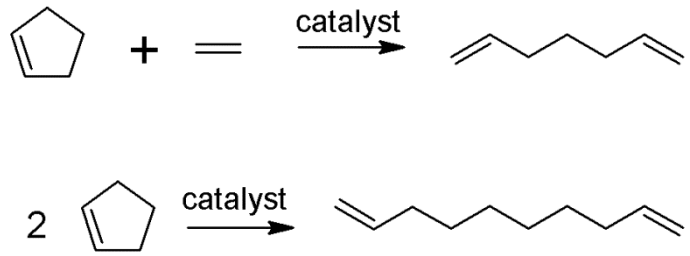

Scheme 3: Ethenolysis (top) and ROMP (bottom) of cyclopentene to produce terminal dienes. The used catalysts are Schrock or Grubbs catalysts [2a][6b]. Both reactions are usually performed at mild reaction temperatures and atmospheric pressure.

Grubbs or Schrock catalysts (Figure 1 and Figure 2) containing transition metals like ruthenium or molybdenum are usually used for these reactions [6b].

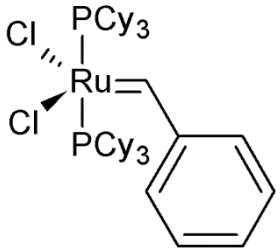

Figure 1: Simplest (1st generation) Grubbs catalyst used for ethenolysis of cycloalkenes [6b].

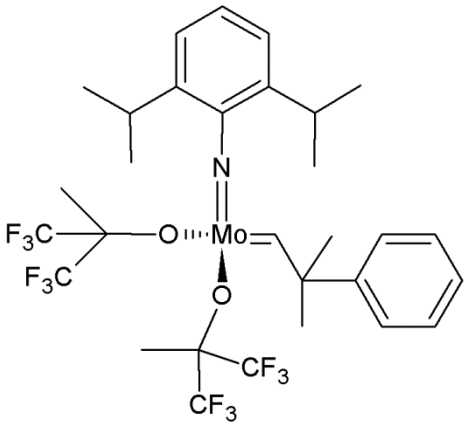

Figure 2: Schrock catalyst used for ethenolysis of cycloalkenes [6b].

All these processes (SHOP, ethenolysis, ROMP) are dependent on fossil fuels. Since fossil resources are depleting and peak oil is probably reached, there is the demand of new synthesis routes for 1-alkenes which are independent of crude oil or gas [8 - 13]. Another drawback is that the educts of these processes are obtained from steam cracking, requiring high reaction temperatures and pressure [1][2b][3]. Further, ruthenium-based catalysts, which are used for ethenolysis [6b][2a], are rather expensive (92.8 €/100 mg for a 2nd generation Grubbs catalyst [14]). Moreover, ruthenium is obtained from mining [15] and is therefore not renewable nor biodegradable.

One alternative for the production of 1-alkenes is the decarbonylation of fatty acids, which can be obtained from renewable resources [8] (Scheme 4). Production of odd numbered α-olefins by decarbonylation of fatty acids (C10 - C18) was achieved by Liu *et al.*, using a Pd catalyst, acetic anhydride and a reaction temperature of about 130 °C. Further, a continuous vacuum is necessary to distill the formed acetic acid as well as volatile olefins. Moreover, carbon monoxide is produced as toxic side product [8] (Scheme 4).

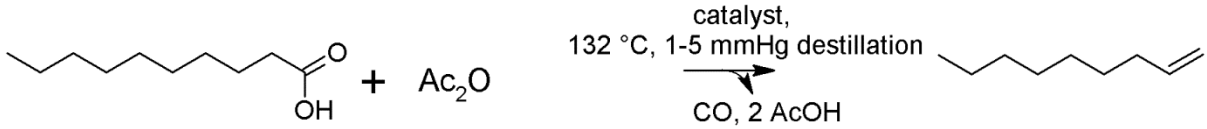

Scheme 4: Decarbonylation of decanoic acid as described by Liu *et al.* For the reaction a Pd-catalyst is used [8].

Further, Pyl *et al.* reported a hydrodeoxygenation of tall oil fraction (320 - 360 °C, 50.5 bar and NiMo catalyst) from Norwegian spruce pulping and the use of the obtained paraffinic hydrocarbon liquids in a steam cracking process (850 °C, 1.7 bar). With this process, typical products obtained from steam cracking of naphtha, especially ethylene and propene, could be produced [1].

While there are several processes for production of α-olefins from renewable resources [1][8], production of terminal dienes is hardly reported. Miller *et al.* achieved decarbonylation of dicarboxylic acids to terminal dienes using acetic anhydride, a Pd or Rh catalyst and a reaction temperature of about 250 °C. With this system, 1,7-octadiene was formed from decanedioic acid and 6-heptenoic acid was obtained form octanedioic acid (depending on the amount of acetic anhydride used) [16] (Scheme 5).

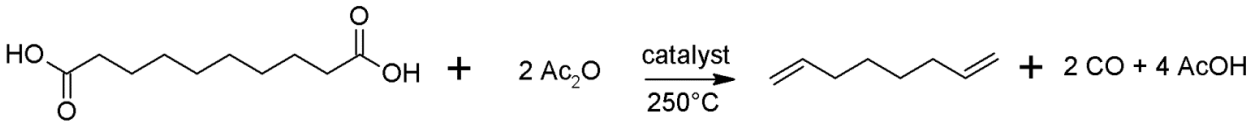

Scheme 5: Decarbonylation of decanedioic acid as described by Miller *et al.* Pd or Rh catalysts are used for the reaction [16].

Although with these methods synthesis of 1-alkenes is independent from petrol resources, there are several drawbacks, such as the rather high reaction temperatures, the need of transition metal catalysts and Ac_2O as well as the formation of carbon monoxide and acetic acid. Hence, a synthetic route to terminal dienes and 1-alkenes starting from renewable resources at mild reaction conditions without hazardous catalyst would be desirable [10][11].

1.2 Biocatalytic approaches for synthesis of 1-alkenes

A biocatalytic approach would present an attractive and environmentally friendly alternative for production of 1-alkenes compared to chemical approaches. To that end, fatty acids would be ideal substrates, since they are abundant, especially in plants (e.g.: hexadecanoic acid in palm oil or cacao butter), and entirely renewable [17]. Main advantages of enzymatic decarboxylation of fatty acids would be operation at mild reaction conditions (RT and atmospheric pressure) and no need of (hazardous) metal catalyst. Contrary to metal catalyst, enzymes are completely biodegradable, which results overall in an environmentally friendly conversion [18a].

The first enzymatic oxidative decarboxylation of saturated fatty acids was reported by Rude *et al*. In their study, decarboxylation of saturated even numbered long-chain fatty acids (C16 - C20) was achieved with the P450 monooxygenase OleT from *Jeotgalicoccus* sp. ATCC 8456 using H_2O_2 as sole oxidant. However, α/β-hydroxylated fatty acids were detected as side products. OleT amino acid sequence shows 36 % and 41 % homology with peroxygenases $P450_{SP\alpha}$ and $P450_{BS\beta}$, respectively [19], which catalyse the hydroxylation of fatty acids at the α/β- ($P450_{BS\beta}$) or only α-position ($P450_{SP\alpha}$) [20]. Based on these results, Rude *et al.* also tested $P450_{BS\beta}$, $P450_{SP\alpha}$ and 3 other enzymes in the decarboxylation of fatty acids. They found that all enzymes that were able to catalyse β-hydroxylation could also catalyse decarboxylation. However, OleT was the only enzyme that was more selective for decarboxylation than for hydroxylation [19].

Thereafter, Belcher *et al.* solved the crystal structure of OleT and the quite narrow substrate scope of OleT was expanded to C12 saturated fatty acid [21], although OleT was initially thought to preferably convert medium and long chain fatty acids (C22 - C14), due to good interactions with the amino acids inside the substrate channel [21][17].

In 2014, Liu *et al.* reported a H_2O_2-independent decarboxylation of fatty acids using OleT. In-vivo and in-vitro production of 1-alkenes was achieved using two different systems. On the one hand, in-vitro conversion (using purified enzymes) of fatty acids (C12 - C20) was tested by creating a fusion protein, in which a P450 reductase domain RhFRED from *Rhodococcus sp.* was fused to the C-terminus of OleT. Additionally, conversion with OleT, purified flavodoxin and flavodoxin reductase (Fld/FdR) from *E. coli* and NADPH was carried out. Further, in-vivo conversion in *E. coli* (using living *E. coli* cells, overexpressing the enzymes,

under fermentation conditions) was performed with OleT or OleT-RhFRED and addition of NADPH. Liu *et al.* found that decarboxylation of most tested fatty acids with OleT-RhFRED was less efficient than conversion with OleT and addition of H_2O_2. In-vivo decarboxylation of fatty acids with OleT in *E. coli* using NADPH and O_2, however, resulted in formation of a mixture of alkenes (97.6 $mg.L^{-1}$) over 40 h cultivation time, in which 1,10-heptadecadiene was the major product (41.4 $mg.L^{-1}$). Despite the rather low product titers, avoiding the problematic peroxide shunt could be an advantage for production of 1-alkenes, especially as whole cell process [22].

Additionally, decarboxylation of fatty acids by the non-heme iron decarboxylase UndA was reported by Rui *et al*. It was shown that UndA catalyses oxidative decarboxylation of fatty acids using Fe^{2+} and O_2. However, UndA has a quite narrow substrate scope and is only able to decarboxylate medium-chain fatty acids (C10 - C14), further limitation is that low product titers were obtained (< 3 $ng.mL^{-1}$ 1-undecene) [23]. Another method investigated to raise final product concentration was the photobiocatalytic regeneration of H_2O_2, however also resulting in low product titer (≈ 0.12 $mg.mL^{-1}$ 1-heptadecene) [24].

The so far most promising system was described by Dennig *et al*. The in-vitro decarboxylation of fatty acids was achieved using OleT, O_2, electron transfer components of spinach or putidaredoxin CamAB as electron transfer system and NAD(P)H in combination with an efficient NAD(P)H recycling system (Scheme 6). Using this system, the substrate scope was greatly expanded (C4 - C22), showing for the first time production of propene from butyric acid [17]. Furthermore, rather high product titers of 1-alkenes up to 1 $g.L^{-1}.h^{-1}$ (compared to 4 - 48 $mg.L^{-1}.h^{-1}$ with various whole cell approaches) were reached [22][25]. However, so far the described system from Dennig *et al*. is limited to saturated fatty acids [17].

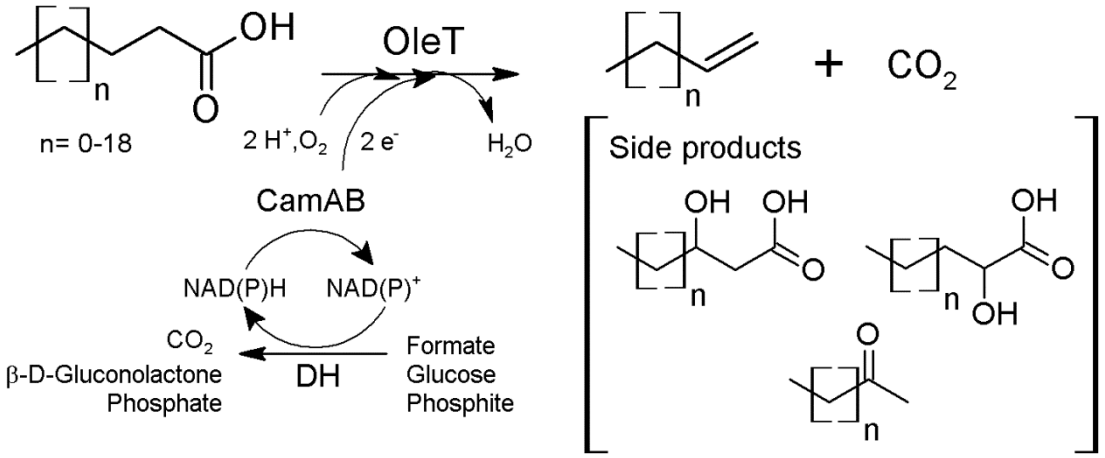

Scheme 6: Reaction scheme for decarboxylation of saturated fatty acids with OleT as described by Dennig *et al.* DH → dehydrogenase (used for cofactor recycling) [17].

1.3 Cytochrome P450 monooxygenases

1.3.1 General Introduction

All cytochrome P450 monooxygenases contain a cysteinato-heme group and their name is derived from the unusual property of their heme iron to form a ferrous-CO complex (Fe^{II}-CO). The CO can bind to reduced heme iron [Fe(II)] and thereupon induces a characteristic shift of absorbance from 420 to 450 nm (P450 = peak at 450 nm). The resulting pigment was called cytochrome [26]. In Figure 3 the prosthetic group found in all of cytochrome P450s is shown: an iron(III) protoporphyrin IX, which is covalently linked to the sulphur of a near cystein [27].

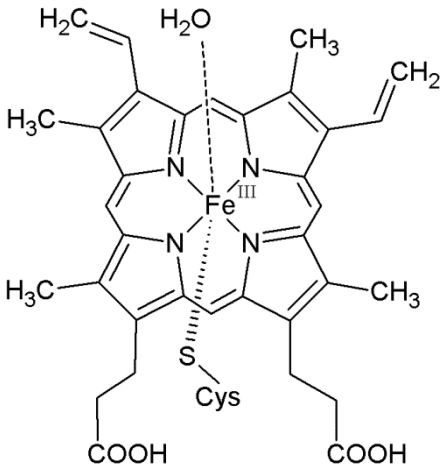

Figure 3: Prosthetic group of P450s: iron(III) protoporphyrin IX linked to a nearby cystein [27].

P450 monooxygenases are abundant in all organisms (bacteria, plants, fungi and animals) [27] and now have more than 26,000 annotated members [28][29]. One typical reaction catalysed by P450 monooxygenases is the introduction of one oxygen atom derived from cleavage of O_2 into a substrate, while the other oxygen atom is reduced to H_2O (equation 1) [18b][27].

$$2\,H^+ + 2\,e^- + O_2 + Sub \rightarrow SubO + H_2O \qquad (1)$$

P450 monooxygenases catalyse about 21 different types of reactions [28], e.g. hydroxylation and decarboxylation of fatty acids [30][17][19][20][22]. Although the reaction mechanism can be quite different depending on the catalysed reaction, activation of O_2 is always done in the same way [18b].

1.3.2 **Oxygen activation and electron transfer**

The reaction requires the transport of two electrons, derived from NAD(P)H, to the heme Fe-S cluster according to Scheme 7. First the substrate binds near to the heme in the active site by replacing a H_2O molecule that is coordinated as 6^{th} ligand (B) [18b][31a][27], which is driven by an entropy change [27]. Afterwards, the Fe(III) is reduced by one electron to Fe(II) (ferrous state; C) and hence catalysis is initiated. This is possible due to the increasing distance of the iron from the plane of the porphyrin ring and hence the heme becomes a better electron sink [27]. Furthermore, it is supposed that a negative charge is delocalized over the whole ferrous complex, which has later a great influence on O-O bond cleavage. This Fe(II) complex is a very efficient reducing agent and therefore reaction with a triplet dioxygen can take place, forming an iron(III)-oxygen bond (D) [27]. After formation of this iron(III)-oxygen bond, a second electron is transported to the complex resulting in a negatively charged iron(III)-peroxo complex (E), which is considered to be the rate limiting step [27][31a]. Due to this reduction, the O-O bond is weakened and subsequently two protonation steps cleave the O-O bond, forming H_2O and an iron(IV)-oxo radical cation (F) [18b]. This species is called compound I and usually regarded as the reactive intermediate that catalyses P450 reactions. Compound I is a strong electrophile and thus reacts with a substrate molecule [18b], resulting in the release of an oxygenated substrate and coordination of a water molecule to the heme (A) [18b][27][31a].

Beside the use of molecular oxygen and NAD(P)H, oxidation reaction can also occur using the peroxide shunt, where the iron(III)-substrate complex (B) is transformed to the Fe(III)-hydroperoxo complex (E) using H_2O_2 as sole oxidant [31].

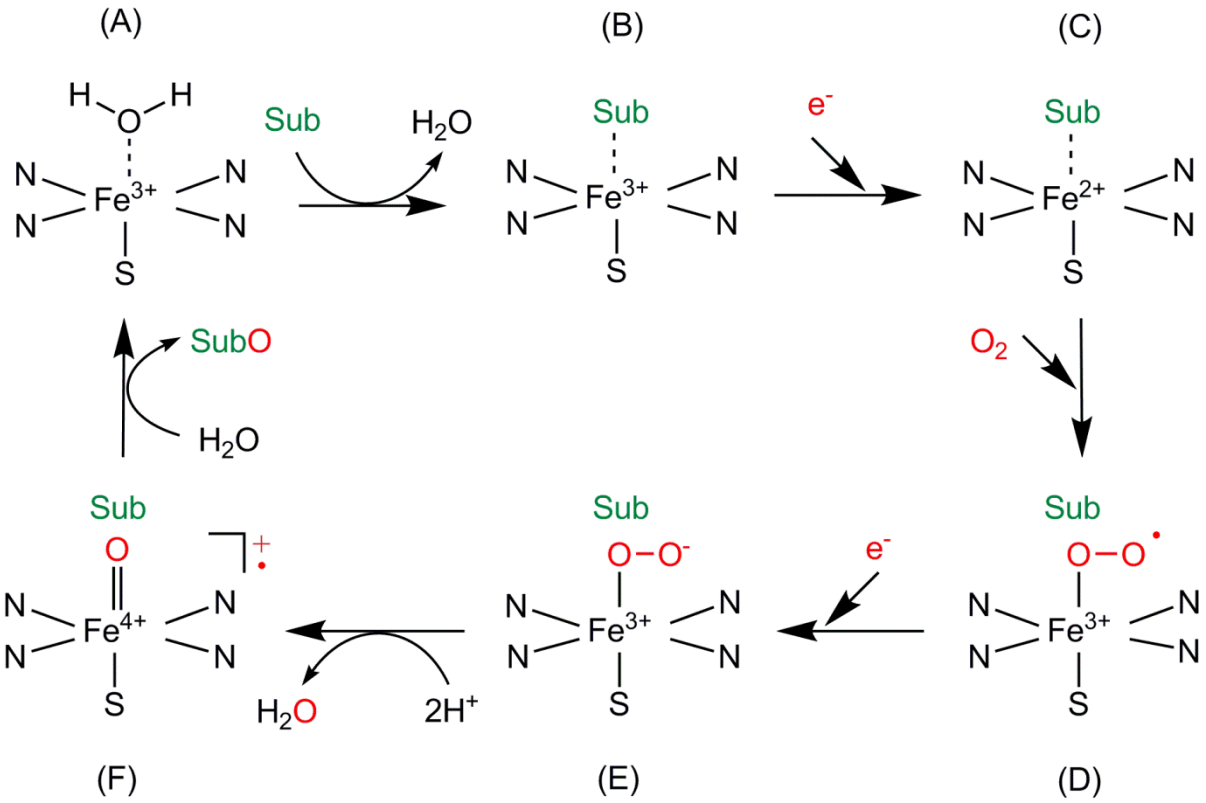

Scheme 7: Summary of the catalytic cycle of cytochrome P450 monooxygenases. A simplified scheme for oxygen activation and oxygenation of a substrate is shown [18b].

Transport of the electrons from nicotinamide to P450 monooxygenases is usually regulated by an electron transfer system. Depending on the type of organism and location of the monooxygenase in the organism, different electron transfer systems are used. They can usually be divided into bacterial, mitochondrial, microsomal and self-sufficient cytochromes [18b]. Class I (bacterial, mitochondrial) and class II (microsomal) electron transfer systems are most abundant. A self-sufficient system is described for BM-3 [18b][32][31a].

Class I electron transfer systems belong to bacterial cytochrome and mitochondrial, eukaryotic P450 systems (Scheme 8). In this group, three separate proteins are involved in catalysis. A FAD dependent reductase accepts hydride equivalents from a NAD(P)H cofactor. Further a ferredoxin, which usually harbours a 2Fe-2S iron-sulfur cluster, shuttles the single electrons derived from the reductase to the heme unit, which is subsequently reduced [18b][32][31a].

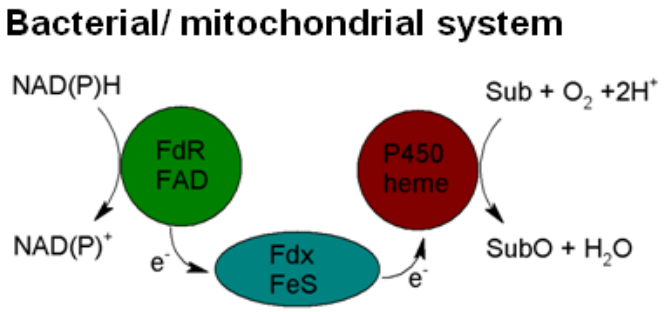

Scheme 8: Class I electron transfer system (bacterial, mitochondrial) used by P450 monooxygenases. FdR = ferredoxin reductase; FAD = flavin adenine dinucleotide; Fdx = ferredoxin; FeS = iron-sulfur cluster; P450 heme = cytochrome P450. Overall reaction requires two times a single electron transfer [18b].

The best studied system, belonging to class I P450s, is $P450_{cam}$ from *Pseudomonas putida*, which catalyzes the hydroxylation of camphor. Its electron transfer depends on a FAD-containing putidaredoxin reductase (ferredoxin reductase), which is depending on NAD(P)H and a putidaredoxin - a 2Fe-2S containing ferredoxin. The putidaredoxin transfers two electrons, one by one, from the putidaredoxin reductase to the P450, while the reductase accepts two electrons from NAD(P)H [32][33][34].

The microsomal (class II) electron transfer system is the most commonly used system in eukaryotes (Scheme 9). It is more simple than the class I system. In this system either a cytochrome P450 reductase, which possesses a FAD or FMN cofactor, transfers the electrons from NAD(P)H directly to the cytochrome or a cytochrome b5 is used and there is no need of an additional transfer enzyme [18b][32][31a].

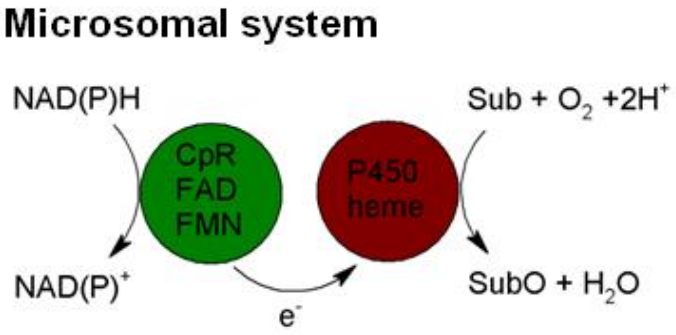

Scheme 9: Class II electron transfer system (microsomal) used by P450 monooxygenases. CpR = cytochrome P reductase; FAD = flavin adenine dinucleotide; FMN = flavin mononucleotide; P450 heme = cytochrome P450. Overall reaction requires two times a single electron transfer [18b].

Moreover, a self sufficient system without separate transporter, BM-3 monooxygenase from *Bacillus megaterium*, was described (Scheme 10). This system consists of a natural fusion

protein of a cytochrome P450 reductase, which contains a FMN and a Fe-S cluster, and the P450 enzyme [18b][32][31a].

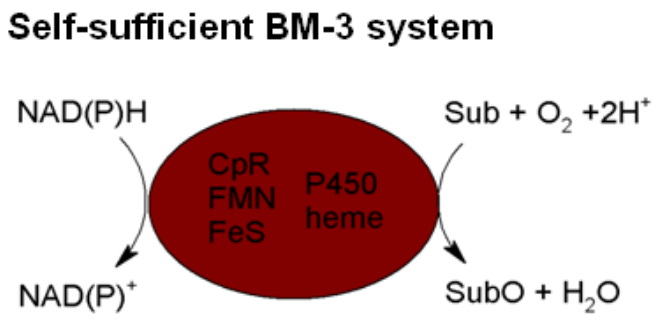

Scheme 10: Self-sufficient BM-3 system. CpR = cytochrome P reductase; FMN = flavin mononucleotide; FeS = iron-sulfur cluster; P450 heme = cytochrome P450 [18b].

1.3.3 Limitations in industrial applications

Although P450 monooxygenases catalyse a broad range of chemically important reactions (such as activation of C-H bond) and therefore are highly studied enzymes, their application in industrial processes is rare and still challenging. Compared to other enzyme-catalysed reactions, cytochrome P450 monooxygenases require a quite complex system [28][29][31b].

There is the need of an electron transfer system as well as expensive NAD(P)H cofactor. Therefore one of the major challenges is recycling of the cofactor, which is usually done by the use of a second enzyme and co-substrate, e.g. glucose dehydrogenase and glucose. Limitations of cofactor availability might be solved by whole cell processes. However, in these systems, problems such as inhibition by toxic substrates or products and limitations due to substrate transfer or product degradation could occur. Hence, for whole cell approaches the choice of a proper expression host is absolutely necessary. Overcoming cost limitations due to the cofactor might be also achieved by the use of H_2O_2 as oxidant (using the peroxide shunt), instead of NAD(P)H and an electron transfer system, resulting in a more simple reaction system. Nonetheless, there are only a few P450s that work efficiently with H_2O_2 and reactive oxygen species might lead to degradation of the heme or oxidative protein damage [28][31b].

Furthermore, enhancing the efficiency of the electron transport system is necessary and could be done by co-expression with the cytochrome P450 or by design of fusion proteins. On the other hand, the use of separate, heterologous electron transfer systems such as putidaredoxin or bacterial flavodoxins could also enhance the activity of the system [28][31b].

The overall stability could pose another problem. During activation of O_2 (Scheme 7), a side reaction can occur, called uncoupling reaction, in which the consumption of NAD(P)H is

uncoupled from product formation. This could occur when the Fe(III)-hydroperoxo complex (Scheme 7; compound E) dissociates into Fe(III) and a superoxide anion, which consequently leads to formation of H_2O_2 [33][27]. The formed H_2O_2 could lead to enzyme inactivation due to degradation of the heme and moreover NAD(P)H is consumed without product formation. Hence, there is the need to increase the coupling efficiency, which is mainly achieved by directed evolution [28][31b].

Next, substrates converted by P450s are usually unpolar (unfunctionalized alkanes and alkenes) and therefore insoluble in water. The use of a cosolvent is very often necessary; however, P450 monooxygenases are often less active and less stable, especially in polar organic solvents [18c][31b]. This poses, in whole cell processes, problems and requires proper enzyme engineering for stability enhancement. Finally, P450s are often quite inefficient with respect to industrial applications (low TTN), asking for protein engineering to improve catalyst activity [28][31b].

1.4 OleT and reaction mechanism

As described in chapter 1.2, OleT catalyses the oxidative decarboxylation of fatty acids, which is a quite unusual reaction for P450 monooxygenases. While in chapter 1.2 different ways of producing terminal olefin with OleT were described [17][19][21][22][24], in this section the biochemical properties as well as a possible reaction mechanism for OleT will be covered.

OleT was isolated from the halophilic organism *Jeotgalicoccus sp.* and therefore it is rather stable in high salt solutions (e.g. 1 M NaCl) [21]. Furthermore, OleT is part of the cytochrome P450 family and was classified as CYP152L1 due to the sequence homology to $P450_{BS\beta}$ and $P450_{SP\alpha}$ (41 % and 36 %, respectively). Based on the homology of the active site with $P450_{BS\beta}$ and the ability to convert fatty acids in presence of H_2O_2, OleT was classified as peroxygenase [19]. However, a re-classification as monooxygenase was proposed as higher conversions were achieved using NAD(P)H and an electron transfer system [35][22][17].

Figure 4 shows the crystal structure of the substrate channel of OleT. The substrate channel is highly hydrophobic, providing good properties for binding of long chain fatty acids [21].

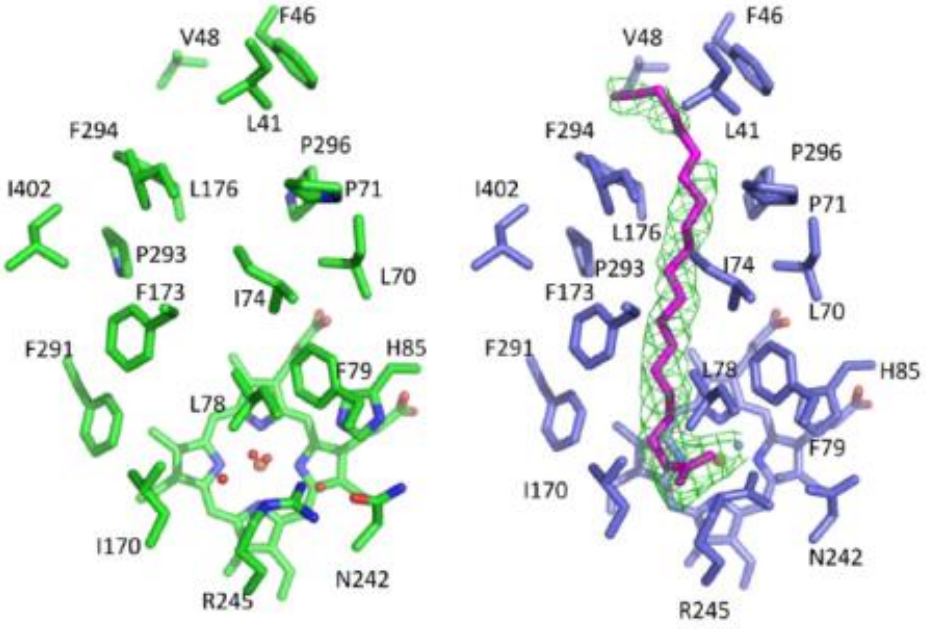

Figure 4: View of OleT active site derived from crystal structure (substrate channel residues), with and without bounded substrate (taken from [21]).

The active site of OleT ressembles that of $P450_{BS\beta}$, whereby the major difference between $P450_{BS\beta}$ and OleT is the Gln-85 ($P450_{BS\beta}$) which is replaced by His-85 (OleT) [19][21]. Rude *et al.* reported that His-85 plays a major role in the decarboxylation reaction, since replacing Gln-85 by His-85 in $P450_{BS\beta}$ resulted in higher preference for decarboxylation reaction over hydroxylation [19]. It was proposed that His-85 acts as proton donor to compound I [Fe(IV)-oxo radical cation], resulting in the abstraction of an electron from the carboxylate moiety of the substrate and reduction of compound I to compound II [Fe(IV) hydroxide]. A carboxylic radical is formed, which further results in a homolytic C-C_α bond cleavage. On the other hand, it was proposed that P450 monooxygenases, such as $P450_{BS\beta}$, without a His, abstract a hydrogen atom (not an electron) from the substrate. Furthermore, Arg-245 and Pro-246 are found in the active site of OleT like in the peroxygenases $P450_{BS\beta}$ and $P450_{Cla}$. These amino acids where supposed to support positioning and binding of the fatty acids in the substrate channel and thus are essential to catalyze the decarboxylation or hydroxylation reactions [19][21].

More recently, Grand *et al.* also proposed a mechanism for decarboxylation of fatty acids by OleT (Scheme 11). They proposed that the first reaction step is identical to P450 oxygenation reactions. There, a hydrogen atom is abstracted from the C_β-atom of the substrate by compound I, resulting in the formation of a substrate radical and a Fe(IV) hydroxide (compound II). Afterwards, recombination of the substrate radical with compound II results in the formation of an hydroxylated substrate and reformation of the ferric state of the enzyme [35].

Based on kinetic isotope experiments, they claimed that decarboxylation is initiated by abstraction of a hydrogen atom from the substrate on C_β position rather than electron abstraction from the fatty acid carboxylate. After hydrogen abstraction, a substrate radical and a Fe(IV) hydroxide (compound II) is formed. Next, a single electron transfer, either to compound II or to another oxidant, results in the formation of a substrate carbocation or a substrate diradical. Finally, formation of the corresponding 1-alkene is achieved by loss of the leaving group CO_2 [35].

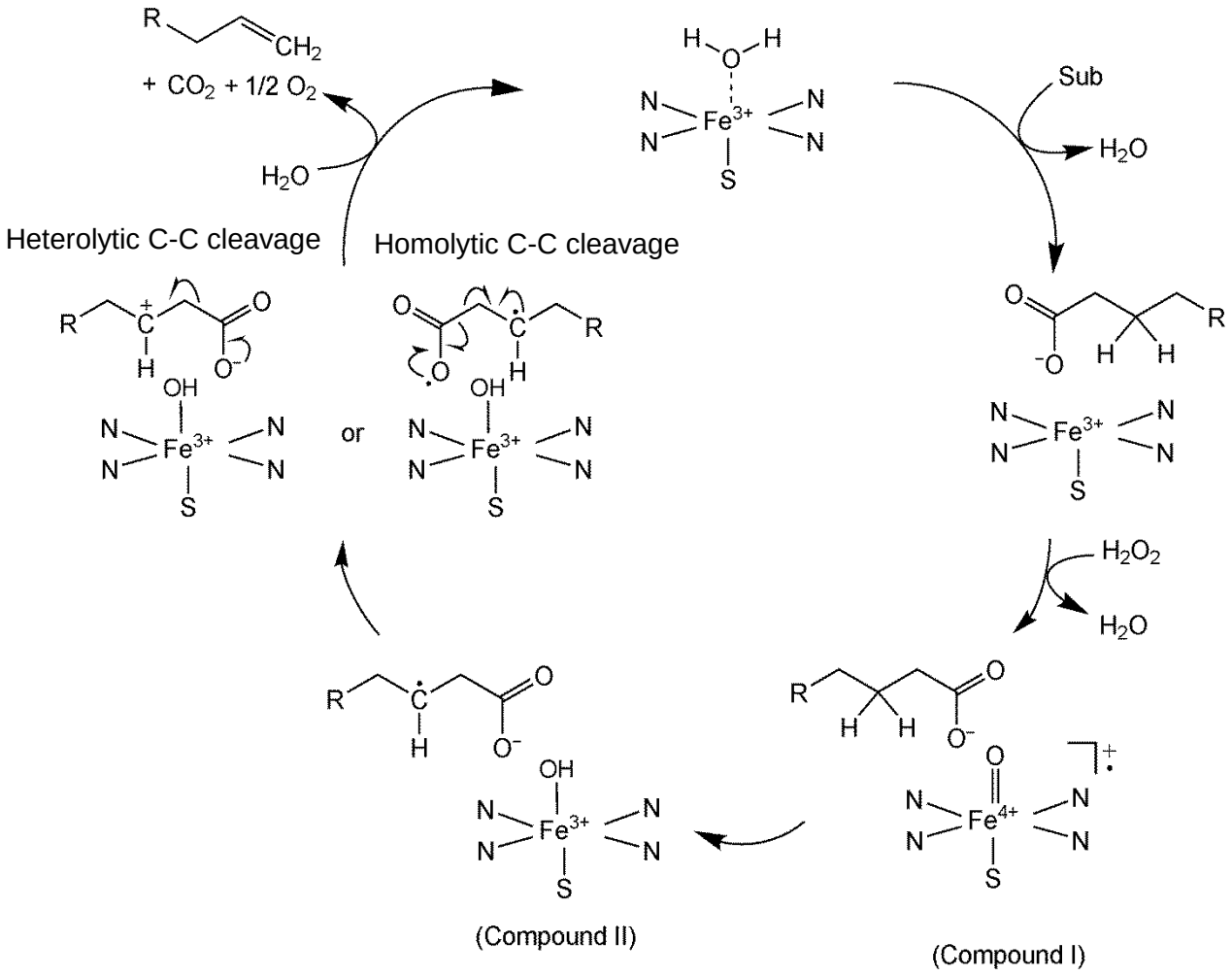

Scheme 11: Proposed reaction mechanism for oxidative decarboxylation of fatty acids by OleT [35].

1.5 Aim of this thesis

In this work, the oxidative decarboxylation of dioic acids by the P450 monooxygenase OleT was investigated. The basis of this research was the reaction system established by Dennig *et al.* for the decarboxylation of saturated fatty acids. Dennig *et al.* used purified OleT in combination with an electron transfer system (CamAB) and NAD(P)H with efficient cofactor recycling. With this system, decarboxylation of fatty acids from C22 - C4 was achieved [17] (Scheme 6, section 2.1).

Dioic acids are widely distributed in nature and they are part of various metabolic pathways [36 - 41]. Another possibility to obtain dioic acids is their production via enzymatic ω-oxidation of fatty acids, where high yields (> 100 $g.L^{-1}$) could be reached [42]. First the fatty acid is hydroxylated on ω-position to the corresponding alcohol with an oxygenase, then oxidized to the aldehyde by an alcohol dehydrogenase and finally oxidized to the dioic acid by an aldehyde dehydrogenase (Scheme 12) [43]. Polyester waste materials are another source of dioic acids, such as adipic acid [12]. Therefore, oxidative decarboxylation of dioic acid with OleT-CamAB-FDH system would present an environmental friendly and sustainable way to access terminal dienes.

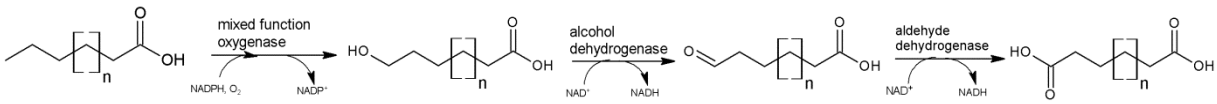

Scheme 12: Reaction scheme for biocatalytic ω-oxidation of fatty acids to yield dioic acids [43].

The aim of this study is:

- Study of the reactivity of dioic acids (C18 - C6) in the oxidative decarboxylation reaction using OleT.
- Investigation of the reactivity of potential reaction intermediates (ω-enoic acids).
- Investigation of branched fatty acids as the third substrate class containing a carboxylic acid functionality.
- Investigation of the influence of reaction temperature (RT, 4 °C) on conversion of the different substrates.
- Quantification and characterization of final products (terminal dienes) using commercial product standards or via scale-up followed by product isolation and purification.

- Optimization of system efficiency (variation of substrate and enzyme concentration, type of electron transfer system and co-solvent).

2 Results and discussion

2.1 Exploration of the substrate scope of OleT

To explore the substrate scope of OleT, three different types of substrates were investigated with OleT-CamAB-FDH cascade [17]: dioic acids, ω-enoic acids and branched fatty acids. In the following chapters, the results obtained with OleT-CamAB-FDH cascade on these substrate classes will be discussed.

In Scheme 13 and Scheme 14, conversions of the substrates to the corresponding products, are shown.

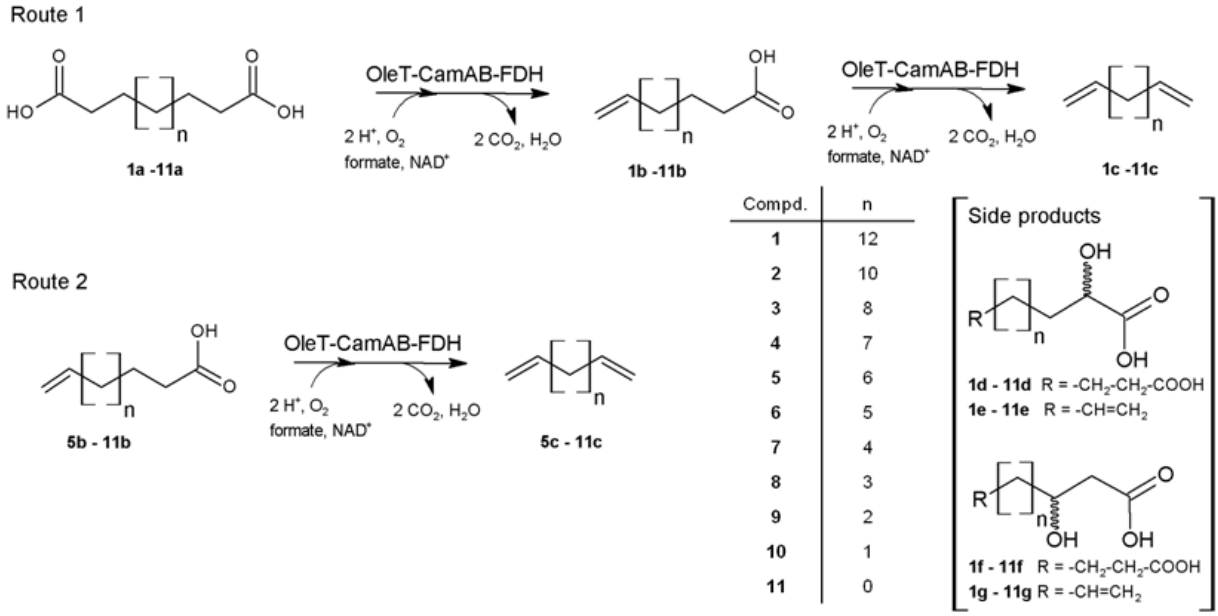

Scheme 13: Conversion of dioic acids and ω-enoic acids by OleT. One CO_2 molecule comes from the oxidation of formate, one from the decarboxylation.

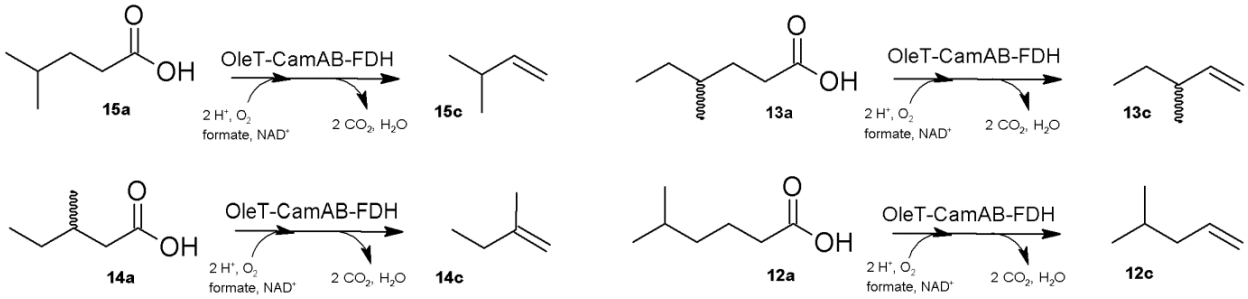

Scheme 14: Conversion of selected branched fatty acids by OleT. One CO_2 molecule comes from the oxidation of formate, one from the decarboxylation.

2.1.1 **Decarboxylation of dioic acids using OleT-CamAB-FDH cascade**

In previous studies, it was shown that decarboxylation of saturated fatty acids with OleT-CamAB-FDH system yields 1-alkenes [17] (Scheme 6, chapter 1.2). In this study, the influence of a second carboxyl group on the catalyst performance was studied by testing dioic acids (**1a - 11a**) in the decarboxylation reaction (Scheme 13).

The first conversion was tested with **3a** at room temperature (RT). Measurement on GC-FID showed the formation of **3c** as well as various side products, such as **3f** and **3g** (Figure 5). Hence it was proven that decarboxylation of dioic acids is possible with the current reaction system. Therefore, conversion of 11 dioic acids from C18 to C6 (**1a - 11a**) was investigated.
Figure 5 shows GC-MS chromatrogram obtained after conversion of **3a** with OleT-CamAB-FDH cascade and the reaction control without OleT (negative control) as one typical example of the conversion of dioic acids. Here the three products that are mainly formed are shown: terminal diene (**3c**), 3-hydroxy-ω-enoic acid (**3g**) and 3-hydroxy-dioic acid (**3f**). Although decarboxylation was the major reaction catalyzed by OleT, formation of hydroxy-dioic acids and hydroxy-ω-enoic acids as side products was expected, as hydroxylation was already observed on saturated fatty acids [17][22][19]. Detailed results regarding the side product formation will be discussed in chapter 2.1.3.

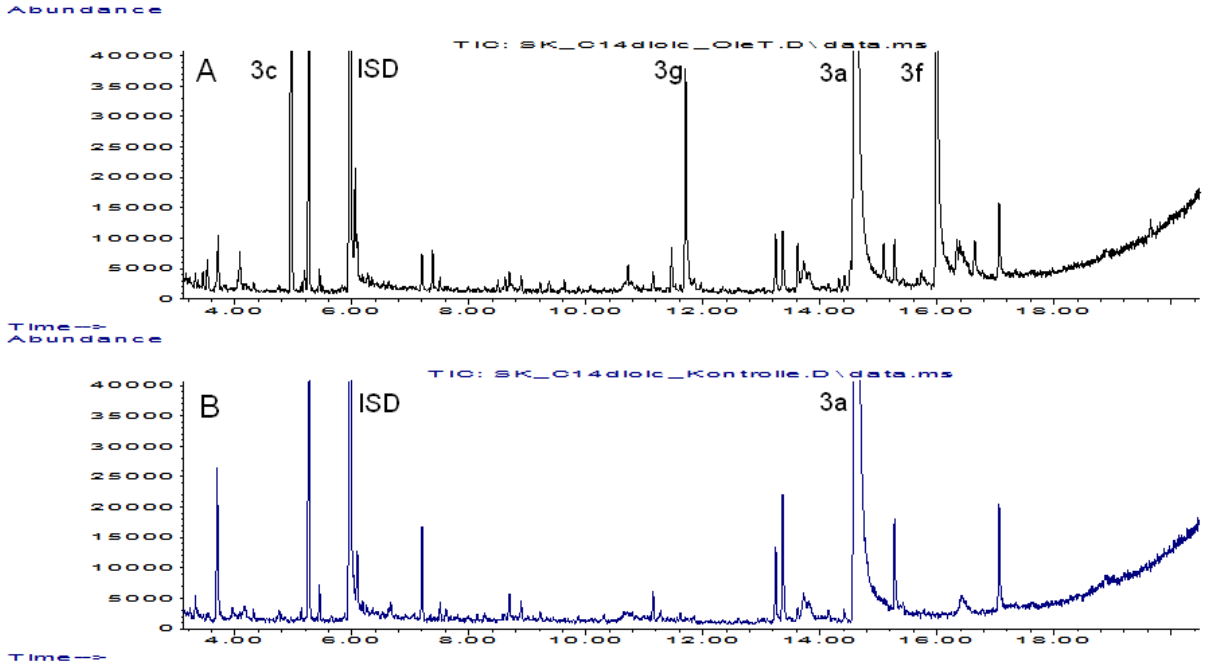

Figure 5: A: Conversion of **3a** (10 mM) using OleT-CamAB-FDH reaction cascade. **B:** Reaction control without OleT (negative control). From **3a**, **3f** and **3g** the corresponding methylester are shown (derivatization with TMS-diazomethane), ISD: internal standard (0.1 % 1-decanol).

Further, since catalyst performance is usually strongly dependent on the temperature [17], the influence of the reaction temperature on the cascade was also investigated. Therefore all biotransformations were performed at RT for 24 h as well as at 4 °C for 72 h, while all other parameters were kept constant.

Figure 6 shows the TTN (calculated based on quantification of terminal dienes formed, $TTN_{conv.diacids} = \frac{c_{diene}}{c_{OleT}} * 2$) obtained by conversion of **2a** - **10a** with OleT-CamAB-FDH cascade. As already expected, it was found that not only the type of substrate (chain length) but also the reaction temperature had an influence on the conversion [17]. In Table 1 detailed information about conversion, TTN and STY (space time yield) of all converted dioic acids are listed.

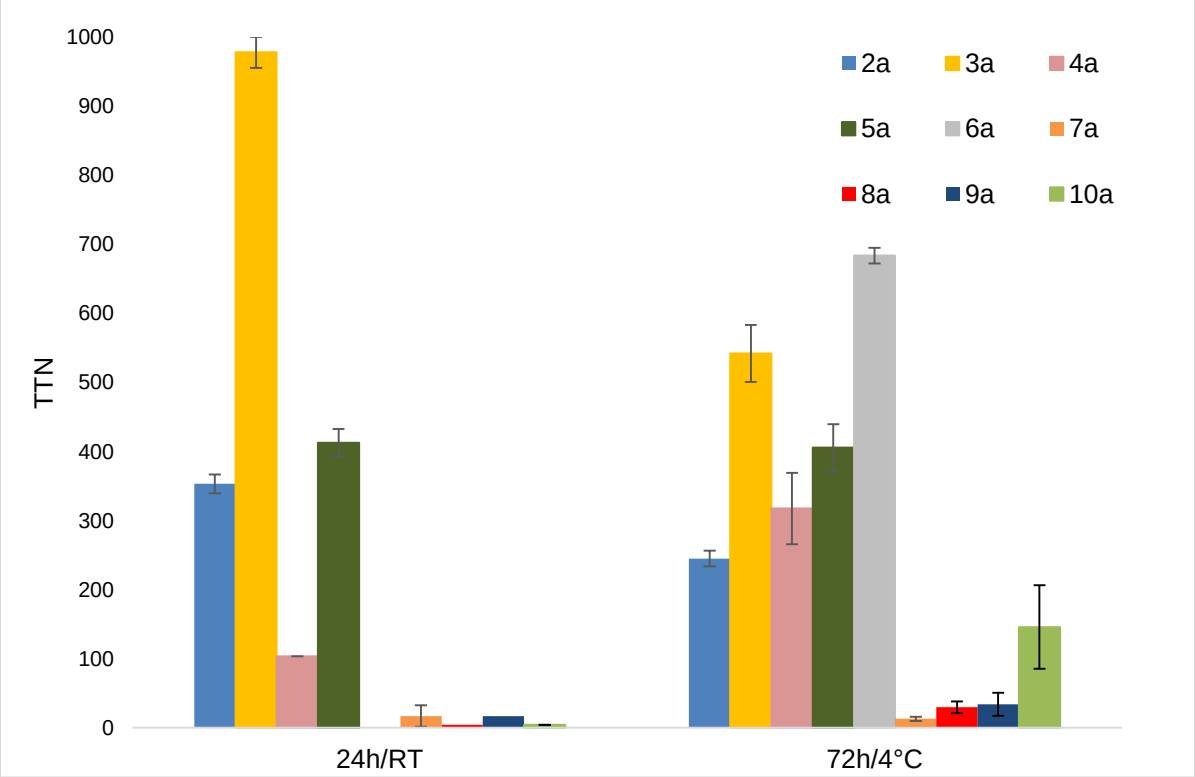

Figure 6: Total turnover numbers of **2a** - **10a** obtained from conversion with OleT-CamAB-FDH cascade at RT/24 h and 4 °C/72 h.

$TTN_{conv.diacids} = \frac{c_{diene}}{c_{OleT}} * 2.$

First it was found that **1a** - **10a** were converted with OleT-CamAB-FDH system and only with **11a** no conversion was observed. It might be that polarity of **11a** (shortest substrate) is too high to allow proper binding due to the rather hydrophobic substrate channel of OleT [21][17]. Moreover the chain length appears to have a great influence, since there were large differences observed between all product concentrations (0 - 2.9 mM terminal diene; Table 1;

Figure 6) obtained with the single substrates. In general it was observed that higher dioic acids were better converted, which is not astonishing since OleT has a higher affinity towards long-chain fatty acids (C20 - C14) [21][17].

The best conversion (defined as % terminal diene formed related to starting substrate concentration) was achieved with **3a** at RT (29 %) (Figure 6, Table 1). Interestingly, at 4 °C the best substrate was **6a**, while at RT there was no terminal diene formed with **6a**. Similarly, the corresponding C11 mono acid previously showed no conversion at RT and only 1.9 % conversion at 4 °C, which was explained by ineffective binding of medium-chain fatty acids (C10, C11) in the binding pocket of OleT [17]. This might also explain the very low conversions of **7a** (< 1 %). However, with **7a** no improvement was observed by lowering the temperature; a similar observation was made with corresponding C10 mono acid at 4 °C with no significant increase in product concentration (0.04/0.07 mM, respectively) [17]. This indicates that **6a** is overall better accepted by OleT than **7a**. Interestingly, conversion of smaller substrates increased when lowering the temperature (e.g. with **10a**, ≈ 35 times higher TTN; 4/146, respectively).

Overall, lowering the reaction temperature led to better conversions. The TTN values increased in most cases by performing the biotransformation at 4 °C.

A significant decrease in conversion was observed at 4 °C only with long-chain substrates **2a** and **3a**. Compared to most other substrates, conversion at RT with **2a** and **3a** was rather high (11 % and 30 %, respectively). This indicates that substrates that are well converted are properly binding in the substrate channel, while substrates that show low conversions are poorly accepted by OleT. Substrate binding might be improved at 4 °C, resulting in an increased stability of OleT and therefore increased productivity [17].

Beside the catalyst stability, productivity might also be influenced by the electron transfer system. The efficiency of the electron transfer system strongly influences productivity of P450 monooxygenases. Additionally the productivity is influenced by activation of O_2 resulting in the formation of a reactive oxygenated species [28]. Hence substrate turnover and catalyst lifetime is determined by those parameters [27][33]. Moreover, the redox-potential of the mediator CamB is also depending on the temperature. At 5 °C there is a redox potential of -0.195 V and at 25 °C the redox potential is -0.242 V [44], which again has an influence on the productivity of OleT [28][27][33][32].

Table 1: Analytical data obtained by conversion of dioic acids with OleT-CamAB-FDH cascade at RT and 4 °C. Biotransformations were carried out at standard reaction conditions (10 mM substrate, 6 µM OleT, 0.05 U.mL^{-1} CamAB, 1 mg.mL^{-1} FDH, 100 mM ammonium formate, 200 µM NADH, 500 U.mL^{-1} catalase).

$$TTN_{conv.diacids} = \frac{c_{diene}}{c_{OleT}} * 2$$

	RT				4 °C	
Substrate	**terminal diene [mM] (conversion [%])**	**TTN**	**TON[a] [h^{-1}]**	**STY [mg.L^{-1}.d^{-1}]**	**terminal diene [mM] (conversion [%])**	**TTN**
1a[b]	n.d.	n.d.	n.d.	n.d.	n.d.	n.d.
2a	1.06 ± 0.04 (11)	353 ± 14	18 ± 0.5	206 ± 6	0.74± 0.03 (7)	245 ± 11
3a	2.93 ± 0.07 (29)	978 ± 22	73 ± 2	487 ± 11	1.63 ± 0.12 (16)	542 ± 41
4a	0.31 ± 0.04 (3)	104 ± 13	36 ± 2	51 ± 6	0.95 ± 0.15 (10)	317 ± 52
5a	1.24 ± 0.06 (12)	413 ± 20	91 ± 9	171 ± 8	1.22 ± 0.10	406 ± 34
6a	0 (0)	n.d.	n.d.	86[d] ± 1	2.05 ± 0.03 (20)	684 ± 11
7a	61*10^{-3} ± 58*10^{-3} [g] (<1)	17 ± 16 [g]	n.d.	6 ± 5 [g]	39*10^{-3} ± 9*10^{-3} (<1)	13 ± 3
8a	12*10^{-3} ± 2*10^{-3} (<1)	4 ± 1	n.d.	1	88*10^{-3} ± 26*10^{-3} (<1)	30 ± 9
9a	0.12[e]	38	n.d.	9	0.10[c] ± 0.5	34 ± 17
10a	12*10^{-3} [f]	4[f]	n.d.	10[d]	0.44 ± 0.18	146 ± 60

n.d.: not determined
a) determined from biotransformation at RT for 1 h.
b) Quantification of **1c** was not possible since no commercial product standard was available. Proof of product formation was done by isolation and purification of **1c** (see chapter 2.4.1). Unfortunately isolation of **1c** did not result in high yield so that a product standard could not have been generated for quantification.
c) Reaction was done over 5 days at 4 °C.
d) Determined from biotransformations at 4 °C for 72 h.
e) Only single determination.
f) Only double determination, mean of the two values is shown, no standard deviation was determined.
g) High standard deviation: For **7a** boiling point was too low for extraction and GC-FID analysis (114 - 121 °C), however, GC-MS measurements were performed at 80 °C, which led to the high variation.

Regarding the TON there are also big differences between the different substrates, where observed TTN values were 3 to 14 times higher than the corresponding TONs. This shows that, depending on the substrate, inactivation of the catalyst is more or less fast. In P450s it is observed that inactivation often occurs, due to uncoupling reactions. Uncoupling of NAD(P)H consumption from product formation leads to production of H_2O_2. Consequently H_2O_2 might inactivate the enzyme due to degradation of its heme [28][33]. Additionally, uncoupling also results in the consumption of NADH without product formation, which could decrease the TTN [28][33].

Furthermore, with **4a** and **2a**, no side product formation was observed after one hour, but after 24 h significant amount of side products could be detected. This is probably a problem of analysis. Given the low conversion levels, it can be expected that concentration of side products was below the limit of detection.

Moreover, it is interesting that the TON of **5a** (91 h^{-1}) was 25 % higher than that of **3a** (73 h^{-1}), however, the TTN of **3a** after 24 h was finally 2.3 times higher (978 and 413, respectively). This shows that the type of substrate has a great influence on catalyst performance. The catalyst lifetime probably be higher when converting **3a** than **5a**. This might be again due to the preference of OleT for long chain substrates [17][21] and therefore uncoupling reaction might occur more frequently with **5a** than **3a** probably due to poorer binding into the substrate channel [33]. Furthermore, the TON of **2a** was the lowest (18 h^{-1}) but TTN did not differ much from that of **5a**, which supports the assumption that **5a** has a higher impact on the catalyst stability than other substrates. It could be concluded that high initial reaction rates do not necessarily lead to high conversions and good overall catalyst performance. Low activity and low operational stability are major problems in the application of P450 monooxygenases [28][29].

Next, STY was determined and highest productivity was achieved with **3a,** reaching almost 0.5 $g.L^{-1}.d^{-1}$ (Table 1). In comparison, whole cell approaches with OleT in *E. coli* so far only reached a maximum of 48 $mg.L^{-1}.d^{-1}$ [25][22]. Whole cell approaches for decarboxylation of fatty acids are quite challenging since reactions might compete with host organism's fatty acid metabolism [29][45]. Furthermore since the host organism contains many different fatty acids, which can be decarboxylated by OleT, there will be a mixture of several 1-alkenes formed [22]. Also the use of a co-solvent is difficult in whole cell approaches, due to low resistance of whole cells agaist organic solvents, and also substrates or products might be toxic to the organism [28][31b]. Therefore the obtained STY of 0.5 $g.L^{-1}.d^{-1}$ (TTN = 980) from **3a** is satisfying in the context of a decarboxylation reaction by a P450 monooxygenase [28][29][45]. In comparison, conversion of saturated fatty acids led to product titers up to 1 $g.L^{-1}.d^{-1}$ (TTN = 1300) [17]. This indicates that the second carboxylic acid group on the ω-position has an impact on the overall activity of the enzyme, which is probably due to the fact that the substrate channel of OleT is rather hydrophobic [21] and especially mid to short chain dioic acids show an increased polarity compared to the saturated fatty acids. This could result in less binding efficiency and more frequently occuring uncoupling reactions [33].

2.1.2 Decarboxylation of ω-enoic acids using OleT-CamAB-FDH cascade

Interestingly, no reaction intermediate (ω-enoic acids) could be observed during biotransformation of dioic acids. Hence, to answer the question whether a reaction intermediate was formed during the reaction and how decarboxylation occurs, ω-enoic acids were tested with the OleT-CamAB-FDH system (Scheme 13).

First, **5b** was converted under standard reaction condition (see chapter 4.3) at RT for 24 h. Interestingly, with 10 mM substrate concentration, no product was formed from **5b** and also convertion of **6b** showed only traces of **6c**. This indicates again a strong influence of the ω-functionality on the catalytic activity of OleT. However, compared to corresponding C11 and C10 saturated fatty acid, conversions with OleT-CamAB-FDH cascade were also quite low (0 %/0.4 % at RT and 1.9 %/0.7 % at 4 °C, respectively) [17]. Since conversions of C11 and C10 saturated fatty acid were also poor, it could be assumed that the low conversions of **5b** and **6b** are rather due to the chain length than due to the ω-terminus. Another hint for this assumption is that **5a** and **6a** were also poorly converted at RT (see chapter 2.1.1).

Due to the low conversion of **5b** and **6b**, the influence of the substrate concentration on the conversion of **5b** and **6b** was studied (Figure 7) and indeed at a substrate concentration ≤ 6 mM product formation was also observed with **5b**.

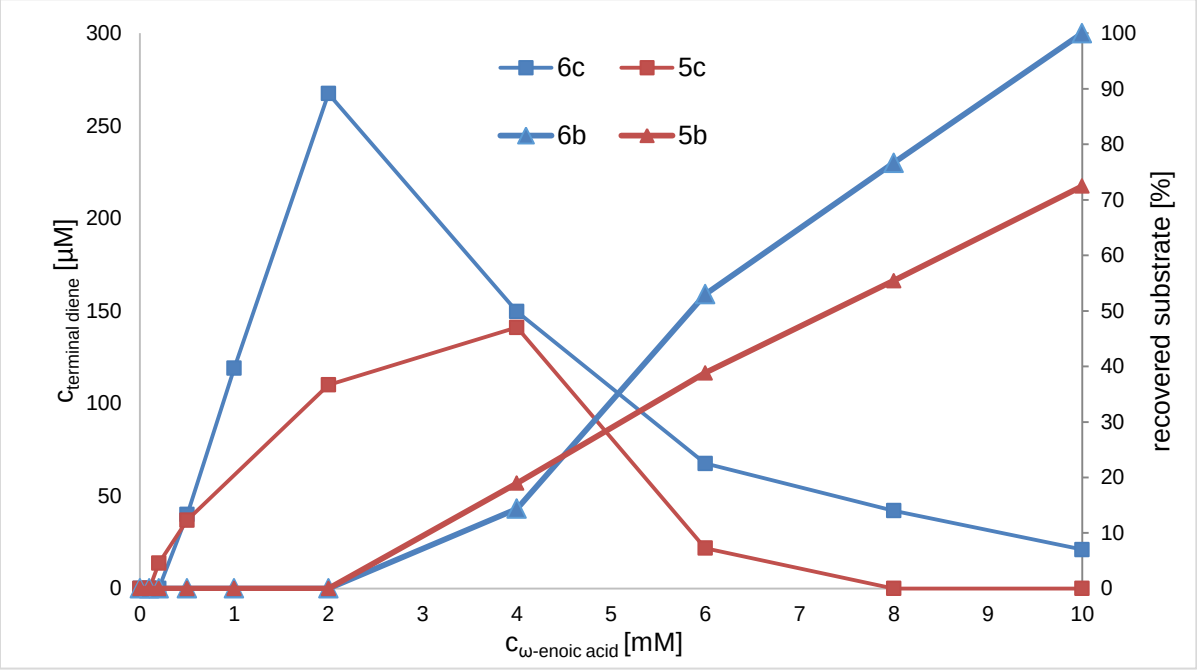

Figure 7: Influence of **5b** and **6b** concentration on conversion levels. Biotransformations were done according to the standard protocol at RT/24 h in 1 mL scale. Substrate concentrations varied from 0 to 10 mM. A reaction control without OleT was performed to be able to calculate the recovery of unconverted substrate, at substrate concentrations < 2 mM no substrate was recovered, which is probable a problem of the detection limit of GC-FID.

Also the conversion of **6b** increased when lowering the substrate concentration reaching an optimum at 2 mM (compared to 4 mM for **5b**). These results may indicate a potential substrate inhibition; however, this was not studied any further.

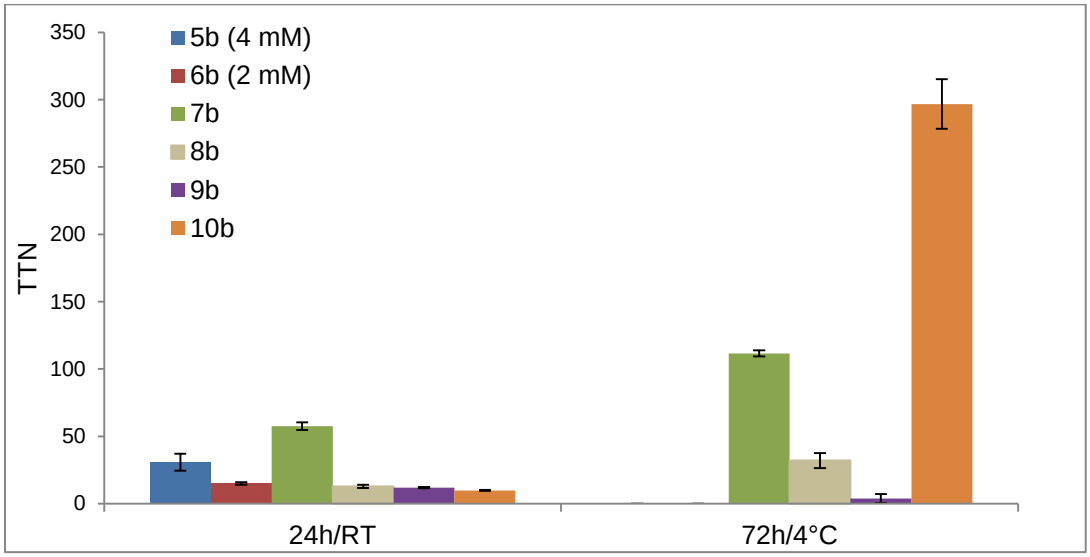

Figure 8: Total turnover numbers for conversion of **5b - 10b** with OleT-CamAB-FDH cascade at RT/24 h and 4 °C/72 h. For **5b** TTN was determined from biotransformation with 4 mM **5a**, for **6b** 2 mM **6a** were used.

$TTN_{conv.enoic} = \frac{c_{diene}}{c_{OelT}}$.

On the other hand, as shown in Figure 8 and Table 2, the short chain ω-enoic acids ≤ C9 (**7b - 10b**) were well converted with 10 mM substrate concentration, yielding higher product concentrations and TTNs than obtained with the corresponding dioic acids (**7a - 10a**) (e.g.: TTN were 60 with **7b** compared to 17 with **7a**; Table 1 and Table 2). Moreover, lowering the reaction temperature resulted in improved conversions, as seen for dioic acids (Table 1, chapter 2.1.1), with the most significant improvement in the conversion of **10b**.

This supports the assumption that the poor results achieved with **5b** and **6b** were not only due to the C=C bond on ω-position but also due to the chain length of the substrate. Nonetheless, decarboxylation of short chain saturated fatty acids (< C10) resulted in conversions between 5 % and 25 % [17], while conversions of the corresponding ω-enoic acids (**7b - 9b**) showed a maximum of 7 % and of 18 % with **10b**.

Table 2: Analytical data obtained from conversion of ω-enoic acids with OleT-CamAB-FDH cascade at RT and 4 °C. Biotransformations were carried out at standard reaction conditions (10 mM substrate, 6µM OleT, 0.05 U.mL^{-1} CamAB, 1 mg.mL^{-1} FDH, 100 mM ammonium formate, 200 µM NADH, 500 U.mL^{-1} catalase).

$TTN_{conv.enoic} = \frac{c_{diene}}{c_{OelT}}$.

Substrate	RT α,ω-diene [µM] (conversion [%])	TTN	4 °C α,ω-diene [µM] (conversion [%])	TTN
5b (10 mM)	0	n.d.	0[a]	n.d.
5b (4 mM)	184 ± 31 (5)	31 ± 6	n.d.	n.d.
6b (10 mM)	30 ± 6 (< 1)	n.d.	0[a]	n.d.
6b (2 mM)	137 ± 70 (7)	23 ± 12	n.d.	n.d.
7b	345 ±17 (3)	58 ± 3	669 ± 14 (7)	112±2
8b	77 ± 8 (< 1)	13 ± 1	192 ± 34 (2)	32 ± 6
9b	71 ± 3 (< 1)	12 ± 1	34[b] (< 1)	6[b]
10b	59[b] (< 1)	10[b]	$1.78*10^3$ ± $0.11*10^3$ (18)	297 ± 18

n.d.: not determined
a) Only determined for 10 mM substrate concentration.
b) Only double determination. The mean of both values is shown. No standard deviation was determined.

After comparing the conversions of the different substrate classes (saturated fatty acids, dioic acids and ω-enoic acids), it can be concluded that the ω-terminus has an impact on the performance of OleT. These results lead to the assumption that OleT works best if there is no functional group at the ω-position, such as in saturated fatty acids. It could be concluded that the C=C bond of the ω-enoic acid might slightly influence conversions. However, a substrate with an unpolar ω-terminus (fatty acids, ω-enoic acids) is probably more accepted by OleT than one with a polar ω-terminus (dioic acids). This corresponds to the fact that the substrate channel of OleT is rather hydrophobic and hence hydrophobic substrates probably interact better than hydrophilic ones [21].

The possible conversion of the ω-enoic acids (**5b** - **10b)** to terminal dienes is a strong indication for the formation of a reaction intermediate. Later isolation of **6g** was achieved from conversion of **6a** and thus proving the supposed formation of a reaction intermediate (chapter 2.4.2). Therefore, it could be concluded that decarboxylation takes place in two steps. First the dioic acid is decarboxylated once to the corresponding ω-enoic acid. This reaction intermediate leaves the substrate channel and then the second carboxy-group rebinds to the

active centre and the substrate gets decarboxylated again. Hydroxylation of the intermediate product occurs as side reaction.

It might be assumed that the first decarboxylation step is rate limiting. This is indicated by several factors such as the absence of accumulation of reaction intermediate or by the higher conversion levels achieved with the ω-enoic acids (< C10) compared to dioic acids with the same chain length. However, these are only assumptions; no kinetic values (v_{max}, K_M, k_{cat}) for both ω-enoic and dioic acids have been determined so far.

2.1.3 **Selectivity of biotransformations with OleT-CamAB-FDH cascade**

As already mentioned, beside formation of terminal dienes, significant amounts of side products were also formed during the biotransformation (Figure 9). It was found that the main side products that were formed are 3-hydroxy-dioic acids and 3-hydroxy-ω-enoic acids followed by 2-hydroxy-dioic acids and 2-hydroxy-ω-enoic acids (Scheme 15). Further there were some unidentified side products formed with a few substrates.

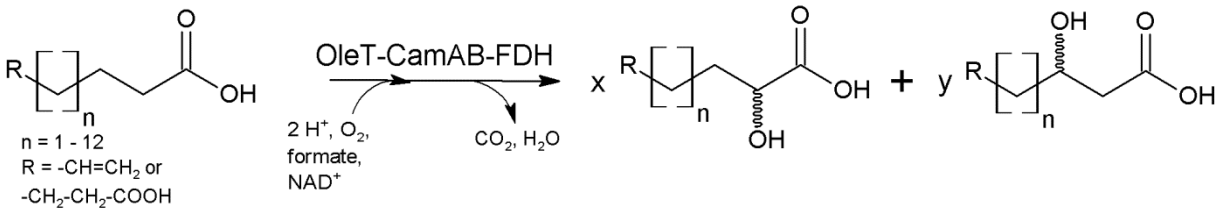

Scheme 15: Scheme of side-products formed by conversion of either dioic acids or ω-enoic acids (hydroxylation on α- or β-position). Usually formation of β-hydroxylated products was higher.

Figure 9 shows the selectivity of the conversion of substrates **1a** - **6a** as well as of **5b** - **6b**. Concerning lower chain substrates, a side product was detected with **7b** only (probably hydroxylation occurred; no quantification or identification was done). Detection of the side products was done via extraction from the biotransformation samples and analysis on GC-FID after headspace GC-MS measurement. For all other substrates, side products were either not detected (**8a**, **8b** and **9b**) or not determined.

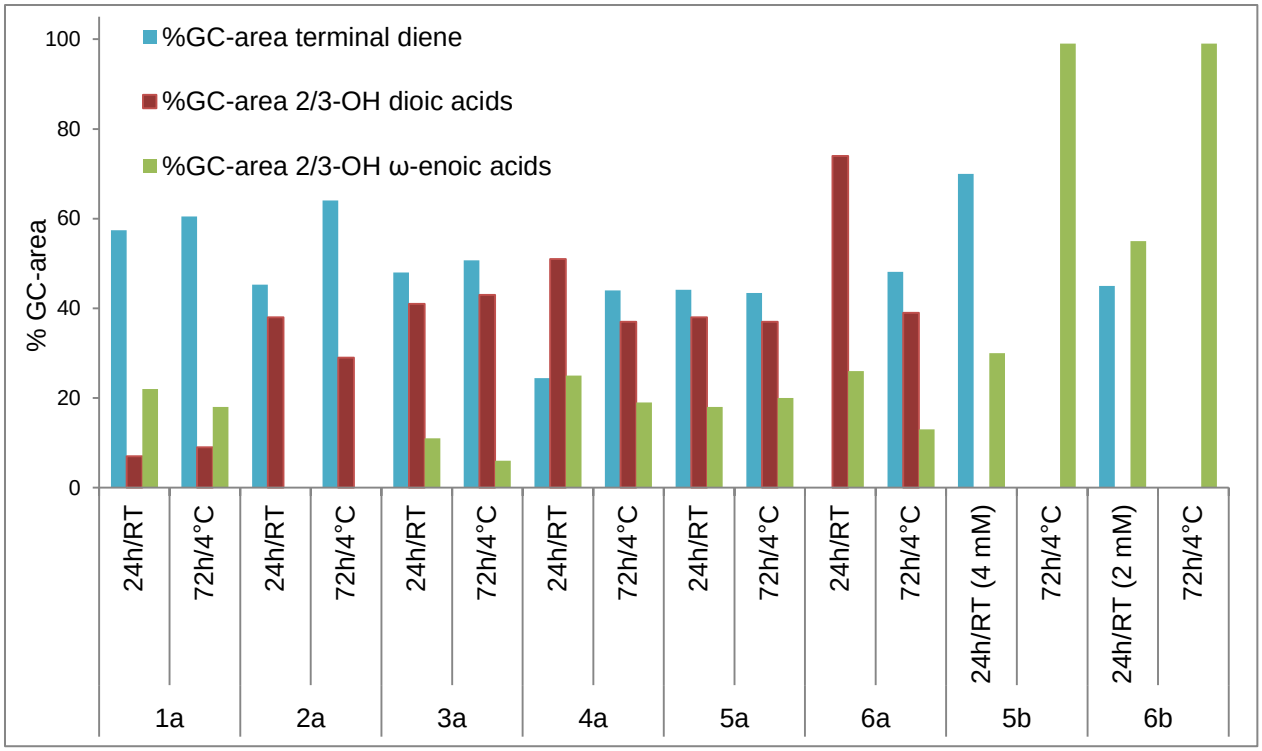

Figure 9: Relative amounts of the main products formed during biotransformation of **1a - 6a** and **5b - 6b**. Concerning the conversion of **5b** and **6b** (10 mM) at 4 °C, there was no **5c/6c** formed. However hydroxylation was observed and comparison of these signals with the signal of ISD (0.1 % 1-decanol) gave a ratio (peak area ISD)/(peak area product) of 0.11 (**5b**) and 0.03 (**6b**) compared to the ratio (peak area ISD)/(peak area substrate) of 4 (**5b**) and 5 (**6b**).

The amounts of side products formed during the reaction and hence the selectivity (determined as % GC-area of one product compared to the GC-area of all products) depended strongly on the substrate. Generally formation of side products ranged (with a few exceptions) from 30 % to 60 % and also the reaction conditions had an influence on the selectivity, with some substrates (Figure 9).

Conversion of **6a** and **4a** showed high dependency of selectivity on the reaction temperature. Regarding **4a**, almost 80 % of **4g** and **4f** were formed at RT while with **6a**, although no formation of **6c** was observed, formation of **6g** could be detected, indicating that single decarboxylation occurred. Therefore it might be assumed that for conversion of **4a** and **6a**, selectivity of OleT shifted towards hydroxylation reaction. Interestingly, at 4 °C formation of terminal dienes clearly increased in both cases, up to nearly 50 %. Hence one can assume that the reaction temperature influences the selectivity of OleT, which was already observed in the conversion of saturated fatty acids [17].

Surprisingly, **1a** and **2a** were the only substrates where other side products beside hydroxy-acids were formed. Unfortunately, clear identification of those side products was not possible on GC-MS due to low concentrations. On the one hand, it is possible that 2-alkanones were

formed as these compounds were already suggested to occur from reaction with C18 and C16 saturated acid [17]. Interestingly, also with the saturated fatty acids, this was only observed at chain lengths C16 and C18 [17], indicating that side product formation depends highly on the chain length of the substrate. Another possibility for high side product formation with **1a** and **2a** might be the rather low purities of those two substrates (95 % and 96 %, respectively). Since it is probably that these impurities are mainly other fatty acids, which can also be converted by OleT, it is quite possible that these side products are formed due to conversion of impurities of the substrate. For **1a** it was shown that **7a** is present in significant amounts (Figure S1) and therefore hydroxylation of **7a** might have occured.

Concerning the ω-enoic acids, 3-hydroxy-ω-enoic acids were detected as sole side products (Figure 9). Interestingly, for **6b** and **5b** there was (hardly) no terminal diene formed at a substrate concentration of 10 mM. However, for **5b** at both RT and 4 °C and for **6b** at 4 °C, formation of 3-hydroxy-ω-enoic acids was detected. Furthermore, both substrates showed side product formation at RT, when converting them at their optimal substrate concentration (2 mM for **6b** and 4 mM for **5b**); at 4 °C biotransformation were only performed with 10 mM substrate concentration. This indicates that the selectivity of OleT in the reaction with **5b** and **6b** is improved when performing the biotransformations at 4 °C. Moreover, it was observed that at a substrate concentration of 2 mM (for both **6b** and **5b**), there was no substrate left after conversion. This indicates that selectivity shifted very likely towards hydroxylation (Figure 7). In comparison to that, conversion of corresponding C11 and C10 saturated fatty acid did not show any side product formation, neither at RT nor at 4 °C [17], indicating a dependency of selectivity on the substrate type.

All these results allow the conclusion that reaction selectivity of OleT is primarily dependent on the substrate type – chain length and functional group at ω-terminus – and could be further influenced by the reaction temperature.

2.1.4 Decarboxylation of branched fatty acids using OleT-CamAB-FDH cascade

Previously, it was shown that decarboxylation of saturated fatty acids worked with OleT-CamAB-FDH cascade [17]. Dioic acids and ω-enoic acids are accepted as substrates by OleT. Therefore four branched fatty acids were selected to investigate the influence of substitution on the performance of OleT.

Scheme 14 in chapter 2.1 shows the reaction scheme for conversion of the 4 branched fatty acids that were investigated. In Table 3 analytical data from the conversion of the branched fatty acids are listed.

Table 3: Analytical data obtained from conversion of the four branched fatty acids by OleT-CamAB-FDH cascade at RT and 4 °C. Biotransformations were carried out at standard reaction conditions in 2 mL scale (10 mM substrate, 6µM OleT, 0.05 U.mL^{-1}CamAB, 1 mg.mL^{-1} FDH, 100 mM ammonium formate, 200 µM NADH, 500 U.mL^{-1} catalase).

$TTN_{conv.fatty\ acid} = \frac{c_{1-alkene}}{c_{OelT}}$.

Substrate	1-alkene [mM] 24h/RT (conversion [%])[b]	1-alkene [mM] 72h/4°C (conversion [%])[b]	Side-products [% GC-area][c,d]	TTN 24h/RT	TTN 72h/4°C
12a	1.7 ± 0.1 (17)	1.2 ± 0.1 (12)	detected	283 ± 8	200 ± 19
13a	1.9 ± 0.1 (19)	1.4 ± 0.3 (14)	detected	314 ± 8	227 ± 56
14a[a]	detected[e]	2.4 (24)	0	n.d.	400
15a	3.0 ± 0.2 (30)	0.6 ± 0.1 (6)	detected	503 ± 40	95 ± 14

n.d.: not determined

a) Product was detected, but derivatisation via bromination to identify product structure was not possible. For product identification comparison with the commercial standard of **14c** was done (Figure S164 and Figure S166). Additionally comparison of the conversion of **14a** at 4 °C with the GC-MS library gave a score of 87 % for 2-methyl-1-butene (**14c**).

b) Headspace GC-MS detection; Verification of the formed product was done through in-situ bromination (**12c**, **13c** and **15c**) and through comparison with the analytical product standard.

c) For detection of the side-products, samples (24h/RT) were extracted with EtOAc after headspace GC-MS measurements.

d) Identification of the side products was not possible since measurements were only done on GC-FID and there was no reference material available. However, it is quite probable that hydroxylation occurs as with the other tested substrates. Also the retention times (higher than those of the substrate) would support this assumption.

e) Product concentration was too low to be quantified.

Conversions of the short chain branched fatty acids yielded quite high product concentrations compared to the short chain dioic and ω-enoic acids (**10a**, **9a**, **10b** and **9b**). Except from **14a** at RT, the obtained product concentrations ranged from 1.7 mM to 3 mM (17 - 30 % conversion). In comparison, the best converted dioic acid (**3a**) yielded 2.9 mM **3c** (29 % conversion) and with the short chain dioic acids (**8a - 10a**) obtained conversions were around 1 %. The obtained product concentrations were also up to 2 times higher than those from decarboxylation of C7 and C6 saturated fatty acids (1.3 mM and 1.2 mM olefin, respectively) [17].

On the other hand, at 4 °C the best result was obtained with **14a** (24 %), while conversion of **15a** achieved only 6 %. This proves again the strong influence of the temperature on the

catalyst performance [17]. It was already discussed in chapter 2.1.1 that decreasing the reaction temperature could enhance productivity, especially for poorly converted substrates.

For conversion of **12a, 13a** and **15a**, product formation was proven by in-situ bromination (chapter 2.5.3). However, with **14a** in-situ bromination of the biotransformation did not lead to any conclusive result. This is probably due to the fact that in-situ bromination was done at RT. At RT the conversion of **14a** was < 1 % and therefore it is reasonable that the concentration of **14c** was too low to be clearly detected on GC-MS after bromination. At 4 °C the product concentration would have been high enough, however, the in-situ bromination system was not adapted to be used at 4 °C. To exclude the possibility of formation of 2-methyl-2-butene comparison of the biotransformation with a commercial product standard of **14c** (2-methyl-1-butene) was done. Comparing the obtained spectra (Figure S165 and Figure S167) supports the assumption that **14c** was formed and not 2-methyl-2-butene.

2.2 Optimization of OleT-CamAB-FDH reaction system

For better understanding of the performance of OleT-CamAB-FDH reaction system, some parameters (co-solvent, enzyme-, substrate-, and FDH concentration) were varied.

2.2.1 Solvent study – influence of the used co-solvent on OleT performance

Most substrates that are converted by P450 monooxygenases, like fatty acids and dioic acids, are poorly soluble in aqueous phase, even at low concentration, and therefore addition of a polar co-solvent is necessary to increase solubility [27][31b]. Therefore EtOH or DMSO was used as co-solvent for biotransformation of dioic acids with OleT-CamAB-FDH cascade. EtOH was generally used in the biotransformations because in previous studies it led to good conversions [17]. DMSO was chosen for substrates, which were insoluble in EtOH. Unfortunately polar solvents are known to greatly decrease enzyme activities, especially when using P450 monooxygenases, and often can only be added up to a concentration of around 10 % [31b][18c]. To investigate whether other co-solvents are more compatible with OleT, a solvent study with stearic acid as model substrate was done. Biotransformations were carried out at RT for 24 h using the standard OleT-CamAB-FDH protocol (see chapter 4.3). The co-solvent concentration was varied from 0 - 20 % (v/v) and instead of 6 µM OleT only 1.5 µM were used. In Table 4 the used co-solvents and solubility of stearic acid in the pure solvent as well as in the final reaction solution are described.

Table 4: List of co-solvents used for conversion of stearic acid by OleT and solubility of stearic acid.

Cosolvent	Solubitilty of 200 mM stearic acid in the co-solvent	Solubility of 10 mM stearic acid with co-solvent in the final reaction solution
THF	well soluble at RT	The solution was slightly cloudy, the substrate was not soluble, however, it was well suspended in the solution
EtOH	soluble when treated with ultrasonication; precipitation at RT	Increased solubility when higher co-solvent concentration were used, however, remained cloudy up to 20 % co-solvent content
1,4-Dioxane	well soluble when treated with ultrasonication	Increased solubility when higher co-solvent concentration were used, however, remained cloudy up to 20 % co-solvent content
DMF	well soluble at RT	With all concentration of co-solvent the substrate precipitated, however, at 20 % the substrate was better suspended in the solution (smaller particles)
DMSO	soluble when treated with ultrasonication; viscous liquid at RT	Very poor solubility of the substrate, even at higher co-solvent concentration, strong precipitation of the substrate
Isopropanol	soluble at RT	Cloudy solution, substrate was poorly soluble at all concentrations and strong precipitation of the substrate was observed

Figure 10 shows the performance of the OleT-CamAB-FDH system with different co-solvents.

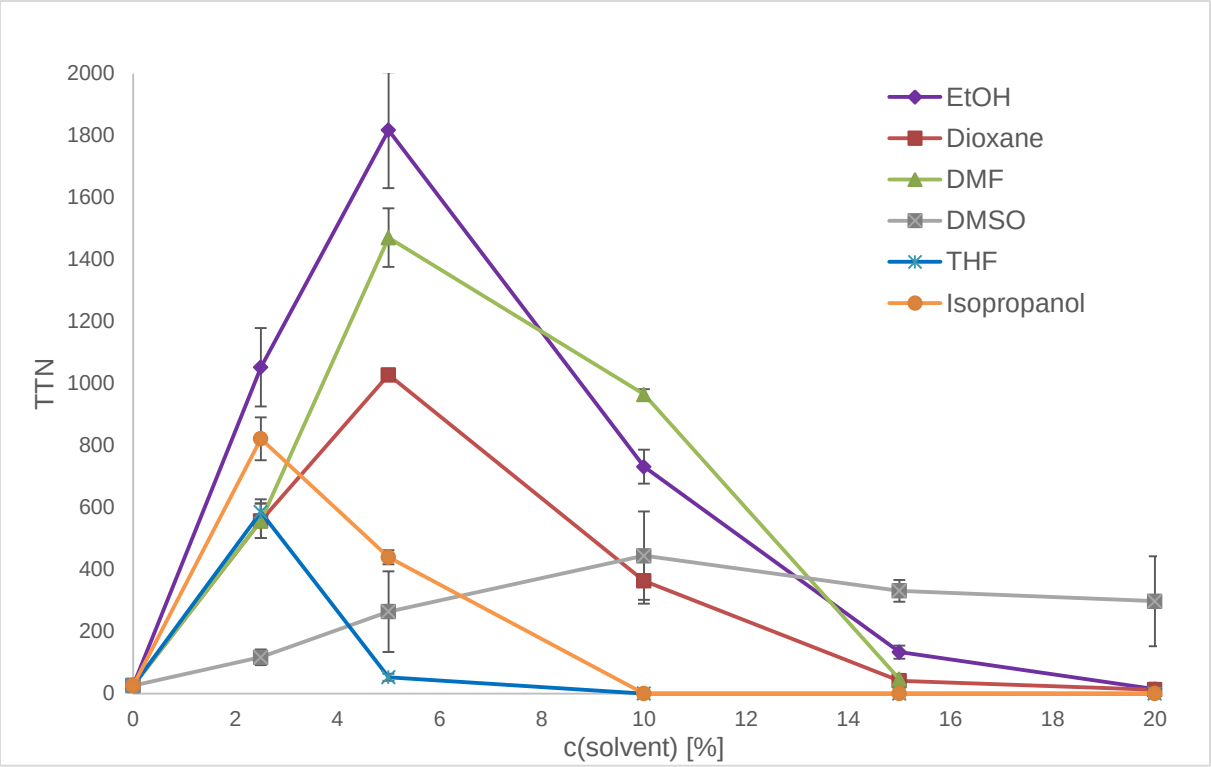

Figure 10: TTN values from conversion of 10 mM stearic acid by OleT-CamAB-FDH standard reaction cascade with selected co-solvents. The influence on catalytic activity of OleT was studied. Proper volume of the co-solvent was adjusted by replacing KPi-buffer.

$$TTN_{fatty\ acids} = \frac{c_{1-alkene}}{c_{OleT}}$$

First, it was shown that there is no conversion when no co-solvent was used, which is probably due to the poor solubility of the substrate in water and hence mass transfer limitations. Further, EtOH, DMF and dioxane led to the best conversions and with those co-solvents, highest TTNs were obtained at a concentration of 5 %. At 2.5 % co-solvent, solubility of the substrate might be limited. On the other hand, co-solvent contents beyond 5 % led to a fast decrease of enzyme activity and at 20 % there was no activity left. This corresponds to the general assumption that higher concentrations of polar co-solvents often result in enzyme deactivation [18c]. Moreover, isopropanol and THF seem to be strongly deactivating OleT – the maximum conversion with these co-solvents was achieved with a concentration of 2.5 %; at 10 % there was no activity detected anymore. Interestingly, conversion with DMSO as co-solvent gave very different results. Although DMSO led to the lowest TTNs at 2.5 % and 5 % (117 and 264, respectively) it was the only solvent in which OleT was still active at 20 %. This leads to the assumption that DMSO is very compatible with OleT-CamAB-FDH system and well suited when higher amounts of co-solvent are necessary (in particular for higher substrate concentration).

Conversion of stearic acid showed that, beside EtOH as co-solvent, 5 % (v/v) DMF was best accepted, and this condition was selected for conversion of **3a**. In addition, various concentrations of DMSO were studied (Figure 11).

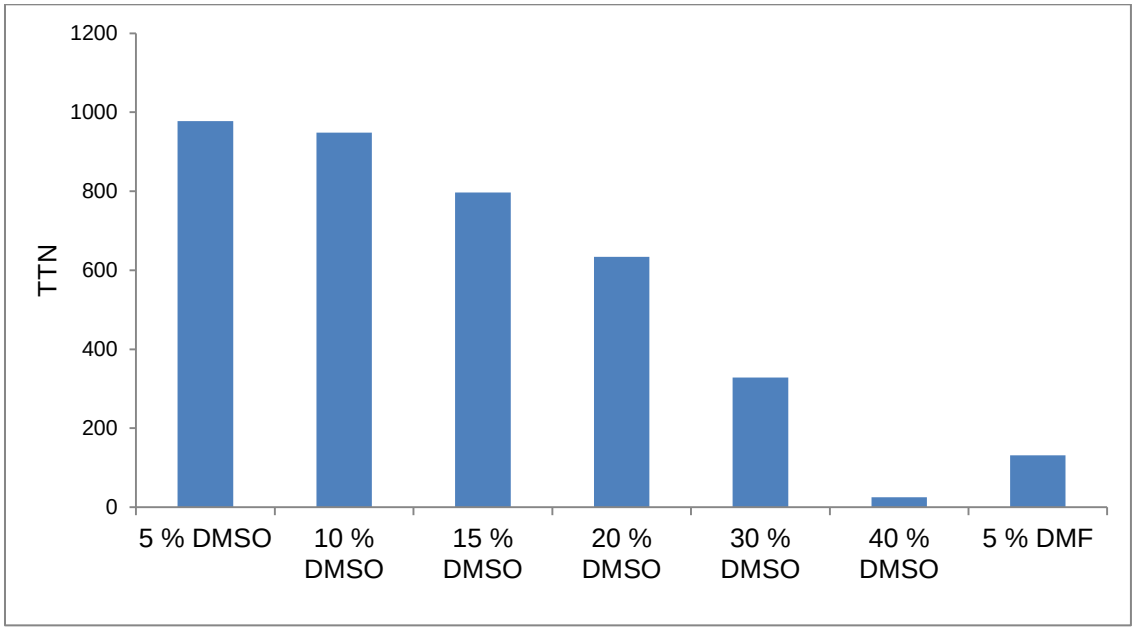

Figure 11: Conversion of 10 mM **3a** by OleT-CamAB-FDH standard reaction cascade with varying DMSO concentrations as well as with 5 % DMF. The influence of catalytic activity of OleT was studied. Proper volume of the co-solvent was adjusted by replacing KPi-buffer.

Conversion of **3a** with DMSO led to high TTN values compared to stearic acid (TTN for **3a** was 978, compared to 264 for stearic acid with 5 % (v/v) DMSO). On the other hand the use of DMF for **3a** led to 7.5 times lower TTN (TTN: 131 and 978, respectively). In comparison, conversion of stearic acid was 5.6 times higher with DFM than with DMSO (TTN 1471 and 264, respectively).

Since one can assume that the tolerance of OleT against one co-solvent is not influenced by the used substrate, these differences might be due to differences in substrate solubility. While **3a** is very well soluble in DMSO, stearic acid is only soluble when treated with ultrasonication and the resulting solution is very viscous (Table 4). Furthermore, the poor solubility of stearic acid resulted in high precipitation of the substrate in the final reaction mixture. **3a**, however, was rather well suspended in the reaction mixture when using DMSO. No conversion in absence of co-solvent and worse conversion when using only 2.5 % co-solvent (Figure 10) support the assumption that low substrate solubility leads to low substrate availability and hence to less conversion. Moreover, the enzyme activity decreased constantly from 5 % to 40 % DMSO in the conversion of **3a** (Figure 11). At 20 % DMSO, 60 % of the

maximal TTN of **3a** was obtained [TTN 978 (5 % DMSO); 634 (20 % DMSO)], indicating a high tolerance of OleT towards DMSO.

In conclusion it was found that beside the co-solvent itself, the substrate solubility has a significant influence on the conversion.

2.2.2 Influence of the substrate and enzyme concentration on the performance of OleT-CamAB-FDH system

To achieve higher TTN and conversions, **3a** was also converted using lower substrate concentrations (2 mM and 5 mM) or enzyme concentrations (1 µM). Figure 12 and Figure 13 show the TTN values as well as conversions for those systems in comparison with the standard reaction system (6 µM OleT and 10 mM substrate).

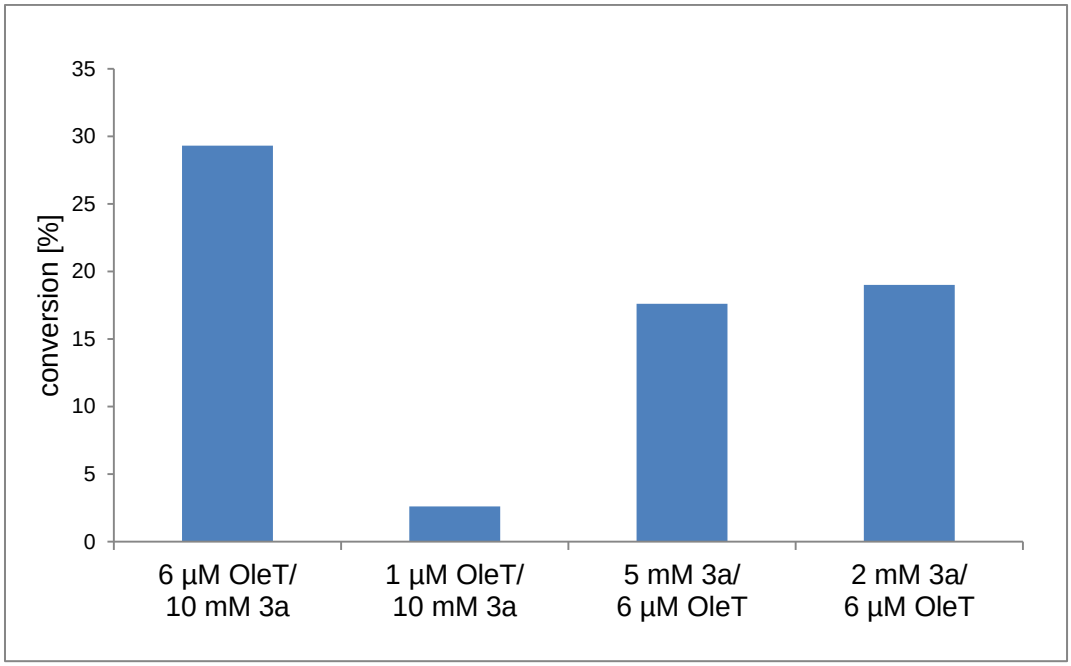

Figure 12: Conversions obtained from biotransformation of **3a** using varied OleT and substrate concentrations.

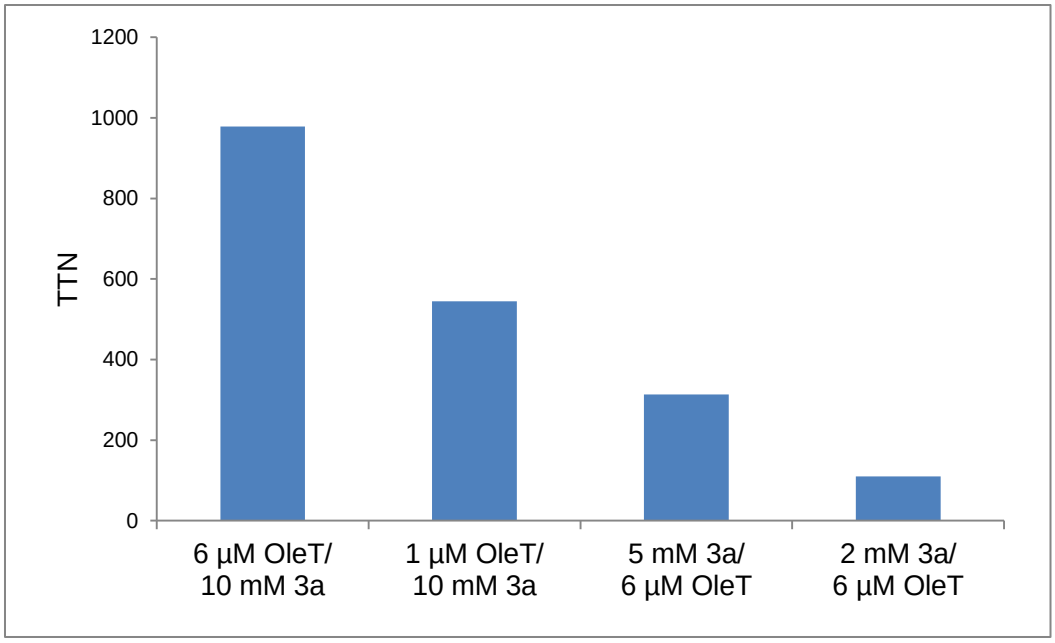

Figure 13: TTN values obtained from biotransformation of **3a** using varied OleT and substrate concentrations.

Lowering the enzyme concentration led to decreased TTN values, and lowering substrate concentration led to reduced conversions (Figure 12, Figure 13).

A lower enzyme concentration is expected to result in lower activity and therefore lower conversions. On the other hand, the lower TTN value obtained with 1 µM OleT indicates an increased efficiency of the OleT-CamAB-FDH system, when higher OleT concentrations were used.

Interestingly, lower substrate concentration led to about 30 % lower conversions (2 mM and 5 mM **3a**), indicating that the reaction is favored at a higher substrate concentration.

While the TTN and conversion with **6b** and **5b** (see chapter 2.1.2) increased by lowering the substrate concentration, it seems that with **3a** a higher substrate concentration is the better choice to obtain high conversions and TTN. With **5b** and **6b**, a substrate inhibition was assumed (Figure 7) and therefore it is not astonishing that lower substrate concentrations led to better conversions and TTN.

Hence, it can be concluded that depending on the used substrate, different reaction conditions, such as enzyme concentration, substrate concentration or reaction temperature, can lead to optimal results.

2.2.3 Influence of FDH concentration on the performance of OleT-CamAB-FDH system

Further optimization of the reaction system was attempted by increasing the FDH concentration. **3a** was converted at varying FDH concentrations (1 - 20 mg.mL^{-1}) (Figure 14). With 4 - 8 mg.mL^{-1} FDH, an optimum was reached before activity decreased again. It is probably that NADH recycling is accelerated at increasing FDH concentration and thus increasing electron and proton transport from NADH to OleT. Thus, using 1 mg.mL^{-1} FDH might results in lower reaction velocities. At increasing FDH concentration, reaction velocity will increase and therefore it seems that FDH concentrations beyond 8 mg.mL^{-1} will result in too fast reaction rates. Generally for the formation of Compound I efficient and distinct delivery of two protons to the peroxo-intermediate (Scheme 7, chapter 1.3.2, E → F) is required. On the other hand proton and electron transfer to the oxo-ferryl state (Scheme 7, chapter 1.3.2, F → B) probably leads to uncoupling reactions [33][46]. Therefore, higher FDH concentrations and hence higher velocities of electron/proton transfer might lead to unspecific reaction, uncoupling and hence enzyme inactivation due to formation of H_2O_2.

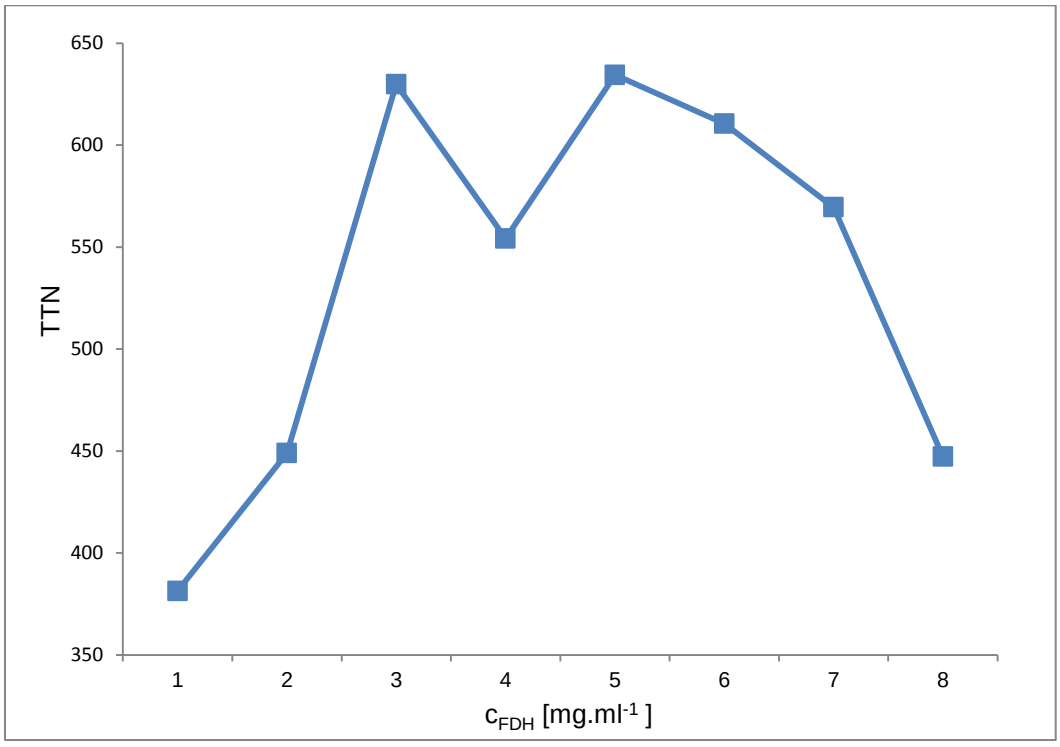

Figure 14: TTN values obtained from conversion of **3a** at varied FDH concentrations, ranging from 1 - 20 mg.mL^{-1}. The influence on the performance of OleT was tested. Here a preparation of OleT was used, in which some enzyme precipitated, and therefore TTNs are lower than usually observed with conversion of **3a** using a fully soluble OleT preparation.

2.3 Decarboxylation of 3a using alternative reaction systems

Additionally to the standard reaction system (OleT-CamAB-FDH cascade), reactions were also performed with Fdr/FldA electron transfer system [22][47] and with H_2O_2 as sole oxidant [19][17][21][22][24] (Scheme 16 and Scheme 17).

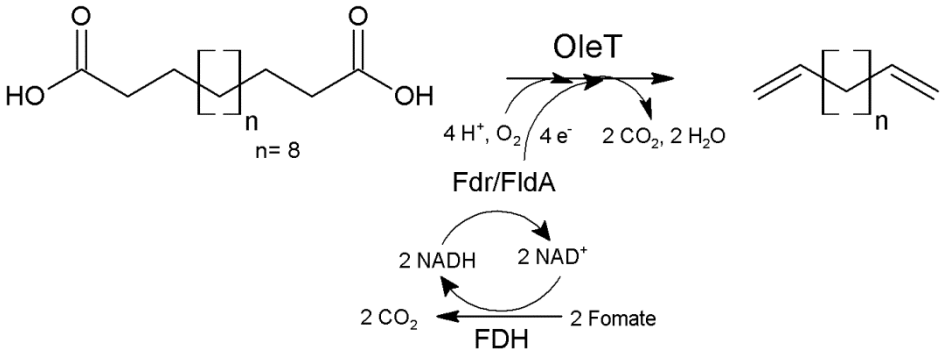

Scheme 16: Conversion of **3a** using OleT-Fdr/FldA-FDH cascade.

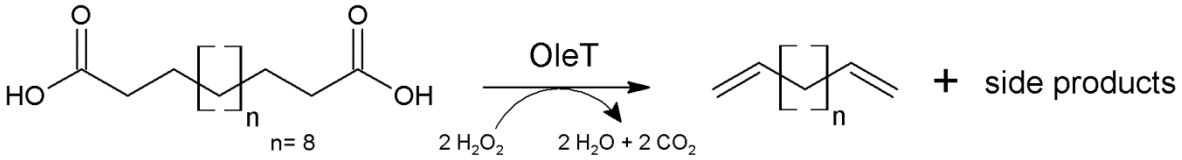

Scheme 17: Conversion of **3a** using H_2O_2 as sole oxidant.

Comparing these three reaction systems, it is obvious that the standard reaction system led to highest effiency (Figure 15) [TTN: 32 (H_2O_2), 185 (50 µL Fdr/FldA), 978 (CamAB)]. However, it has to be mentioned that the other two systems were not optimized.

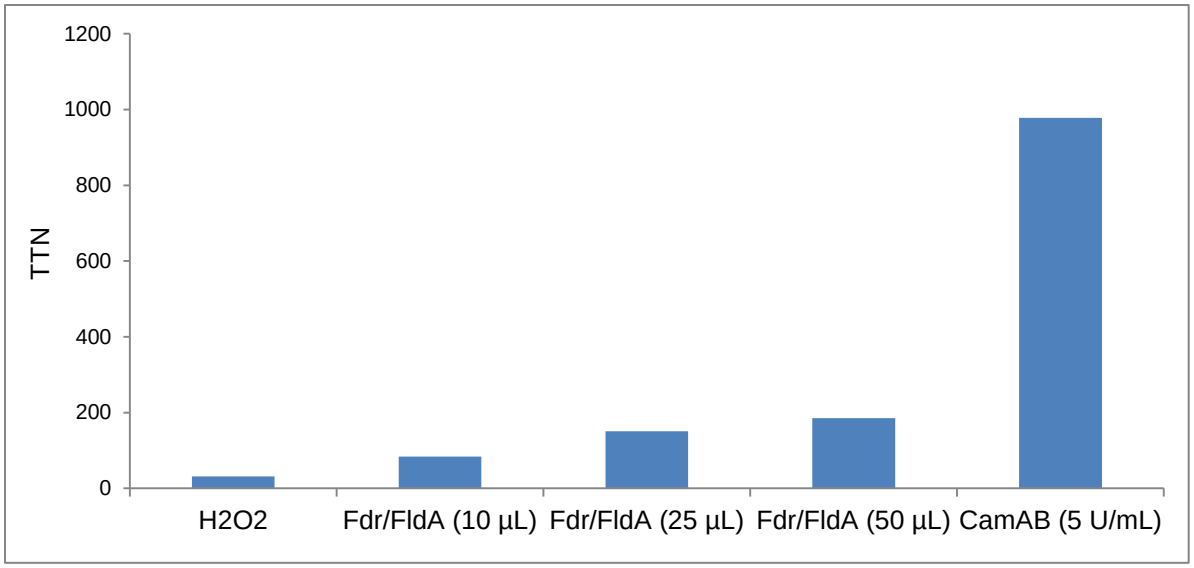

Figure 15: Comparison of the performance of OleT, when converting **3a**, using either standard OleT-CamAB-FDH reaction cascade, OleT-Fdr/FldA-FDH reaction cascade or H_2O_2 as sole oxidant.

The OleT-CamAB-FDH system is about 5 times more efficient than the Fdr/FldA system. Higher amounts of Fdr/FldA led to higher TTN values [TTN values: 84 (10 µL), 151 (25 µL) and 185 (50 µL)], and compared with CamAB, only 10 - 20 µL of the lysate were used. Therefore it could be assumed that the CamAB system (class I/ferredoxin-based electron transfer system) has a better compatibility with OleT [17][32]. Conversion of the substrate was also observed with H_2O_2 as sole oxidant, however, the TTN was 31 times lower than with the standard system. These results support a re-classification of OleT as monooxygenase not as peroxygenase [17][22][35]. The acceptance of H_2O_2 has already been reported several times [19][21]. Liu *et al.* explained this by the assumption that monooxygenases developed from peroxygenases, since in the early Earth environment H_2O_2 was probably more abundant that O_2; thus the use of H_2O_2 is a remnant function derived from the evolutionary origin of monooxygenases [22]. The low terminal diene concentration obtained with H_2O_2 is probably explained by enzyme inactivation. In general many enzymes are sensitive towards H_2O_2 and especially for P450 monooxygenases it was shown that high H_2O_2 concentrations lead to degradation of the heme [28][31a]. Interestingly, conversion of **3a** with H_2O_2 showed significant side product formation (**3f** and **3g**; around 90 % of total product formation), which indicates that the use of H_2O_2 might lead preferably to hydroxylation rather than to decarboxylation (Figure S194). The conversion of **3a** with the Fdr/FldA system did not show clear formation of hydroxylated products (Figure S193). The used electron transfer system has a significant influence on the catalyst selectivity.

2.4 Preparative scale reactions with 1a, 3a and 6a using OleT-CamAB-FDH cascade

On the one hand, biotransformations on preparative scale were done to allow identification and characterization of the main products formed (terminal dienes, 3-hydroxy-dioic acids and 3-hydroxy-ω-enoic acids). On the other hand, these were conducted for determination of isolated yields.

2.4.1 Isolation and purification of 1c and 3c

Scheme 18 shows the overall reaction for decarboxylation of **1a** and **3a**.

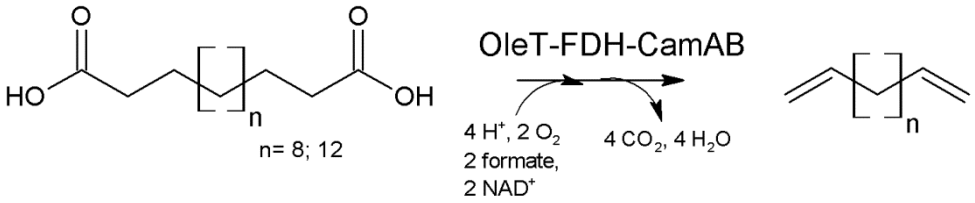

Scheme 18: Decarboxylation of **1a** or **3a** to obtain **1c** or **3c** using OleT-CamAB-FDH reaction cascade.

First biotransformations of **1a** and **3a** were done on a 50 mL scale to allow formation of enough material (1 - 10 mg) for ^{1}H-NMR analysis. This was necessary especially for **1c** since there was no commercial product standard available. Isolation of the product was possible in both cases, however, the isolated yields were very low [3.9 mg (3.5 %) **1c** and 6 mg (7.2 %) **3c**].

Only 0.72 mM of **3c** could be isolated, compared to almost 3 mM detected in the 1 mL scale reactions. This correlates with 25 % of the maximal expected yield by comparison with 1 mL scale reactions. There are several possible reasons for the low isolated yields. Most probably the conversion of the **3a** is worse in the reaction vessel than in the glass vials. From 10 mL scale reaction, conversion from GC analysis showed formation of 1 mM **3c** (compared to 3 mM in 1 mL scale biotransformations). This might be due to faster inactivation of OleT by stirring in the vessel than by shaking. Hence it might be assumed that an increase of the reaction volume from 10 mL to 50 mL under same reaction conditions (stirred in a 250 mL round bottom flask at 200 rpm, 24 h and RT, standard OleT-CamAB-FDH cascade) would also show lower conversions than found in 1 mL scale reactions.

Other losses might be explained by the purification method. Terminal dienes are unpolar and insoluble in aqueous phase and hence they can accumulate in the gaseous phase. In industrial scale, dienes are produced via ethenolysis of cycloalkenes in large quantities (e.g. production

of **5c** ca. 3000 t/a [2a]). The usual isolation and purification method of olefins is fractionated distillation instead of column chromatography [5][6a], which was not investigated in the frame of this project.

2.4.2 **Isolation and purification of 3f and 6g**

Scheme 19 and Scheme 20 show the overall reactions for hydroxylation of **3a** and **6a**, respectively.

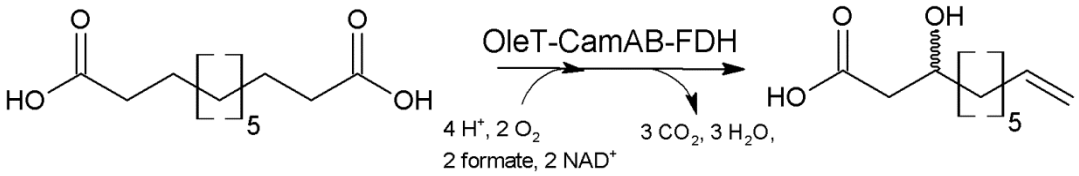

Scheme 19: Hydroxylation and decarboxylation of **6a** to obtain **6g** using OleT-CamAB-FDH reaction cascade.

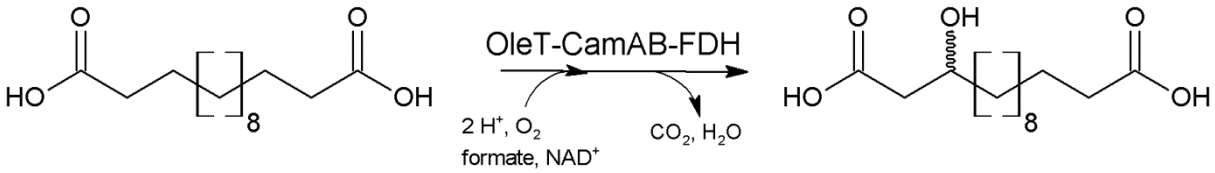

Scheme 20: Hydroxylation of **3a** to obtain **3f** using OleT-CamAB-FDH reaction cascade.

In most biotransformations, 3-hydroxy-dioic acids and 3-hydroxy-ω-enoic acids were formed as main side products beside the terminal dienes (Figure 9 in chapter 2.1.3). To confirm the formation of those products, biotransformations were done on a preparative scale. Conversions of **3a** and **6a** led to rather high formation of side products. For that reason, conversion of **3a** was performed to isolate the **3f**-dimethylester and **6a** was chosen to isolate the **6g**-methylester.

Esterification of the acids was done because several trials of column chromatography to isolate the underivatized 3-hydroxy acids (**3f** and **6g**) failed. This is probably due to the low difference in polarity between the hydroxy-dioic acid and the dioic acid, which results in very similar R_f values. Additionally to that, the dioic acids interact strongly with the silica of the column. This makes the separation of the single compounds even more difficult because the substrates (**3a** and **6a**) as well as the products (**3f** and **6g**) do not elute in single fractions but over a broad range, depending on the mobile phase. Separation of **3a** from **3f** on silica-column was tried twice. Once EtOAc with about 1 % acetic acid was used as mobile phase, where R_f's ranged from 0.46 - 0.57 for **3f** and 0.64 - 0.71 for **3a.** Next 2-butanone:acetone:acetic acid:H_2O (35:25:15:10) as mobile phase was tried, here **3f** and **3a**

were clearly separated, however, still close together [R_f = 0.56 (**3f**) and 0.69 (**3a**)]. With both mobile phases, no separation was achieved.

Therefore, purification of the 3-hydroxy acids was achieved via esterification to the corresponding methyl-esters. Due to the esterification, product isolation and analysis (GC-MS and ^{1}H-NMR) was feasible. 3-hydroxy-dioic acids and 3-hydroxy-ω-enoic acids were confirmed to be formed as main side products (Figure S38, Figure S88).

In chapter 2.1.2 , ω-enoic acids are proposed to form as reaction intermediate. The successful isolation of **6g**-methylester confirms this assumption. Isolated yields, obtained from the biotransformations with **3a** and **6a**, were 7 mg (11.5 %) for **3f**-dimethylester and 8 mg (8 %) for **6g**-methylester.

In comparison with terminal dienes, isolation and purification of **3f**-dimethylester and **6g**-methylester were straightforward and isolated yields appeared slightly higher than those for the terminal dienes (chapter 2.1.3, Figure 9).

2.5 Analysis of low boiling olefins - derivatization experiments

Analysis of higher terminal dienes (**2c** - **6c**) was done via GC-FID. Product concentrations were high enough to achieve clear identification of the formed products by comparison with product standards. **7c** could not be analysed via GC-FID but via headspace GC-MS, due to its relatively low boiling point (114 - 121 °C) combined with the unpolar character and hence insolubility in aqueous phase. However, in biotransformations of **7a** and **7b**, comparison and quantification via the corresponding product standard of **7c** was feasible. Since Dennig *et al.* achieved quantification of low boiling α-olefins via in-situ bromination [17], such product derivatization was tried with **8c** - **10c** and **12c** - **15c**.

2.5.1 Derivatization and quantification of 8c - 10c

First, bromination of **9c** and **10c** was attempted. Analogous to the bromination of 1-alkenes (mechanism see Scheme 22 [50a]), tetrabrominated product standards were expected to form (Scheme 21).

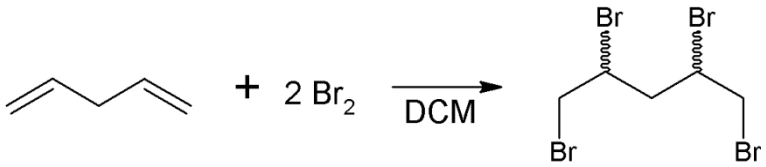

Scheme 21: Expected product formation obtained from reaction of **10c** with Br_2.

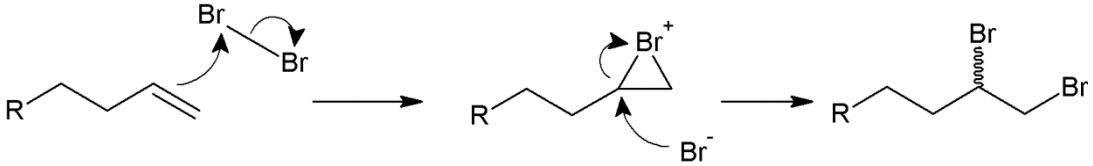

Scheme 22: General reaction mechanism of electrophilic addition of Br_2 to 1-alkenes [50a].

First it was necessary to produce standards through to bromination of commercial standards from **9c** - **10c**, since there was no tetrabrominated product standard available (see chapter 4.7.2). After bromination, orange coloured solids were obtained from derivatization of both **9c** and **10c**. This indicated remaining bromine in the solids; however, it was not possible to get rid of it through multiple washs with DCM. Staining of brominated alkenes on TLC was not achieved and therefore purification via silica column chromatography was not possible. Hence ^{1}H-NMR was used for analysis but it was not possible to identify a clear product.

It might happened that bromination not only occurred at the C=C bond but also on the allylic position. It is known that radical bromination, induced by light, can brominate the allylic

carbon, instead of the double bond, which is usually competing with addition to the double bond (Scheme 23) [50b].

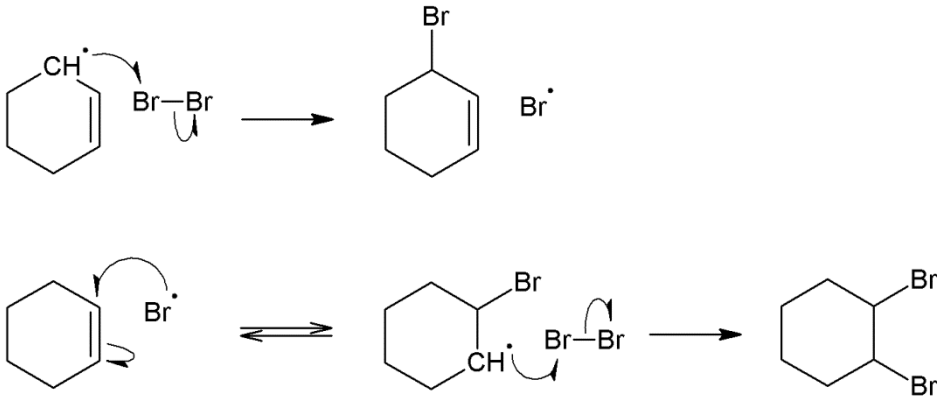

Scheme 23: Possible reactions occurring by radical bromination of an alkene: bromination of allylic carbon (top) versus radical addition of Br_2 on C=C (bottom) [50b].

Therefore it might happen that bromination occurred on various positions, since Br_2 was used in excess (≈ 6 times), resulting in formation of a mixture of products, which is not distinguishable with ^{1}H-NMR. So it was not possible to do analysis and quantification of **9c** and **10c** via bromination.

The next option that was tried was epoxidation of **8c** - **9c** using *m*CPBA. Again since there was no product standard available production of standards from 8c - 9c was done (see chapter 4.7.1). It was supposed to obtain bis-epoxides (Scheme 24) according to the reaction mechanism (Scheme 25).

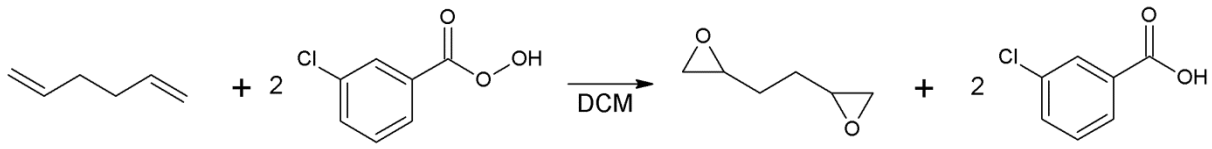

Scheme 24: Recation scheme for epoxitation of **9c** with *m*CPBA.

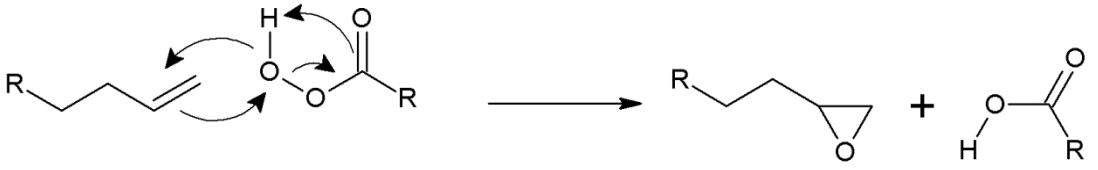

Scheme 25: General reaction mechanism for epoxidation of a 1-alkene with *m*CPBA [50b].

Epoxidation in the stirred round flasks worked as expected (confirmed by GC-MS). However, since *m*CPBA was used in excess, purification of the epoxide from remaining chlorobenzoic acids was absolutely necessary to generate a product for later quantification. Unfortunately purification did not work ideally. Since epoxides are rather unstable under acidic conditions

(ring opening of the epoxide), purification via column chromatography using silica as stationary phase was not possible. Separation of the single compounds succeeded on TLC, when using neutral aluminium oxide as stationary phase and EtOAC:hexane 1:6 as mobile phase. Therefore column chromatography was tried under those conditions. Unfortunately the obtained yields of the bis-epoxides were too low for calibration [< 10 mg after column chromatography and still containing EtOAc (detected by ^{1}H-NMR)]. This might be due to low solubility (especially for *m*-chlorobenzoic acid, but probably also for the bis-epoxide) in the mobile phase, since there was a lot of white precipitant in the concentrated solution, which could not have been entirely loaded onto the column.

Since purification of derivatized products (from bromination and epoxidation) did not succeed, no in-situ derivatization experiments were done. While for biotransformations with **8a** and **9a** there was no doubt that the terminal dienes were formed (comparison with product standard of **8c** and **9c**), for biotransformation of **10a** we wondered whether **10c** (terminal diene) or 1,3-pentadiene (conjugated form) was formed (Scheme 26).

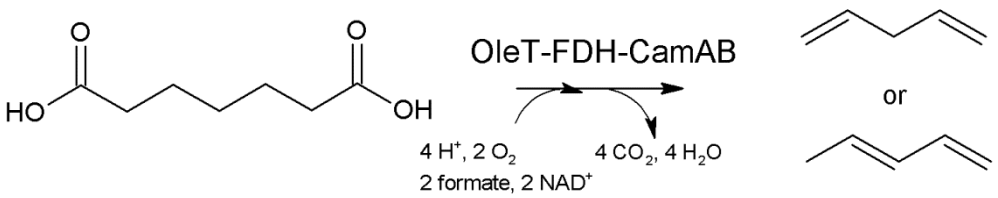

Scheme 26: Reaction scheme from conversion of **10a** to the corresponding diene. The question was whether 1,3-pentadiene or 1,4-pentadiene (**10c**) was formed.

2.5.2 Derivatization and quantification of 10c

To verify formation of **10c**, Wacker oxidation was tried as a further derivatization method (Scheme 27).

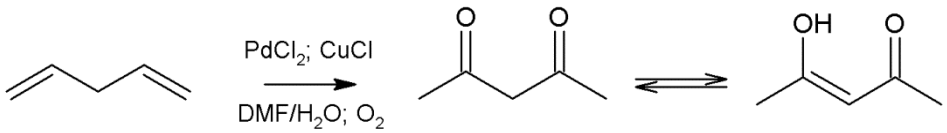

Scheme 27: Reaction scheme for derivatization of **10c** to the corresponding di-ketone via Wacker Oxidation.

For that acetyl-acetone was available as product standard and therefore in-situ derivatization was tried right away (see chapter 4.8.4). Unfortunately there was no product formation observed. This is probably due to the fact that derivatization was done in an unstirred system, which might have resulted in mass transfer limitations, especially since the catalyst was solid.

Another possibility might be that product concentration was too low (12.2 µM – Table 3, chapter 2.1.4) to achieve a detectable amount of derivatized product.

Due to the difficulties of product derivatization of **10c**, product identification was achieved by comparison of the biotransformation with product standards of **10c** and 1,3-pentadiene (Figure S146 and Figure S148). Surprisingly, it was shown that **10c** (non-conjugated form) was produced, since it was expected that the more stable, conjugated 1,3-pentadiene is formed. This indicates that OleT precisely controls β-radical formation and therefore selectively cleaves the C-C_α bond.

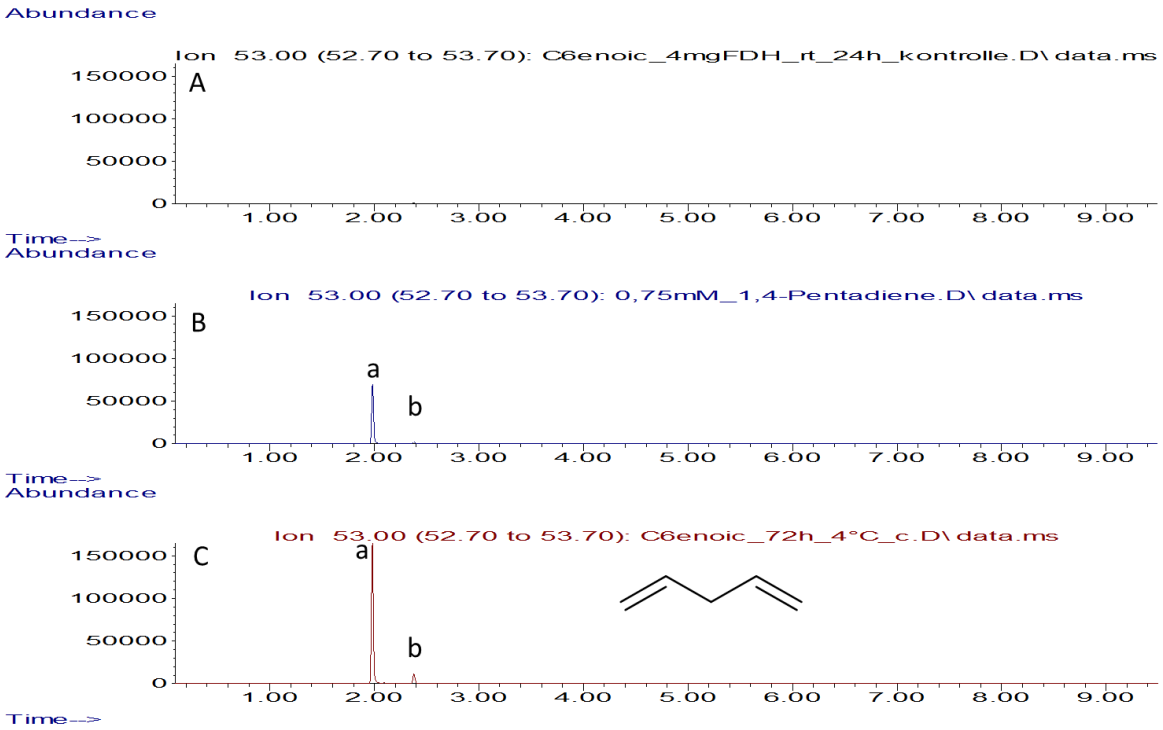

Figure 16: Headspace GC-MS chromatograms obtained by conversion of **10b** (10 mM) (signals from extracted ion *m*/z = 53 are shown). A = Conversion of **10b** in the absence of OleT (negative control). B = Commercial standard of **10c**. C = Conversion of **10b** with the OleT-CamAB-FDH system. a = **10c**; b = 2-butanone; 5 % (v/v) EtOH was used as co-solvent.

2.5.3 **Bromination of 12c-15c**

Due to the similarity of branched 1-alkenes to linear 1-alkenes, bromination was tried again as derivatization method. Again standards were produced starting from **12c** - **15c** (see chapter 4.8.1) followed by analysis via GC-MS. It was shown that bromination did not work selectively resulting in formation of di- and tri-brominated species (Figure S174, Figure S180 and Figure S185). Tri-bromination might have occurred due to the bromination of the allylic position of the substrates (Scheme 23) [50c] as well as dibromination of the double bond [an excess of Br_2 (> 2 equivalents) was used].

The brominated species were used for product identification by comparison with in-situ bromination of the biotransformations of **12a - 15a**. Product quantifiaction was done with commercial product standards of **12a - 15a** by headspace GC-MS.

2.5.4 **Derivatization of 11c**

Last also **11b** was successfully converted by OleT-CamAB-FDH cascade (Scheme 13, Figure 17; Figure S154) and **11c** was supposed as product. However, due to the low product concentrations and the gaseous character of **11c** (comparison with a product standard is more difficult) there is the need of a proper derivatization method to confirm production of **11c**.

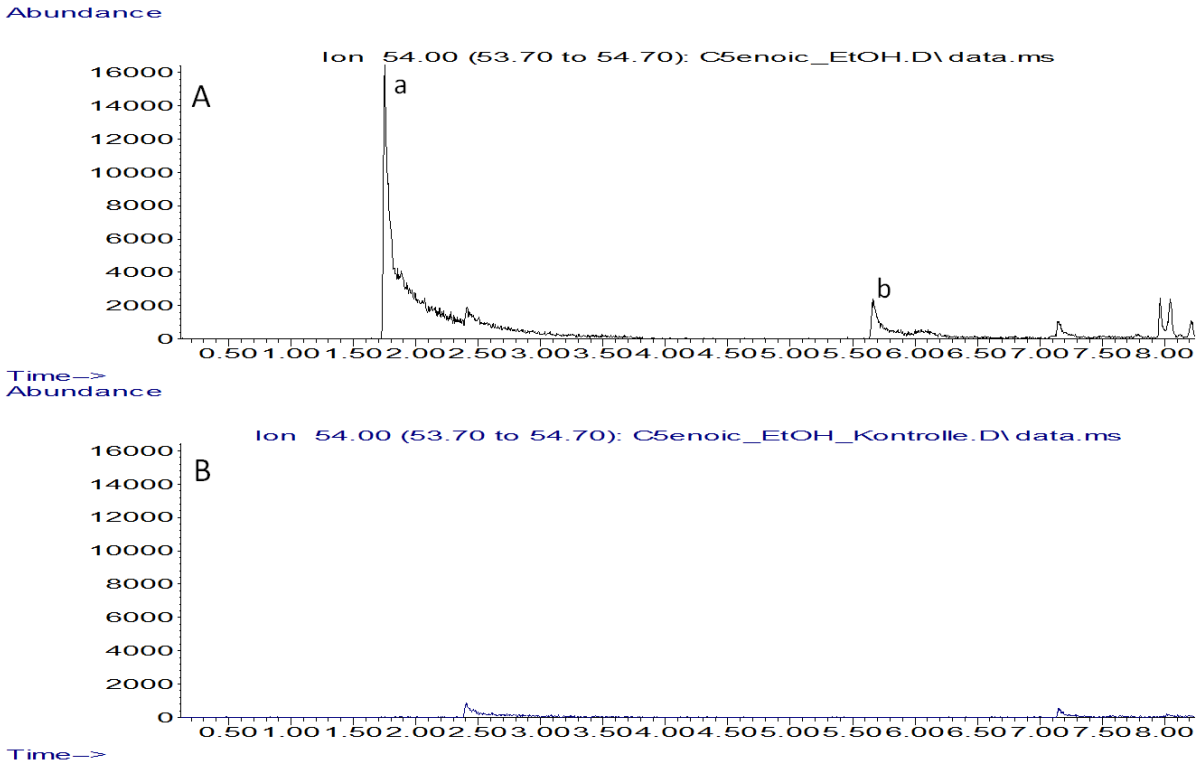

Figure 17: Headspace GC-MS analysis by conversion of **11b** (10 mM). A = Conversion of **11b** with the OleT-CamAB-FDH system. B = Conversion of **11b** in the absence of OleT (negative control). a = **11c**. b = unidentified side product. 5 % (v/v) EtOH was used as co-solvent. The signal of extracted ion *m*/z = 54 is shown.

For **11c** there was a tetra-brominated product standard available and therefore first bromination was tried. Unforetunately, no clear product formation was observed, indicating that product concentration was too low and noise of the bromination solution was too high for detection of any derivatized product.

Furthermore derivatization was tried via sulfonation with H_2SO_3 and Diels-Alder reaction with maleic anhydride and CuCl (Scheme 28 and Scheme 29). Both derivatization methods did not work. Again it might be a problem of mass transfer due to the unstirred system,

especially for Diels-Alder, where a solid catalyst was used. Moreover, product concentration probably was too low to be detected.

Performing derivatization experiments of **11c** at 4 °C and using a stirred reaction set-up might overcome these problems, as it was already shown for biotransformation of **10a** and **15a** that higher product concentrations were obtained at 4 °C (chapter 2.1; Table 1 and Table 3).

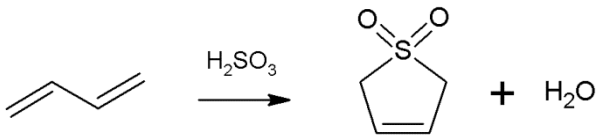

Scheme 28: Sulfonation of **11c** to obtain 3-sulfolene.

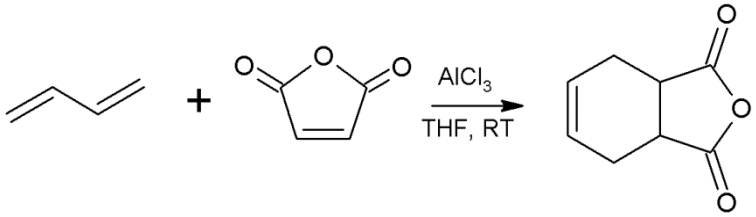

Scheme 29: Diels-Alder reaction of **11c** with maleic anhydride to obtain tetrahydrophthalic anhydride.

Finally, also isovaleric acid was converted by OleT-CamAB-FDH cascade. There was one product detected on GC-MS, which might be isobutene (Figure 18, Figure S172).

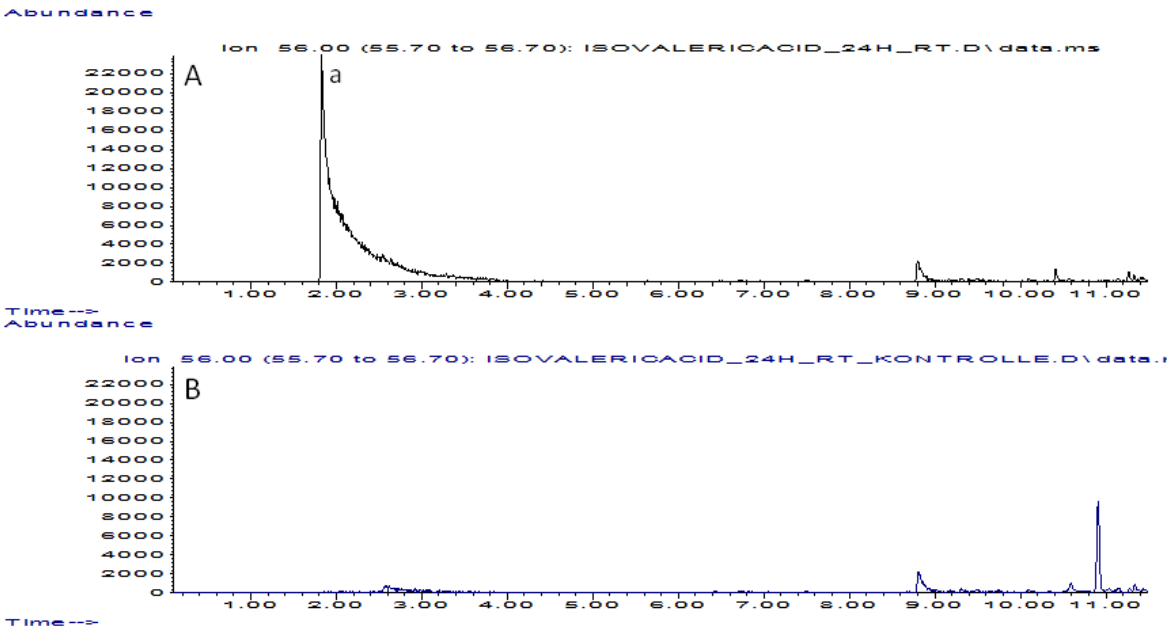

Figure 18: Headspace GC-MS analysis by conversion of isovaleric acid (10 mM). A = Conversion of isovaleric acid with the OleT-CamAB-FDH system. B = Conversion of isovaleric acid in the absence of OleT (negative control). a = isobutene. 5 % (v/v) EtOH was used as co-solvent. The signal of extracted ion *m*/z = 56 is shown.

However, same as for **11c** no proper derivatization method was found so far for identification of isobutene. Since both products (**11c** and isobutene) are gaseous a comparison with the commercial product standards, as it was done for all other conversions, is more difficult with used analytical systems. Proof of the formation of those products and using them directly for further reactions might be a challenge for further studies.

3 Conclusion

Production of terminal dienes with a chain length from C16 to C5 with P450 monooxygenase OleT was shown for the first time. An alternative route was established using ω-enoic acids (C11 - C6). Hence, it was shown that decarboxylation of dioic acids occurs in two steps via formation of ω-enoic acids as reaction intermediate. Conversion of a third substrate class was achieved with short chain branched fatty acids.

Although all these substrates were converted, large differences were observed in conversion levels. The best productivity was achieved with conversion of **3a**, in which 0.49 $g.L^{-1}.d^{-1}$ of 1,11-dodecadiene were produced (TTN = 978). Comparing this with the decarboxylation of saturated fatty acids, it was shown that the ω-terminus still has an impact on the catalyst performance, since conversion of stearic acid led to product titers of 1 $g.L^{-1}.d^{-1}$ 1-heptadecene (TTN = 1300) [17].

Moreover, it was found that catalyst productivity and selectivity can be significantly influenced by reaction temperature, and in most cases, a lower reaction temperature led to higher conversions. Stability and productivity were strongly influenced by enzyme concentration, substrate concentration, co-solvent and co-solvent concentration, FDH concentration and the electron transfer system, and best results were obtained when using the standard reaction set-up.

Last, it was shown that conversion of **11b** and isovaleric acid led to product formation. However, so far it was not possible to identify those products, which might be a challenge for further research.

4 Experimental section

4.1 Materials used in this work

In Table 5 the chemicals and enzymes used in this work are listed. Table 6 shows the substrates and corresponding product standards that were used. All other reagents were of analytical grade or obtained from Sigma Aldrich GmbH (Steinheim, Germany).

Table 5: List of chemicals and enzymes used in this work.

Compound	Supplier
Catalase from bovine liver (2000 - 5000 U.mg^{-1})	Sigma Aldrich (Steinheim, Germany)
Cytochrome C from bovine heart	Sigma Aldrich (Steinheim, Germany)
Lysozyme from chicken egg white (≥ 40000 U.mg^{-1})	Sigma Aldrich (Steinheim, Germany)
Formate dehydrogenase (2.1 U.mg^{-1})	Evocatal (Monheim am Rhein, Germany).
NADH disodium salt	AppliChem (Darmstadt, Germany)
$TMSCHN_2$ (trimethylsilyl diazomethane in diethyl ether)	Sigma Aldrich (Steinheim, Germany)
BSTFA (*N*,*O*-bis(trimethylsilyl)trifluoroacetamide with trimethylchlorosilane)	Sigma Aldrich (Steinheim, Germany)

Table 6: List of substrates and product references with their purity used in this study.

Compound	CAS no.	Supplier	Purity [%]
1a	871-70-5	ABCR	95
2a	505-54-4	Sigma-Aldrich	96
3a	821-38-5	Sigma-Aldrich	99
4a	505-52-2	Sigma-Aldrich	94
5a	693-23-2	Sigma-Aldrich	99
6a	1852-04-6	Sigma-Aldrich	97
7a	111-20-6	Sigma-Aldrich	99
8a	123-99-9	Sigma-Aldrich	98
9a	505-48-6	Fluka	≥ 98
10a	111-16-0	Sigma-Aldrich	98
11a	124-04-9	Sigma-Aldrich	98
5b	112-38-9	Sigma-Aldrich	98
6b	14436-32-9	Sigma-Aldrich	≥ 95

7b	31642-67-8	Sigma-Aldrich	97
8b	18719-24-9	Sigma-Aldrich	97
9b	1119-60-4	ABCR	98
10b	1577-22-6	Sigma-Aldrich	98
11b	591-80-0	ABCR	98
12a	628-46-6	Sigma-Aldrich	-
13a	1561-11-1	Sigma-Aldrich	97
15a	646-07-1	Sigma-Aldrich	99
14a	105-43-1	Sigma-Aldrich	≥ 98
Isovaleric acid	503-74-2	Sigma-Aldrich	99
2c	21964-49-8	ABCR	90
3c	5876-87-9	TCI	> 99
4c	13688-67-0	TCI	> 90
5c	1647-16-1	Sigma-Aldrich	98
6c	4900-30-5	TCI	> 98
7c	3710-30-3	Sigma-Aldrich	98
8c	3070-53-9	TCI	> 99
9c	592-42-7	ACROS ORGANICS	98
10c	591-93-5	Sigma-Aldrich	99
1,3-pentadiene	2004-70-8	TCI	> 95
12c	691-37-2	Sigma-Aldrich	98
13c	760-20-3	ABCR	98
15c	563-45-1	TCI	15 % in DCM
14c	563-46-2	ABCR	98

For GC-FID analysis an Agilent 7890A GC system was used. Helium was used as carrier gas and detection of the analytes was achieved with a flame ionization detector (FID). An Agilent HP-5 column (30 m x 320 µm, 0.25 µm film) was used for separation of the analytes. Further GC-MS analysis was done using an Agilent 7890A GC-system. An Agilent 5975C mass-selective detector was used for detection and separation was achieved with an Agilent HP-5 MS column (30 m x 320 µm, 0.25 µm film). For headspace measurements an Agilent 7697A headspace sampler was used connected to an Agilent 7890A GC-system for GC-MS analysis.

For ^{1}H-NMR analysis a Bruker Avance III 300 MHz NMR spectrometer was used. The reported chemical shifts were relative to TMS (δ = 0.00 ppm) and the unit used for the coupling constants *J* was Hz.

4.2 Enzyme preparation

In this study the substrates (Table 6) were converted using the monooxygenases OleT, $CYP_{BS\beta}$ or $P450_{Cla}$. CamAB or Fdr/FldA were used as electron transfer systems. This section describes the expression and purification of enzymes used in this work.

4.2.1 Expression of OleT

Expression and purification of OleT from *Jeotgalicoccus* sp. was done as described by Dennig *et al*. The identical expression system (pET28a expression vector) and *E. coli* strain (BL21(DE3), C43) was used [17]. In Table 7 the composition of the media used for enzyme expression is shown.

Table 7: Composition of the media used for enzyme expression.

Medium	Compound	Concentration
LB-medium	NaCl	5 $g.L^{-1}$
	Yeast extract	5 $g.L^{-1}$
	Peptone	10 $g.L^{-1}$
TB-medium (solution A) 800 mL	Yeast extract	24 g
	Peptone	12 g
	Glycerol	4 g
TB-medium (solution B) 200 mL	KH_2PO_4	2.31 g
	K_2HPO_4	12.54 g
Trace element solution [49]	$FeCl_3 \cdot 6H_2O$	16.7 $g.L^{-1}$
	Na_2-EDTA	20.1 $g.L^{-1}$
	$CaCl_2 \cdot 2H_2O$	0.5 $g.L^{-1}$
	$ZnSO_4 \cdot 7H_2O$	0.18 $g.L^{-1}$
	$CuSO_4 \cdot 5H_2O$	0.16 $g.L^{-1}$
	$MgSO_4 \cdot H_2O$	0.1 $g.L^{-1}$

The media were filled up with ddH_2O to the final volume and autoclaved (20 min at 121 °C). For the final TB-medium solution A and B were mixed after autoclaving. For the trace element solution all components were dissolved in ddH_2O and the solution was sterile filtrated.

For expression of OleT, first, a preculture was generated using a 250 mL shaking flask (round bottom) filled with LB-medium (30 mL), a kanamycin stock solution (30 µL, 50 $mg.mL^{-1}$) and glycerol stock solution (10 µL) of the culture {750 µL of the preculture mixed with

500 µL glycerol stock [50 % (w/v)]}. The preculture was incubated overnight at 140 rpm and 37 °C. Then the preculture (1 mL) was added to a 1 L shaking flask filled with TB-medium (100 mL), the trace element solution (100 µL) (Table 7) and a kanamycin stock solution (100 µL, 50 mg.mL^{-1}). The culture was incubated at 140 rpm and 37 °C until an optical density (OD_{600}) of 2.0 was reached. At that point an IPTG solution (100 µL, 1 M) and a δ-aminolevulinic acid (ALA) solution (200 µL, 0.5 M) were added to induce protein expression and the culture was incubated for 20 h at 140 rpm and 25 °C. After incubation the cells were centrifuged for 10 min at 4,000 rpm and RT, followed by freezing the remaining cell pellets at -20 °C.

4.2.2 Expression of $P450_{Cla}$ and $CYP_{BS\beta}$

For expression and purification of $CYP_{BSß}$ from *B. subtilis* the protocol of Matsunaga *et al.* was used [20][50]. $P450_{Cla}$ from *C. acetobutylicum* was expressed and purified as described elsewhere [30][17].

Expression of $CYP_{BSβ}$ and $P450_{Cla}$ was done as described for OleT (chapter 4.2.1) with following changes: Induction of protein expression was done at OD_{600} = 0.8. After induction $CYP_{BSβ}$ was incubated at 30 °C and $P450_{Cla}$ at 25 °C for 20 h, respectively.

4.2.3 Purification of OleT, $P450_{Cla}$ and $CYP_{BS\beta}$

Purification of the monooxygenases was done as decribed by Dennig *et al.* [17].

Purification of the enzymes OleT, $P450_{Cla}$ and $CYP_{BSβ}$ was achieved via the His-Tag of the proteins using a 5 mL His-Trap^{TM} FF column (GC-Healthcare Life Science). First, cell disruption was achieved by freezing the pellets, incubation with lysozyme and ultra-sonication. In Table 8 composition of the buffers used for purification are listed. Binding of the enzymes to the Ni^{2+} ions of the column was regulated through different imidazole concentrations. For binding of OleT imidazole (50 mM) was used to avoid binding of host cell proteins onto the column. Elution was then achieved with imidazole (400 mM) that binds stronger to the Ni^{2+} ion than the His-Tag. As last purification step imidazole was removed from the enzyme preparation in order to prevent binding of imidazole to the heme iron and hence influence on activity measurements.

Table 8: Composition of the buffers used for purification of OleT, $CYP_{BS\beta}$ and $P450_{Cla}$.

Buffer	Compound	Concentration
Buffer A (binding/washing buffer)	Imidazole	50 mM
	KCl	300 mM
	Glycerol	20 % (w/v)
Buffer B (elution buffer)	Imidazole	400 mM
	KCl	300 mM
	Glycerol	20 % (w/v)
Dialysis buffer	KCl	300 mM
	Glycerol	20 % (w/v)

The final volume and pH 7 of all solutions (Table 8) was adjusted by adding K_2HPO_4 and KH_2PO_4 buffer (0.1 M). All solutions were filtrated afterwards.

For purification the frozen pellet was warmed up at RT and then re-suspended in about 15 mL of a lysozyme solution (1 $mg.mL^{-1}$ in buffer A). After incubating the suspension for two hours at 37 °C, the cells were disrupted by ultra-sonication (Table 9) (using a Digital Cell Disrupter, Branson, Emerson Electric).

Table 9: Protocol for ultra-sonication used for cell disruption and isolation of OleT, $CYP_{BS\beta}$ and $P450_{Cla}$.

Protocol for ultra-sonication	
Amplitude of the ultra-sonication	30 %
Total time	30 s
Duration of the ultra-sonication	2 s
Pause between the ultra-sonication	4 s

Then the suspension was centrifuged for 15 min at 14,000 rpm and 4 °C, the supernatant was collected and purified using a 5 mL His-Trap™ FF column (GC-Healthcare Life Science). Treatment of the column was done according to the supplier's recommendations [51].

For the enzyme purification the column was first washed with ten column volumes of ddH_2O to remove the ethanol, which was used for storage of the column. After that the column was conditioned with about 20 volumes of buffer A. Then the crude enzyme solution was loaded onto the column and further 10 volumes of buffer A were added to elute non-desired unbound protein. Afterwards the enzyme was eluted with buffer B and the orange-red coloured solution was collected. For cleaning the column buffer B (10 column volumes), water (10 column volumes) and ethanol [20 % (v/v), (10 column volumes)] were used, respectively. Finally the

enzyme was dialysed for 36 h at 4 °C using dialysis buffer (300 mL, each), which was exchanged three times in intervals of 8 to 16 h. OleT was then stored at 4 °C.

The aim of purification was to eliminate fatty acids and other substances that could negatively influence enzyme performance and product formation. Furthermore, concentration of the monooxygenases was achieved by elimination of host proteins. To prove the purity of the enzyme OleT a SDS-gel from all enzyme purification steps was done (Figure 19). Samples were taken from the crude enzyme solution (lysate; Lane 1 and 5 in Figure 19), the unbound protein (protein which was not bound onto the column while loading the enzyme; Lane 2 and 6 in Figure 19), the wash solution (containing protein which eluted while washing with buffer A Lane 3 and 7 in Figure 19), as well as from the purified enzyme before dialyses (Lane 4 and 8 in Figure 19).

The samples for the SDS-gel were prepared according to the protocol from Sigma Aldrich [52]. Samples were mixed 1:1 (100 µL, each) with Laemmli buffer 2x (obtained from Sigma Aldrich, composition: 4 % SDS, 20 % glycerol, 10 % 2-mercaptoethanol, 0.004 % bromophenol blue and 0.125 M Tris HCl, pH approx. 6.8), heated at 95 °C for ten minutes and stored on ice for another ten minutes.

The gel was then prepared in the following way: First the separating gel (Table 10) was poured into the gel casting form and layerd with 200 µL isopropanol to ensure a smooth surface. For addition of the stacking gel about 2 cm space were left. After polymerization of the gel (10 - 15 min), the isopropanol was removed and stacking gel (Table 11) was added and a comb was put in the stacking gel to form slots. After the stacking gel was polymerized the comb was removed and samples were loaded onto the gel.

Table 10: Composition of separating gel mixture for the SDS gel.

Compounds for separating gel	Amounts
Acrylamide (30 %)	1.67 mL
Separating gel buffer (1 M Tris/HCl, pH 8.8)	1.88 mL
ddH_2O	1.36 mL
SDS (10 %) (50 mg SDS in 500 µL H_2O)	50 µL
APS (10 %) (20 mg APS in 200 µL H_2O)	40 µL
TEMED	4 µL

Table 11: Composition of stacking gel mixture for the SDS gel.

Compound for stacking gel	Amounts
Acrylamide (30 %)	0.278 mL
Stacking gel buffer (1 M Tris/HCl, pH 6.8)	0.208 mL
ddH_2O	1.154 mL
SDS (10 %) (50 mg SDS in 500 µL H_2O)	16.7 µL
APS (10 %) (20 mg APS in 200 µL H_2O)	8.3 µL
TEMED	1.67 µL

The volumes for the samples loaded on the gel were 2 µL and 5 µL, respectively, and the volume for the standard was 4 µL. For electrophoresis the SDS gel was incubated in SDS buffer 1x at 100 V for about 30 min. The gel was then incubated with staining solution [1 g coomassie brilliant blue R250 (obtained from BioRad), 500 ml MeOH, 100 mL AcOH, 500 mL H_2O] for 15 min and afterwards incubated with destaining solution (300 ml MeOH, 100 mL AcOH, 600 mL H_2O) over night.

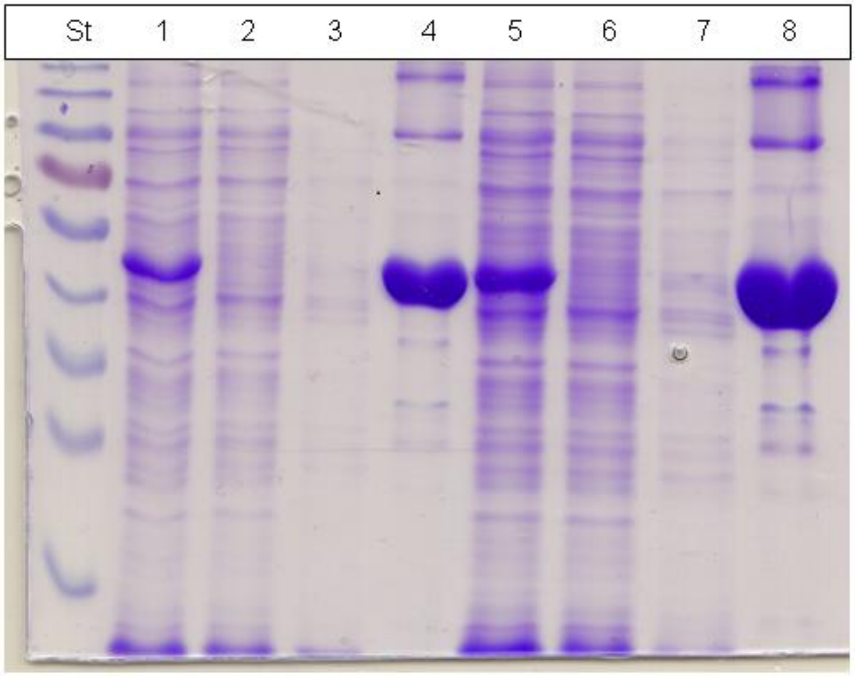

Figure 19: SDS gel of the OleT enzyme purification. St – standard protein layer; 1 cell free lysate; 2 unbound protein; 3 washing fraction; 4 purified protein; 5 cell free lysate; 6 unbound protein; 7 washing fraction; 8 purified protein; for the lines 1 to 4, 2 µL of the solutions were loaded onto the SDS gel and for the lines 5 to 8, 5 µL were taken, respectively.

The SDS gel (Figure 19) shows that purification worked sufficiently. OleT did not elute from the column during loading and washing with buffer A (lanes 2/6 and 3/7). During purification most of the host proteins were eliminated (lanes 4 and 8) and the purity of the enzyme was estimated to be roughly 70 %. Furthermore, overexpression of OleT generally worked well,

however, after dialysis it sometimes occurred that protein precipitated. Therefore the enzyme was diluted by adding 5 to 10 mL buffer B to the purified enzyme before dialysis (final volume of purified enzyme was about 30 mL). It was observed that no protein precipitated when it was diluted.

4.2.4 **Expression and purification of Fdr/FldA**

For expression of Fdr/FldA in *E. coli* BL21 (pTf16) cells the protocols from Jenkins *et al.* were used [47][53].

Two precultures in LB-medium containing ampicillin (150 µg.mL^{-1}) and Fdr or FldA were generated and cells were grown overnight at 37 °C. Then a 1 L shaking flask filled with TB-medium (100 mL), containing $MgCl_2$ (1 mM), NaCl (5 mM) and ampicillin (25 mg.mL^{-1}) was inoculated with the preculture (1 mL), respectively. After incubation at 37 °C and 250 rpm for 4 h, the enzyme expression was induced by adding IPTG (1 mM). Both cultures were incubated for another 5 h at 33 °C.

Afterwards, the cells were centrifuged and the remaining cell pellet was re-suspended in ice-cold KPi buffer (50 mM, pH 7.5 containing 200 mM NaCl, 5 % glycerol and 0.5 µg.mL^{-1} lysozyme). The suspension was left on ice for 30 min and then sonicated (30 % amplitude, duration of sonication 2 s, pause 4 s, total time 1 min). This suspension was centrifuged at 14,000 rpm for 30 min and the supernatant was stored at 4 °C.

4.2.5 **Expression and purification of CamAB**

Regarding the CamAB system co-expression in *E. coli* C43(DE3) cells was achieved as described by Schallmey *et al.* [54].

A preculture was prepared in LB-medium containing chloramphenicol (25 µg.mL^{-1}) and cells were grown overnight. Then the preculture (500 µL) was added to the TB-media (500 mL) containing chloramphenicol (25 µg.mL^{-1}). Cells were incubated at 37 °C and enzyme expression was induced at OD_{600} = 1. For that IPTG (0.8 mM) and ALA (0.5 mM) were added. The culture was further incubated at 30 °C for 48 h. After that cells were centrifuged at 14,000 rpm for 20 min and the cell pellet was frozen at -20 °C.

Cell disruption was done in the following way: The cell pellet was warmed up at RT and re-suspended in buffer [20 mL; TrisHCl (0.1 M), 20 % glycerol (w/v), pH 8; containing 1 mg.mL^{-1} lysozyme]. The solution was incubated at 37 °C for 1 h and further disruption was achieved by ultra-sonication using the following program (Table 12).

Table 12: Protocol for ultrasonication used for cell disruption and isolation of CamAB.

Protocol for ultra-sonication	
Amplitude of the ultra-sonication	30 %
Total time	60 s
Duration of the ultra-sonication	2 s
Pause between the ultra-sonication	4 s

The solution was sonicated twice and in between, it was stored on ice for 5 min. After that the suspension was centrifuged at 14,000 rpm for 10 min, supernatant was taken and stored at -20 °C.

4.2.6 Measurement of enzyme concentration and activity

After enzyme purification, the concentration of active enzyme of the monooxygenases (OleT, $CYP_{BSß}$ and $P450_{Cla}$) was determined by CO-titration. Activity of the electron transfer systems (CamAB; Fdr/FldA) was determined with a photometric cytochrome C assay before each biotransformation.

4.2.6.1 CO-titration for determination of the concentration of active cytochrome P450s

For determination of the concentration of purified cytochrome P450s (OleT, $CYP_{BSß}$ and $P450_{Cla}$) the CO-titration assay was used as described in the original protocol by Omura and Sato [26].

Determination of the concentration of cytochrome P450s was done by the CO-titration assay. First reduction of the heme iron of the enzyme was achieved by addition of sodium dithionite. Then the solution was saturated with CO, which forms an adduct with the reduced heme iron of cytochrome P450s. If the CO binds to the heme iron the absorption of the heme iron shifts from 420 nm to around 450 nm. Since oxygen binds in the same way to the reduced heme iron than CO, an absorbance at 450 nm indicates active enzyme.

For determination of the concentration of active cytochrome P450 a few milligrams of sodium dithionite were dissolved in KPi-buffer (950 µL; pH 7.5, 0.1 M) and filled into a cuvette [cuvette obtained from SARSTEDT (Ref 67.742); composed of polystyrene; 10 x 4 x 45 mm]. Afterwards the purified enzyme (50 µL) was added to the KPi-buffer containing the sodium dithionite and absorbance was measured on a photometer (Thermospectronic™ Genesys 10 UV scanning; software: VISIONlite scan). The reduced enzyme was used as blank over the range from 400 - 520 nm absorbance. Followed by this the reduced enzyme solution was gassed with CO for 30 s. Absorption was measured again in the range from 400 - 520 nm to

obtain a differential spectrum of purified cytochrome P450s after CO-titration. The concentration of active cytochrome P450 could be determined through absorption at 450 nm, while the absorbance maximum of inactive cytochrome P450 is usually at 420 nm (Figure 20).

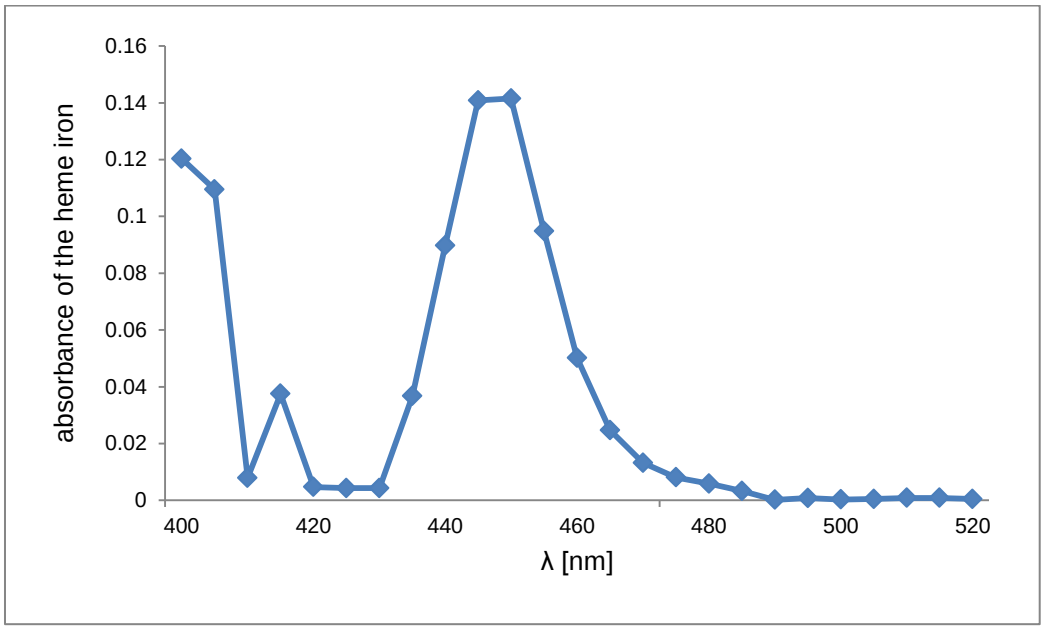

Figure 20: Differential spectrum of purified OleT after CO-titration showing the absorbance of the heme iron of the enzyme over the range of 400 to 520 nm. Here the concentration of active OleT was dermined with 15.5 µM.

Based on the law of Lambeer-Beer (equation 2), the concentration of active cytochrome P450 was calculated in the following way (equation 3):

$$A = \lg\left(\frac{I_0}{I}\right) = \varepsilon * c * d \qquad (2)$$

A → absorbance

I_0 → incident intensity of light [$W.m^{-2}$]

I → transmitted intensity of light [$W.m^{-2}$]

ε → molar extinction coefficient [$(M.m)^{-1}$]

c → concentration [M]

d → path length [m]

The absorbance at 500 nm (baseline) was subtracted from that at 450 nm (active cytochrome P450).

$$c_{active\ enzyme}[\mu M] = \frac{abs * 1000 * 20}{91 * \mathrm{d}} \quad (3)$$

1000 → mM to µM

20 → dilution factor

91 → molar extinction coefficient of the reduced iron-CO complex [$(mM.cm)^{-1}$]

d → path length [cm] = 1

Usually expression of OleT was done in 800 mL fermentation volume. After purification of the enzyme about 30 mL purified enzyme were obtained and concentration of active OleT ranged from 15 to 25 µM.

4.2.6.2 Cytochrome C assay for determination of the activity of the electron transfer system

Activity mesurements for CamAB and Fdr/FldA were done as described by Lacour *et al.* and Schallmey *et al.* [54][55].

Ferredoxin reductases in combination with a ferredoxin are able to transfer electrons from the cofactor NAD(P)H to the heme iron of cytochrome P450 [54]. For activity measurement of the ferredoxin reductases a photometric cytochrome C assay was performed, while the efficiency of electron transfer was measured over the reduction of cytochrome C. Reduced cytochrome C absorbs at 550 nm and hence activity could be measured over an increase of absorbance at 550 nm. The supplier's original protocol was used for activity determination of the CamAB system and Fdr/FldA [56].

Table 13: Composition of the solution used for CamAB and Fdr/FldA activity measurement.

Compounds for the activity assay	Volume
Cytochrome C from bovine heart ($18.4\ mg.mL^{-1}$)	50 µL
Ferredoxin + ferredoxin reductase (CamAB)*	5 µL
NADH stock solution (10 mM)	20 µL
KPi buffer (pH 7.5; 0.1 M)	925 µL

*activity of Fdr/FldA was determined once using 50 µL and 25 µL Fdr/FldA, showing an activity of 0.11 and 0.07 $U.mL^{-1}$, respectively.

The components for activity measurement (Table 13), except from NADH, were mixed in a cuvette (blank solution) and absorbance was measured on a photometer (Thermospectronic™ Genesys 10 UV scanning; software: VISIONlite rate). To start the reduction of cytochrome C and hence activity measurement NADH was added and an increase of the absorbance was directly measured at 550 nm (Figure 21).

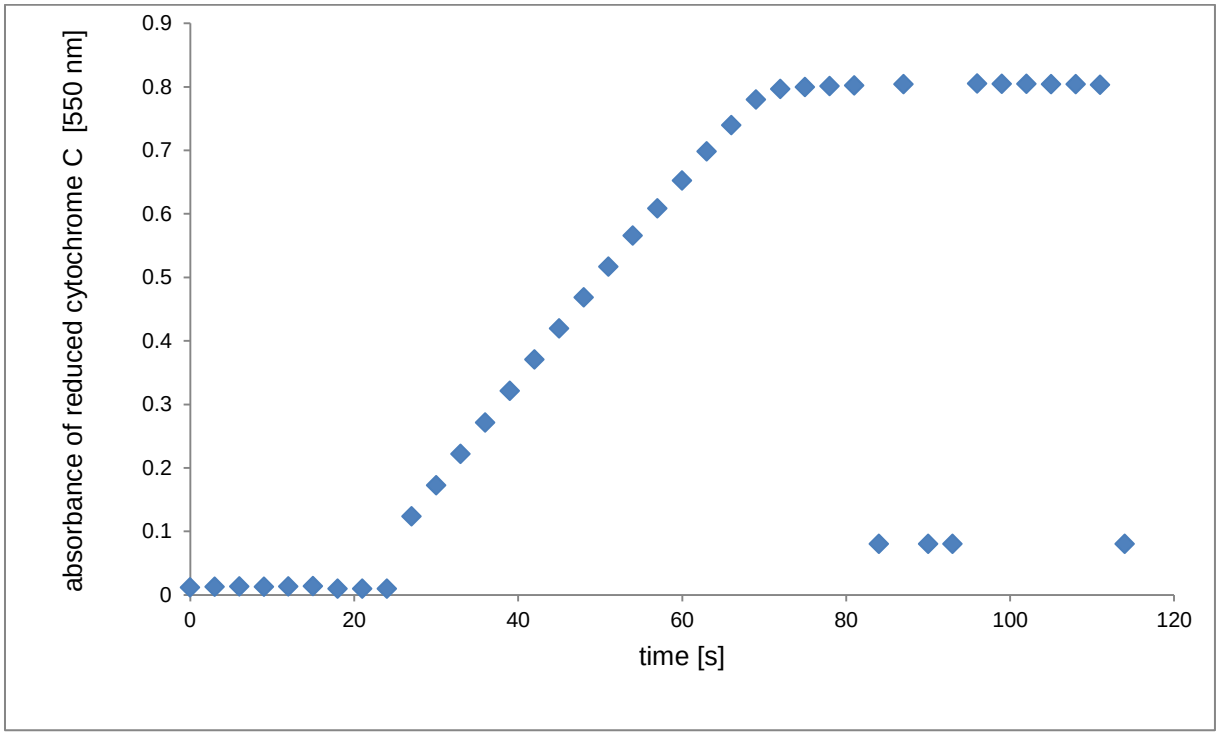

Figure 21: CamAB activity measurement: increase of absorbance of cytochrome C at 550 nm, due to its reduction. Here activity of the CamAB system was determined with 4.9 U.mL^{-1}.

The activity was calculated in the following way (equation 4):

Within the linear range there were taken two points with a time difference of one minute. The lower absorption was subtracted from the higher one.

$$a\left[\frac{U}{mL}\right] = \frac{abs}{0.005 * 28 * \mathrm{d}} \qquad (4)$$

abs → increase of absorbance [min^{-1}]

a → activity [U.mL^{-1}]

0.005 → volume of CamAB = dilution factor

28 → extinction coefficient of reduced cytochrome C [(mM.cm)$^{-1}$]

d → path length [cm] = 1

Usually the activity of CamAB varied from about 2.5 to 5 U.mL^{-1}.

4.3 Biotransformations

4.3.1 General procedure for biotransformations with OleT-CamAB-FDH reaction cascade

Biotransformations with OleT were performed according to the protocol of Dennig *et al.* [17]. Decarboxylation of the substrates (Table 15) with OleT-CamAB-FDH system was done as shown in Scheme 13 and Scheme 14, chapter 1.5.

23 fatty acid substrates (Table 6) were tested to be converted with the OleT-CamAB-FDH reaction cascade to yield the terminal dienes or 1-alkenes.

Table 14: Composition of reaction mixture for biotransfomations with OleT-CamAB-FDH cascade.

Components for biotranformation	c_{final} in the biotransformation
OleT	6 µM
Ammonium formate	0.1 M
CamAB	0.05 $U.mL^{-1}$
Formate dehydrogenase	2.1 $U.mL^{-1}$ = 1 $mg.mL^{-1}$
Catalase	500 $U.mL^{-1}$
Substrate in 5 % (v/v) EtOH or DMSO	10 mM
NADH	0.2 mM

If not stated otherwise biotransformations of all substrates (Table 15) were done in 1 mL scale in 4 mL glass vial closed with a PTFE septum. **1a, 2a** and **3a** were hardly soluble in EtOH and therefore DMSO was used as co-solvent. The components for the biotransformation with OleT are listed in Table 14 and the final reaction volume was adjusted with KPi buffer (0.1 M, pH 7.5). The activity of the CamAB system was determined before each biotransformation and the concentration of active OleT was measured after purification, since OleT was stored at 4 °C for up to one month without observed loss in activity. Biotranformations were carried out at RT for 24 h by shaking samples at 170 rpm or at 4 °C for 72 h stirred at 100 rpm. Additionally, there was one control reaction without OleT performed for each substrate (negative control).

Table 15: List of substrates converted with OleT-CamAB-FDH cascade and co-solvents used in the biotransformation.

Compound	Cosolvent
1a	DMSO 5 % (v/v)
2a	DMSO 5 % (v/v)
3a	DMSO 5 % (v/v)
4a	EtOH 5 % (v/v)
5a	EtOH 5 % (v/v)
6a	EtOH 5 % (v/v)
7a	EtOH 5 % (v/v)
8a	EtOH 5 % (v/v)
9a	EtOH 5 % (v/v)
10a	EtOH 5 % (v/v)
11a	EtOH 5 % (v/v)
5b	EtOH 5 % (v/v)
6b	EtOH 5 % (v/v)
7b	EtOH 5 % (v/v)
8b	EtOH 5 % (v/v)
9b	EtOH 5 % (v/v)
10b	EtOH 5 % (v/v)
11b	EtOH 5 % (v/v)
14a	EtOH 5 % (v/v)
15a	EtOH 5 % (v/v)
13a	EtOH 5 % (v/v)
12a	EtOH 5 % (v/v)
Isovaleric acid	EtOH 5 % (v/v)

4.3.2 **Decarboxylation of 3a using OleT-Fdr/FldA-FDH system**

Biotransformation were usually done using puditaredoxin based/class I electron transfer system CamAB. Additionally to that the electron transfer system from *E. coli* Fdr/FldA based on flavodoxin was also tested to check whether Fdr/FldA system is better compatible with OleT or not. For that decarboxylation of **3a** was done using Fdr/FldA (10, 25 and 50 µL of *E. coli* cell free lysate, respectively), instead of CamAB to mediate electrons from NADH to OleT (see Scheme 16, chapter 2.3) [22]. The activity of Fdr/FldA was determined as 0.11 $U.mL^{-1}$ (using 50 µL Fdr and FldA, each) and 0.07 $U.mL^{-1}$ (using 25 µL Fdr and FldA, each). All other components were used as listed in Table 14 and biotransformations were done at RT for 24 h shaking at 170 rpm.

4.3.3 Decarboxylation of 3a with OleT using H_2O_2 as sole oxidant

As reported by Rude *et al.* decarboxylation of fatty acids by OleT could be achieved with H_2O_2 as oxidant [19]. Therefore **3a** was also converted using H_2O_2 to explore the performance of OleT in presence of H_2O_2 (see Scheme 17, chapter 2.3). For that, the conversion was done in 4 mL glass vials, using 6 µL of purified OleT, 10 mM substrate and 5 % (v/v) DMSO, filled up to a final volume of 1 mL with KPi buffer (pH 7.5; 0.1 M). To start the reaction H_2O_2 (0.8 mM) was added to the reaction mixture. Supplementation of H_2O_2 was repeated every 45 min for seven times ($c_{H2O2\text{-}total}$ = 5.6 mM). The reactions were done in duplicate and shaken at RT for 24 h at 170 rpm.

4.3.4 Hydroxylation of dioic acids and ω-enoic acids with $P450_{Cla}$ and $CYP_{BSβ}$

The two P450 peroxygenases $P450_{Cla}$ and $CYP_{BSß}$ are able to hydroxylate fatty acids on α- or α- and β-positions, respectively [20][30]. Therefore conversion of the dioic acids and ω-enoic acids (Table 15) was done to obtain α-/ß-hydroxy-dioic acids and α-/ß-hydroxy-ω-enoic acids as reference products (Scheme 30, Scheme 31).

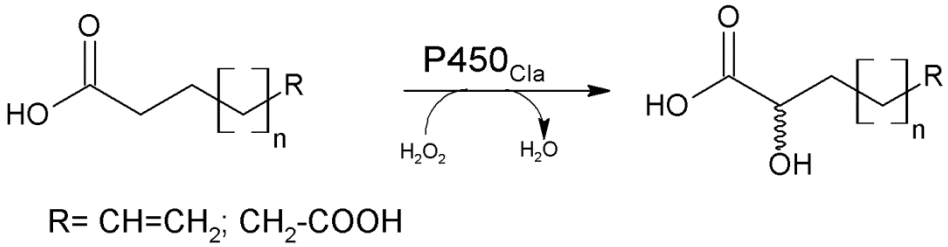

Scheme 30: Reaction scheme for α-hydroxylation of dioic and ω-enoic acids using the peroxygenase $P450_{Cla}$.

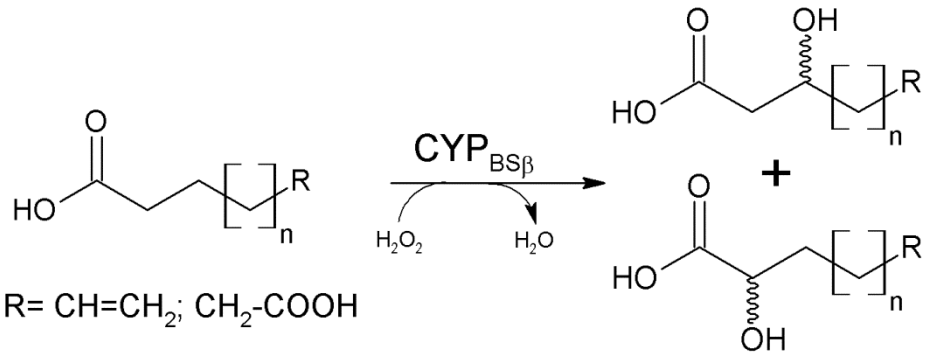

Scheme 31: Reaction scheme for α/β-hydroxylation of dioic and ω-enoic acids using the peroxygenase $CYP_{BSβ}$.

This strategy already succeeded in previous studies for saturated fatty acids [17]. Biotransformations were done in 4 mL glass vials sealed with a PTFE septum and shaking at

RT and 170 rpm for 24 h. The reaction mixture contained 2 µM enzyme, 10 mM substrate (**1a - 6a** and **5b - 6b**) and 5 % (v/v) cosolvent. H_2O_2 (0.8 mM) was added every 45 min for seven times ($c_{H2O2\text{-}total}$ = 5.6 mM).

4.4 Product extraction and derivatization

Product extraction and derivatization was done as described by Dennig *et al.* [17]. All biotransformations were treated in the same way. First the formed products and remaining substrate were extracted from the aqueous phase. Then esterification of the carboxylic group was achieved with $TMSCHN_2$ in order perform GC-FID and GC-MS analysis.
Reactions were quenched by adding HCl (5 N, 100 µL) followed by extraction with EtOAc [500 µL; containing 0.1 % 1-decanol as internal standard (ISD)]. After centrifuging the solution for 5 min at 14,000 rpm the supernatant (organic phase) was collected and dried with Na_2SO_4. Thereafter dry supernatant (150 µL) was mixed with methanol (60 µL) in a GC-vial and esterification was done by adding $TMSCHN_2$ (15 µL). The samples were analysed by GC-FID and GC-MS.

For the identification of the position of the hydroxy-groups (α- or β-position), silylation of the hydroxy-group was done after esterification. Silylation was achieved with BSTFA according to the protocol of Matsunaga *et al.* [20]. For that, the samples were prepared in the following way: After analysing the esterified samples by GC-FID and GC-MS, solvent was evaporated under dry airflow. Then the remaining solids were dissolved in BSTFA (300 µL) and incubated at 60 °C for 30 min. Finally, compound analysis was done by GC-MS to assign α/ß-hydroxy acids.
Although, in the publication of Matsunaga *et al.* detection of α- and β-trimethylsilyl derivatives of the hydroxy-acids was described, we were only able to assign β-trimethylsilyl derivatives. This is quite interesting, because Mantsunaga *et al.* also did derivatization with $TMSCHN_2$, followed by treatment with BSTFA and GC-MS analysis. The sole difference was that they synthesized diazomethane from *N*-nitroso-*N*-methylurea instead of using commercial $TMSCHN_2$. Further the temperature programm for GC-MS was different, using higher initial temperature (150 °C vs. 100 °C) and slower temperature increase (4 °C/min up to 270 °C vs. 10 °C/min up to 300 °C). These factors might have influenced analysis.
Figure 22 shows one example of silylated hydroxy-acid (TMS-**3g**-methylester obtained from the conversion of **3a** with OleT-CamAB-FDH cascade). For all TMS derivatives of β-hydroxy acids the characteristic fragment *m/z* = 175 was obtained due to cleavage between C_3 and C_4. Further the fragment *m/z* = 299 derives from cleavage of Si and CH_3. Therefore in all spectra from slilyated hydroxy-acids a peak *m/z* = M - 15 (loss of one methyl group) is observed [20].

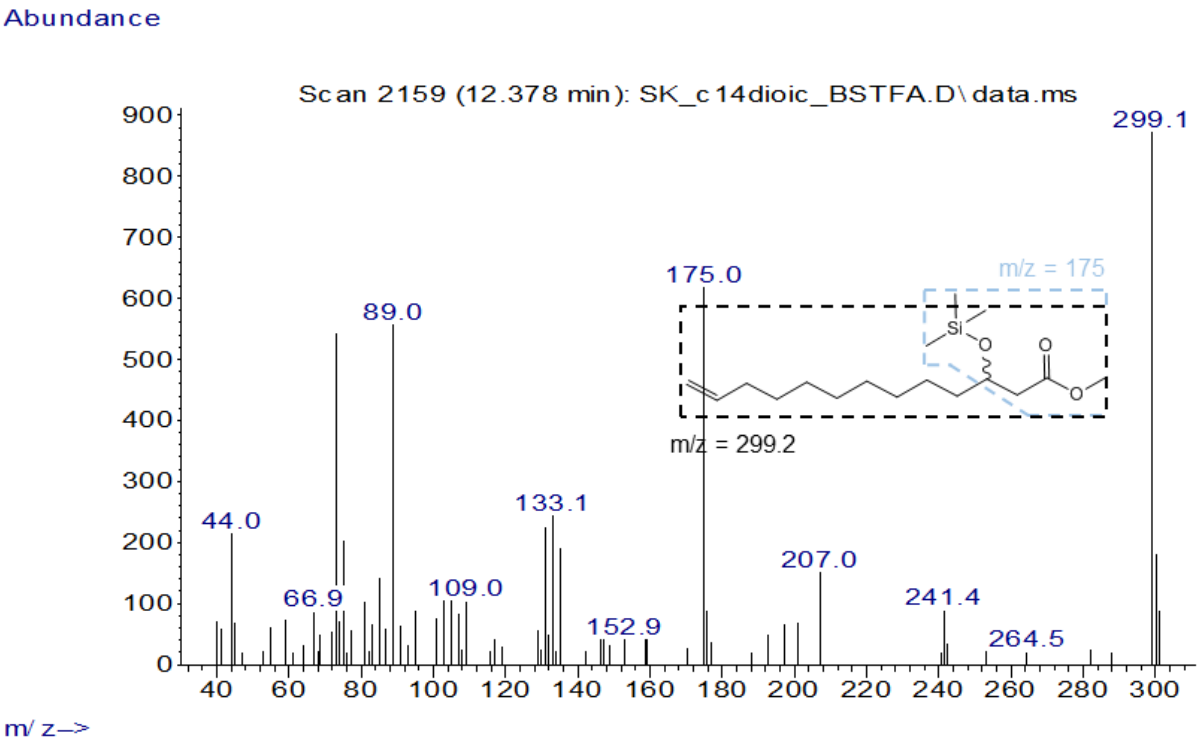

Figure 22: GC-MS spectra of TMS-**3g**-methylester obtained by conversion of **3a** (10 mM) with the OleT-CamAB-FDH system (corresponds to peak c in Figure S39 A). The characteristic ions *m*/z = 175 and *m*/z = 299.2 were used to assign the product as described elsewhere [20].

For analysis of **7c - 9c** headspace GC-MS with manual injection was used. All biotransformations were performed in 4 mL reaction vials that were tightly closed with a PTFE septum to avoid evaporation. The biotransformations were stopped by heating the closed reaction vials to 80 °C for 10 min followed by headspace GC-MS analysis. In order to prevent product condensation, the syringe (Agilent syringe FN 26/50/cone; V = 10 µL) used for headspace injection was also incubated at 80 °C for 10 min. After incubation, 9 µL from the reaction headspace were injected into the GC-MS.

For analysis of **12c - 15c** and **10c** headspace GC-MS with auto sampler (see chapter 4.5.2) was used. Biotransformations of **12a - 15a**, **10a** and **10b** were performed in 2 mL scale in 20 mL vials tightly closed with a PTFE-septum provided by Agilent and samples were heated to 80 °C for 2 min.

4.5 Analytical methods

4.5.1 GC-FID and GC-MS analysis

In Table 16 all methods used for analysis of biotransformations with **1a - 6a** and **5b - 6b** on GC-FID and GC-MS are listed. All biotransformations as well as the product standards of the terminal dienes (**1c - 6c)** were treated as described in chapter 4.4 (extraction, derivatization and analysis). The product standards were used as product reference and for quantification.

Table 16: GC-FID/MS programs for analysis of products (**1c - 6c)** derived from enzymatic conversions.

Detector*	Substrate	Column	Heating program
GC-MS	**1a - 6a**; **5b - 6b**	HP-5MS	100 °C/hold 0.5 min; 10 °C min^{-1} to 300 °C; hold 0 min; Injection temperature = 250 °C
GC-MS	**5a - 6a**; **5b - 6b**	HP-5MS	40 °C/hold 2 min; 10 °C min^{-1} to 180 °C; hold 1 min; Injection temperature = 250 °C
GC-FID	**1a - 5a**; **5b**	HP-5	100 °C/hold 5 min; 20 °C min^{-1} to 320 °C; hold 0 min; Injection temperature = 300 °C
GC-FID	**6a**; **6b**	HP-5	80 °C/hold 10 min; 40 °C min^{-1} to 320 °C; hold 0 min; Injection temperature = 300 °C

*Detector temperature was in all cases 300 °C.

4.5.2 Headspace GC-MS analysis

Table 17 shows the methods used for headspace GC-MS analysis of **7c - 10c** and **12c - 15c**. Again biotransformations were treated as described in chapter 4.4 and identical procedure was used for the product standards for comparison and quantification.

Table 17: GC- MS headspace programs for analysis of volatile products (**7c** - **10c**; **12c** - **15**c) derived from enzymatic conversions.

Detector	Product	Column	Heating program
GC-MS	**7c**	HP-5MS	inlet: 250 °C; 40 °C/hold 5 min; 20 °C min^{-1} to 170 °C/hold 0 min; splittless
GC-MS	**8c-9c**	HP-5MS	inlet: 250 °C; 40 °C/hold 5 min; 40 °C min^{-1} to 170 °C/hold 0 min; splittless
GC-MS	**10c, 14c**	HP-5MS	inlet: 250 °C; 50 °C/hold 4 min; 20 °C min^{-1} to 160 °C/hold 0 min; gas flow 35 $mL.min^{-1}$; split ratio 35:1
GC-MS	**12c-15c**	HP-5MS	inlet: 250 °C; 100 °C/hold 4 min; 20 °C min^{-1} to 160 °C/hold 0 min; gas flow 35 $mL.min^{-1}$; split ratio 35:1

4.5.3 Quantification of terminal dienes

4.5.3.1 Quantification of 1c - 6c

Calibration of **1c - 6c** was done in a range from 50 µM to 5 mM. Therefore stock-solutions of the product standards were prepared and dilution was done as shown in Table 18.

Table 18: Dilution scheme for calibration of terminal dienes.

c_{final} [mM]	$c_{stock\text{-}solution}$ [mM]	Dilution scheme
0	0	solvent
0.05	1	100 µL (2 mM stock) + 100 µL solvent
0.1	2	100 µL (4 mM stock) + 100 µL solvent
0.2	4	80 µL (10 mM stock) + 120 µL solvent
0.5	10	100 µL (20 mM stock) + 100 µL solvent
1	20	100 µL (40 mM stock) + 100 µL solvent
2	40	100 µL (80 mM stock) + 100 µL solvent
3	60	60 µL (100 mM stock) + 40 µL solvent
4	80	160 µL (100 mM stock) + 40 µL solvent
5	100	100 mM stock solution

In a 4 mL glass vial KPi-buffer (950 µL; pH 7; 0.1 M) were mixed with HCl (100 µL; 5 N) and EtOAc (500 µL) containing the internal standard (0.1 % (v/v) 1-decanol) and finally the stock solutions containing the product standard (50 µL) were added and mixed thoroughly. The product standard was added last to avoid evaporation due to the poor solubility of the terminal dienes in KPi-buffer. Derivatization was done as described in chapter 4.4 followed by analysis with GC-FID. The calibration for **6c** and **5c** was done on ice with ice-cooled solutions to prevent evaporation of the products. Figure 23 shows the calibration curve of **3c** as one example for calibration of medium and long chain terminal dienes.

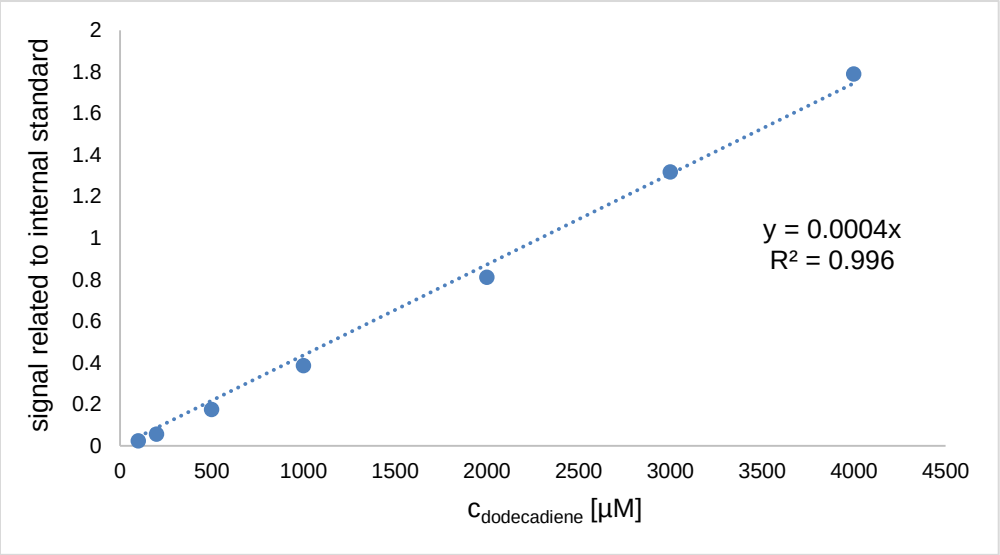

Figure 23: Calibration curve of **3c** within the linear range (0.05 to 4 mM) measured on GC-FID.

4.5.3.2 Quantification of 7c - 10c and 12c - 15c

Calibration for quantification of **7c - 9c** was done in a range from 50 µM to 2 mM, since product concentrations did not exceed 2 mM. For quantification the same dilution scheme than for the higher terminal dienes (Table 18) was used. In 4 mL glass vials pre-filled with KPi-buffer (950 µL; pH 7.5; 0.1 M) the stock solutions containing the product standard (50 µL) were added. All steps were done at 4 °C with ice-cooled solution and for **9c** the solutions (KPi-buffer, EtOH and product standard) were pre-cooled in liquid nitrogen. While the KPi-buffer was frozen, EtOH and the terminal diene remained liquid when cooling them for about 20 s in liquid nitrogen. Measurements were done by headspace GC-MS (see chapter 4.5.2). For detection and quantification of **9c** and **8c** the ion extraction mode of the detector was used, since there was a strong overlapping of products with the signals of CO_2 and EtOH (Figure S104 and Figure S109). Figure 24 shows the calibration curve of **9c** as one example for calibration of short chain terminal dienes, where extracted ion mode (*m*/z = 68) was used.

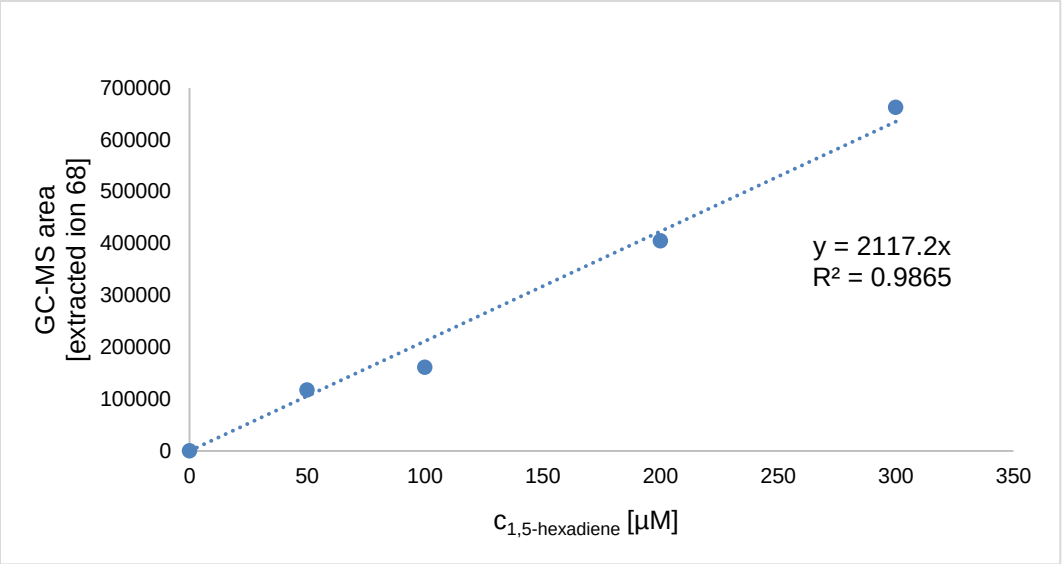

Figure 24: Calibration curve of **9c** within the linear range (0 to 300 µM) measured on Headspace GC-MS. Extracted ion *m*/z = 68 was used for analysis.

Quantification of **12c - 15c** and **10c** was done in a range from 50 µM to 3 mM using the dilution scheme shown in Table 19. Calibration was done in 2 mL scale in 20 mL vials tightly closed with a PTFE-septum. The vials were pre-filled with KPi-buffer (1.9 mL; pH 7.5; 0.1 M) and of the stock solutions containing the product standard (100 µL) were added. All steps were done at 4 °C with ice-cooled solution and for **10c** the solutions were pre-cooled in liquid nitrogen. Preparation of the calibration solution for **10c** was done as described before (see chapter 4.5.3.2). Headspace GC-MS measurement with auto sampler were done for analysis. Also for detection and quantification of **12c - 15c** and **10c** the ion extraction mode of the detector was used (Figure S148, Figure S156, Figure S160, Figure S164 and Figure S168).

Table 19: Dilution scheme for calibration of **10c** and **12c – 15c**.

c_{final} [mM]	$c_{stock\text{-}solution}$ [mM]	Dilution scheme
0	0	solvent
0.05	1	500 µL (2 mM stock) + 500 µL EtOH
0.1	2	300 µL (4 mM stock) + 600 µL EtOH
0.3	6	600 µL (10 mM stock) + 400 µL EtOH
0.5	10	600 µL (15 mM stock) + 300 µL EtOH
0.75	15	500 µL (30 mM stock) + 500 µL EtOH
1.5	30	500 µL (60 mM stock) + 500 µL EtOH
3	60	600 µL (100 mM stock) + 400 µL EtOH

4.6 Upscaling of selected biotransformations for product isolation and identification

Upscaling of biotransformations with **6a**, **3a** and **1a** were done for two reasons. First there was the need of product isolation to verify the formation of the main products (terminal dienes, β-hydroxy-dioic and β-hydroxy-ω-enoic acids). For that product isolation and analysis via ^{1}H-NMR was necessary since there were no commercial standards available for **1c** as well as for the β-hydroxy-dioic and β-hydroxy-ω-enoic acids. Further isolated yields were determined to estimate application of the system in larger scale synthesis.

4.6.1 Isolation and purification of 1c and 3c from biotransformations with 1a and 3a

For the isolation and purification of **1c** and **3c** biotransformations with **1a** and **3a**, respectively, were done in a 50 mL scale (stirred in a 250 mL round bottom flask at 200 rpm, 24 h and RT) using the standard OleT-CamAB-FDH system as described in chapter 4.3.1. The reaction was quenched either by freezing in liquid nitrogen and adding dichloromethane (DCM) to the frozen solution (**3a**) or directly adding DCM (**1a**). Freezing of the biotransformation was done to prevent evaporation of **3c**. Then product extraction from the biotransformations (**1a** and **3a**) was done with DCM (3 times, 50 ml, each). After combining and drying all organic phases with Na_2SO_4 evaporation of the solvent was done (850 mbar and 40 °C for **1c** and dry air-flow for **3c**). Subsequently, the terminal diene (**1c** or **3c**) was purified over silica column-chromatography with DCM as mobile phase. A thin-layer chromatography (TLC; silica plates) of all collected fractions (DCM as mobile phase; staining with $KMnO_4$) was done to identify the fractions containing the target products. Since terminal dienes are unpolar they eluted in the first fractions (R_f = 1). The fractions containing the product (**1c** or **3c**) were combined, dried with Na_2SO_4 and residual solvent was evaporated (850 mbar; 40 °C). Isolated yield was determined and analysis was done with GC-MS and ^{1}H-NMR (solvent for both, **1c** and **3c,** was $CDCl_3$).

4.6.2 Isolation and purification of 3f-dimethylester

For isolation and purification of the **3f**-dimethylester two biotransformations with **3a** (10 mM) were done in a 10 mL scale (stirred in a 100 mL round bottom flask at RT for 24 h and 200 rpm), each, using standard OleT-CamAB-FDH system as described in chapter 4.3.1. The

reactions were quenched with HCl (1 mL, 5 N) and then the product was extracted with EtOAc (3 times, 5 mL, each). After combining the organic phases the solvent was evaporated (230 mbar; 40 °C) until a solid was obtained. Elimination of remaining water was achieved by freeze drying under vacuum. Afterward the sample was dissolved in EtOAc (8 mL), dried with Na_2SO_4 and mixed with methanol (3.2 mL). Esterification was achieved by adding $TMSCHN_2$ (3 times 50 µL, each) over a period of 30 min. After evaporating the solvent (210 mbar; 40 °C) **3f**-dimethylester was purified over silica column chromatography (mobile phase: hexane:EtOAc 3:1). TLC (eluent: hexane:EtOAc 3:1; staining: $KMnO_4$) of all fractions was done to identify the fractions that contain the target product (R_f = 0.26). After combining all fractions containing **3f**-dimethylester, they were dried with Na_2SO_4 and solvent was evaporated (200 mbar; 30 °C). Isolated yield was determined and analysis was done with GC-MS and ^{1}H-NMR (solvent $CDCl_3$).

4.6.3 **Isolation and purification of 6g-methylester**

For the isolation and purification of the product a biotransformation with **6a** was done in a 50 mL scale (stirred in a 250 mL round bottom flask at RT for 24 h and 200 rpm) using standard OleT-CamAB-FDH system as described in chapter 4.3.1. The reaction was quenched with HCl (1 mL, 5 N) followed by extraction of the product with EtOAc (3 times, 50 mL, each). After combining the organic phases the solvent was evaporated (230 mbar; 40 °C) until a solid was obtained. Elimination of remaining water was achieved by freeze-drying under vacuum. Afterwards, the sample was dissolved in EtOAc (8 mL), dried with Na_2SO_4 and mixed with methanol (3.2 mL). Esterification was achieved by adding $TMSCHN_2$ (3 times 50 µL, each) over a period of 30 min. The solvent was evaporated (210 mbar; 40 °C) followed by purification of the **3g**-methylester over silica column chromatography (mobile phase: hexane:EtOAc 3:1). Fractions containing the target product were identified by TLC (mobile phase: hexane:EtOAc 3:1; staining: $KMnO_4$; R_f of the product was 0.5) and combined. After drying the fraction with Na_2SO_4 solvent was evaporated (210 mbar; 40 °C), isolated yield was determined and analysis was done with GC-MS and ^{1}H-NMR (solvent $CDCl_3$).

4.7 Product derivatization methods for low-boiling alkenes

Product derivatization was done to be able to verify product formation and to do analysis and quantification of low boiling dienes (**8c - 10c**) and alkenes (**12c - 15c**). First it was tried to obtain the corresponding product standards, since bis-epoxides and tetra-brominated standards of **8c - 10c** are not commercially available.

4.7.1 Epoxidation of 8c - 9c using mCPBA

The aim of the epoxidation of terminal dienes was to obtain a bis-epoxide of the product standard to prove the formation of the terminal dienes during biotransformation and further quantify the products. First epoxidation of the product standards (**8c, 9c**) was done. For each derivatization reaction mCPBA (1.6 g, ≈ 10 mmol) was dissolved in DCM (> 99.8 %; 100 mL) using a 250 mL round bottom flask and afterwards the reaction was started by adding **8c** or **9c** (140 µL; ≈ 1 mmol), respectively. The flask was closed with a glass plug and stirred overnight. Afterwards ddH_2O (50 mL) was added to the reaction, the organic phase was collected and washed with $NaHCO_3$ solution (5 %; 5 times with 100 mL, each). The formation of the bis-epoxide was confirmed by GC-MS, followed by evaporation of the solvent (850 mbar, 40 °C) and purification over column chromatography (stationary phase: Al_2O_3 neutral; mobile phase: EtOAc:hexanes 1:6). Fractions containing the target product were identified by TLC [mobile phase: EtOAc:hexanes 1:6; staining with UV and cerium molybdate; R_f of the products (**8c**-bis-epoxide and **9c**-bis-epoxide) was 0.6]. The fractions containing the product were combined and solvent was evaporated (240 mbar; 40 °C). Analysis was done via GC-MS and ^{1}H-NMR.

4.7.2 Bromination of 9c - 10c and 12c - 15c

The aim of the bromination of terminal dienes was to obtain a tetra-brominated product standard to prove the formation of the terminal dienes during biotransformation and further quantify the products. First bromination of the product standards (**9c**; **10c**) was done. For that a 50 mL round bottom flask was pre-filled with DCM (15 mL; > 99.8 %), Br_2 (510 µL, ≈ 20 mmol) were added and finally the reaction was started by adding the terminal diene (≈ 300 µL, ≈ 3 mmol). The flask was closed with a drying tube filled with $CaCl_2$ and covered with aluminium foil to prevent side reactions caused by moisture or light. The reaction was stirred over night, the solvent was evaporated under dry airflow and the product was washed with DCM (3 times, 10 mL). Analysis was done with GC-MS and ^{1}H-NMR (solvent $CDCl_3$).

Formation of branched 1-alkenes (**12c - 15c**) from branched fatty acids (**12a - 15a**) was identified by in-situ bromination. First all brominated product standards were synthesized. For each product standard a 4 mL closed glass vials was filled with dry DCM (1 mL) mixed with Br_2 (100 µL, ≈ 2 mmol) and **12c - 15c** (200 µL, ≈ 1.7 mmol), respectively. Reaction vials were covered with aluminium foil and stirred for 1.5 h at 100 rpm. Solvent was evaporated under dry air flow and washed with DCM (5 times, 1 mL, each). Analysis was done with GC-MS and ^{1}H-NMR (solvent $CDCl_3$).

4.8 In-situ derivatization of low boiling products (10c – 15c)

There were several in-situ derivatisation experiments performed for identification of **12c - 15c, 10c** and **11c**. For all derivatisation methods a biotransformation with OleT-CamAB-FDH cascade was carried out in 10 mL scale stirred at 100 rpm in a 50 mL 2-necked round bottom flask using standards reaction conditions. One neck was tightly closed with a glass plug and the other one was closed with an impinger, where product trapping and derivatisation should take place. The derivatisation reagents were filled into the impinger and the derivatization solution was cooled with ice (when necessary) and not stirred. (Figure 25)

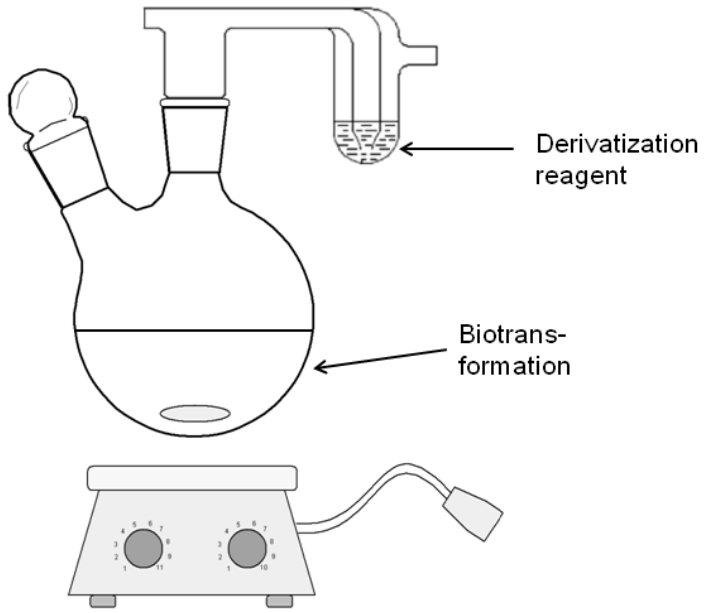

Figure 25: Reaction set-up for in-situ derivatization of low-boiling products.

4.8.1 In-situ bromination of biotransformations with 11a – 15a

Bromination for quantification and characterization of volatile 1-alkenes was already described by Dennig *et al.* [17]. In-situ bromination of biotransformation of **11a - 15a** was

done to obtain the corresponding brominated derivatives of **11c - 15c**. Biotransformations of **11a - 15a** were done in 10 mL scale at RT for 24 h using the standard reaction set-up as described in chapter 4.3.1. The impinger was filled with Br_2 in $CDCl_3$ (10 mL, 24 mM). After biotransformations were finished analysis of the brominated solutions was directly done by GC-MS and ^{1}H-NMR.

4.8.2 Product derivatization of 11c via sulfonation

Another derivatization method that was tried for **11c** was sulfonation to obtain the 3-sulfolene Scheme 28, chapter 2.5.4). For that the impinger was filled with H_2SO_3. After the reaction was finished the H_2SO_3-solution was extracted with chloroform (3 times, 30 mL, each). After evaporation of the solvent a yellow solid remained that was dissolved in $CDCl_3$. Analysis was done via ^{1}H-NMR and comparison with 3-sulfolene standard.

4.8.3 Product derivatisation of 11c by Diels-Alder reaction

Further a biotransformation with **11b** using standard reaction conditions was done and product trapping was tried by Diels-Alder reaction (Scheme 29, chapter 2.5.4). For the Diels-Alder reaction maleic anhydride was used as dienophile, $AlCl_3$ as catalyst and THF as solvent [57]. For that the impinger was filled with $AlCl_3$ (0.005 mmol) and maleic anhydride (1 mmol) suspended in THF (4 mL). After reaction was finished, the solvent was evaporated (40 °C, 280 mbar) and the residue was dissolved in EtOH (3 mL) and 4 drops of concentrated H_2SO_4 were added. This solution was stirred for about 2 h. Product and substrate standards were also dissolved in EtOH and esterified with H_2SO_4. A TLC (hexane:EtOAc 3:1) was done to check product formation.

4.8.4 Wacker oxidation of 10c

Derivatisation of **10c** was tried by Wacker Oxidation (Scheme 27, chapter 2.5.2). For that **10c** (200 µL, ≈ 2 mmol) was mixed with KPi-buffer (10 mL) in the round bottom flask. The impinger was filled with CuCl (2 mmol) and $PdCl_2$ (0.2 mmol) suspended in 10 mL DMF:H_2O (7:1). Reaction was performed at RT for 24 h and then the solution was quenched with ice-cold HCl (20 mL; 3 M). The solution was extracted with di-ethylether (4 times, 20 mL, each) and then the organic phase was washed with saturated $NaHCO_3$ solution (2 times, 50 mL, each). After drying the organic phase with Na_2SO_4 analysis was done by GC-MS and compared to acetyl-acetone product standard [58].

5 Abbreviations

ALA	δ-aminolevulinic acid
APS	Ammonium persulfate
Bp	Boiling point
BSTFA	*N*,*O*-bis(trimethylsilyl)trifluoroacetamide with trimethylchlorosilane
DCM	Dichloromethane
DMF	Dimethylformamide
DMSO	Dimethylsulfoxide
EtOAc	Ethyl acetate
EtOH	Ethanol
FAD	Flavin adenine dinucleotide
FDH	Formate dehydrogenase
FID	Flame ionization detector
FMN	Flavin mononucleotide
GC	Gas chromatography
HS	Headspace
IPTG	Isopropyl β-D-1-thiogalactopyranoside
ISD	Internal standard
KPi	Potassium phosphate
LB	Lysogeny broth
*m*CPBA	Meta chloroperoxybenzoic acid
MeOH	Methanol
MS	Mass spectrometer
NAD(P)H	Nicodinamide adenine dinucleotide (phosphate) hydrogen
PTFE	Polytetrafluoroethylene
ROMP	Ring opening metathesis polymerization
RT	Room temperature
SDS	Sodium dodecyl sulfate
SHOP	Shell higher olefin process
TB	Terrific broth
TEMED	Tetramethylethylenediamine
THF	Tetrahydrofuran
TLC	Thin layer chromatography
$TMSCHN_2$	Trimethylsilyl diazomethane in diethyl ether
TON	Turnover number
TTN	Total turnover number

6 Literature

[1] S. P. Pyl, T. Dijkmans, J. M. Antonykutty, M. F. Reyniers, A. Harlin, K. M. Van Geem, G. B. Marin, *Bioresour. Technol.* **2012**, *126*, 48–55.

[2] H.-J. Arpe, *Industrielle Organische Chemie*, 6th ed., WILEY-VCH: Weinheim Germany, 2007; a) p. 96, b) pp. 68-72.

[3] http://www.standort-ludwigshafen.basf.de/group/corporate/site-ludwigshafen/de/about-basf/worldwide/europe/Ludwigshafen/Education/Lernen_mit_der_BASF/steamcracker/Reaktionsbedingungen. [Accessed: 06-Jun-2016].

[4] http://refiners-notes.blogspot.co.at/2013/06/steam-cracking-part-2.html. [Accessed: 06-Jun-2016].

[5] W. Keim, *Angew. Chem. Int. Ed.* **2013**, *52*, 12492–12496.

[6] J. Hagen, *Industrial Catalysis*, 3th ed., WILEY-VCH: Weinheim Germany, 2015; a) pp. 59-61, b) p. 71, pp. 388-389.

[7] P. W. N. M. V. E. van Leeuwen in *Sci. Synth., C-1 Build. Blocks Org. Synth.* **2014**, *2*, 349–353.

[8] Y. Liu, K. E. Kim, M. B. Herbert, A. Fedorov, R. H. Grubbbs, B. M. Stoltz, *Adv. Synth. Catal.* **2014**, *356*, 130–136.

[9] J. Murray, D. King, *Nature* **2012**, *481*, 433–435.

[10] J. C. Philp, R. J. Ritchie, J. E. Allan, *Trends Biotechnol.* **2013**, *31*, 219–222.

[11] R. Cernansky, *Nature* **2015**, *519*, 379-380.

[12] A. J. J. Straathof, *Chem. Rev.* **2014**, *114*, 1871–1908.

[13] U. Biermann, U. Bornscheuer, M. A. Meier, J. O. Metzger, H. J. Schäfer, *Angew. Chem. Int. Ed.* **2011**, *50*, 3854–3871.

[14]http://www.sigmaaldrich.com/catalog/search?term=grubbs+catalyst&interface=All&N=0&mode=match partialmax&lang=de&region=AT&focus=product. [Accessed: 06-Jun-2016].

[15] H. Rudolph, *Das Edelmetall-Buch Gold-Silber-Platin-Palladium-Ruthenium-Rhodium-Osmium-Iridium*, epubli GmbH: Berlin Germany, 2013; p. 189.

[16] J. A. Miller, J. A. Nelson, M. P. Byrne, *J. Org. Chem.* **1993**, *58*, 18–20.

[17] A. Dennig, M. Kuhn, S. Tassoti, A. Thiessenhusen, S. Gilch, T. Bülter, T. Haas, M. Hall, K. Faber, *Angew. Chem. Int. Ed.* **2015**, *54*, 8819–8822.

[18] K. Faber, *Biotransformations in Organic Chemistry*, 6th ed., Springer-Verlag: Berlin Heidelberg, 2011; a) p. 4, b) pp. 177-181, c) pp. 315-321, d) pp. 80-81.

[19] M. A. Rude, T. S. Baron, S. Brubaker, M. Alibhai, S. B. Del Cardayre, A. Schirmer, *Appl. Environ. Microbiol.* **2011**, *77*, 1718–1727.

[20] I. Matsunaga, A. Ueda, N. Fujiwara, T. Sumimoto, K. Ichihara, *Lipids* **1999**, *34*, 841–846.

[21] J. Belcher, K. J. McLean, S. Matthews, L. S. Woodward, K. Fisher, S. E. Rigby, D. R. Nelson, D. Potts, M. T. Baynham, D. A. Parker, D. Leys, A. W. Munro, *J. Biol. Chem.* **2014**, *289*, 6535–6550.

[22] Y. Liu, C. Wang, J. Yan, W. Zhang, W. Guan, X. Lu, S. Li, *Biotechnol. Biofuels* **2014**, *7*, 28–39.

[23] Z. Rui, X. Li, X. Zhu, J. Liu, B. Domigan, I. Barr, J. H. Cate, and W. Zhang, *Proc. Natl. Acad. Sci. U. S. A.* **2014**, *111*, 18237–18242.

[24] I. Zachos, S. K. Gaßmeyer, D. Bauer, V. Sieber, F. Hollmann, R. Kourist, *Chem. Commun.* **2015**, *51*, 1918–1921.

[25] B. Chen, D. Y. Lee, M. W. Chang, *Metab. Eng.* **2015**, *31*, 53–61.

[26] T. Omura, R. Sato, *J. Biol. Chem.* **1964**, *239*, 2379-2385.

[27] B. Meunier, S. P. de Visser, S. Shaik, *Chem. Rev.* **2004,** *104*, 3947-3980.

[28] R. Bernhardt, V. B. Urlacher, *Appl. Microbiol. Biotechnol.* **2014**, *98*, 6185–6203.

[29] M. T. Lundemo, J. M. Woodley, *Appl. Microbiol. Biotechnol.* **2015**, 99, 2465–2483.

[30] M. Girhard, S. Schuster, M. Dietrich, P. Dürre, V. B. Urlacher, *Biochem. Biophys. Res.*

Commun. **2007**, *362*, 114–119.

[31] P. T. Anatas, *Green Catalysis Volume 3: Biocatalysis*, WILEY-VCH: Weinheim Germany, 2009; a) pp. 3-5, b) pp. 12-18.

[32] F. Hannemann, A. Bichet, K. M. Ewen, R. Bernhardt, *Biochim. Biophys. Acta*. **2007**, *1770*, 330–344.

[33] S. Kadkhodayan, E. D. Coulter, D. M. Maryniak, T. A. Bryson, J. H. Dawson, *J. Biol. Chem.* **1995**, *270*, 28042–28048.

[34] P. W. Roome, J. C. Philley, J. A. Peterson, *J. Biol. Chem.* **1983**, *258*, 2593–2598.

[35] J. L. Grant, C. H. Hsieh, T. M. Makris, *J. Am. Chem. Soc.* **2015**, *137*, 4940–4943.

[36] M. Pollard, F. Beisson, Y. Li, J. B. Ohlrogge, *Trends Plant Sci.* **2008**, *13*, 236–246.

[37] Z. Cong, K. Kawamura, S. Kang, P. Fu, *Sci. Rep.* **2015**, *5*, 9580.

[38] G. Mingrone, M. Castagneto, *Nutr. Rev.* **2006**, *64*, 449–456.

[39] N. M. Carballeira, M. Reyes, A. Sostre, H. Huang, M. F. Verhagen, M. W. Adams, *J. Bacteriol.* **1997**, *179*, 2766–2768.

[40] H. Song, S. Y. Lee, *Enzyme Microb. Technol.* **2005**, *39*, 352–361.

[41] T. Polen, M. Spelberg, M. Bott, *J. Biotechnol.* **2013**, *167*, 75–84.

[42] S. Picataggio, T. Rohrer, K. Deanda, D. Lanning, R. Reynolds, J. Mielenz, L. D. Eirich, *Nat. Biotechnol.* **1992**, *10*, 894–898.

[43] D. L. Nelson and M. M. Cox, *Lehninger Biochemie*, 4th ed. Springer: Heidelberg, Germany, 2008; p. 880.

[44] V. Reipa, M. J. Holden, M. P. Mayhew, V. L. Vilker, *Biochim. Biophys. Acta* **2000**, *1459*, 1–9.

[45] M. Schrewe, M. K. Julsing, B. Bühler, A. Schmid, *Chem. Soc. Rev.* **2013**, *42*, 6346–77.

[46] D. Hamdane, Haoming Zhang, P. Hollenberg, *Photosynth. Res.* **2008**, *98*, 657–666.

[47] C. M. Jenkins, M. R. Waterman, *Biochemistry.* **1998**, *37*, 6106–6113.

[48] J. Clayden, N. Greeves, S. Warren, P. Wothers, *Organic Chemistry*, Oxford University Press, 2001; a) pp. 503-505, pp. 510-511, b) pp. 505-508, c) pp. 1039-1040.

[49] A. Dennig, *Engineering of cytochrome P450 monooxygenases for application in phenol synthesis*, dissertation, RWTH Aachen University, 2013.

[50] I. Matsunaga, A. Ueda, T. Sumimoto, K. Ichihara, M. Ayata, H. Ogura, *Arch. Biochem. Biophys.* **2001**, *394*, 45–53.

[51] https://www.gelifesciences.com/gehcls_images/GELS/Related Content/Files/1314735988470/litdoc11000888_20150304212650.pdf. [Accessed: 06-Jun-2016].

[52]http://www.sigmaaldrich.com/catalog/product/sigma/s3401?lang=de&region=AT&gclid=CNzBm_a3pMoCFVTNGwodFY8JUg. [Accessed: 06-Jun-2016].

[53] C. M. Jenkins, I. Pikuleva, N. Kagawa, M. R. Waterman, *Arch. Biochem. Biophys.* **1997**, *347*, 93–102.

[54] A. Schallmey, G. den Besten, I. G. P. Teune, R. F. Kembaren, D. B. Janssen, *Appl. Microbiol. Biotechnol.* **2011**, *89*, 1475–1485.

[55] T. Lacour, T. Achstetter, B. Dumas, *J. Biol. Chem.* **1998**, *273*, 23984–23992.

[56] http://www.sigmaaldrich.com/technical-documents/protocols/biology/enzymatic-assay-of-ferredoxin-nadp-reductase.html. [Accessed: 06-Jun-2016].

[57] F. Fringuelli, R. Girotti, F. Pizzo, L. Vaccaro, *Org. Lett.* **2006**, *8*, 2487–2489.

[58] J. Tsuji, H. Nagashima, H. Nemoto, *Org. Synth.* **1990**, *7*, 137-139.

7 Appendix

7.1 Conversion of diacids (1a-9a) with the OleT-CamAB-FDH cascade

7.1.1 Conversion of 1a

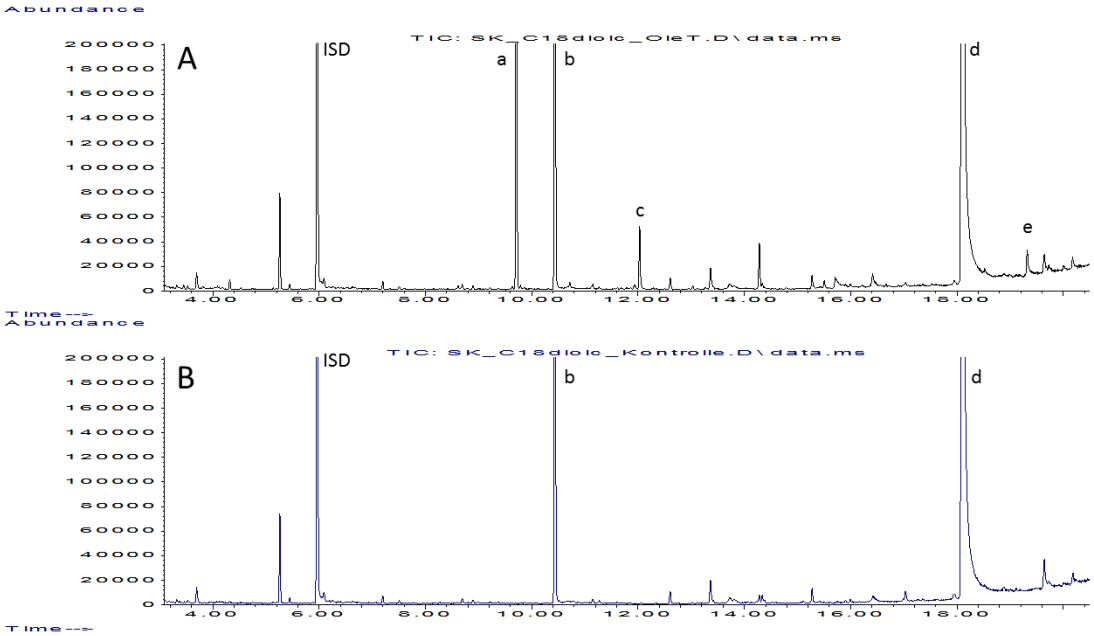

Figure S1. GC-MS chromatograms obtained by conversion of **1a** (10 mM). **A** = Conversion of **1a** with the OleT-CamAB-FDH system. **B** = Conversion of **1a** in the absence of OleT (negative control). **ISD** = internal standard (0.1 % (v/v) 1-decanol); **a** = **1c**; **b** = dimethyl ester of **7a** (present in all conversions and controls); **c** = side product (9 % GC area of all detected products); **d** = substrate (dimethyl ester of **1a**); **e** = **1f** (side product).

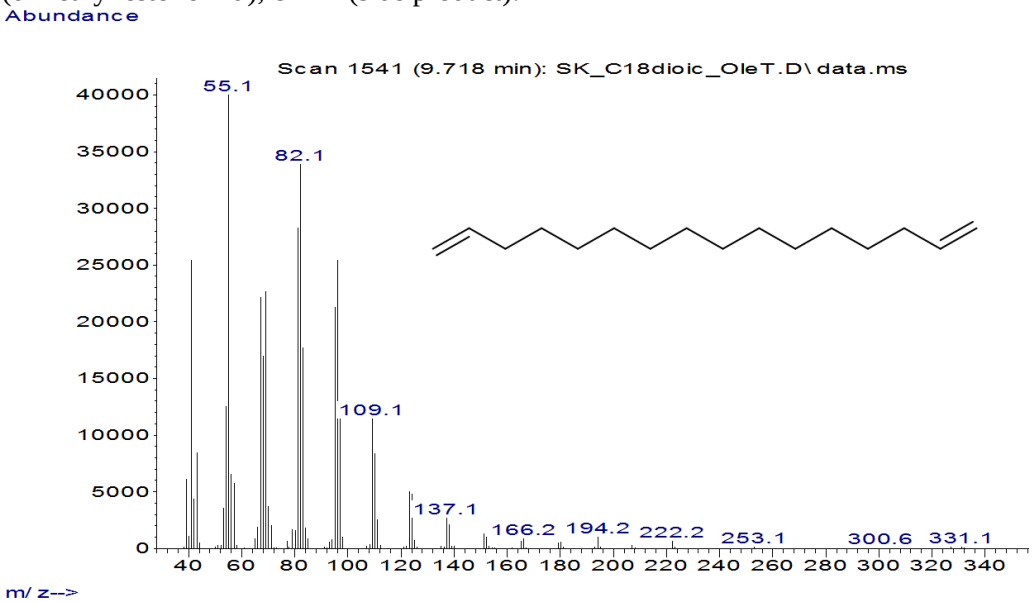

Figure S2. GC-MS spectra of crude **1c** (222.23 g mol^{-1}) obtained by conversion of **1a** (10 mM) with the OleT-CamAB-FDH system (corresponds to peak a in Figure S1 A).

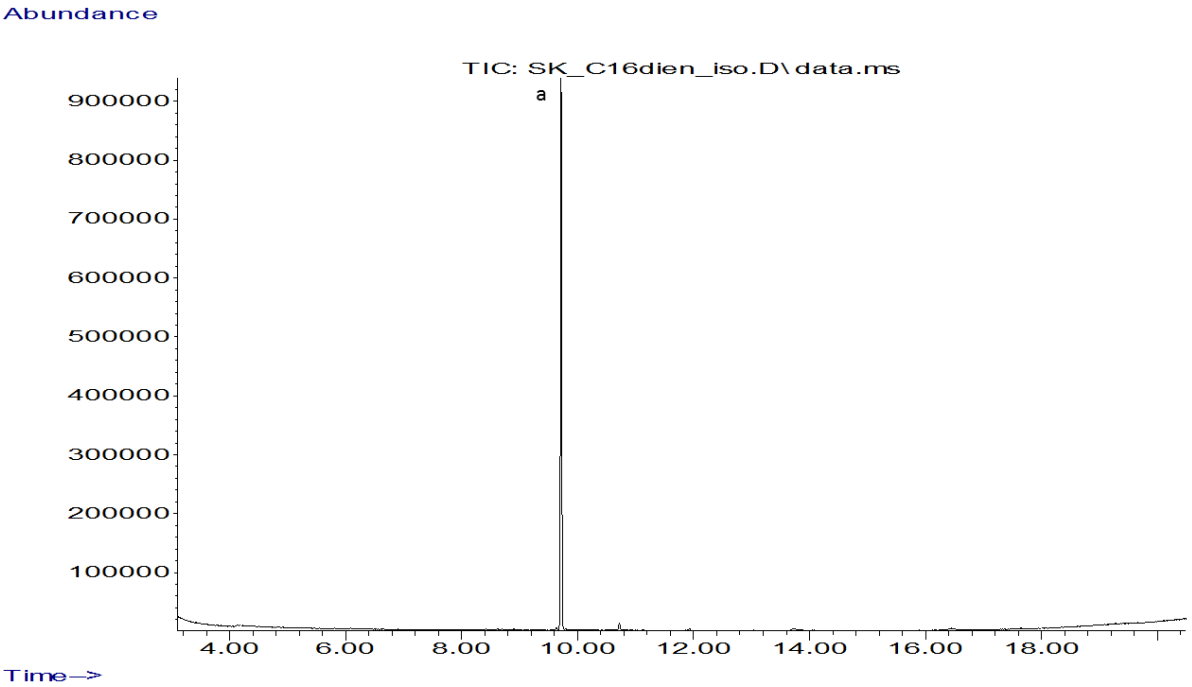

Figure S3. GC-MS chromatograms of isolated and purified **1c** (**a;** purity: ~93% GC-MS area) obtained by conversion of 10 mM **1a** with the OleT-CamAB-FDH system (50 mL scale).

1,15-Hexadecadiene (**1c**): Isolated yield from 50 mL reaction volume starting from 10 mM **1a** substrate. Clear oil (4.9 mg). ^{1}H-NMR (300 MHz, $CDCl_3$): δ = 5.90-5.77 (m, 2 H, C**H**=CH_2), 5.04-4-93 (m, 4 H, C$\mathbf{H_2}$=CH), 2.09-2.02 (m, 4 H, C$\mathbf{H_2}$CH=CH_2), 1.42-1.28 (m, 20 H, CH_2(C$\mathbf{H_2}$)$_{10}$$CH_2$).

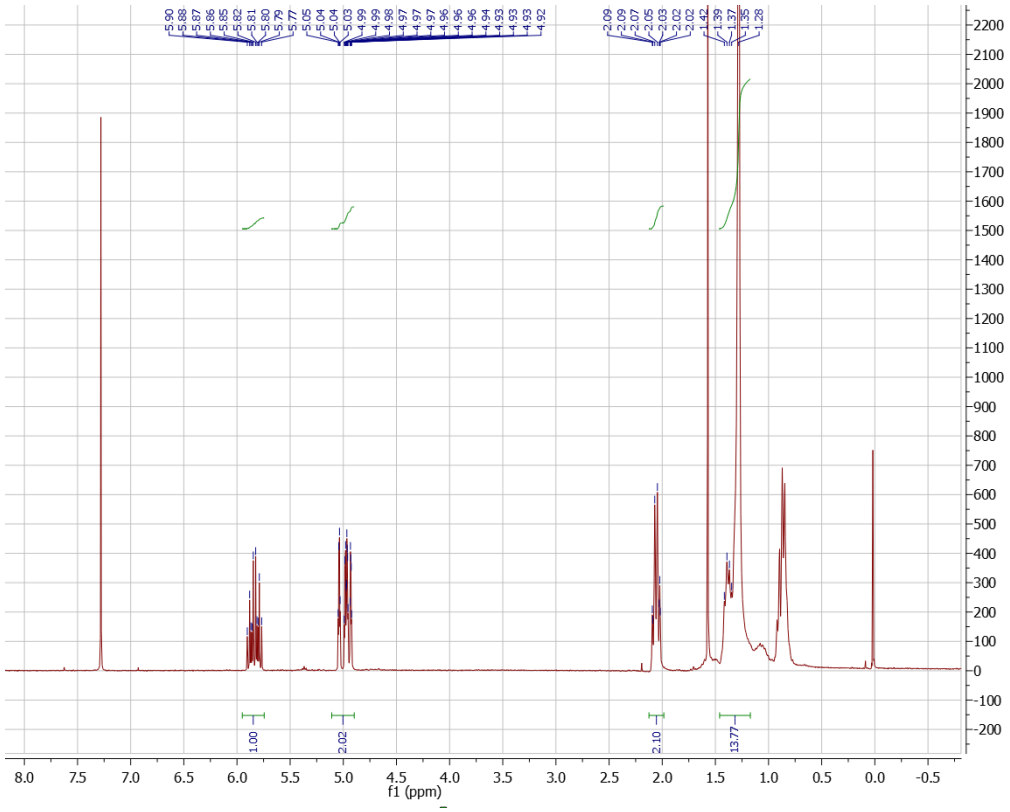

Figure S4. [1]H-NMR spectra of isolated and purified **1c** from a 50 mL conversion of 10 mM **1a** with the OleT-CamAB-FDH cascade.

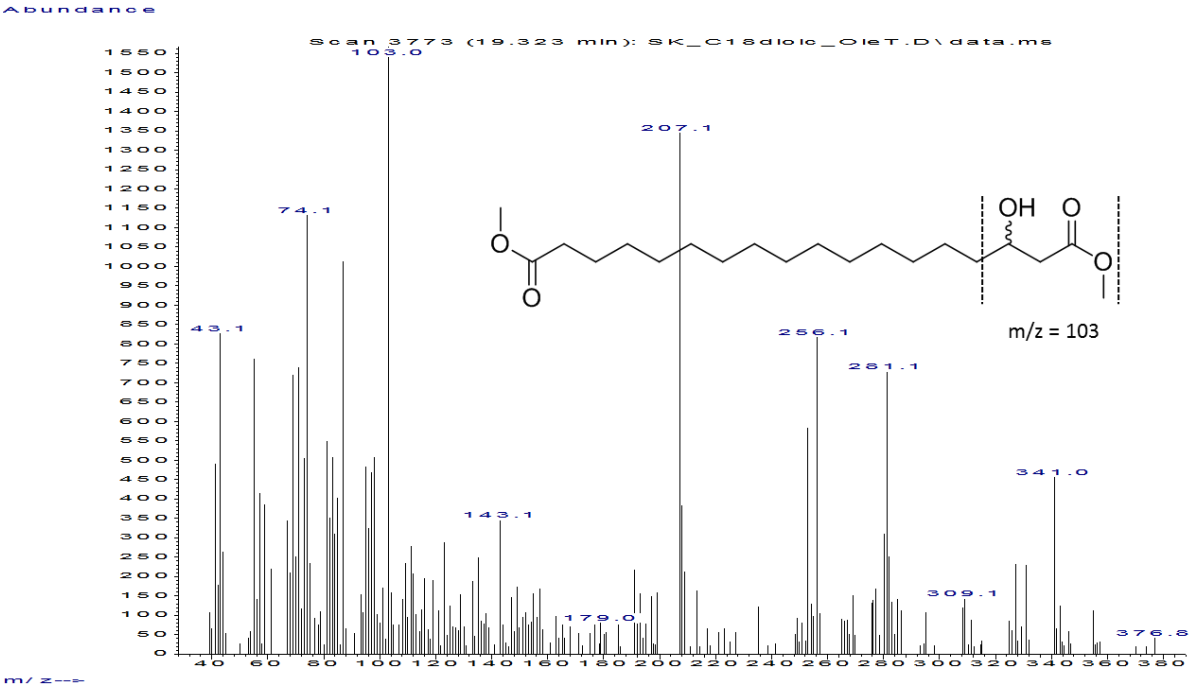

Figure S5. GC-MS spectra of dimethyl ester of **1f** obtained by conversion of **1a** (10 mM) with the OleT-CamAB-FDH system (corresponds to peak e in Figure S1). The ion *m*/z = 103 is characteristic for 3-hydroxy acid methyl esters.[1]

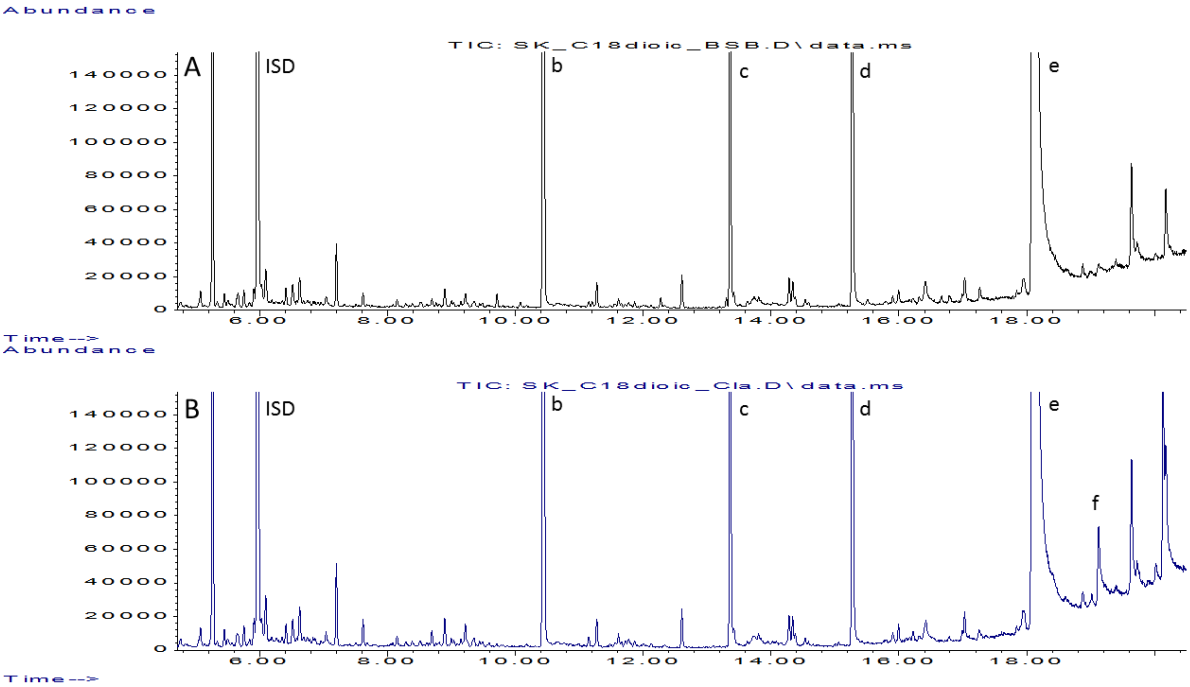

Figure S6. GC-MS chromatograms of conversion of **1a** (10 mM) with $CYP_{BSß}$ (**A**) and $P450_{Cla}$ (**B**) using H_2O_2 as oxidant. **ISD** = internal standard (0.1 % (v/v) 1-decanol); **b** = dimethyl ester of **6a** (present in all conversions); **c** and **d** = hexadecanoic acid methyl ester (270.26 g mol^{-1})/octadecanoic acid methyl ester (298.29 g mol^{-1}, suggested by GC-MS library; score/probability 99 %); **e** = substrate; dimethyl ester of **1a**; **f** = dimethyl ester of **1d**. Purity of the substrate was 95 %.

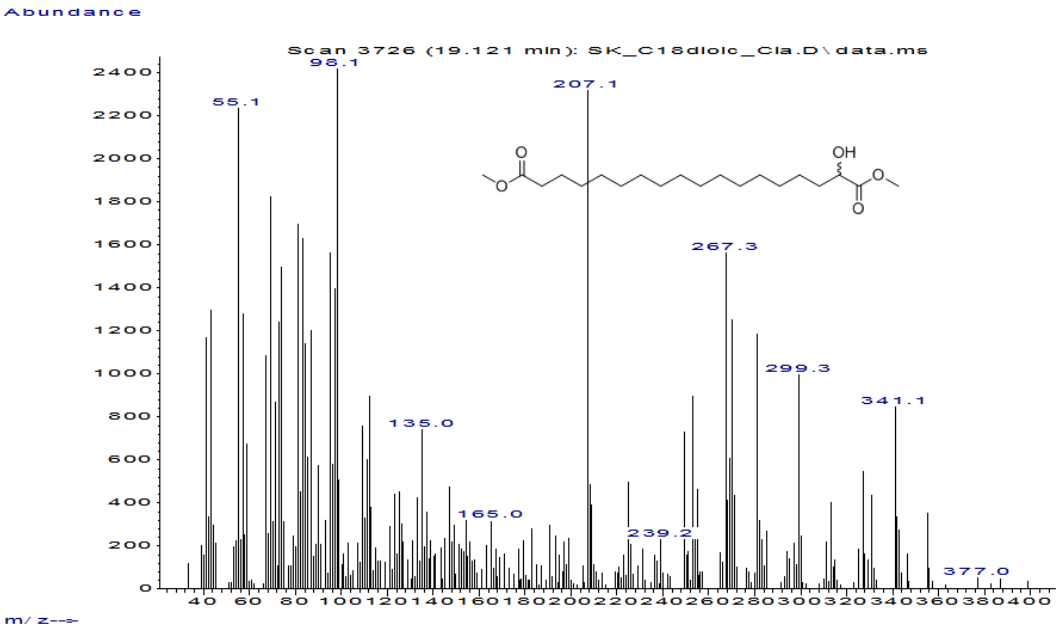

Figure S7. GC-MS spectra of dimethyl ester of **1d** (358.27 g mol^{-1}) obtained by conversion of **1a** (10 mM) with $P450_{Cla}$ and H_2O_2 as oxidant (corresponds to peak f in Figure S6 B).

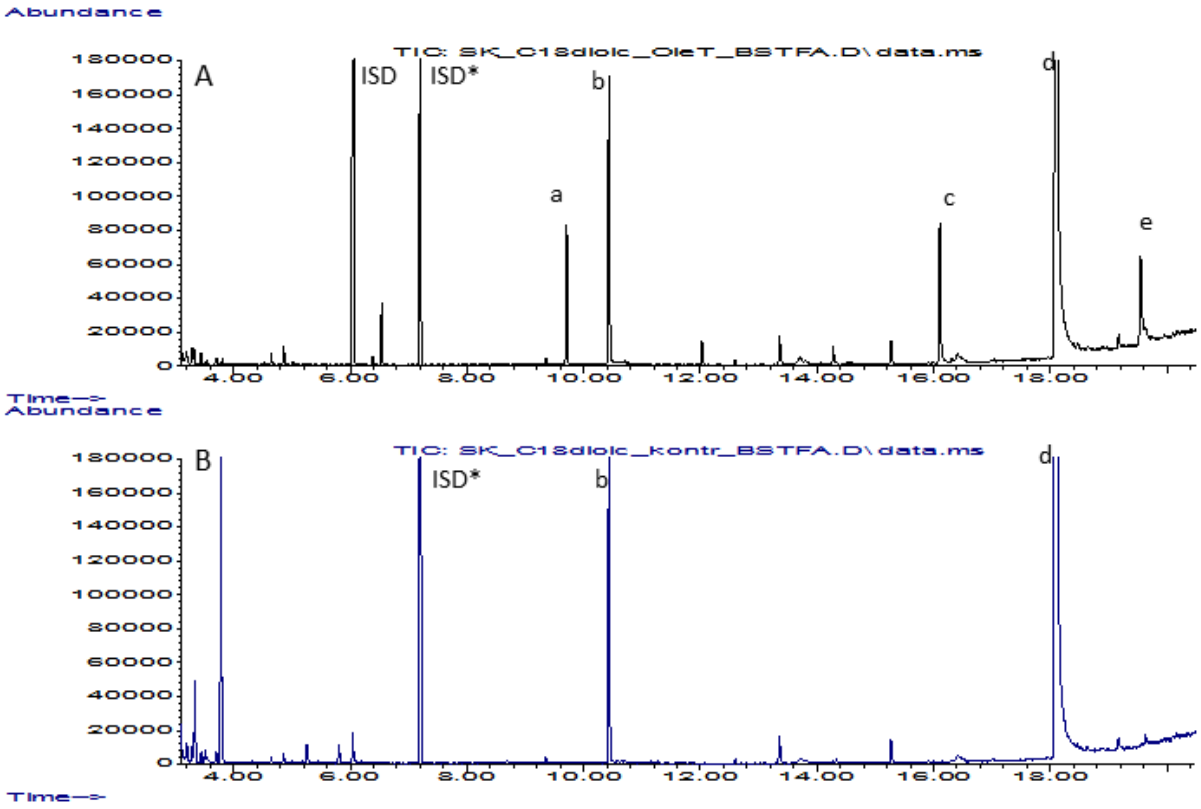

Figure S8. GC-MS chromatograms obtained by conversion of **1a** (10 mM) after derivatization with $TMSCHN_2$ and BSTFA. **A** = Conversion of **1a** with the OleT-CamAB-FDH system. **B** = Conversion of **1a** in the absence of OleT (negative control). **ISD** = internal standard (0.1 % (v/v) 1-decanol); **ISD*** = silylated internal standard (TMS-1-decanol); **a** = **1c**; **b** = dimethyl ester of **6a** (present in all conversions); **c** = TMS-**1g** dimethyl ester; **d** = substrate; dimethyl ester of **1a**; **e** = TMS-**1f**-dimethyl ester.

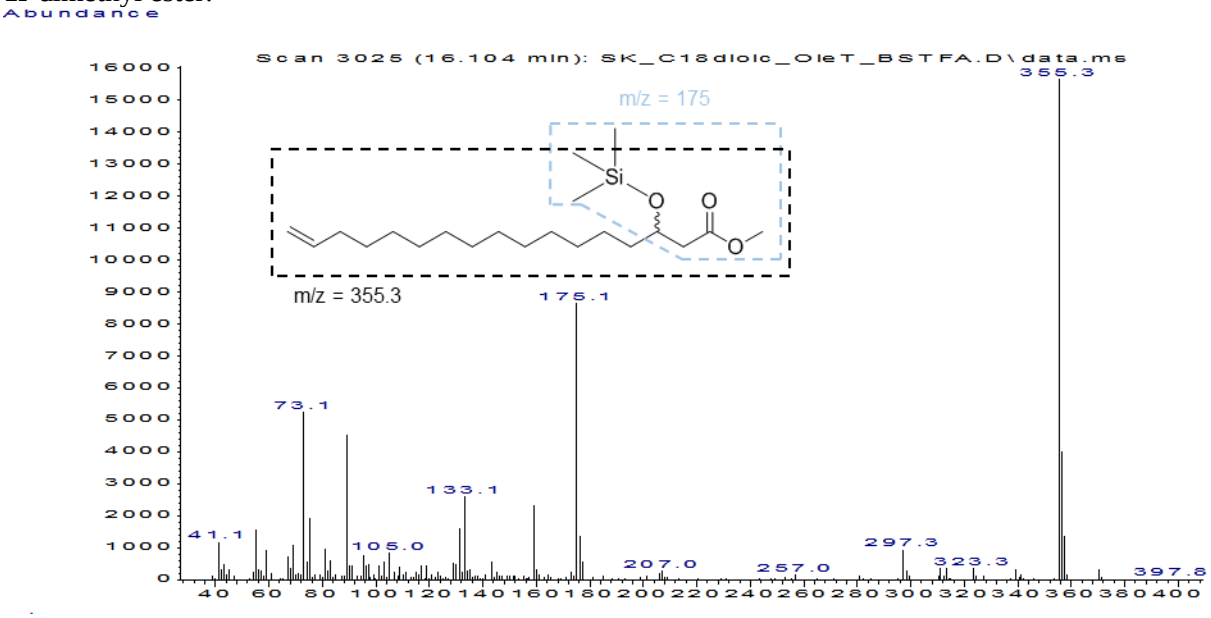

Figure S9. GC-MS spectra of TMS-**1g** dimethyl ester obtained by conversion of **1a** (10 mM) with the OleT-CamAB-FDH system (corresponds to peak c in Figure S8 A). The characteristic ions *m*/z = 175.1 and *m*/z = 355.3 were used to assign the minor side product as described elsewhere.[2]

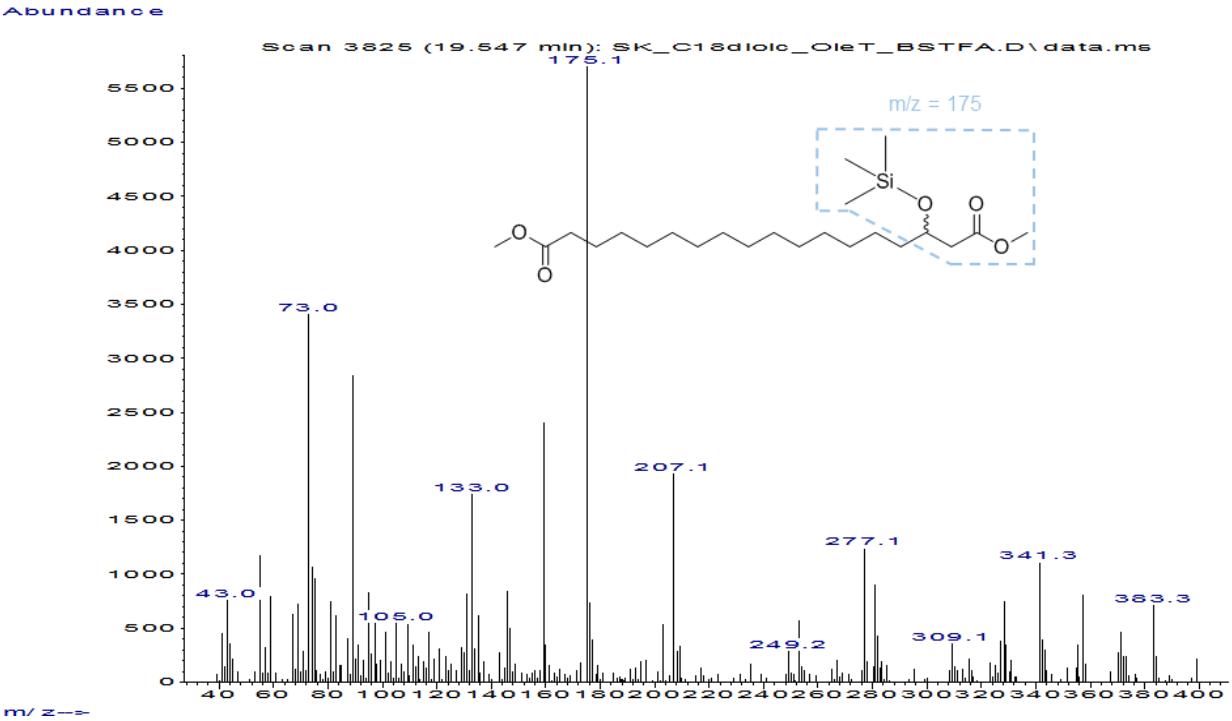

Figure S10. GC-MS spectra of TMS-**1f**-dimethyl ester obtained by conversion of **1a** (10 mM) with the OleT-CamAB-FDH system (corresponds to peak e in Figure S8 A). The characteristic ion *m*/z = 175.1 was used to assign the product as described elsewhere.[2]

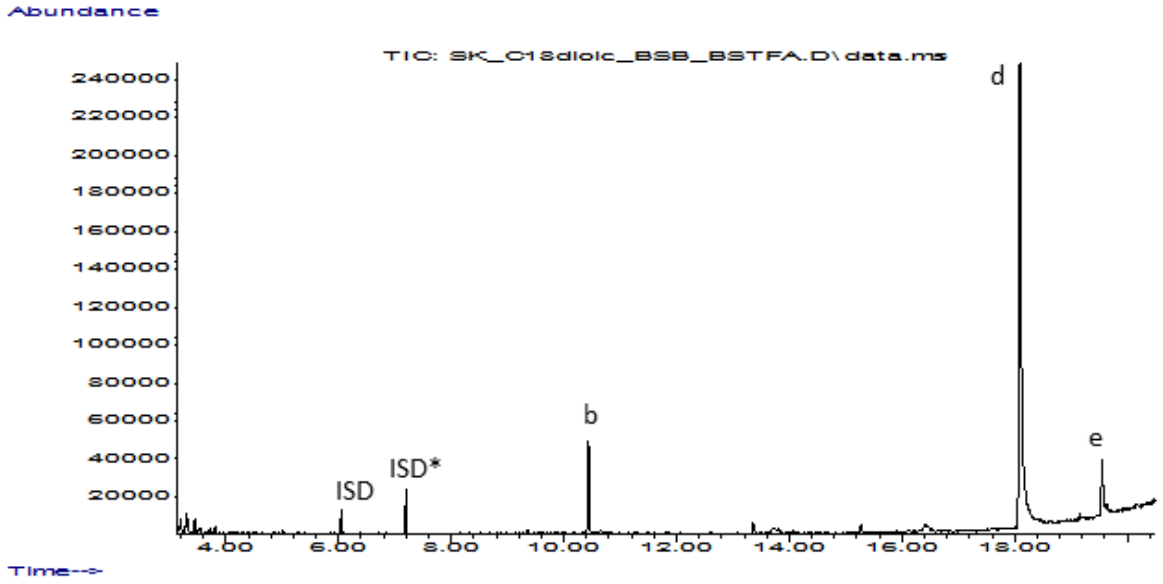

Figure S11. GC-MS chromatograms obtained by conversion of **1a** (10 mM) with $CYP_{BS\beta}$ and H_2O_2 as oxidant after derivatization with $TMSCHN_2$ and BSTFA. **ISD** = internal standard (0.1 % (v/v) 1-decanol); **ISD*** = silylated internal standard; **b** = dimethyl ester of **6a** (present in all conversions); **d** = substrate; dimethyl ester of **1a**; **e** = TMS-**1f**-dimethyl ester.

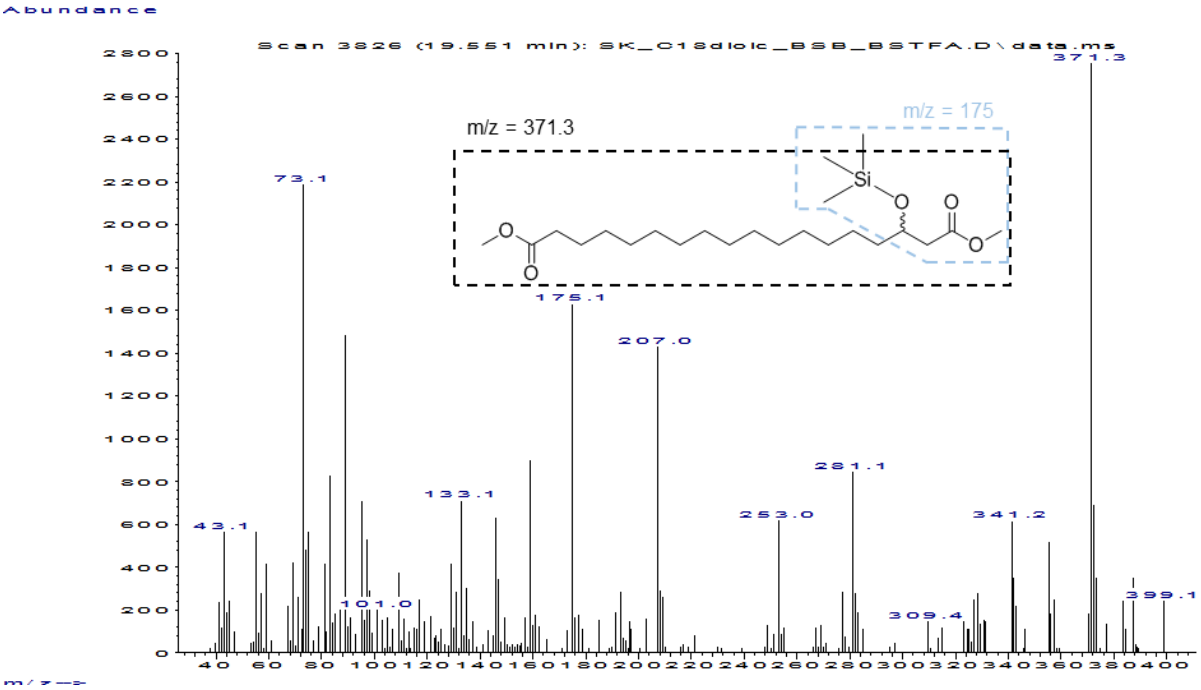

Figure S12. GC-MS spectra of TMS-**1f**-dimethyl ester obtained by conversion of **1a** (10 mM) with $CYP_{BS\beta}$ and H_2O_2 as oxidant (corresponds to peak e in Figure S11). The characteristic ions *m*/z = 175 and *m*/z = 371 were used to assign the minor side product as described elsewhere.[2]

7.1.2 **Conversion of 2a**

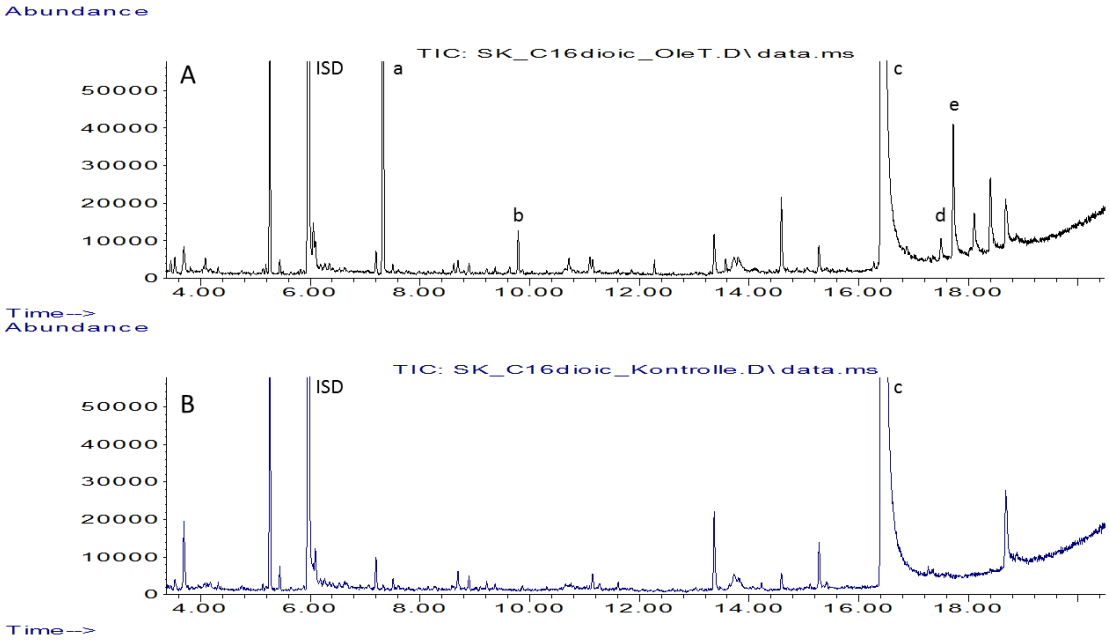

Figure S13. GC-MS chromatograms obtained by conversion of **2a** (10 mM). **A** = Conversion of **2a** with the OleT-CamAB-FDH system. **B** = Conversion of **2a** in the absence of OleT (negative control). **ISD** = internal standard (0.1 % (v/v) 1-decanol); **a** = **2c**; **b** = side product (2.5 % GC area); **c** = dimethyl ester of **2a** (substrate); **d** = dimethyl ester of **2d**; **e** = dimethyl ester of **2f**.

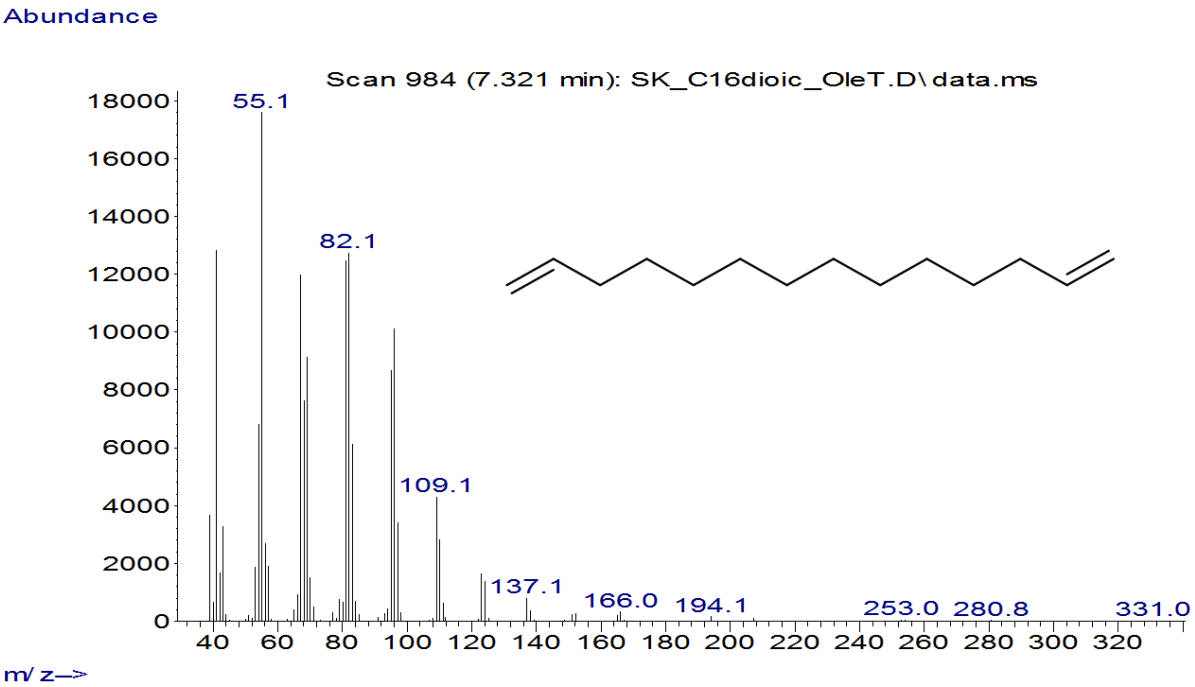

Figure S14. GC-MS spectra of **2c** (194.20 g mol^{-1}) obtained by conversion of **2a** (10 mM) with the OleT-CamAB-FDH system (corresponds to peak a in Figure S14 A).

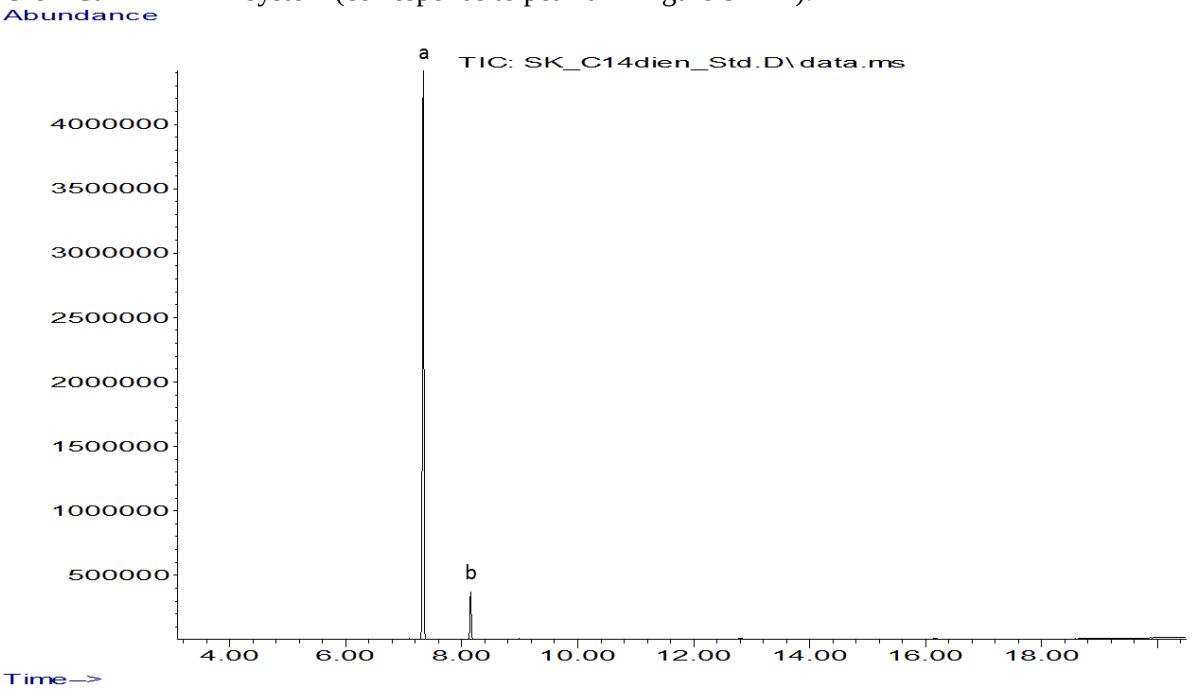

Figure S15. GC-MS chromatogram of a commercial standard of **2c**. **a** = **2c**; **b** = 11-bromo-1-undecanol (according to GC-MS compound library) impurity in the reference material (purity of a commercial **2c** was 90 %).

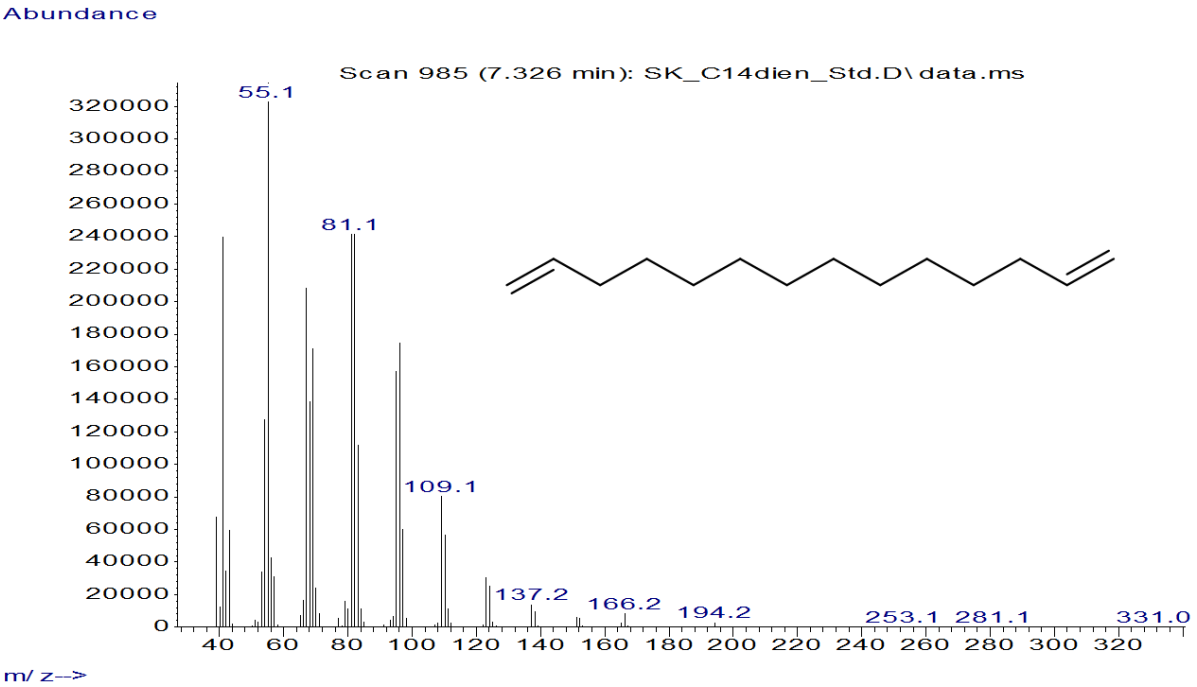

Figure S16. GC-MS spectra of a commercial standard of **2c** (194.20 g mol^{-1}, corresponds to peak a in Figure S15).

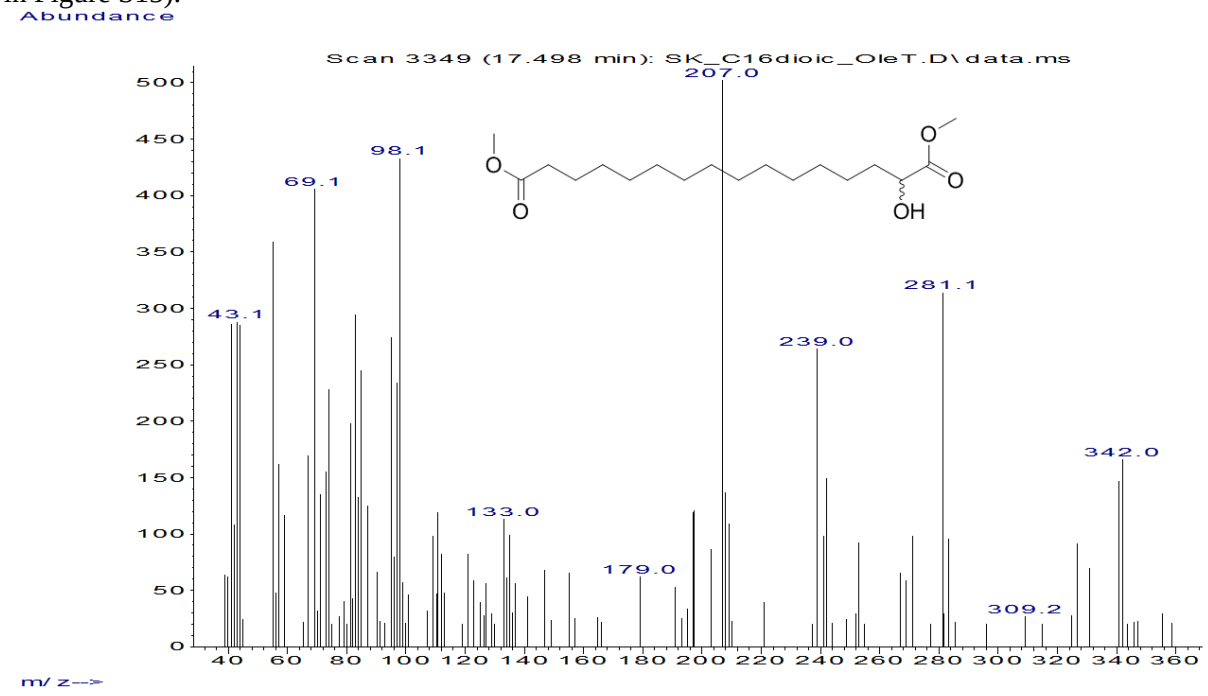

Figure S17. GC-MS spectra of dimethyl ester of **2d** (330.24 g mol^{-1}) obtained by conversion of **2a** (10 mM) with the OleT-CamAB-FDH system (corresponds to peak d in Figure S13 A).

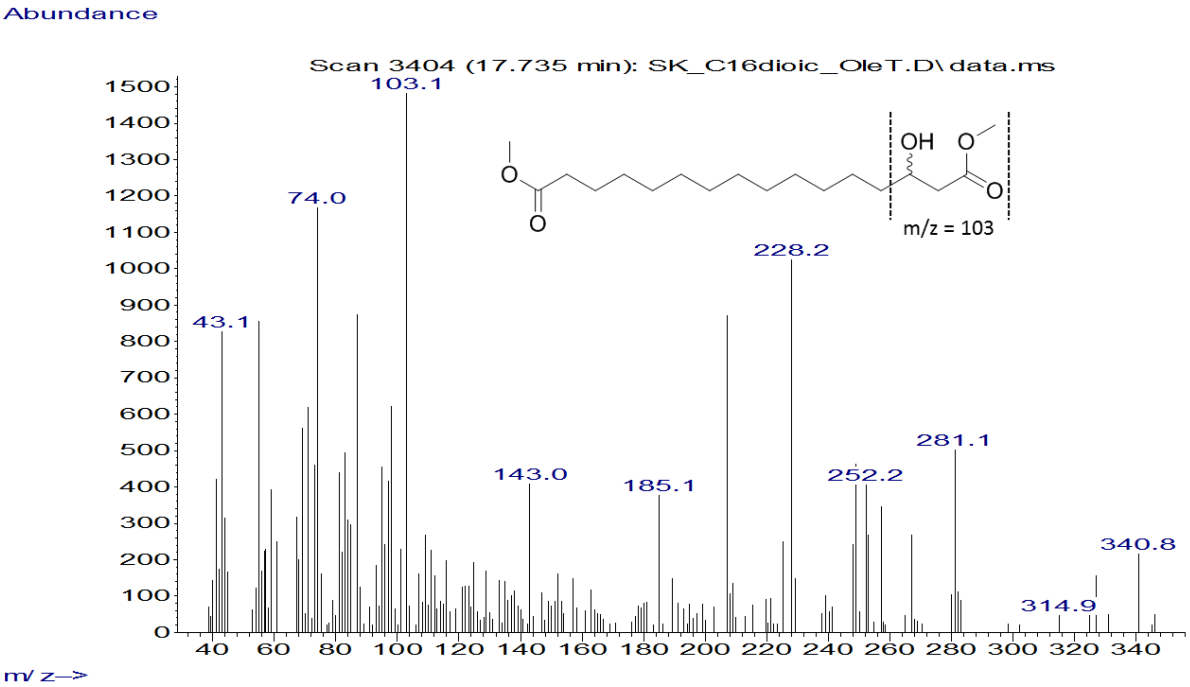

Figure S18. GC-MS spectra of dimethyl ester of **2f** obtained by conversion of **2a** (10 mM) with the OleT-CamAB-FDH system (corresponds to peak e in Figure S13 A). The characteristic ion *m*/z = 103 was used to assign the minor side product.

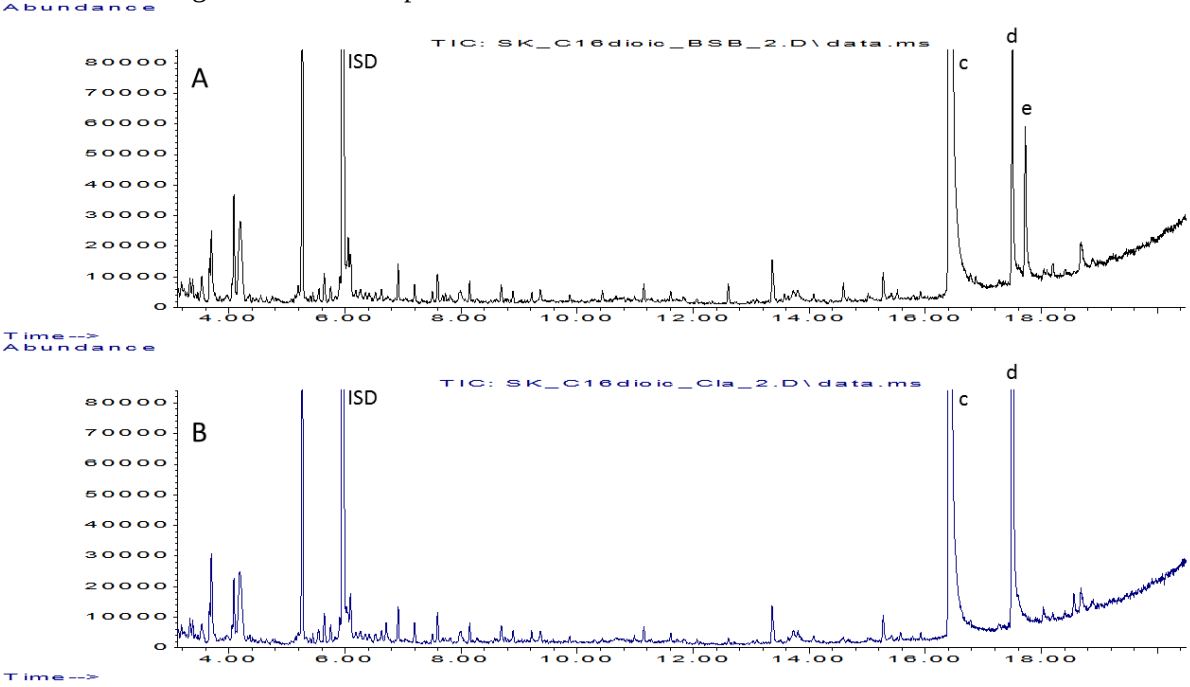

Figure S19. GC-MS chromatograms obtained by conversion of **2a** (10 mM) with $CYP_{BSß}$ (**A**) and $P450_{Cla}$ (**B**) using H_2O_2 as oxidant. **ISD** = internal standard (0.1 % (v/v) 1-decanol); **c** = dimethyl ester of **2a** (substrate); **d** = **2d** dimethyl ester; **e** = **2f**-dimethyl ester.

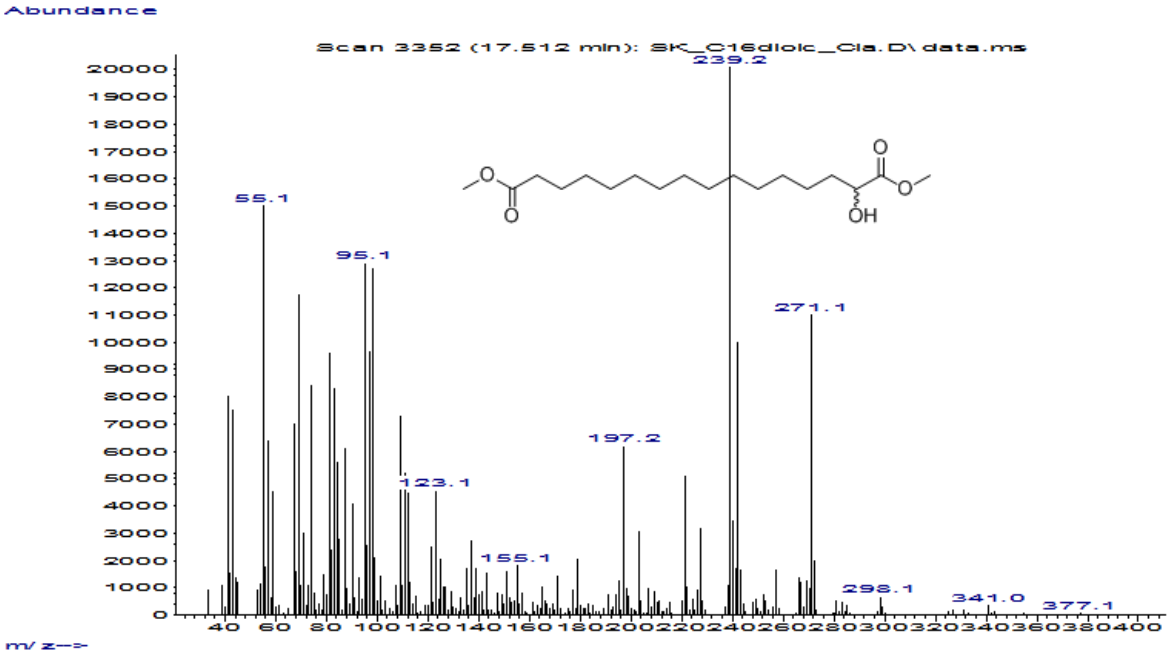

Figure S20. GC-MS spectra of **2d** dimethyl ester (330.24 g mol^{-1}) obtained by conversion of **2a** (10 mM) with $P450_{Cla}$ and H_2O_2 as oxidant (corresponds to peak d in Figure S19).

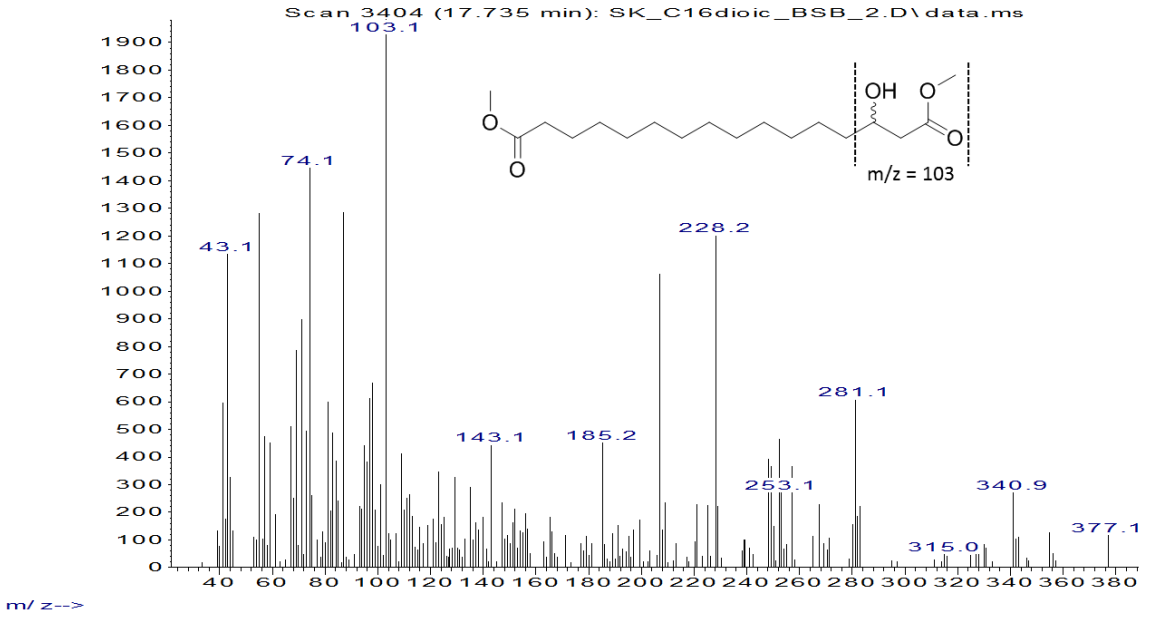

Figure S21. GC-MS spectra of **2f** dimethyl ester obtained by conversion of **2a** (10 mM) with $CYP_{BSß}$ and H_2O_2 as oxidant (corresponds to peak e in Figure S19). The characteristic ion *m*/z = 103 was used to assign the product.

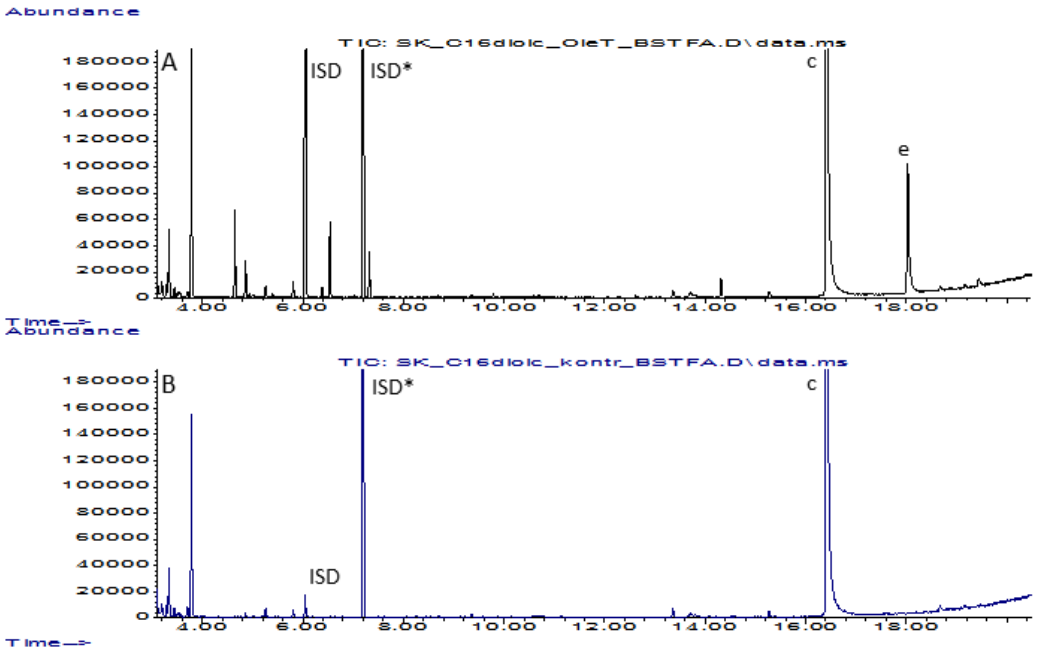

Figure S22. GC-MS chromatograms obtained by conversion of **2a** (10 mM) after derivatization with $TMSCHN_2$ and BSTFA. **A** = Conversion of **2a** with the OleT-CamAB-FDH system. **B** = Conversion of **2a** in the absence of OleT (negative control). **ISD** = internal standard (0.1 % (v/v) 1-decanol); **ISD*** = silylated internal standard (TMS-1-decanol); **c** = dimethyl ester of **2a** (substrate); **e** = **2f**-dimethyl ester.

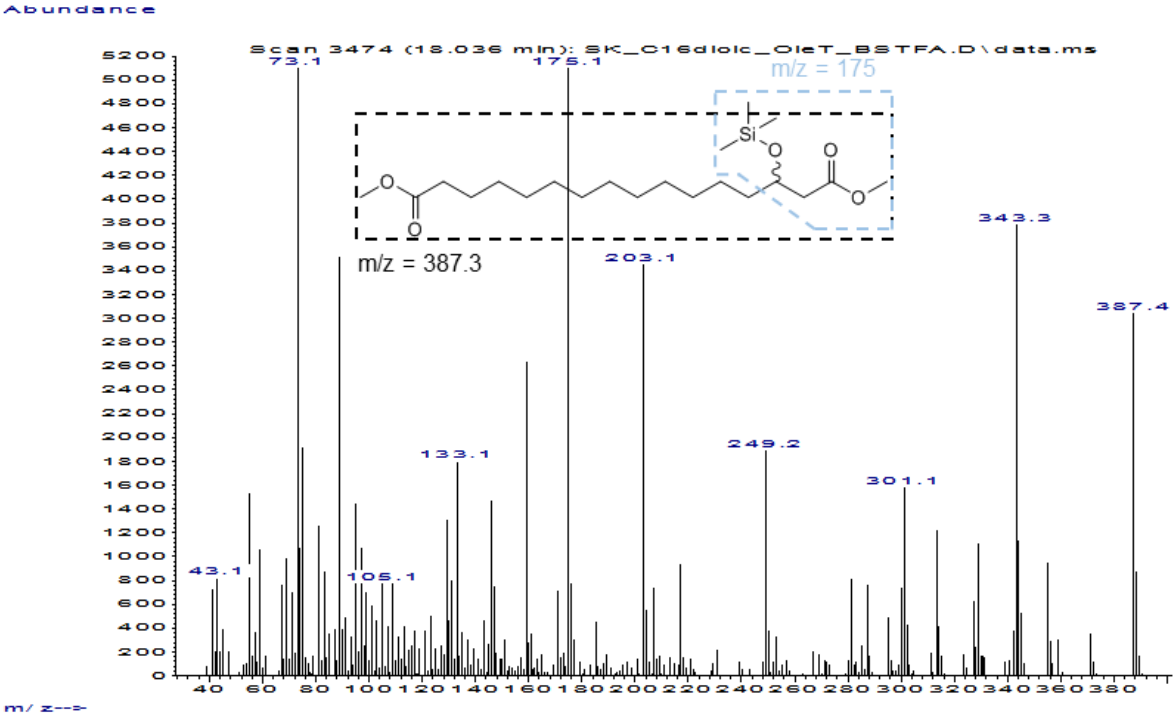

Figure S23. GC-MS spectra of **2f**-dimethyl ester obtained by conversion of **2a** (10 mM) with the OleT-CamAB-FDH system (corresponds to peak e in Figure S22 A). The characteristic ions *m*/z = 175 and *m*/z = 387.3 were used to assign the product as described elsewhere.[2]

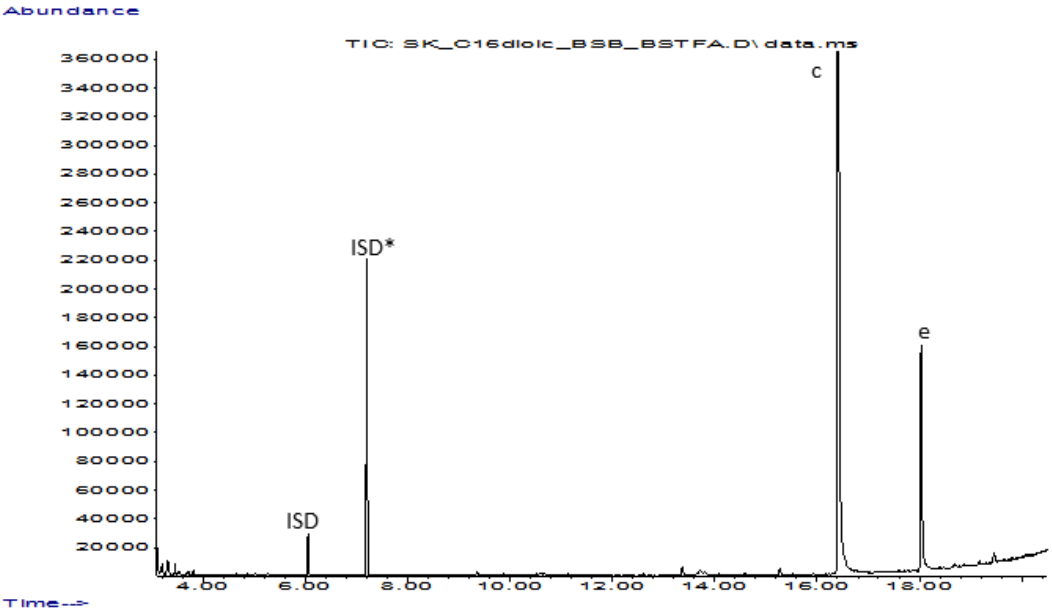

Figure S24. GC-MS chromatogram obtained by conversion of **2a** (10 mM) with $CYP_{BS\beta}$ and H_2O_2 as oxidant after derivatization with $TMSCHN_2$ and BSTFA. **ISD** = internal standard (0.1 % (v/v) 1-decanol); **ISD*** = silylated internal standard (TMS-1-decanol); **c** = dimethyl ester of **2a** (substrate); **e** = **2f**-dimethyl ester.

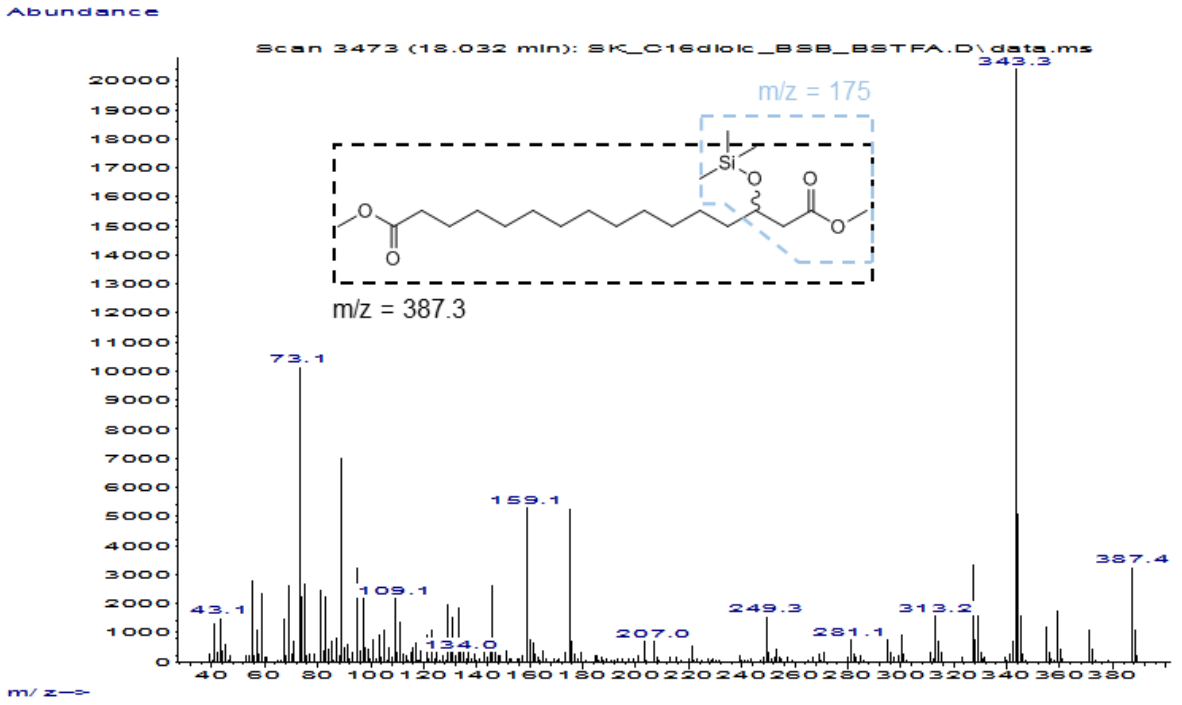

Figure S25. GC-MS spectra of TMS-**2f**-dimethyl ester obtained by conversion of **2a** (10 mM) with $CYP_{BS\beta}$ and H_2O_2 as oxidant (corresponds to peak e in Figure S24). The characteristic ions *m*/z = 175 and *m*/z = 387.3 were used to assign the product as described elsewhere.[2]

7.1.3 **Conversion of 3a**

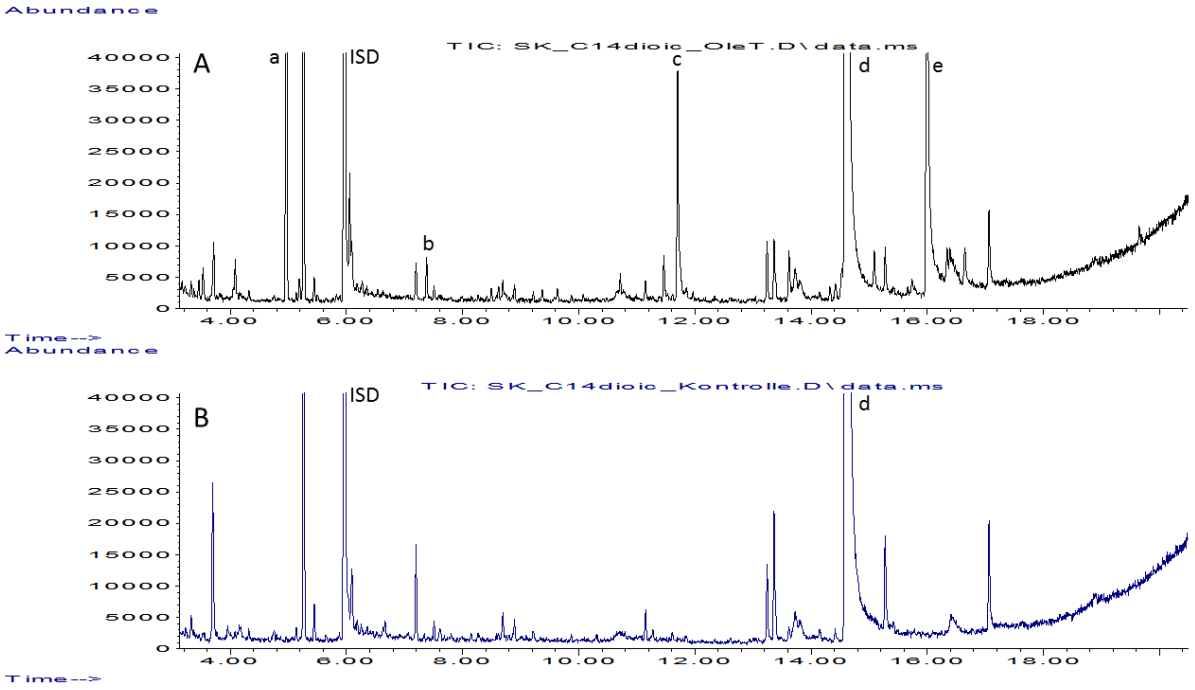

Figure S26. GC-MS chromatograms obtained by conversion of **3a** (10 mM). **A** = Conversion of **3a** with the OleT-CamAB-FDH system. **B** = Conversion of **3a** in the absence of OleT (negative control). **ISD** = internal standard (0.1 % (v/v) 1-decanol); **a** = **3c**; **b** = minor side product (<1 % GC area of all products); **c** = **3g**-methyl ester (see Figure S34, Figure S39 and 0 for comparison; ß-hydroxylated reaction intermediate); **d** = dimethyl ester of **3a** (substrate); **e** = **3f**-dimethyl ester (side product).

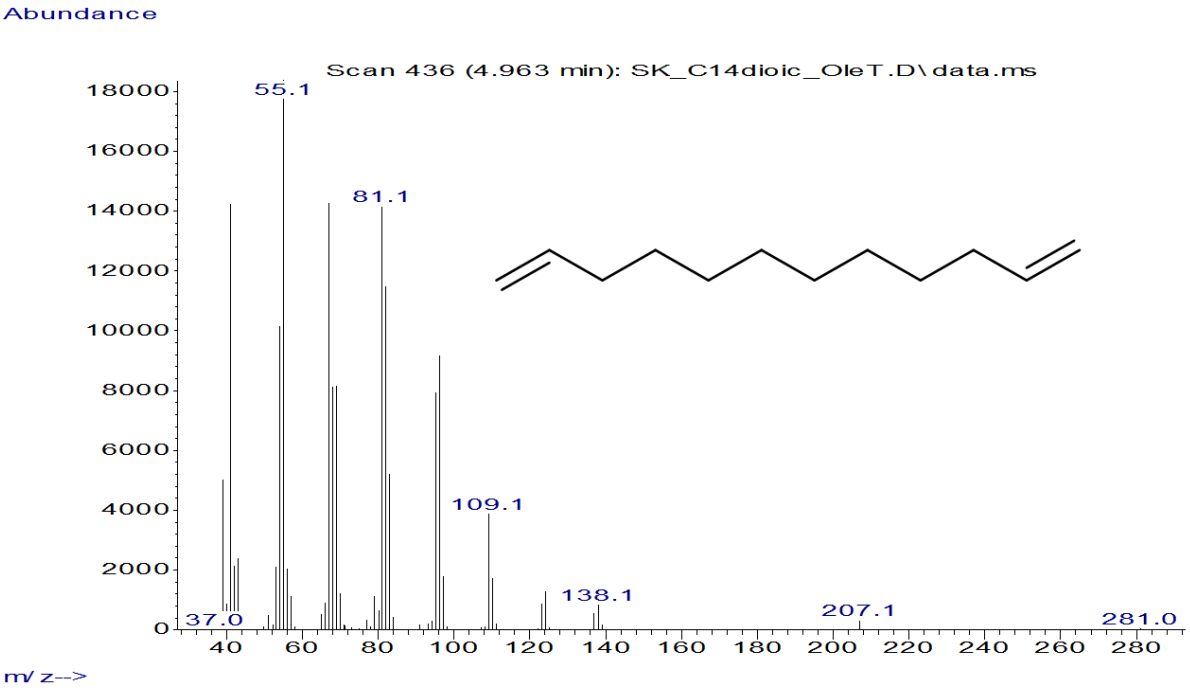

Figure S27. GC-MS spectra of **3c** (166.17 g mol^{-1}) obtained by conversion of **3a** (10 mM) with the OleT-CamAB-FDH system (corresponds to peak a in Figure S26A).

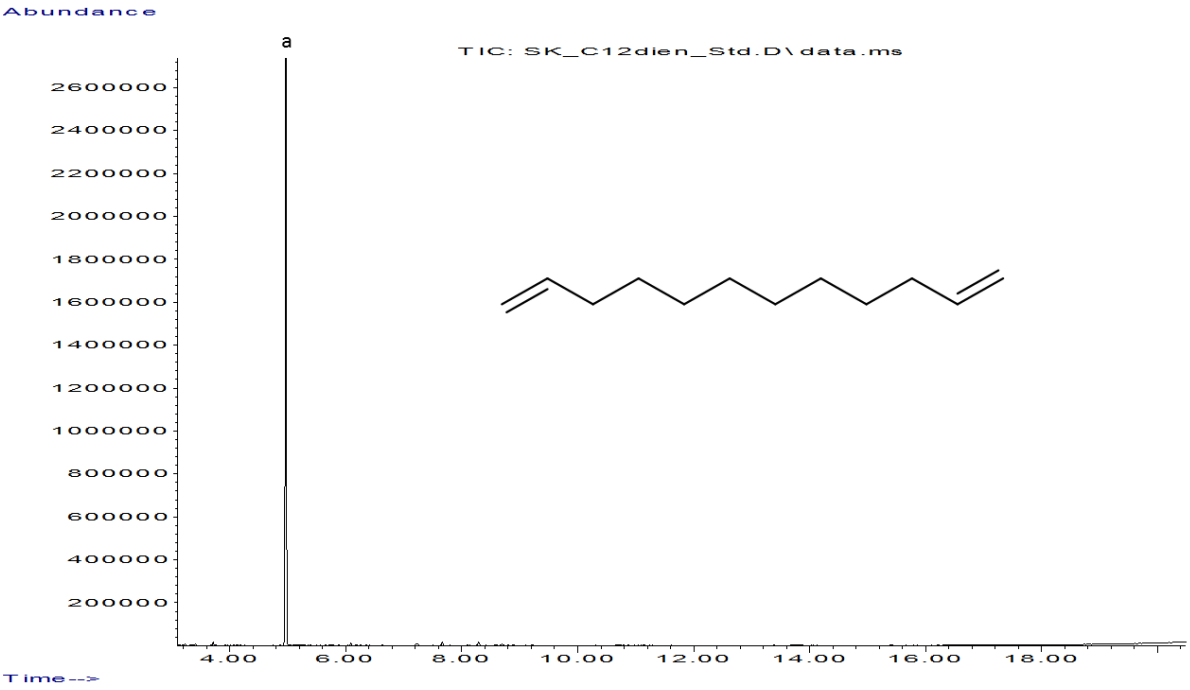

Figure S28. GC-MS chromatogram of a commercial standard of **3c**.

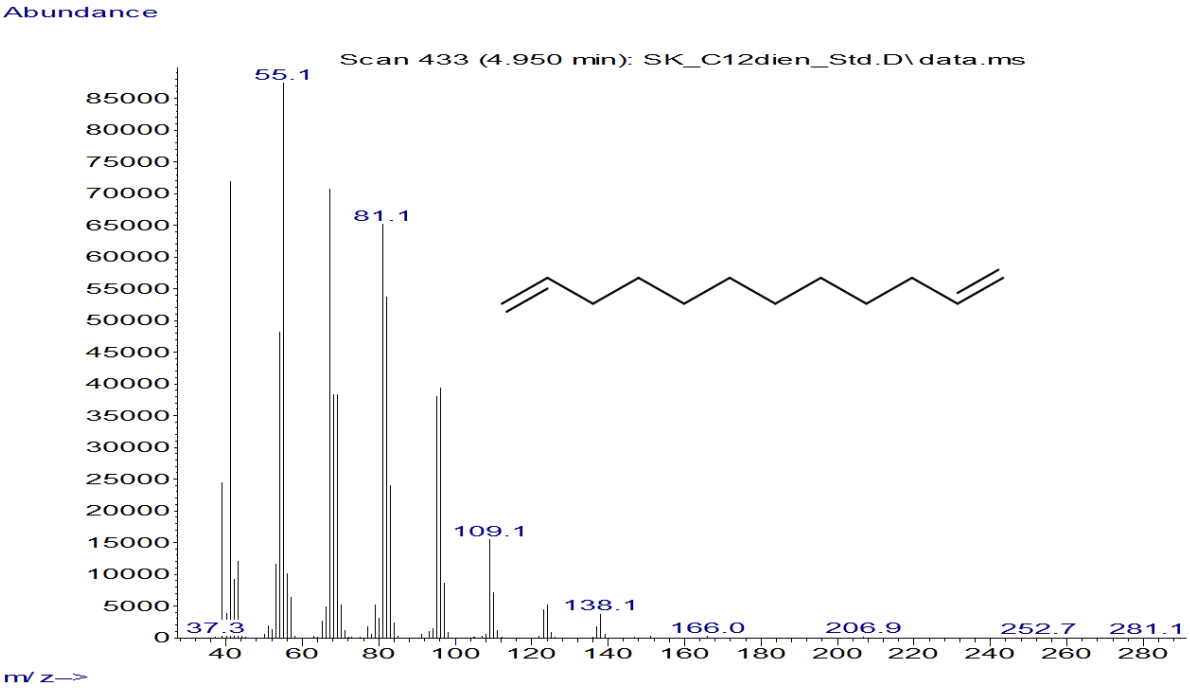

Figure S29. GC-MS spectra of a commercial standard of **3c** (166.17 g mol^{-1}, corresponds to peak a in Figure S28).

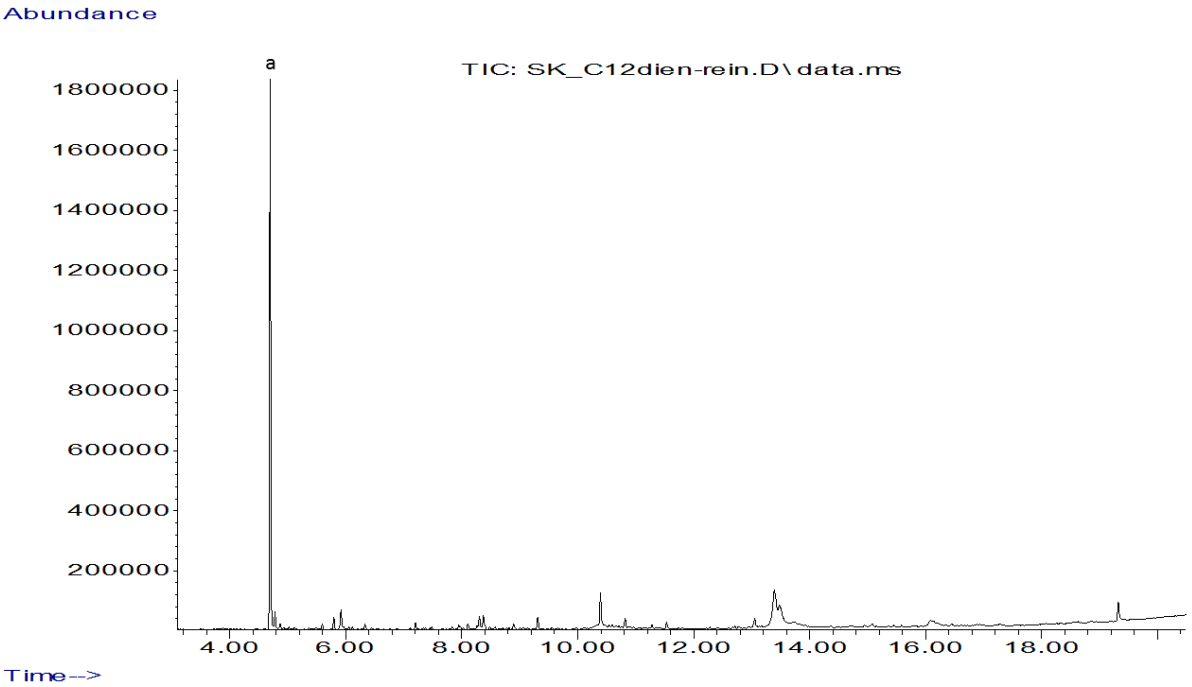

Figure S30. GC-MS chromatogram of isolated and purified **3c** (**a**) by conversion of **3a** with the OleT-CamAB-FDH system (50 mL scale, 10 mM). Purity of the isolated product 86 % (GC-area).

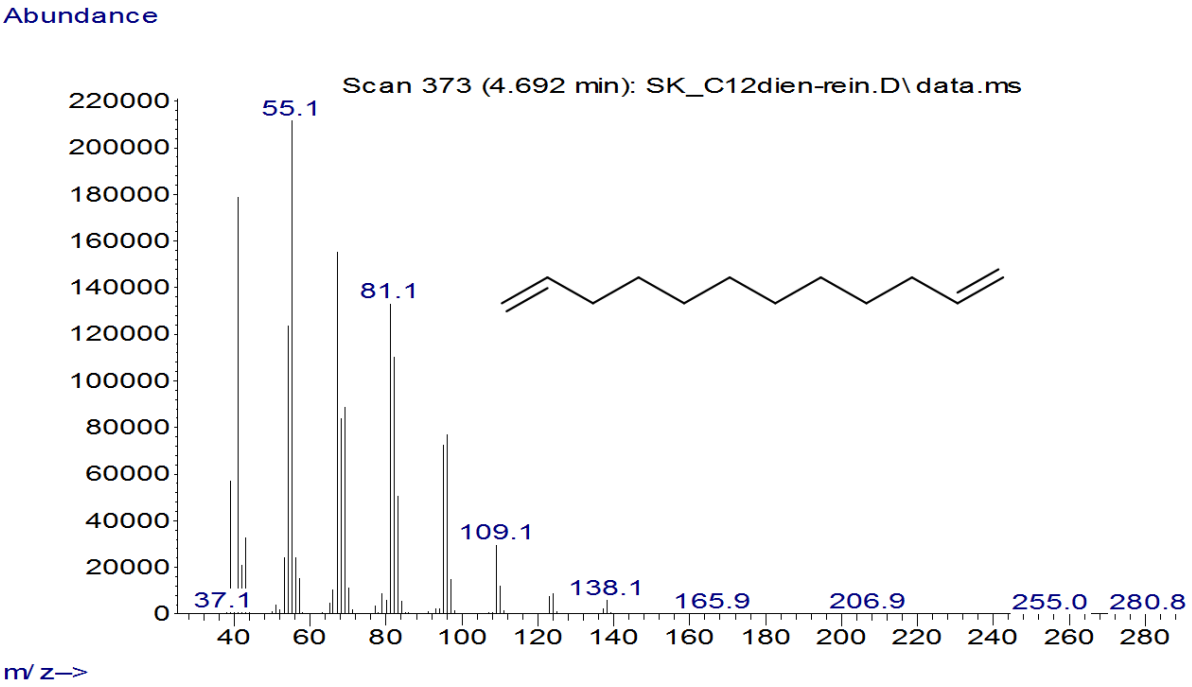

Figure S31. GC-MS spectra of isolated and purified **3c** (166.17 g mol^{-1}) obtained by conversion of **3a** with the OleT-CamAB-FDH system.

Dodeca-1,11-diene, **3c**: Isolated yield from 50 mL reaction volume starting from 10 mM **3a**. Clear oil (6 mg). ^{1}H-NMR (300 MHz, $CDCl_3$): δ = 5.90-5.77 (m, 2 H, C**H**=CH_2), 5.05-4-93 (m, 4 H, C$\mathbf{H_2}$=CH), 2.09-2.02 (m, 4 H, C$\mathbf{H_2}$CH=CH_2), 1.39-1.27 (m, 12 H, CH_2(C$\mathbf{H_2}$)$_6$$CH_2$).

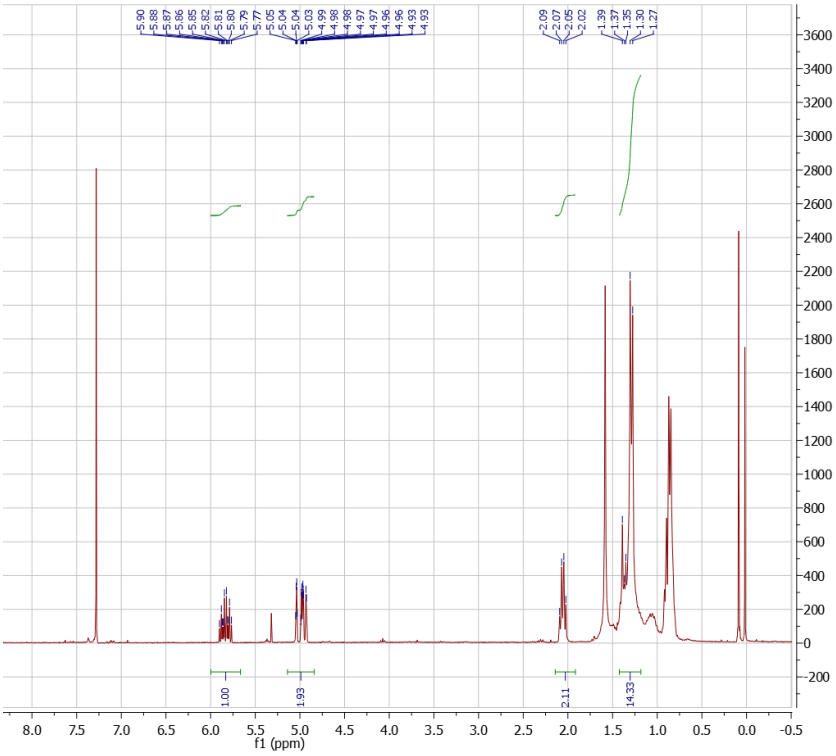

Figure S32. ^{1}H-NMR chromatograms of isolated **3c** by conversion of **3a** with the OleT-CamAB-FDH system.

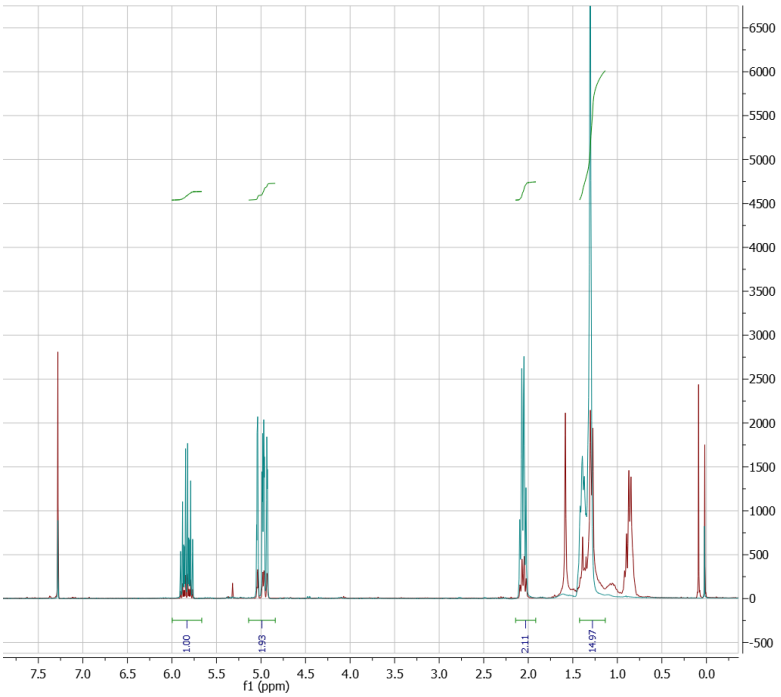

Figure S33. Overlay of ^{1}H-NMR chromatograms of isolated **3c** (red) and commercial standard (turquois).

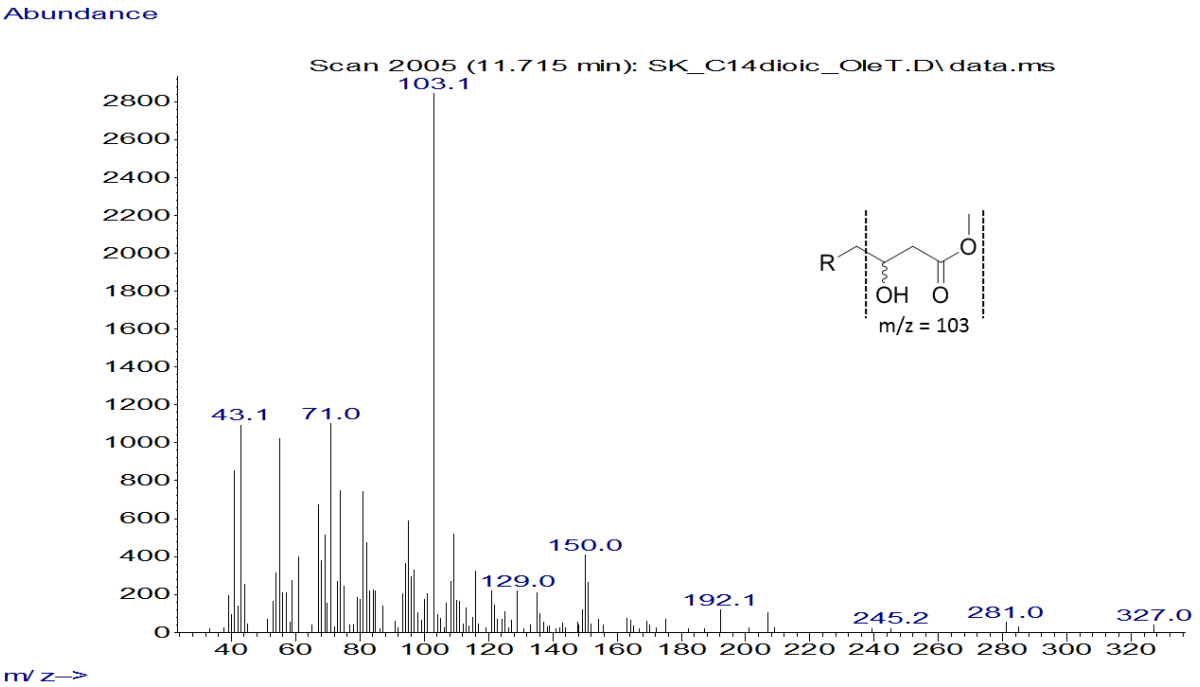

Figure S34. GC-MS spectra of a 3-hydroxy methyl ester side product (6.5 % GC-FID product area; **3g**-methyl ester) obtained by conversion of **3a** (10 mM) with the OleT-CamAB-FDH system (corresponds to peak c in Figure S26 A). The characteristic ion *m*/z = 103 is characteristic for ß-hydroxy acid methyl esters.[1]

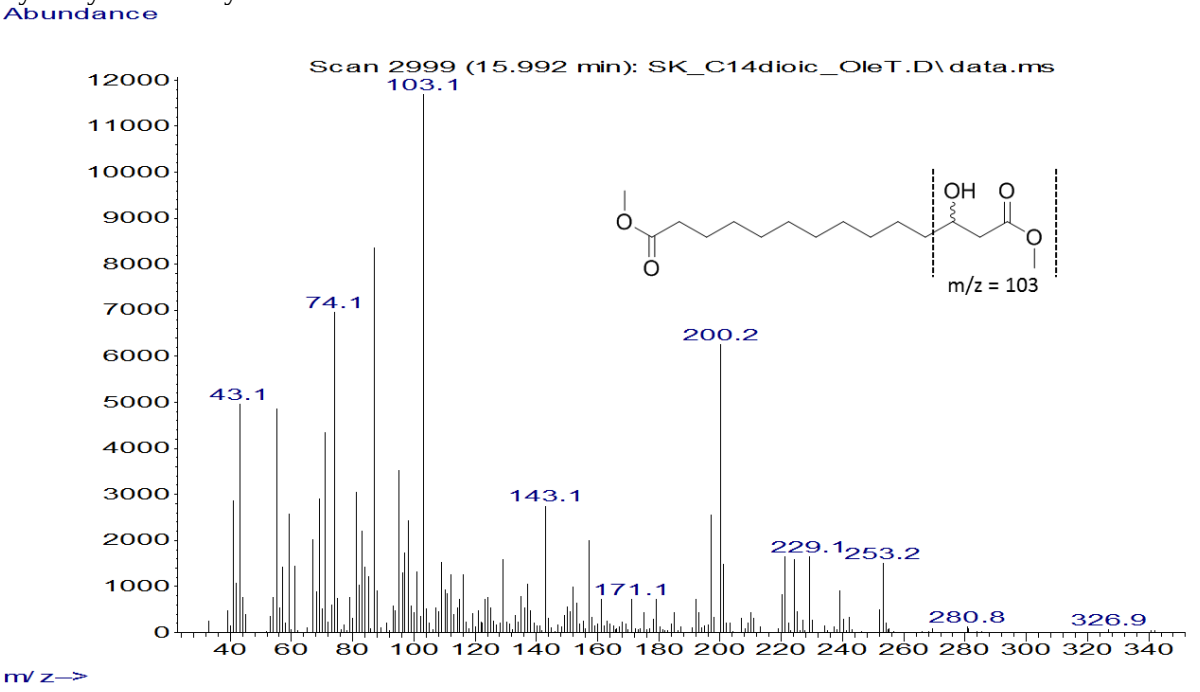

Figure S35. GC-MS spectra of **3f**-dimethyl ester obtained by conversion of **3a** (10 mM) with the OleT-CamAB-FDH system (corresponds to peak e in Figure S26 A). The characteristic ion *m*/z = 103 was used to assign the product.

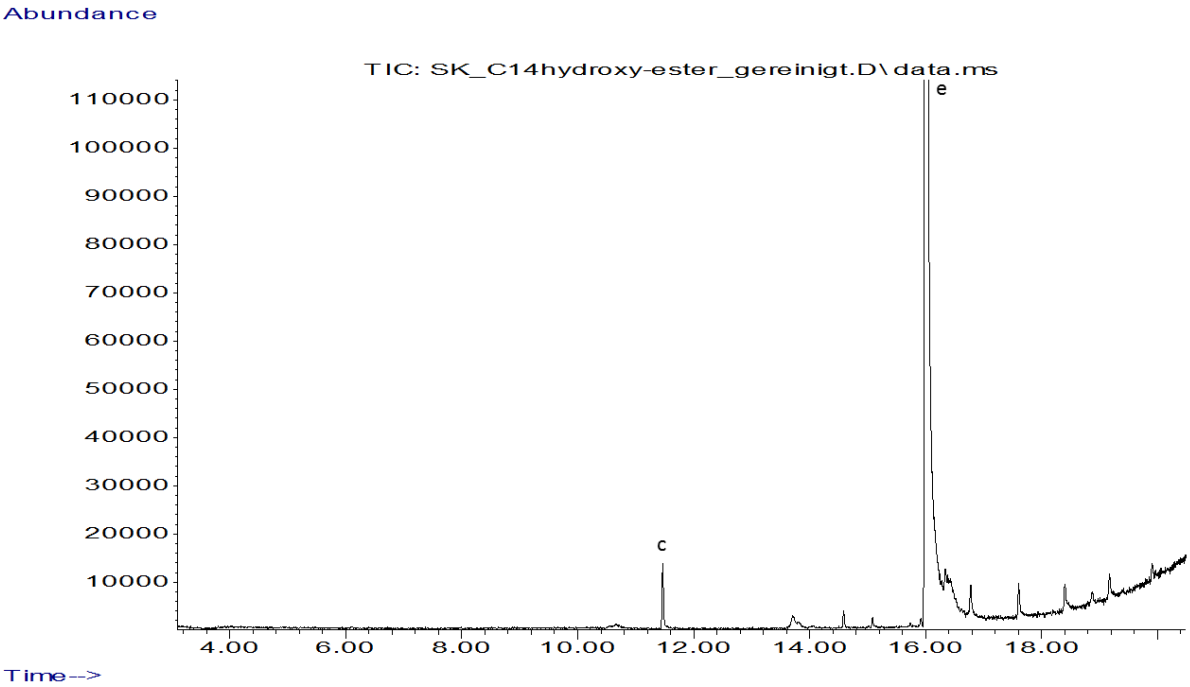

Figure S36. GC-MS chromatogram of isolated and purified **3f**-dimethyl ester (corresponds to peak e in Figure S26 A) obtained by conversion of **3a** with the OleT-CamAB-FDH system. **c** = **3g**-methyl ester.

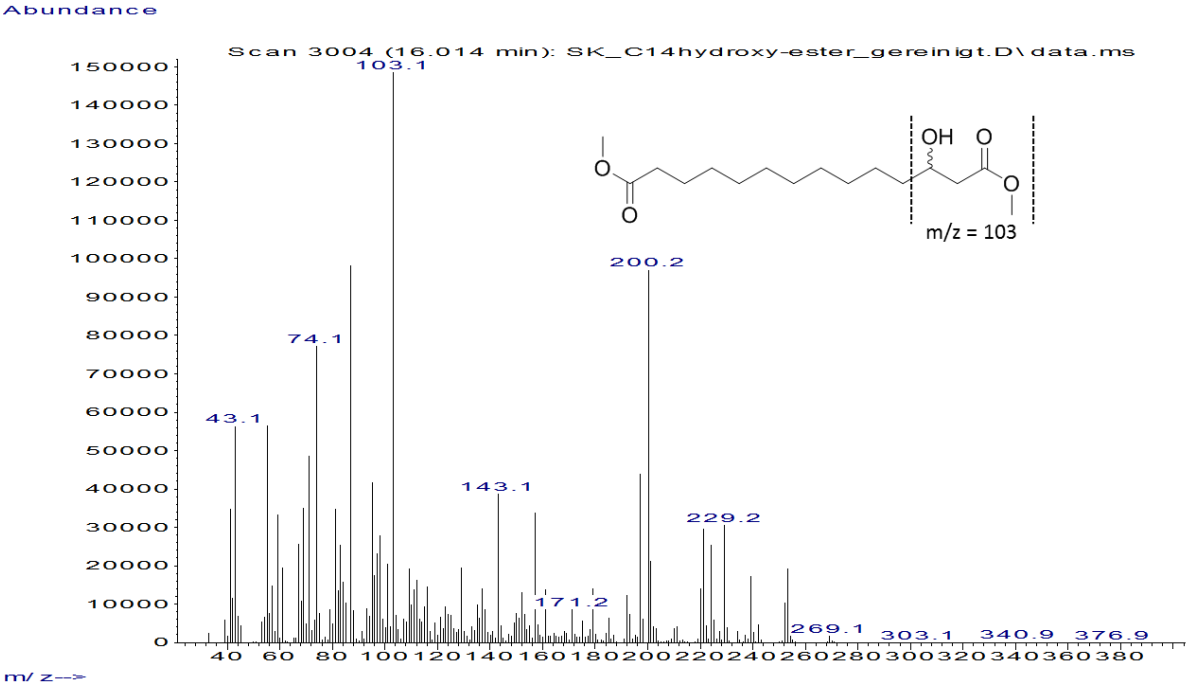

Figure S37. GC-MS spectra of isolated and purified **3f**-dimethyl ester (302.21 g mol^{-1}) obtained by conversion of **3a** with the OleT-CamAB-FDH system (corresponds to peak e in Figure S36).

Dimethyl 3-hydroxytetradecanedioate; **3f**-dimethyl ester: Isolated yield from 20 mL reaction volume starting from 10 mM **3a**. White powder (7 mg). ^{1}H-NMR (300 MHz, $CDCl_3$): δ =

4.04-3.98 (m, 1 H, $CH_2C\mathbf{H}(OH)CH_2$), 3.73 (s, 3 H, OCH_3), 3.68 (s, 3 H, OCH_3), 2.88 (m, 1 H, OH), 2.52-2.29 (m, 4H, $CH_2C\mathbf{H_2}(C{=}O)$), 1.68-1.25 (m, 18 H, $(CH_2)_9$).

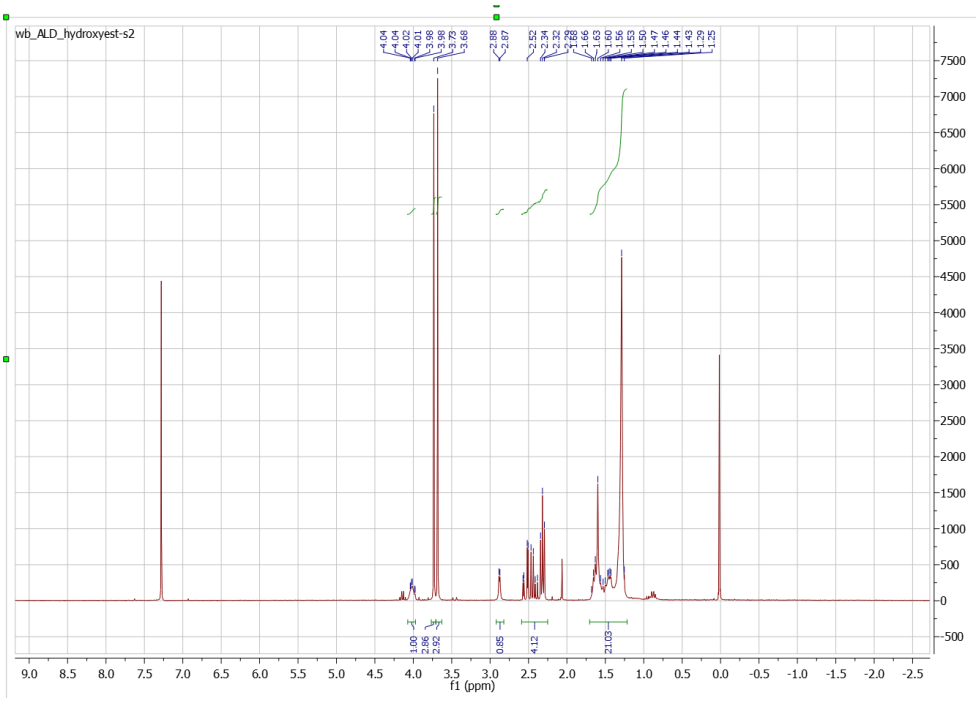

Figure S38. ^{1}H-NMR chromatogram of isolated and purified **3f**-dimethyl ester obtained by conversion of **3a** with the OleT-CamAB-FDH system.

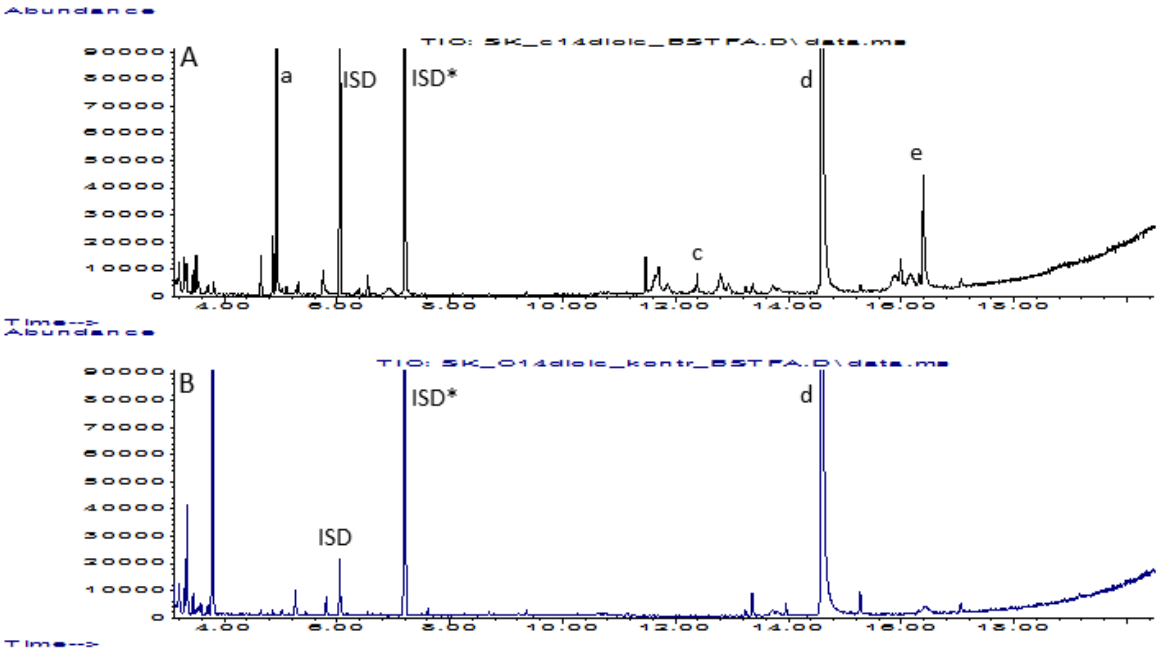

Figure S39. GC-MS chromatograms obtained by conversion of **3a** (10 mM) after derivatization with $TMSCHN_2$ and BSTFA. **A** = Conversion of **3a** with the OleT-CamAB-FDH system. **B** = Conversion of **3a** in the absence of OleT (negative control). **ISD** = internal standard (0.1 % (v/v) 1-decanol); **ISD*** = silylated internal standard (TMS-1-decanol); **a**= **3e**; **c**= TMS-**3g**-methyl ester; **d** = dimethyl ester of **3a** (substrate); **e** = TMS-**3f**-dimethyl ester.

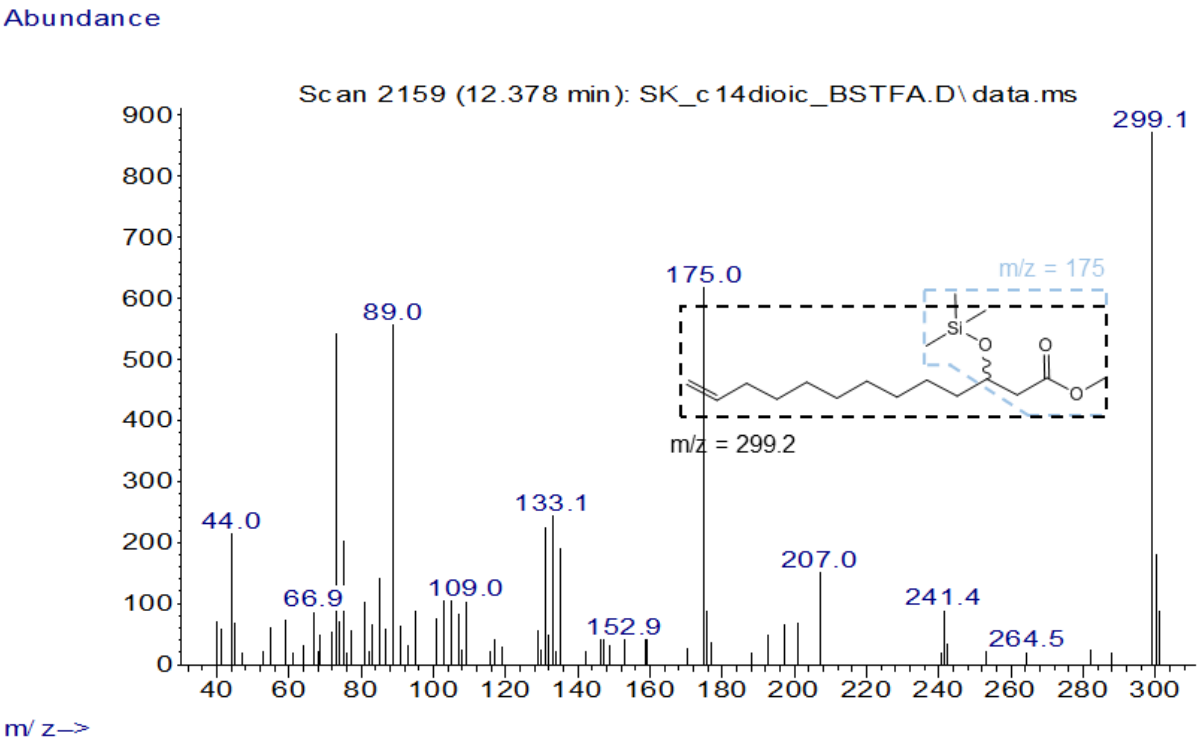

Figure S40. GC-MS spectra of TMS-**3g**-methyl ester obtained by conversion of **3a** (10 mM) with the OleT-CamAB-FDH system (corresponds to peak c in Figure S39 A). The characteristic ions *m*/z = 175 and *m*/z = 299.2 were used to assign the product as described elsewhere.[2]

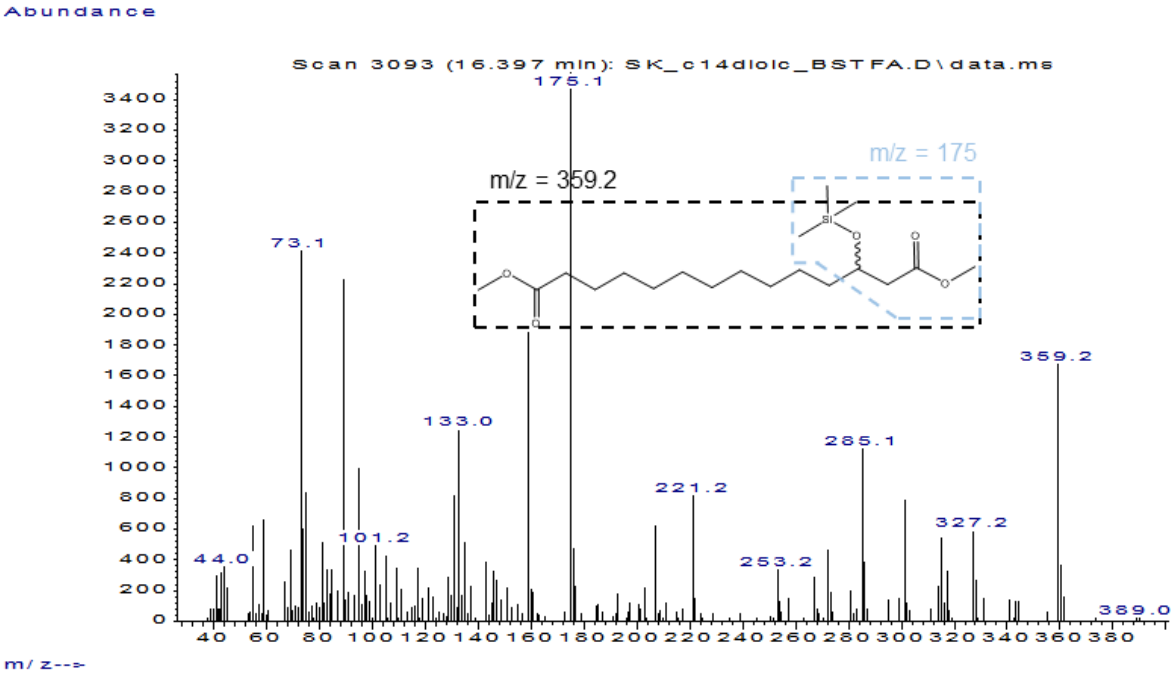

Figure S41. GC-MS spectra of TMS-**3f**-dimethyl ester obtained by conversion of **3a** (10 mM) with the OleT-CamAB-FDH system (corresponds to peak e in Figure S39 A). The characteristic ions *m*/z = 175 and *m*/z = 359.2 were used to assign the product as described elsewhere.[2]

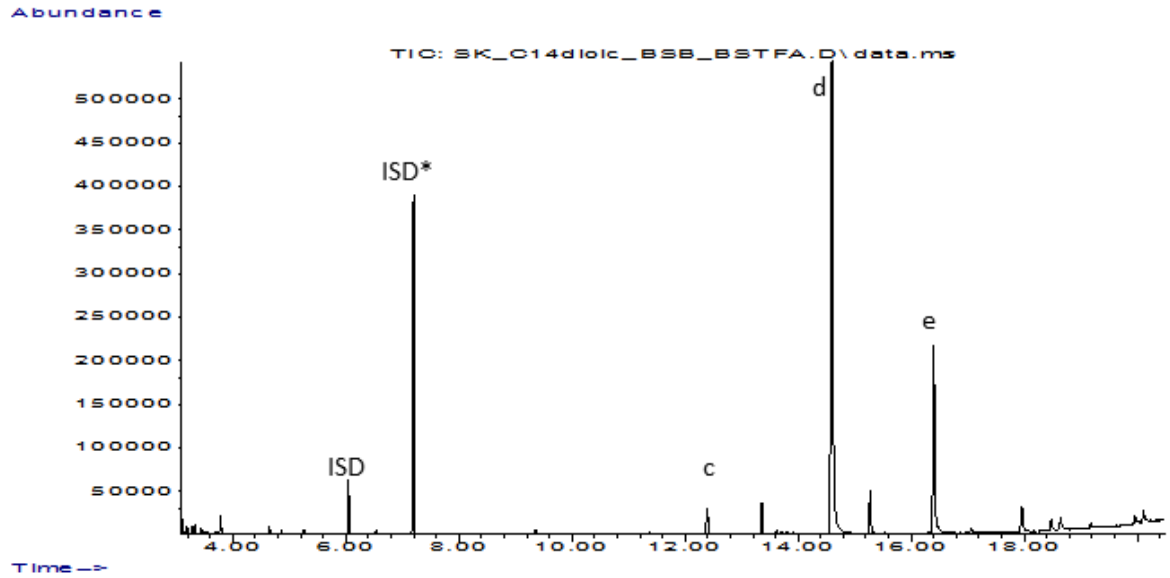

Figure S42. GC-MS chromatograms obtained by conversion of **3a** (10 mM) with $CYP_{BS\beta}$ and H_2O_2 as oxidant after derivatization with $TMSCHN_2$ and BSTFA. **ISD** = internal standard (0.1 % (v/v) 1-decanol); **ISD*** = silylated internal standard (TMS-1-decanol); **c** = TMS-**3g**-methyl ester; **d** = dimethyl ester of **3a** (substrate); **e** = TMS-**3f**-dimethyl ester.

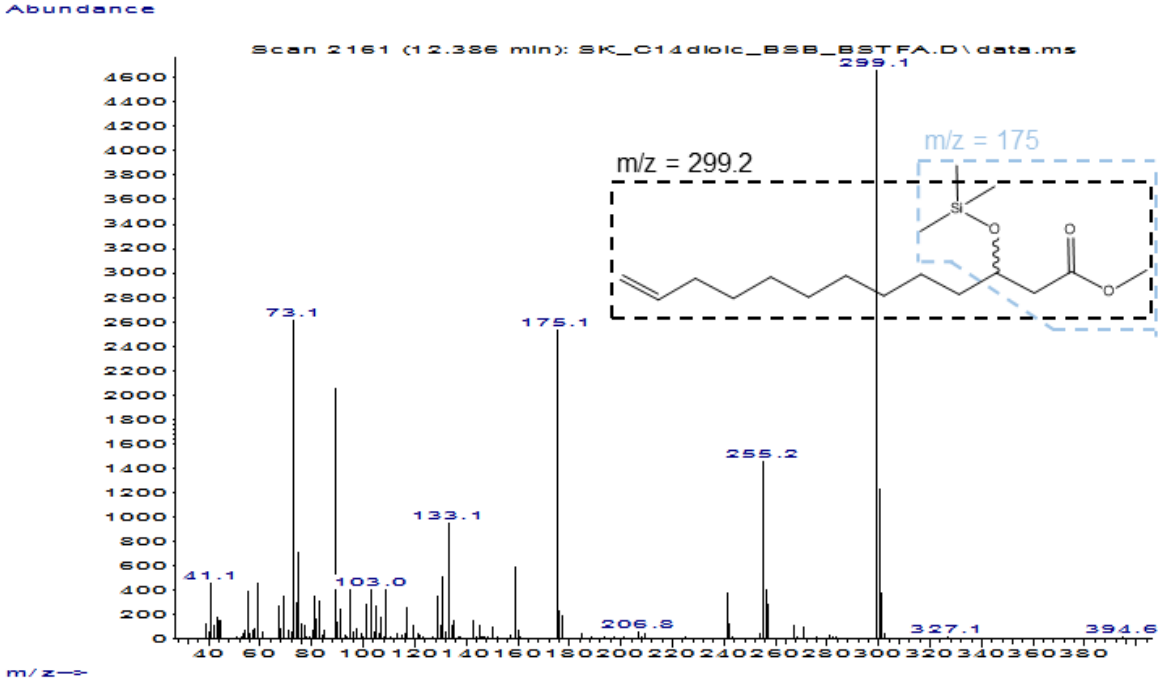

Figure S43. GC-MS spectra of TMS-**3g**-methyl ester obtained by conversion of **3a** (10 mM) with $CYP_{BS\beta}$ and H_2O_2 as oxidant (corresponds to peak c in Figure S42). The characteristic ions *m*/z = 175 and *m*/z = 299.2 were used to assign the minor side product as described elsewhere.[2]

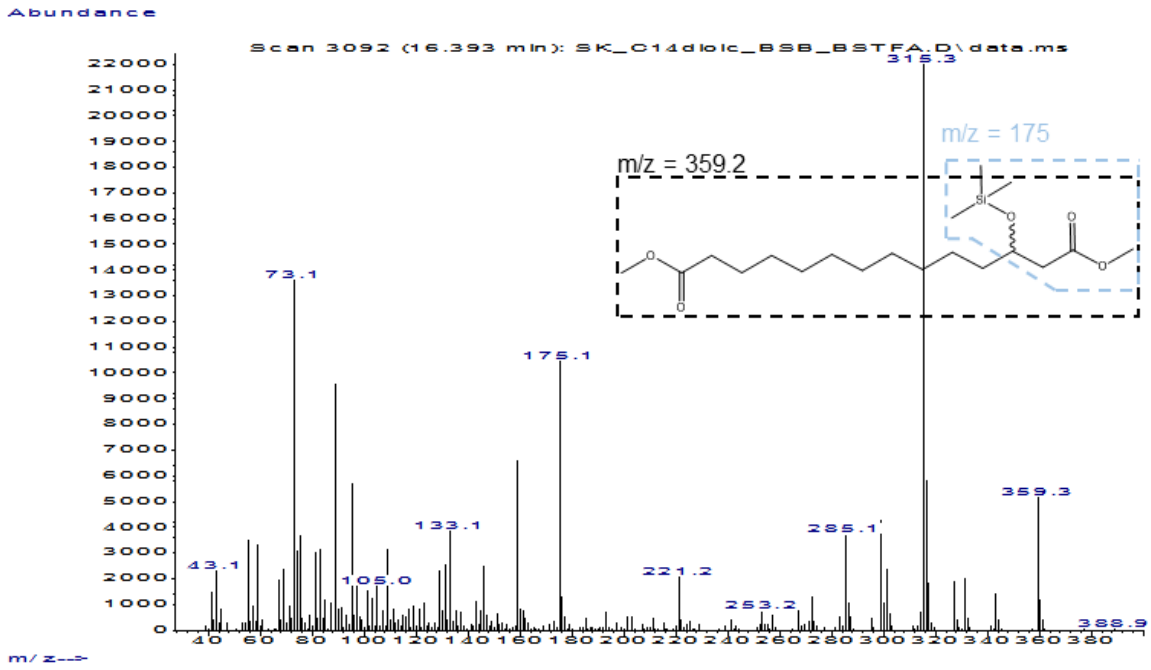

Figure S44. GC-MS spectra of TMS-**3f**-dimethyl ester obtained by conversion of **3a** (10 mM) with $CYP_{BS\beta}$ and H_2O_2 as oxidant (corresponds to peak e in Figure S42). The characteristic ions *m*/z = 175 and *m*/z = 359.2 were used to assign the minor side product as described elsewhere.[2]

7.1.4 **Conversion of 4a**

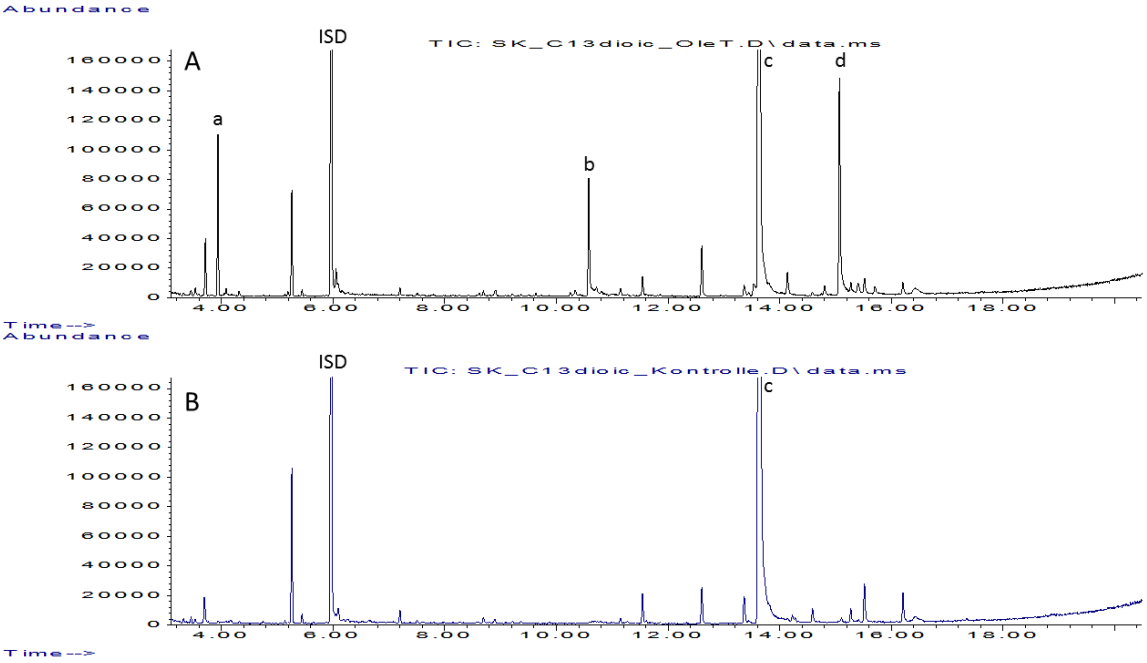

Figure S45. GC-MS chromatograms obtained by conversion of **4a** (10 mM). **A** = Conversion of **4a** with the OleT-CamAB-FDH system. **B** = Conversion of **4a** in the absence of OleT (negative control). **ISD** = internal standard (0.1 % (v/v) 1-decanol); **a** = **4c**; **b** = side product (24 % GC-FID area; see also Figure S49, Figure S52 and Figure S55 for further analytical details for this compound); **c** = dimethyl ester of **4a** (substrate); **d** = **4f**-dimethyl ester.

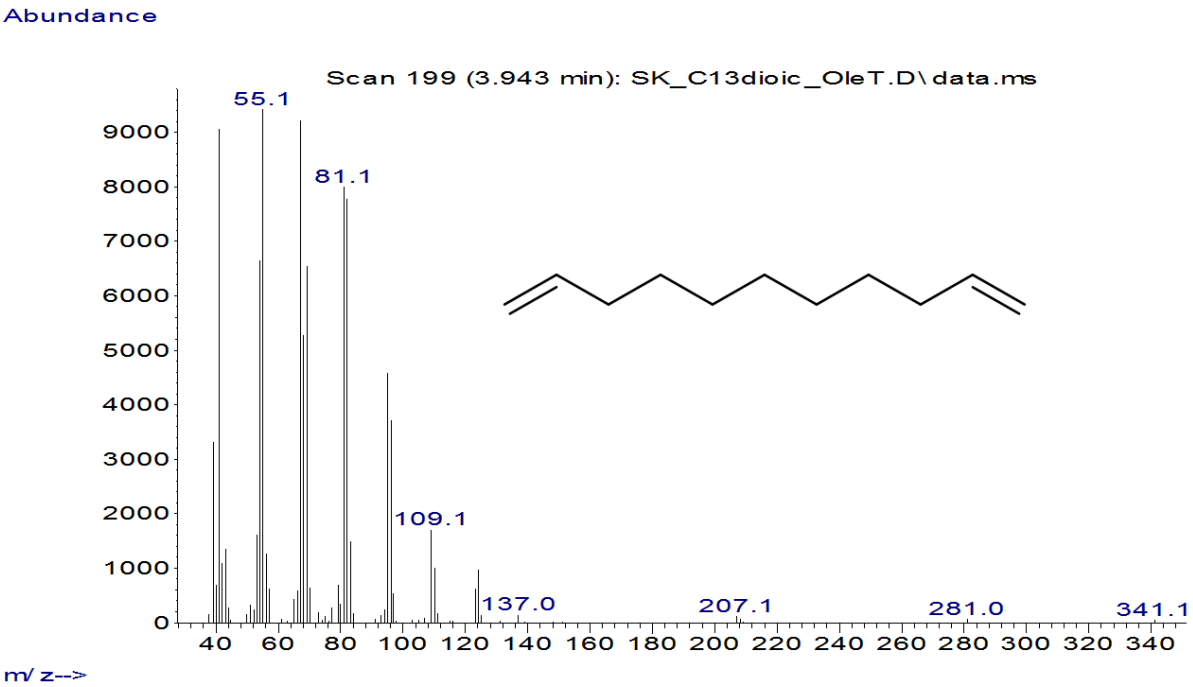

Figure S46. GC-MS spectra of **4c** (152.16 g mol^{-1}) obtained by conversion of **4a** (10 mM) with the OleT-CamAB-FDH system (corresponds to peak a in Figure S45 A).

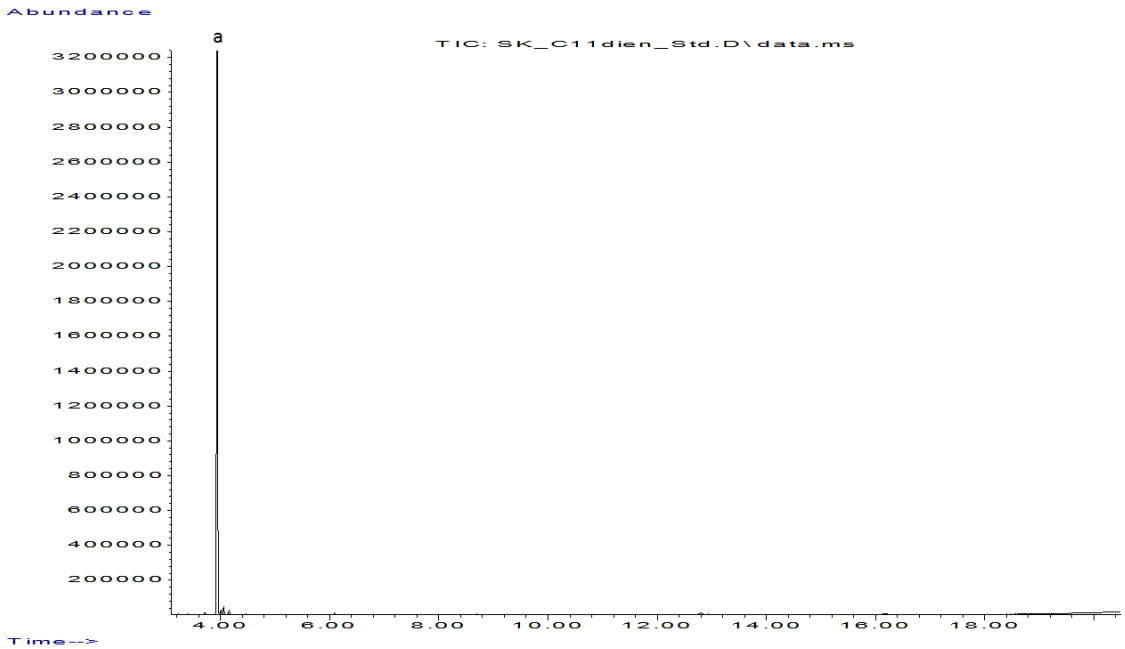

Figure S47. GC-MS chromatogram of a commercial standard of **4c**.

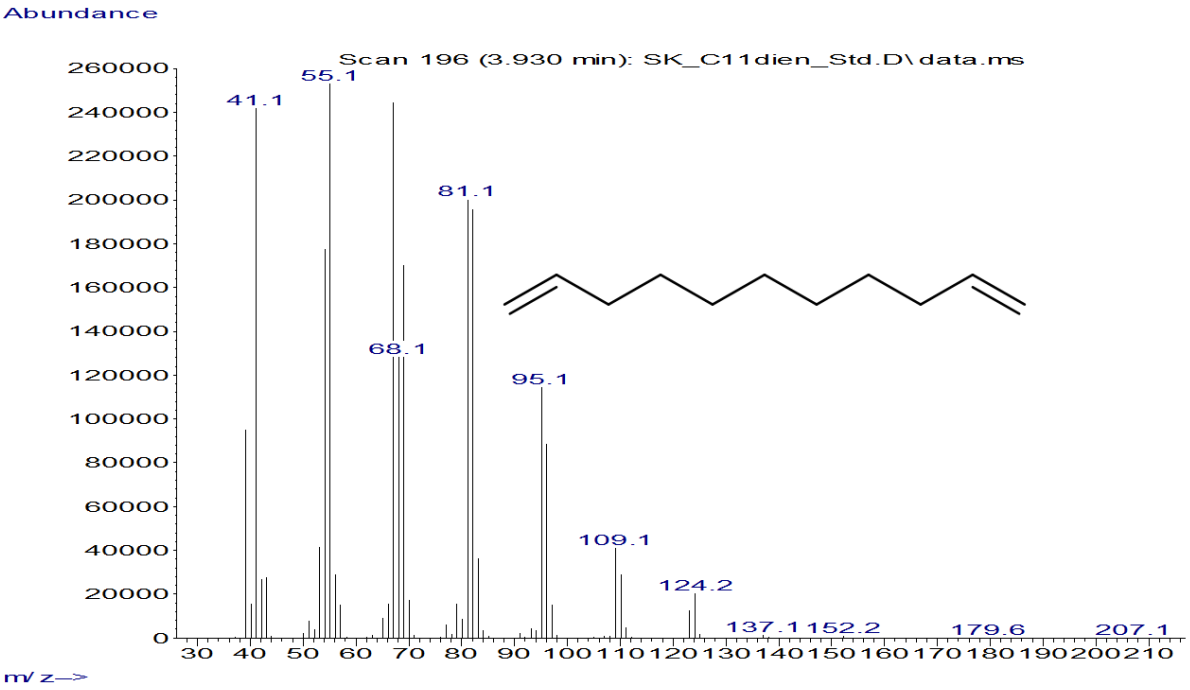

Figure S48. GC-MS spectra of a commercial standard of **4c** (152.16 g mol^{-1}, corresponds to peak a in Figure S47).

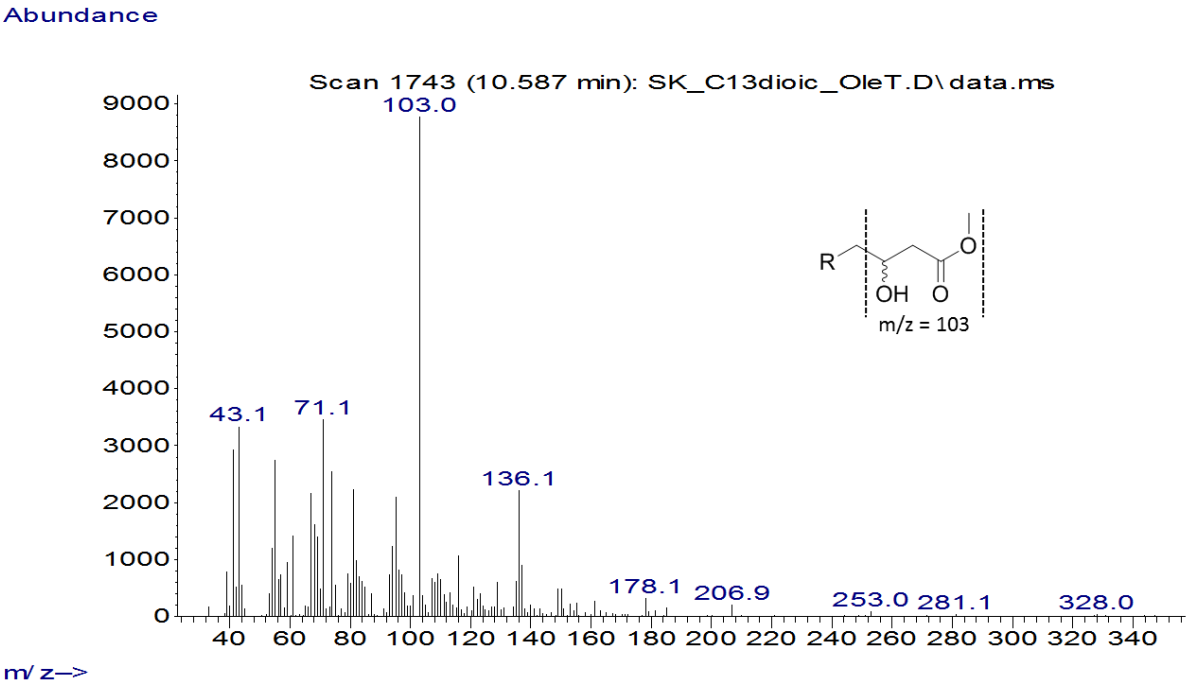

Figure S49. GC-MS spectra of **4g**-methyl ester (24 % GC-FID product area) obtained by conversion of **4a** (10 mM) with the OleT-CamAB-FDH system (corresponds to peak b in Figure S45). The characteristic ion *m*/z = 103 was used for compound assignment, which is characteristic for ß-hydroxy acid methyl esters (see also Figure S52 and Figure S55 for further analysis of the compound).[1]

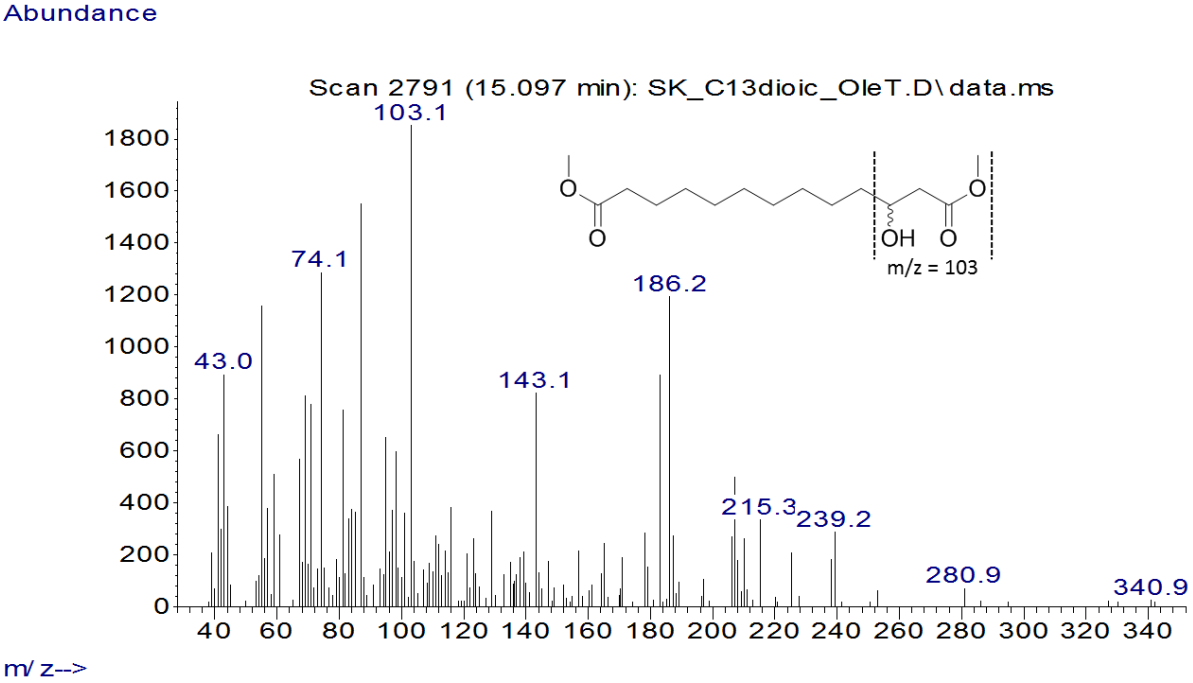

Figure S50. GC-MS spectra of **4f-**dimethyl ester (288.19 g mol^{-1}) obtained by conversion of **4a** (10 mM) with the OleT-CamAB-FDH system (corresponds to peak d in Figure S45). The characteristic ion *m*/z = 103 was used to assign the minor side product.

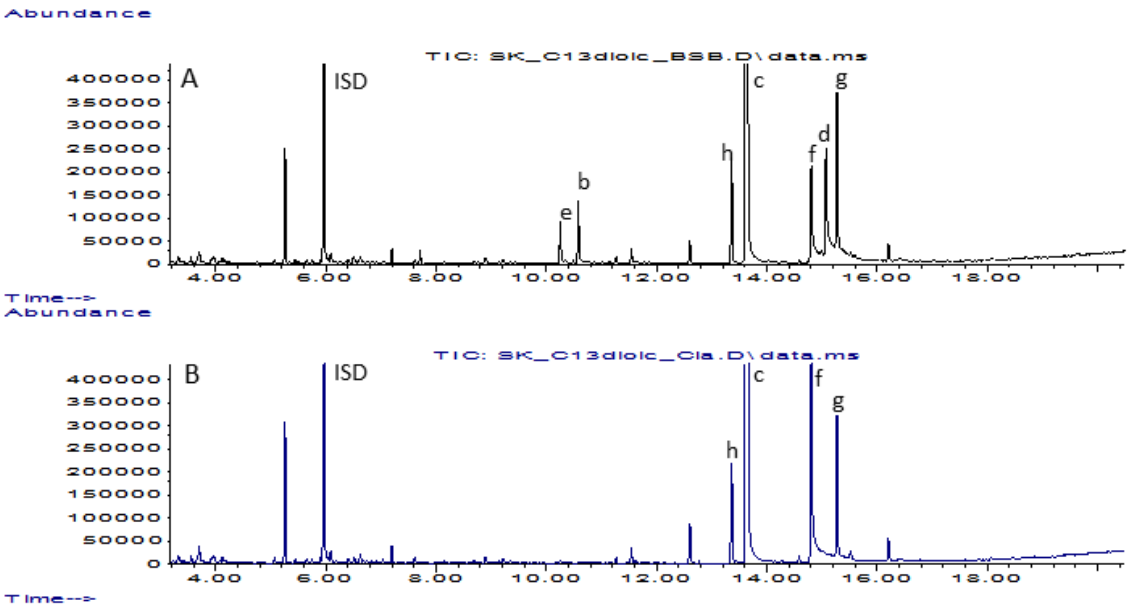

Figure S51. GC-MS chromatograms obtained by conversion of **4a** (10 mM). **A** = Conversion of **4a** with $CYP_{BS\beta}$ and H_2O_2 as oxidant. **B** = Conversion of **4a** with $P450_{Cla}$ and H_2O_2 as oxidant. **ISD** = internal standard (0.1 % (v/v) 1-decanol); **b** = **4g-**methyl ester (see also Figure S52 and Figure S55); **c** = dimethyl ester of **4a** (substrate); **d** = **4f-**dimethyl ester; **e** = side product; **f** = **4d-**dimethyl ester; **g** = octadecanoic acid methyl ester (suggested by GC-MS compound library); **h**= hexadecanoic acid methyl ester (suggested by GC-MS compound library). Purity of **4a** was 94 % leading to side products.

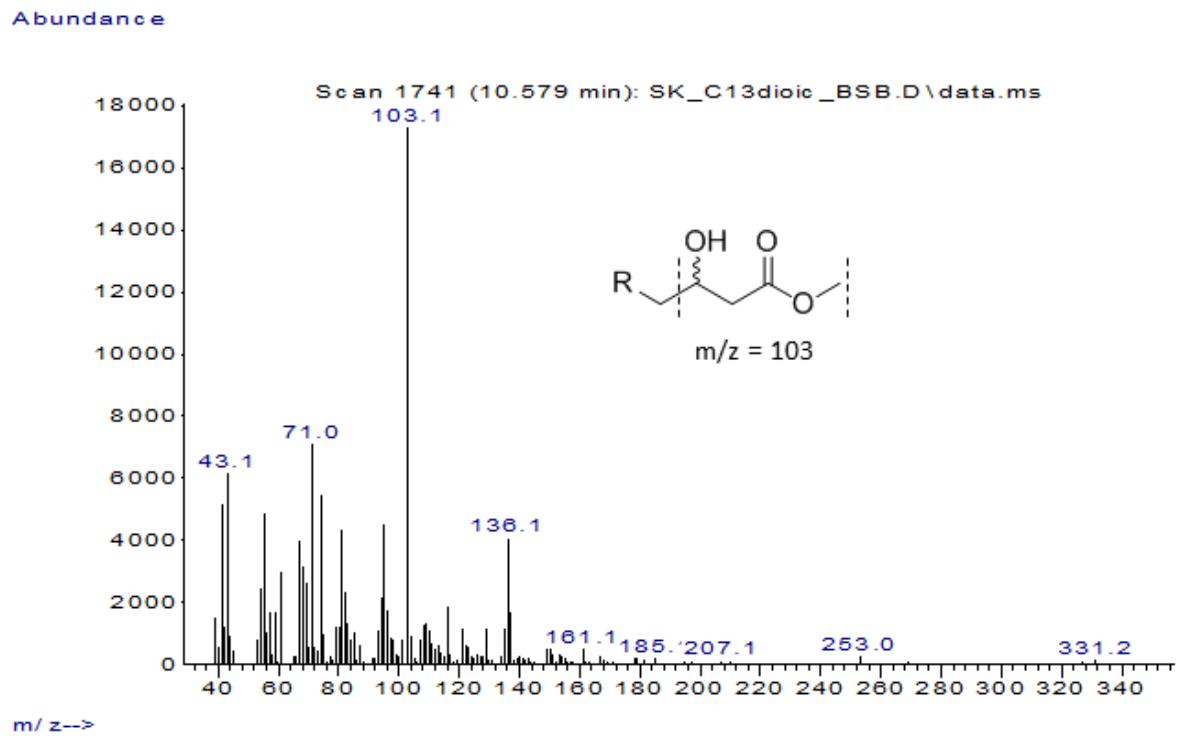

Figure S52. GC-MS spectra of **4g**-methyl ester (24 % GC-FID product area) obtained by conversion of **4a** (10 mM) with $CYP_{BS\beta}$ and H_2O_2 as oxidant (corresponds to peak b in Figure S51 A). The characteristic ion *m*/z = 103 is characteristic for ß-hydroxy acid methyl esters.[1]

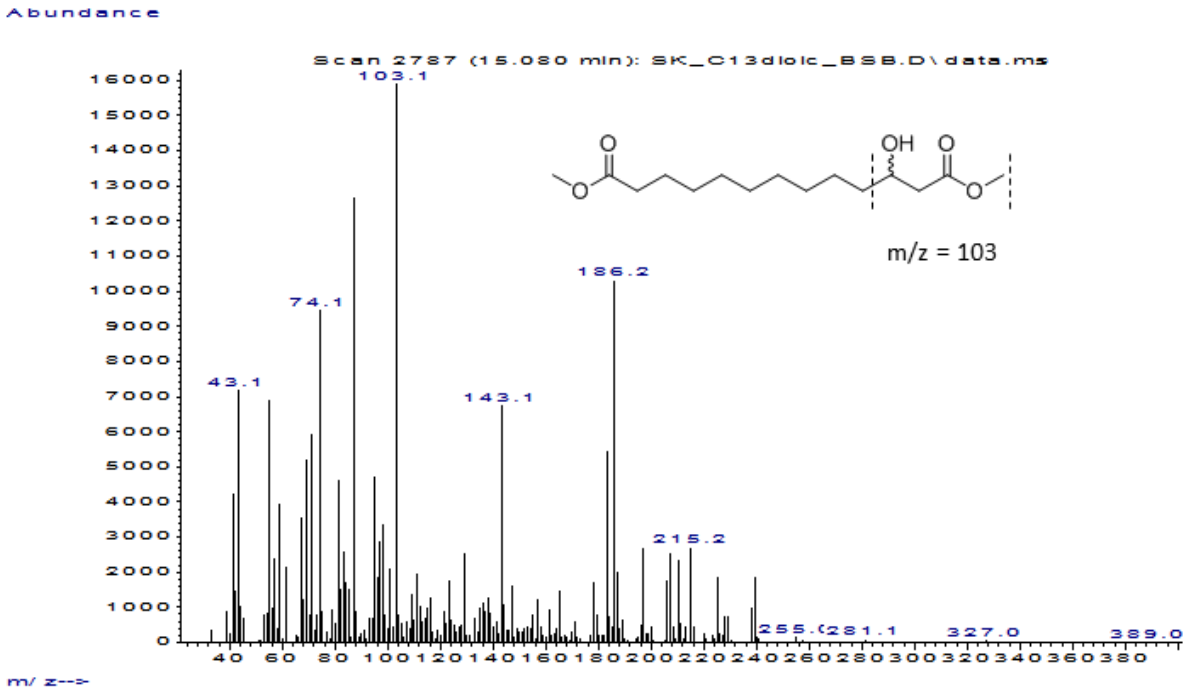

Figure S53. GC-MS spectra of **4f-**dimethyl ester (288.19 g mol^{-1}) obtained by conversion of **4a** (10 mM) with $CYP_{BS\beta}$ and H_2O_2 as oxidant (corresponds to peak d in Figure S51 A). The characteristic ion *m*/z = 103 was used to assign the product.

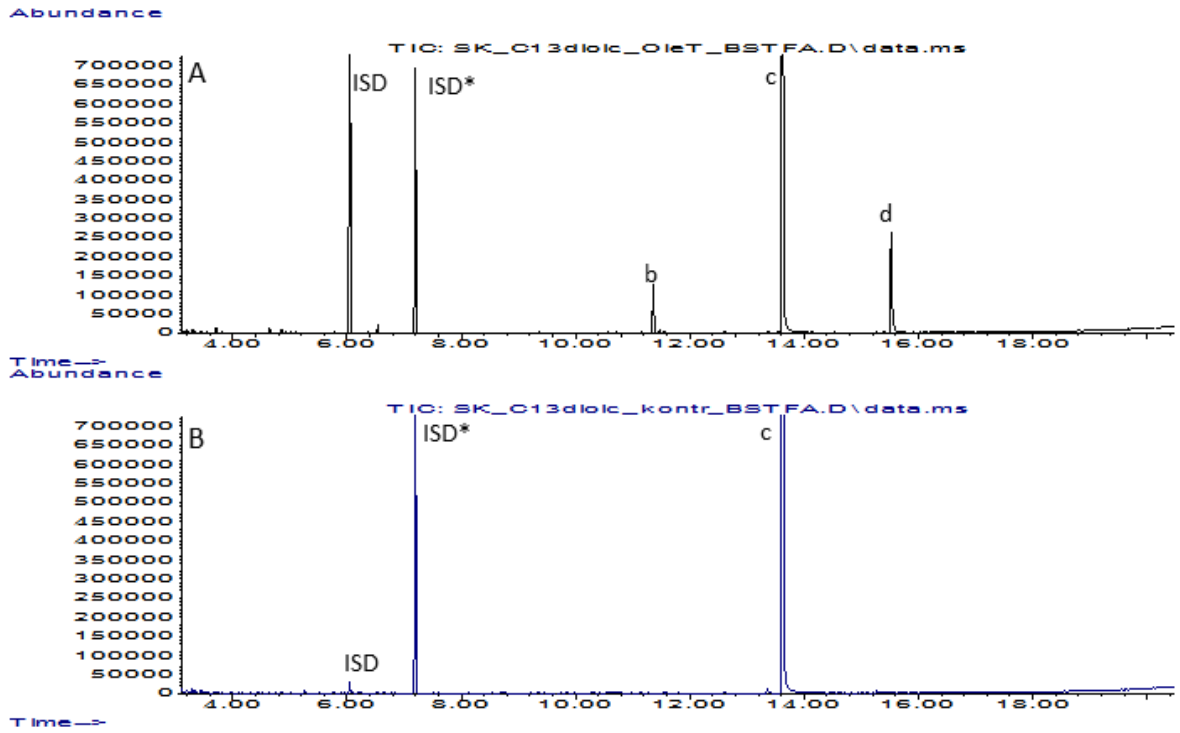

Figure S54. GC-MS chromatograms obtained by conversion of **4a** (10 mM) after derivatization with $TMSCHN_2$ and BSTFA. **A** = Conversion of **4a** with the OleT-CamAB-FDH system. **B** = Conversion of **4a** in the aqbsence of OleT (negative control). **ISD** = internal standard (0.1 % (v/v) 1-decanol); **ISD*** = silylated internal standard (TMS-1-decanol); **b** = TMS-**4g**-methyl ester; **c** = dimethyl ester of **4a** (substrate); **d** = TMS-**4f**-dimethyl ester.

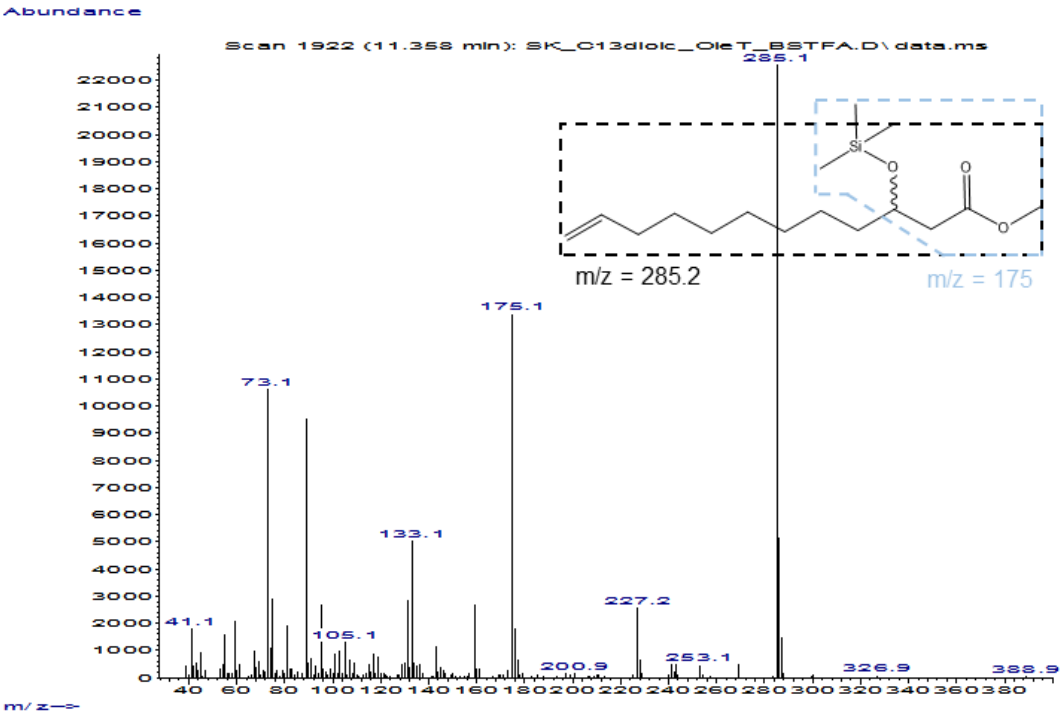

Figure S55. GC-MS spectra of TMS-**4g**-methyl ester obtained by conversion of **4a** (10 mM) with the OleT-CamAB-FDH system (corresponds to peak b in Figure S54 A). The characteristic ions *m*/z = 175 and *m*/z = 285.2 were used to assign the product as described elsewhere.[2]

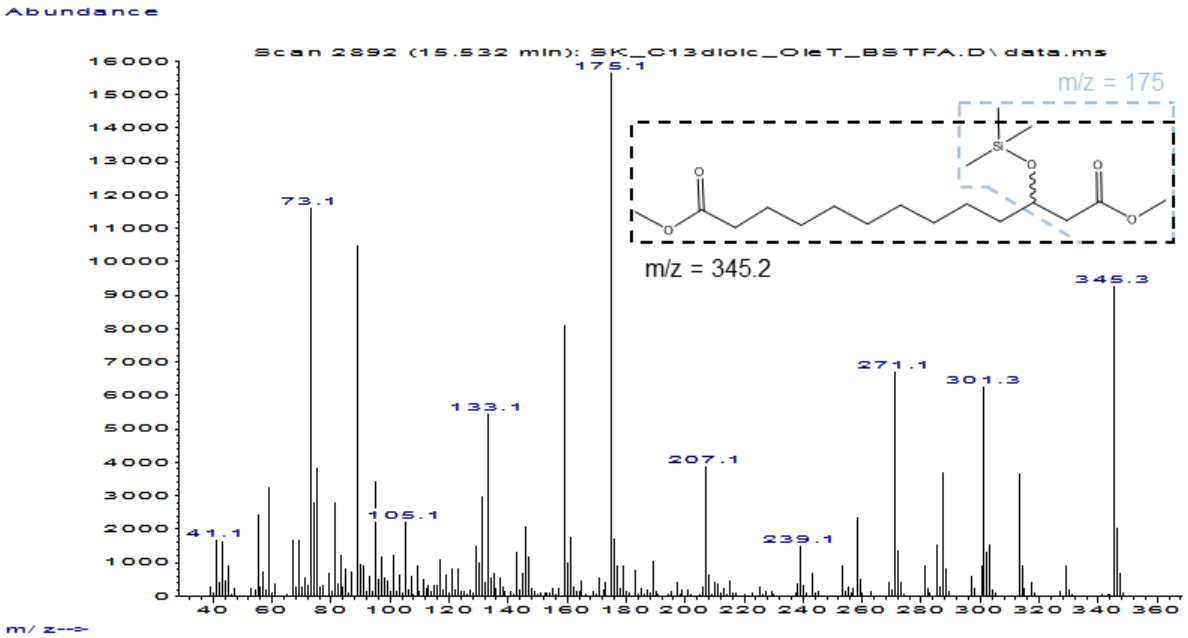

Figure S56. GC-MS spectra of TMS-**4f**-dimethyl ester obtained by conversion of **4a** (10 mM) with the OleT-CamAB-FDH system (corresponds to peak d in Figure S54 A). The characteristic ions *m*/z = 175 and *m*/z = 345.2 were used to assign the product as described elsewhere.[2]

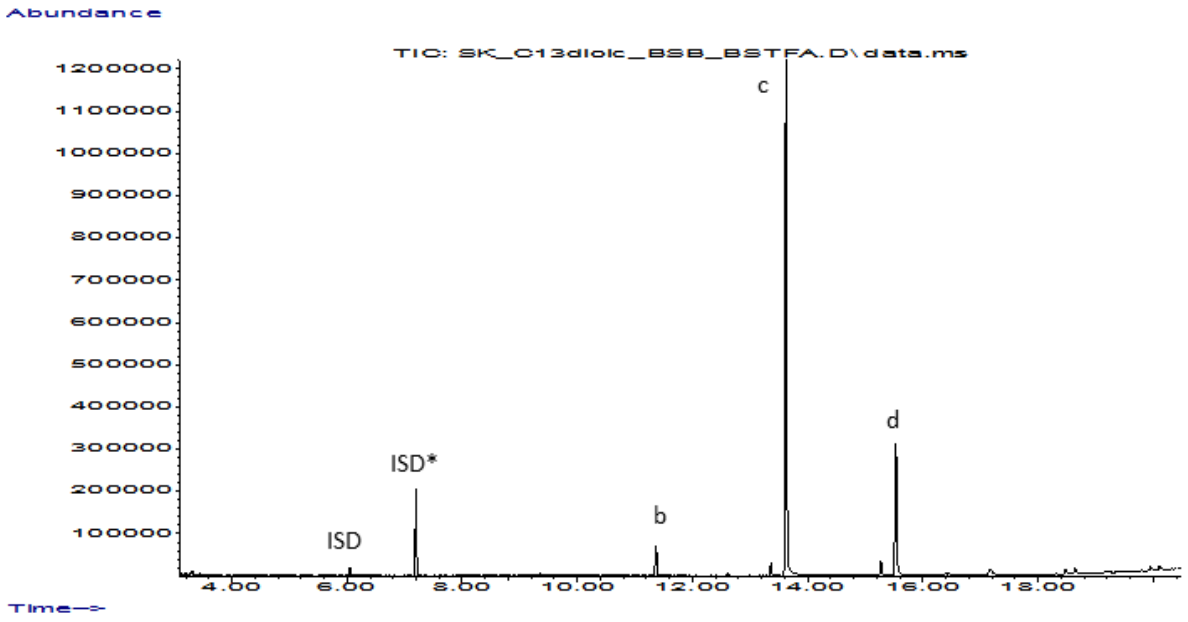

Figure S57. GC-MS chromatograms obtained by conversion of **4a** (10 mM) with $CYP_{BS\beta}$ and H_2O_2 as oxidant after derivatization with $TMSCHN_2$ and BSTFA. **ISD** = internal standard (0.1 % (v/v) 1-decanol); **ISD*** = silylated internal standard (TMS-1-decanol); **b** = TMS-**4g**-methyl ester; **c** = dimethyl ester of **4a** (substrate); **d** = TMS-**4f**-dimethyl ester.

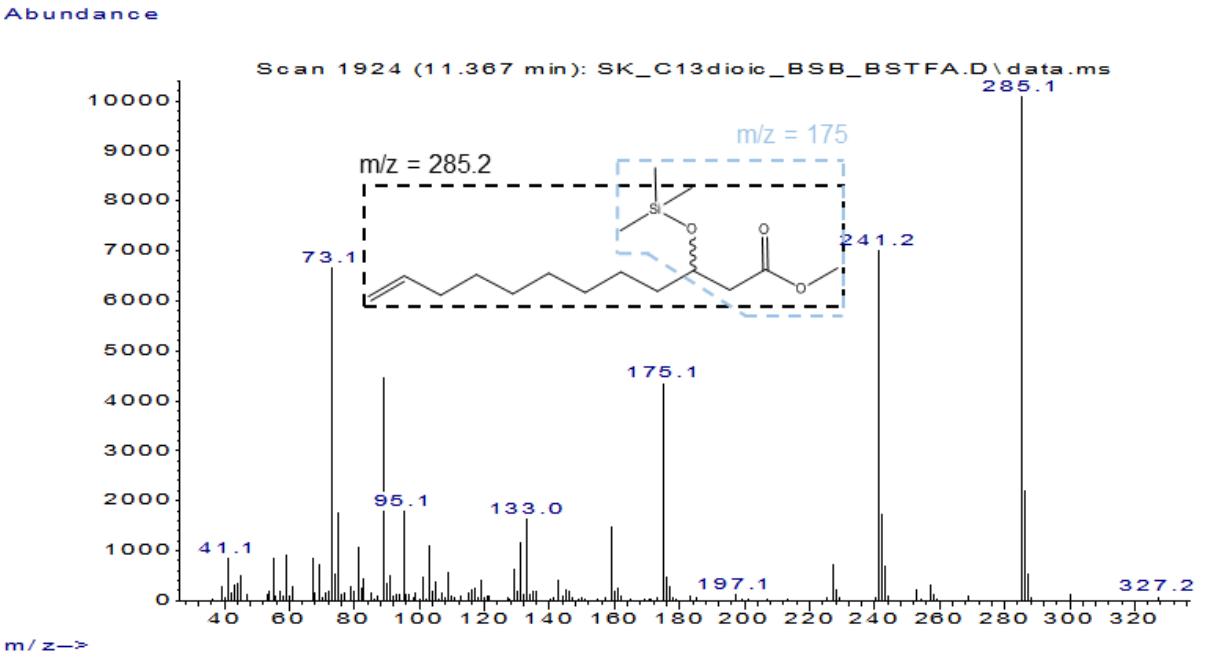

Figure S58. GC-MS spectra of TMS-**4g**-methyl ester obtained by conversion of **4a** (10 mM) with $CYP_{BS\beta}$ and H_2O_2 as oxidant (corresponds to peak b in Figure S57). The characteristic ions *m*/z = 175 and *m*/z = 285.2 were used to assign the product as described elsewhere.[2]

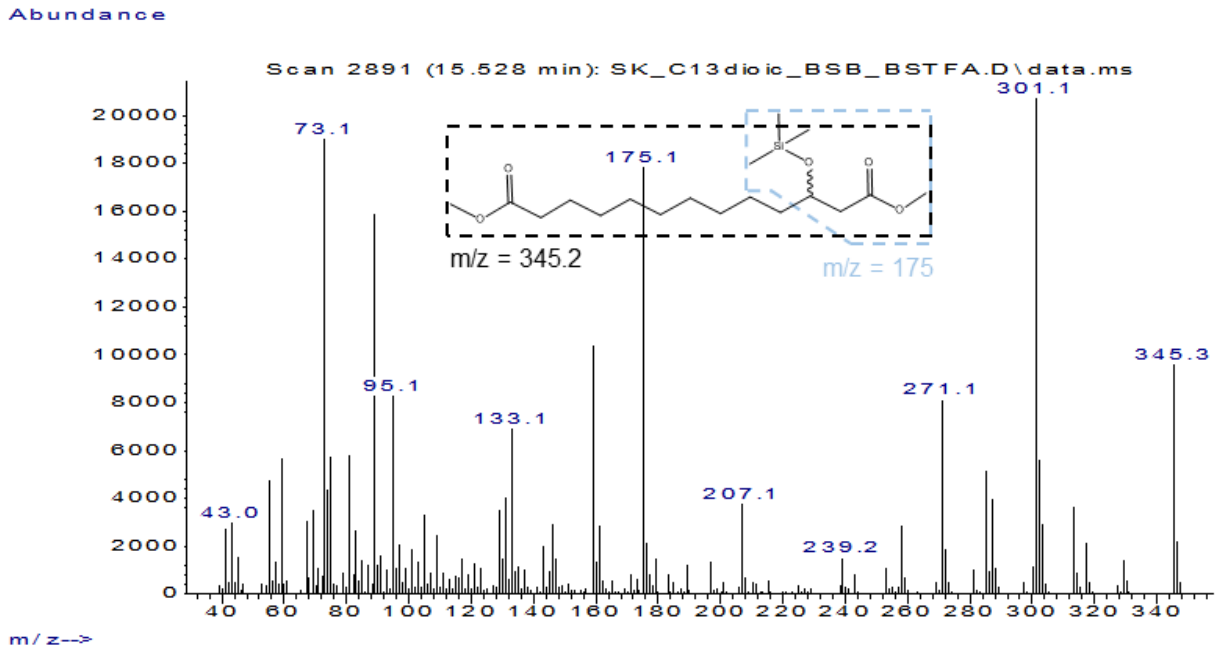

Figure S59. GC-MS spectra of TMS-**4f**-dimethyl ester obtained by conversion of **4a** (10 mM) with $CYP_{BS\beta}$ and H_2O_2 as oxidant (corresponds to peak d in Figure S57). The characteristic ions *m*/z = 175 and *m*/z = 345.2 were used to assign the product as described elsewhere.[2]

7.1.5 **Conversion of 5a**

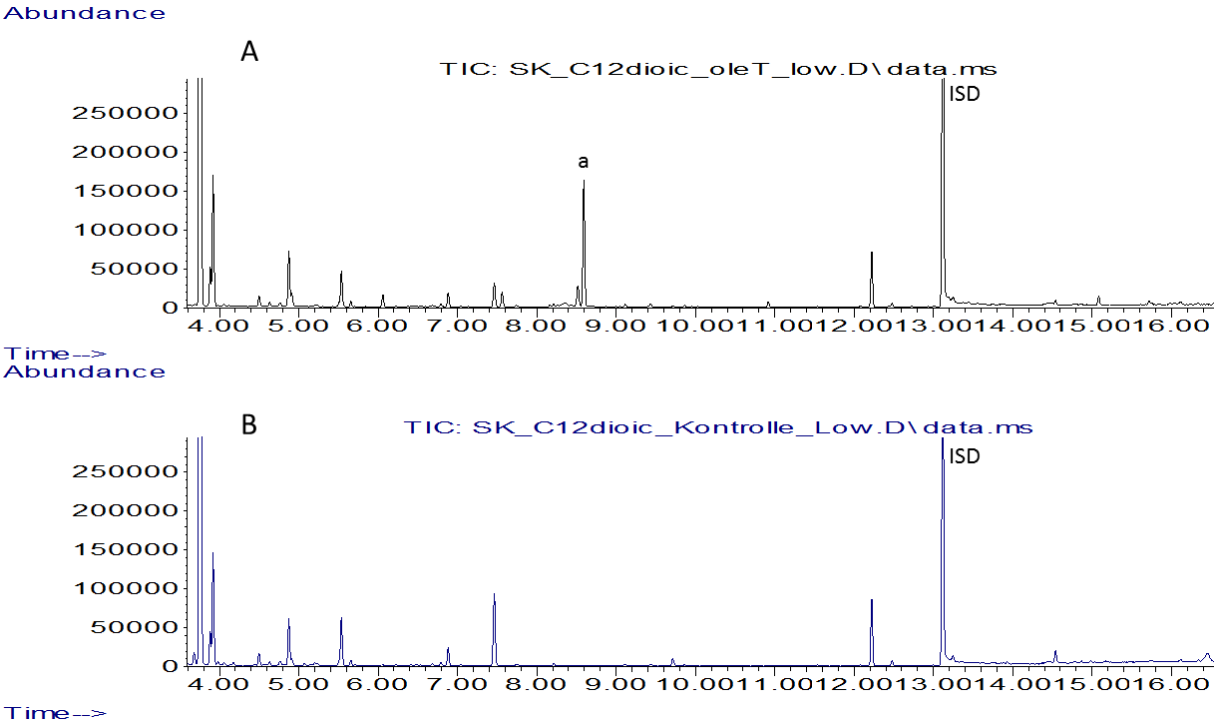

Figure S60. GC-MS chromatograms obtained by conversion of **5a** (10 mM). **A** = Conversion of **5a** with the OleT-CamAB-FDH system. **B** = Conversion of **5a** in the absence of OleT (negative control). **ISD** = internal standard (0.1 % (v/v) 1-decanol); **a** = **5c**.

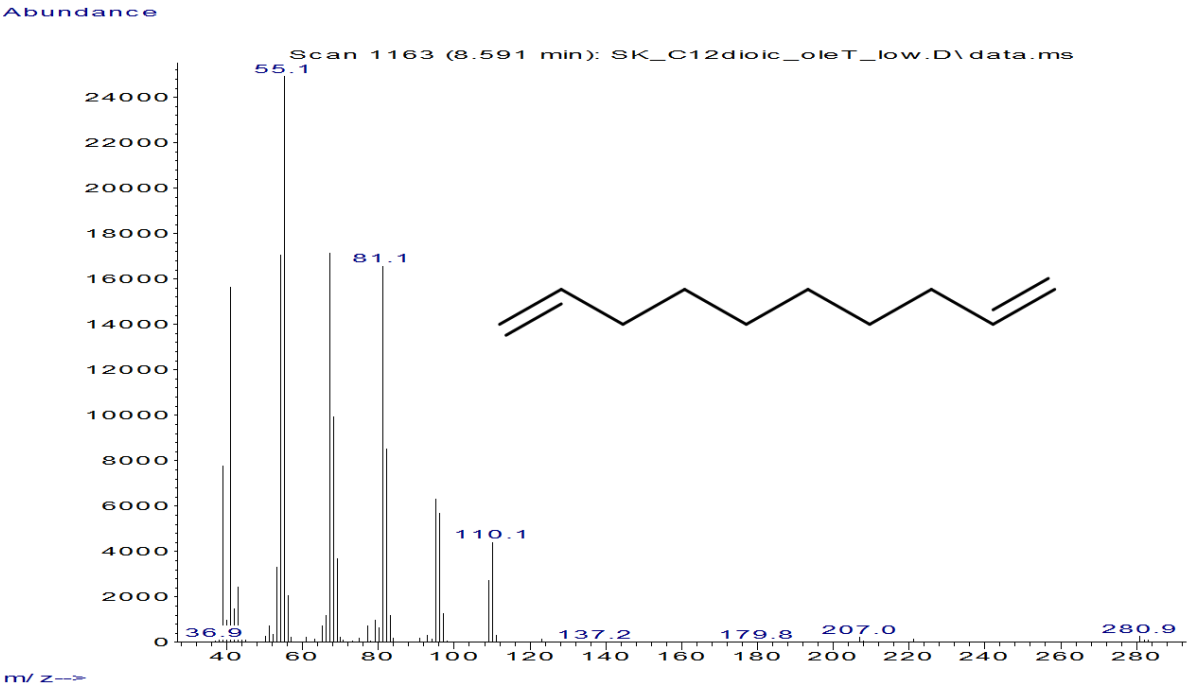

Figure S61. GC-MS spectra of **5c** (138.14 g mol^{-1}) obtained by conversion of **5a** (10 mM) with the OleT-CamAB-FDH system (corresponds to peak a in Figure S60 A).

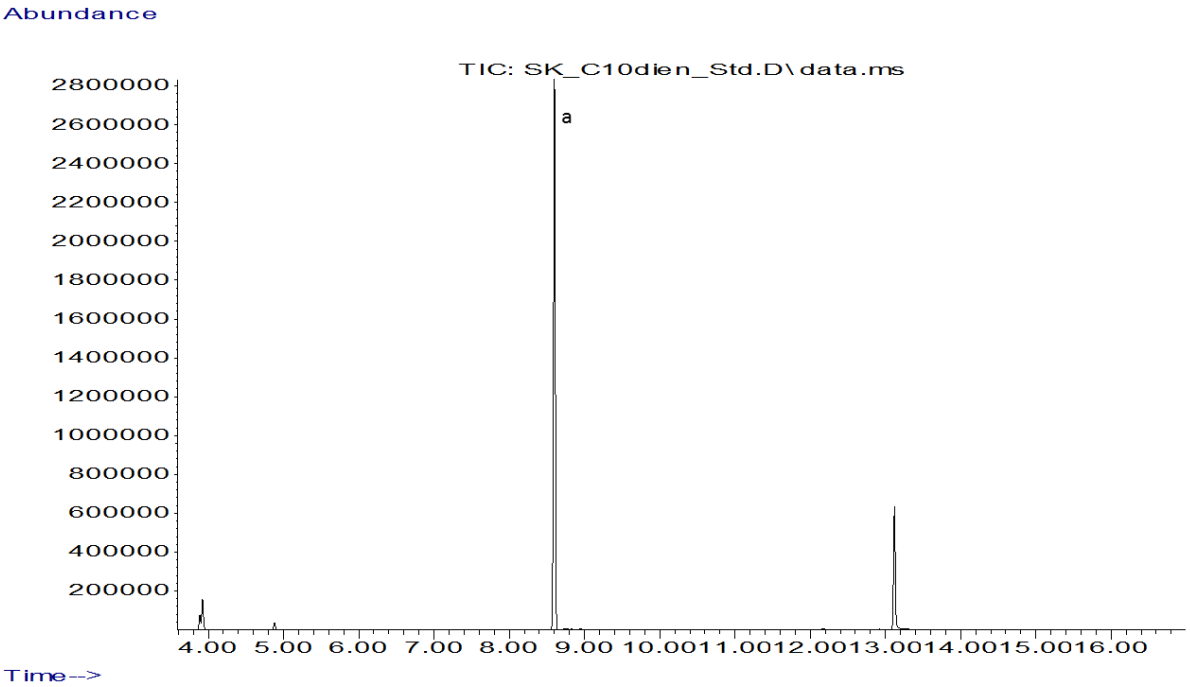

Figure S62. GC-MS chromatogram of a commercial standard of **5a**. **a** = **5a**. The peak at ~13.1 min corresponds to 1-decanol supplemented as internal standard (0.1 % v/v).

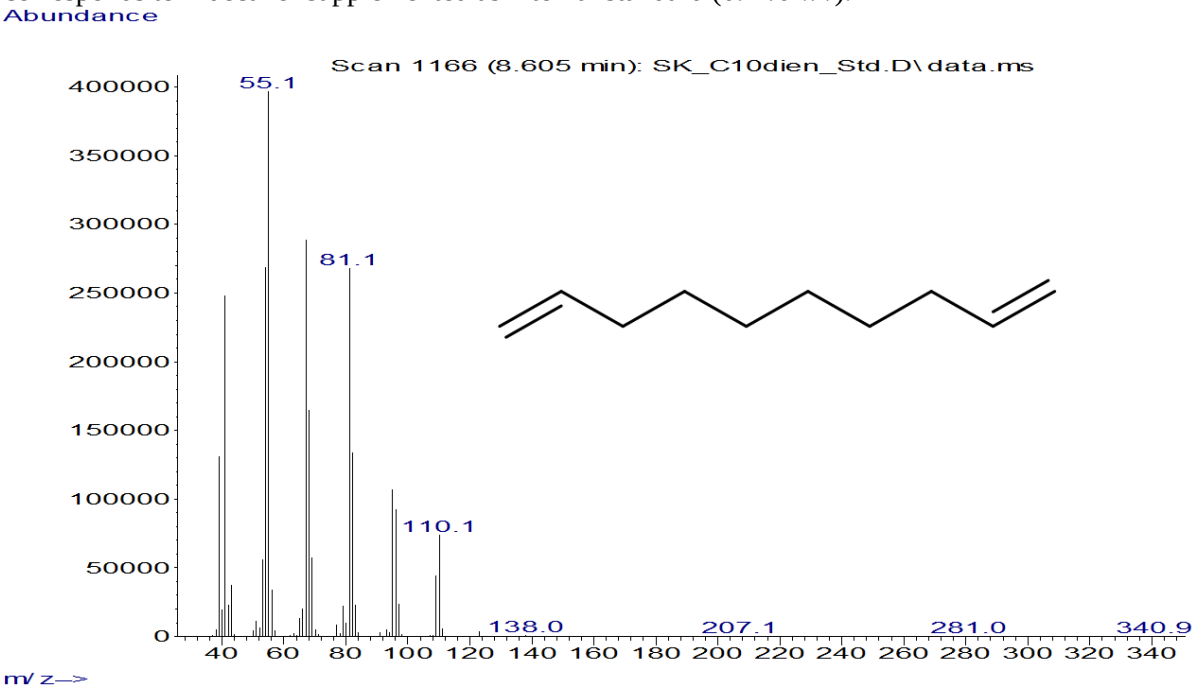

Figure S63. GC-MS spectra of a commercial standard of **5a** (138.14 g mol^{-1}, corresponds to peak a in Figure S62).

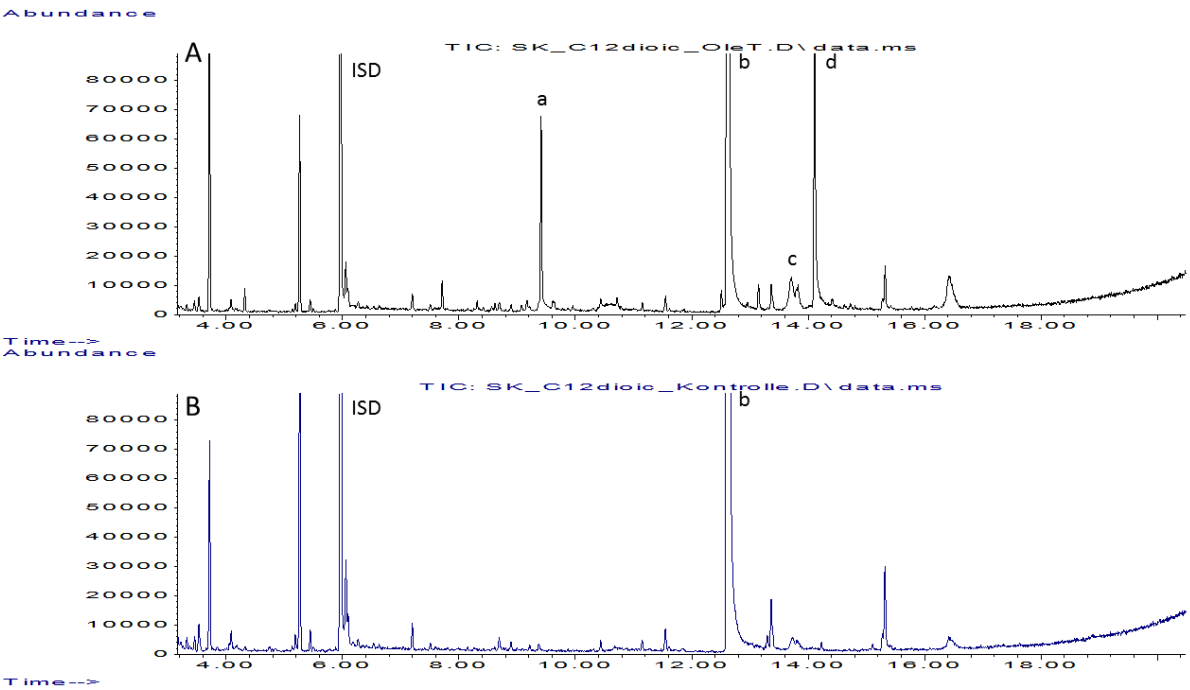

Figure S64. GC-MS chromatograms obtained by conversion of **5a** (10 mM). **A** = Conversion of **5a** with the OleT-CamAB-FDH system. **B** = Conversion of **5a** in the absence of OleT (negative control). **ISD** = internal standard (0.1 % (v/v) 1-decanol); **a** = **5g**-methyl ester (18 % GC-MS area); **b** = dimethyl ester of **5a** (substrate); **c** = **5d-** dimethyl ester; **d** = **5f**-dimethyl ester.

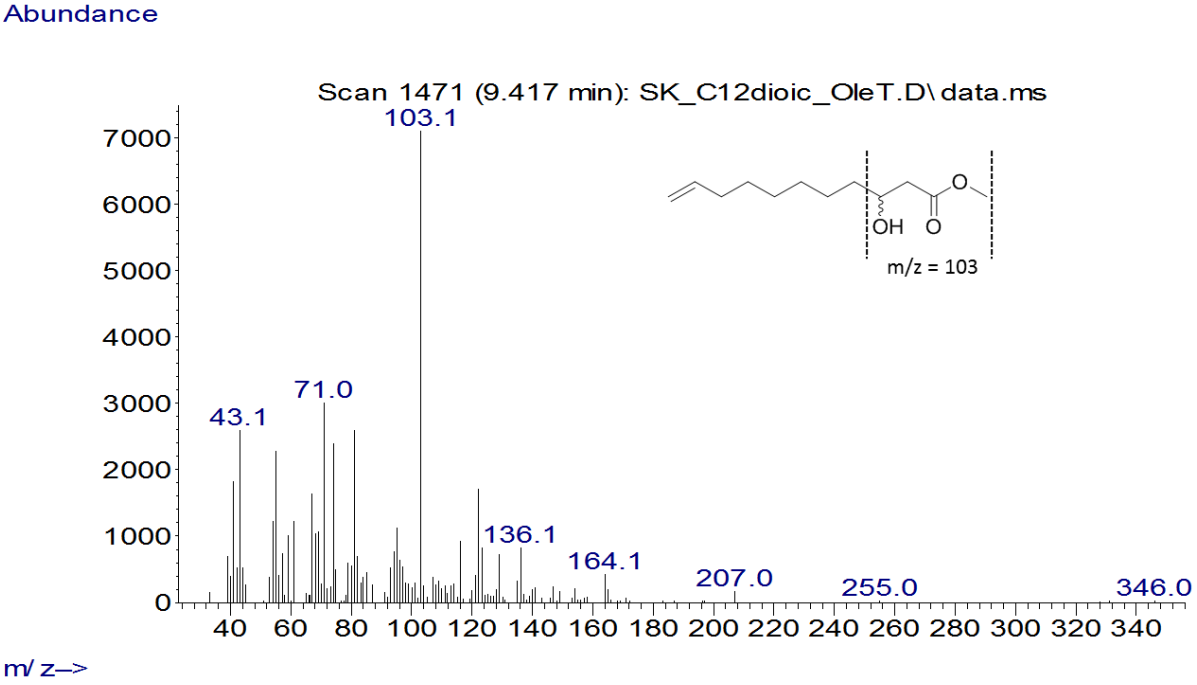

Figure S65. GC-MS spectra of **5g**-methyl ester (214.16 g mol^{-1}) obtained by conversion of **5a** (10 mM) with the OleT-CamAB-FDH system (corresponds to peak a in Figure S64 A). See also Figure S122 (conversion of **5b** with $CYP_{BSß}$), Figure S73, Figure S74, Figure S77, Figure S124 and Figure S126 (BSTFA derivatization) for comparison. The characteristic ion *m*/z = 103 was used to assign the product.

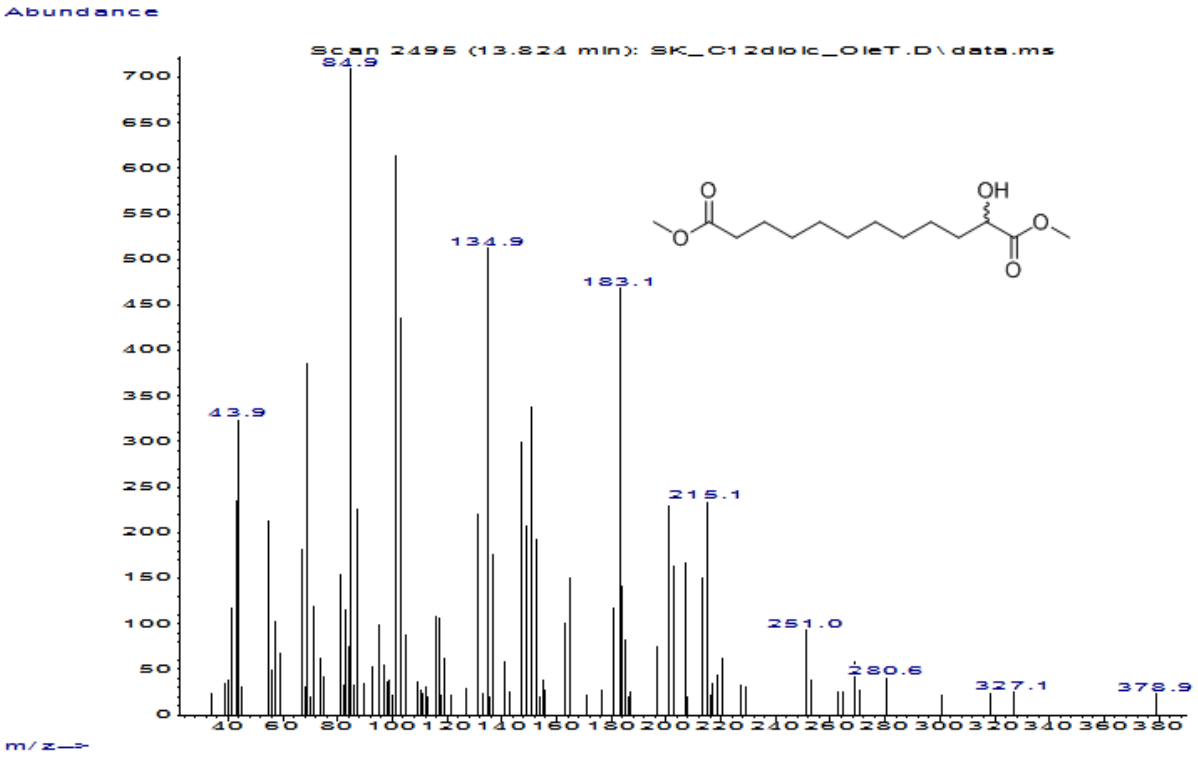

Figure S66. GC-MS spectra of **5d**-dimethyl ester (274.18 g mol^{-1}) obtained by conversion of **5a** (10 mM) with the OleT-CamAB-FDH system (corresponds to peak c in Figure S64 A).

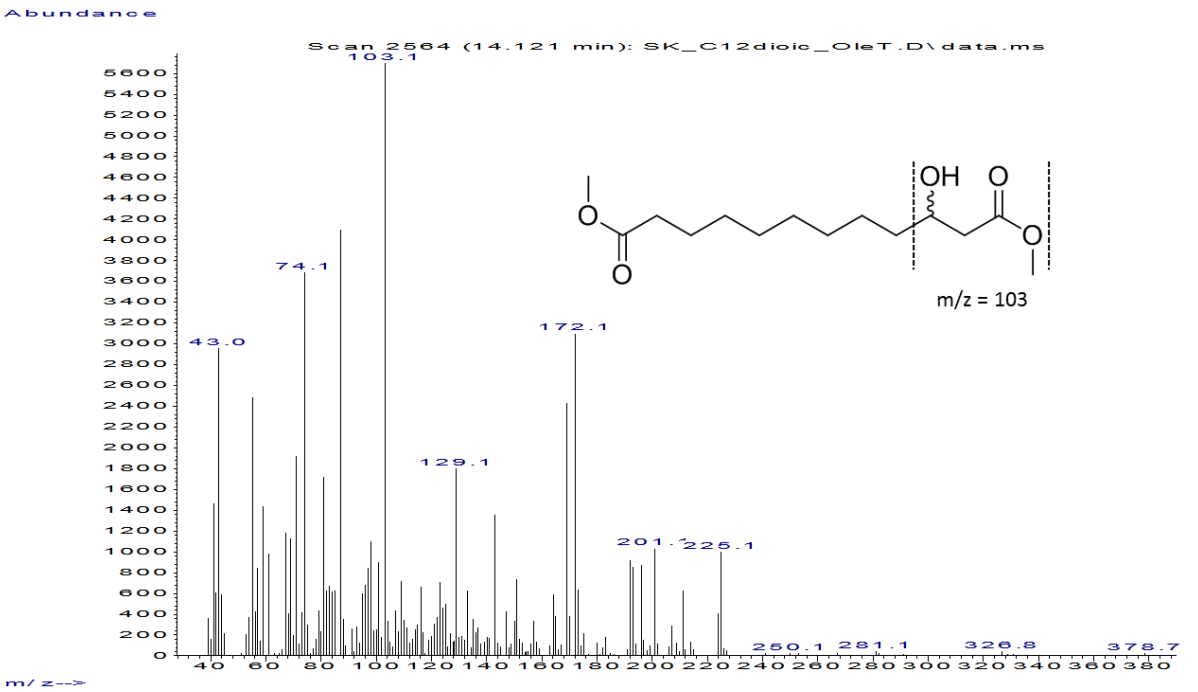

Figure S67. GC-MS spectra of **5f**-dimethyl ester (274.18 g mol^{-1}) obtained by conversion of **5a** (10 mM) with the OleT-CamAB-FDH system (corresponds to peak d in Figure S64 A). The characteristic ion *m*/z = 103 was used to assign the product.

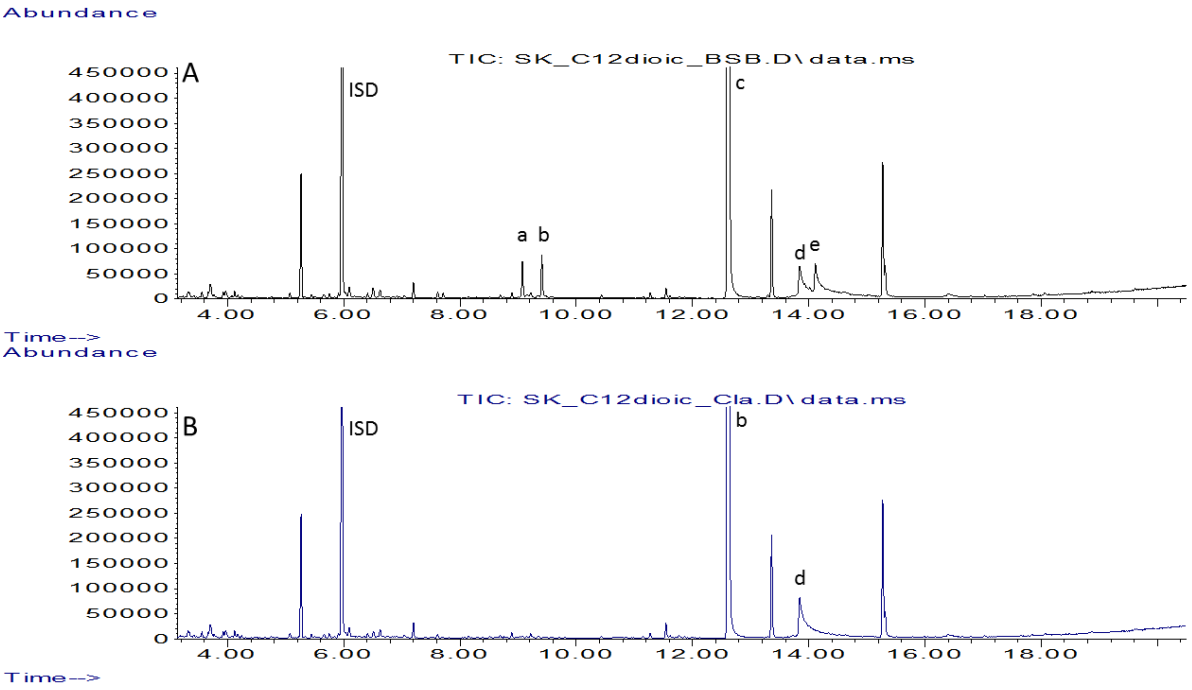

Figure S68. GC-MS chromatograms obtained by conversion of **5a** (10 mM) with $CYP_{BSß}$ (**A**) and $P450_{Cla}$ (**B**) using H_2O_2 as oxidant. **ISD** = internal standard (0.1 % (v/v) 1-decanol); **a** = **5e**-methyl ester (see also Figure S120 B and Figure S122 for comparison); **b** = **5g**-methyl ester (see also Figure S120A and Figure S121 for comparison); **c** = dimethyl ester of **5a** (substrate); **d** = **5d**-dimethyl ester; **e** = **5f**-dimethyl ester.

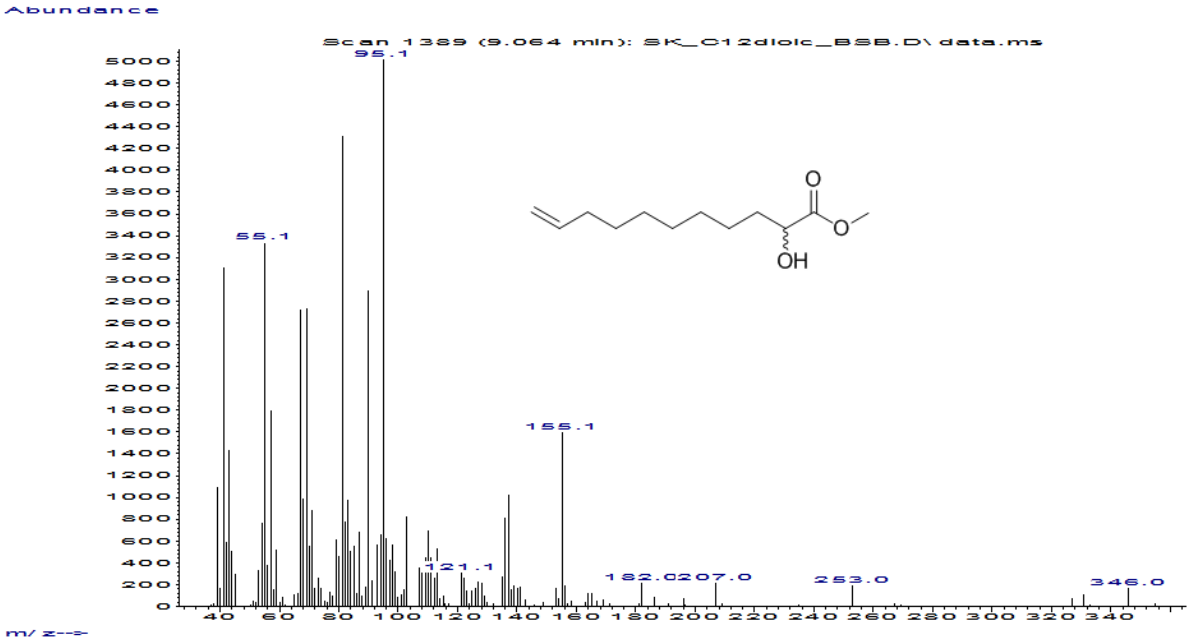

Figure S69. GC-MS spectra of **5e**-methyl ester (214.16 g mol^{-1}) obtained by conversion of **5a** (10 mM) with $CYP_{BSß}$ and H_2O_2 as oxidant (corresponds to peak a in Figure S68 A; compare also to Figure S121 showing conversion of **5b** with $P450_{Cla}$).

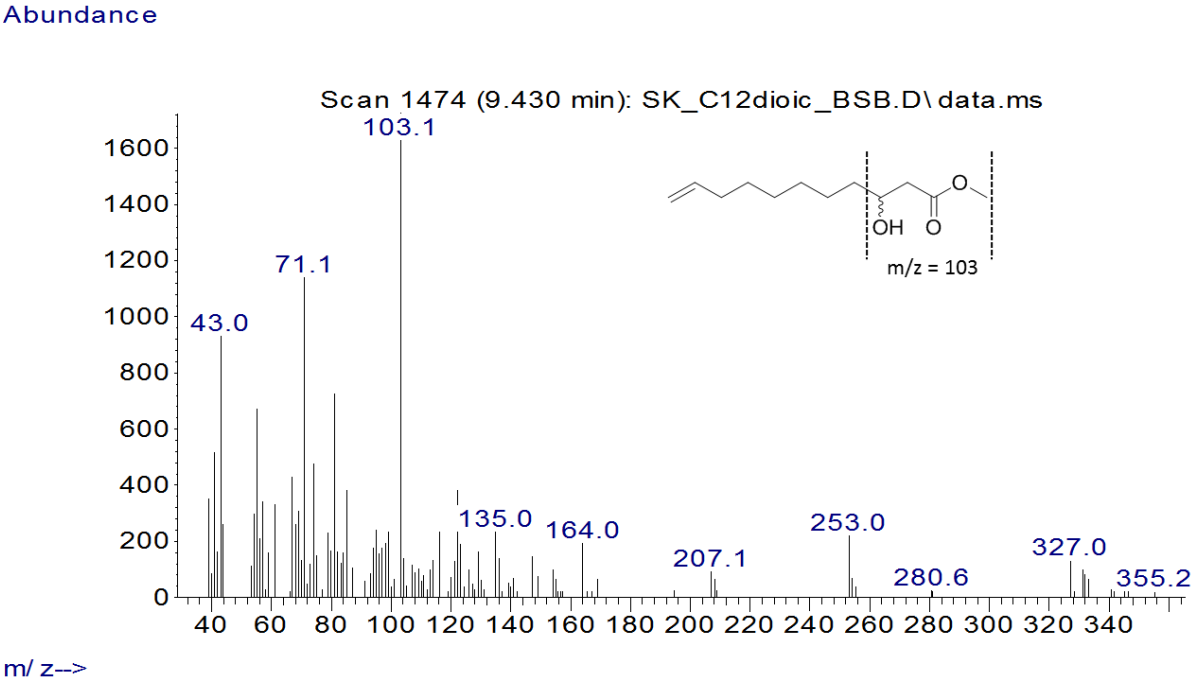

Figure S70. GC-MS spectra of **5g-**methyl ester obtained by conversion of **5a** (10 mM) with $CYP_{BSß}$ and H_2O_2 as oxidant (corresponds to peak b in Figure S68 A; compare also to Figure S121 showing conversion of **5b** with $CYP_{BSß}$). The characteristic ion *m*/z = 103 was used to assign the product.

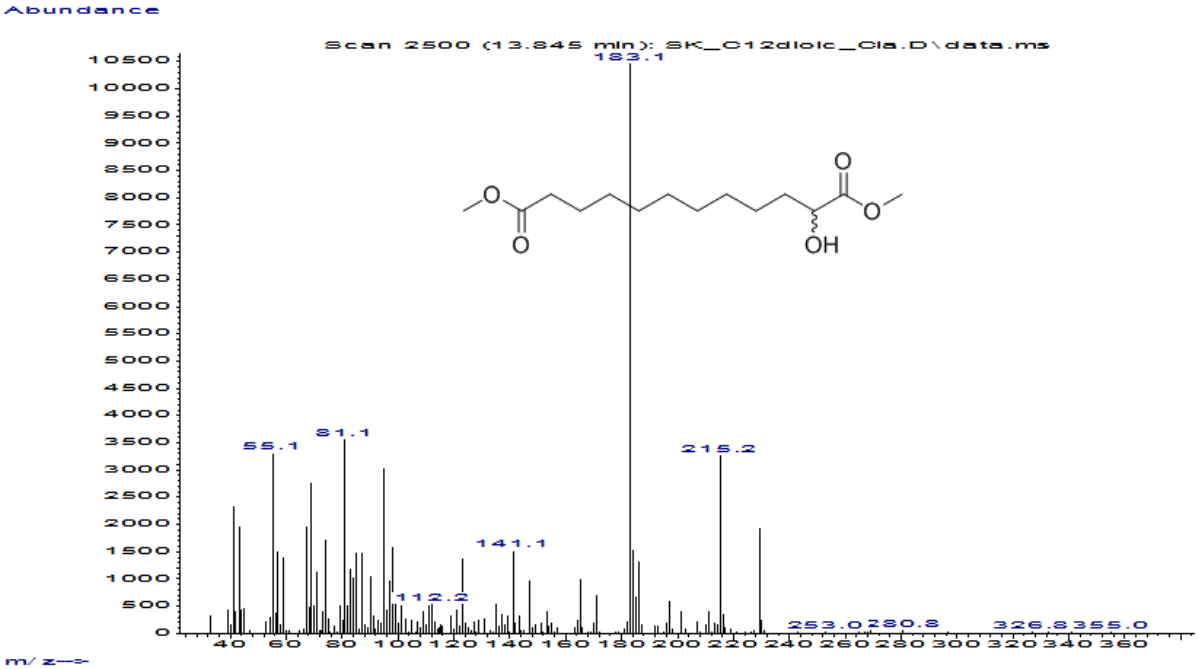

Figure S71. GC-MS spectra of **5d-**dimethyl ester (274.18 g mol^{-1}) obtained by conversion of **5a** (10 mM) with $P450_{Cla}$ and H_2O_2 oxidant (corresponds to peak d in Figure S68 A and B).

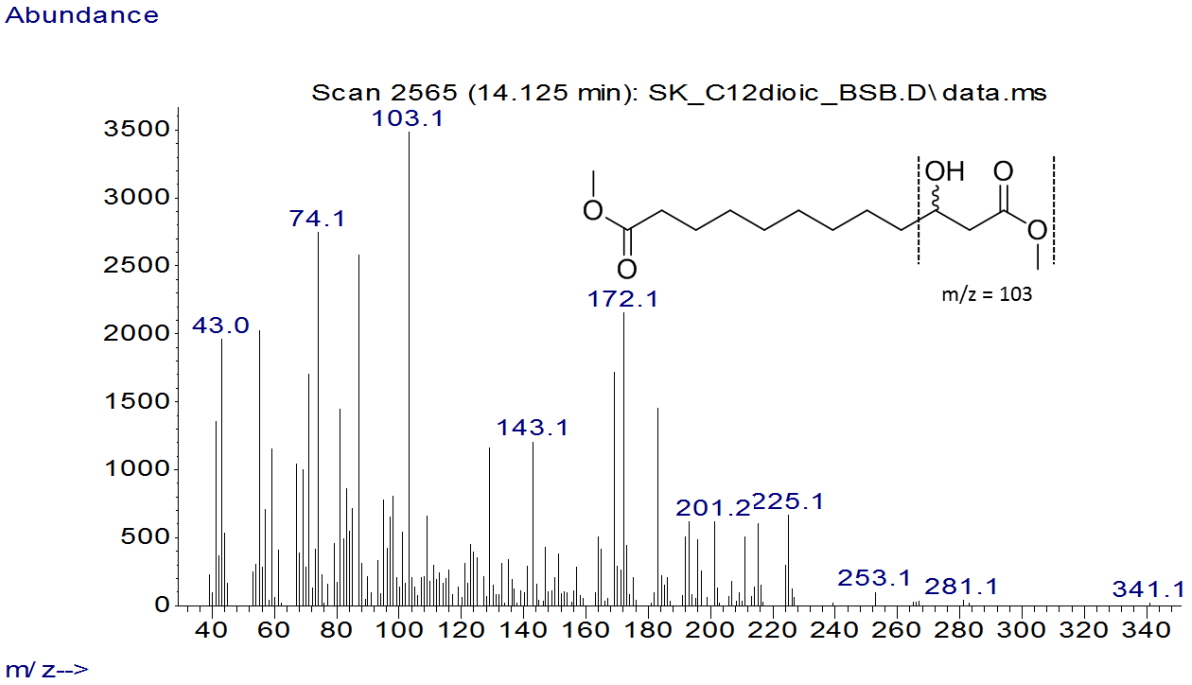

Figure S72. GC-MS spectra of **5f**-dimethyl ester (274.18 g mol^{-1}) obtained by conversion of **5a** (10 mM) with $CYP_{BSß}$ and H_2O_2 as oxidant (corresponds to peak e in Figure S68 A). The characteristic ion *m*/z = 103 was used to assign the product.

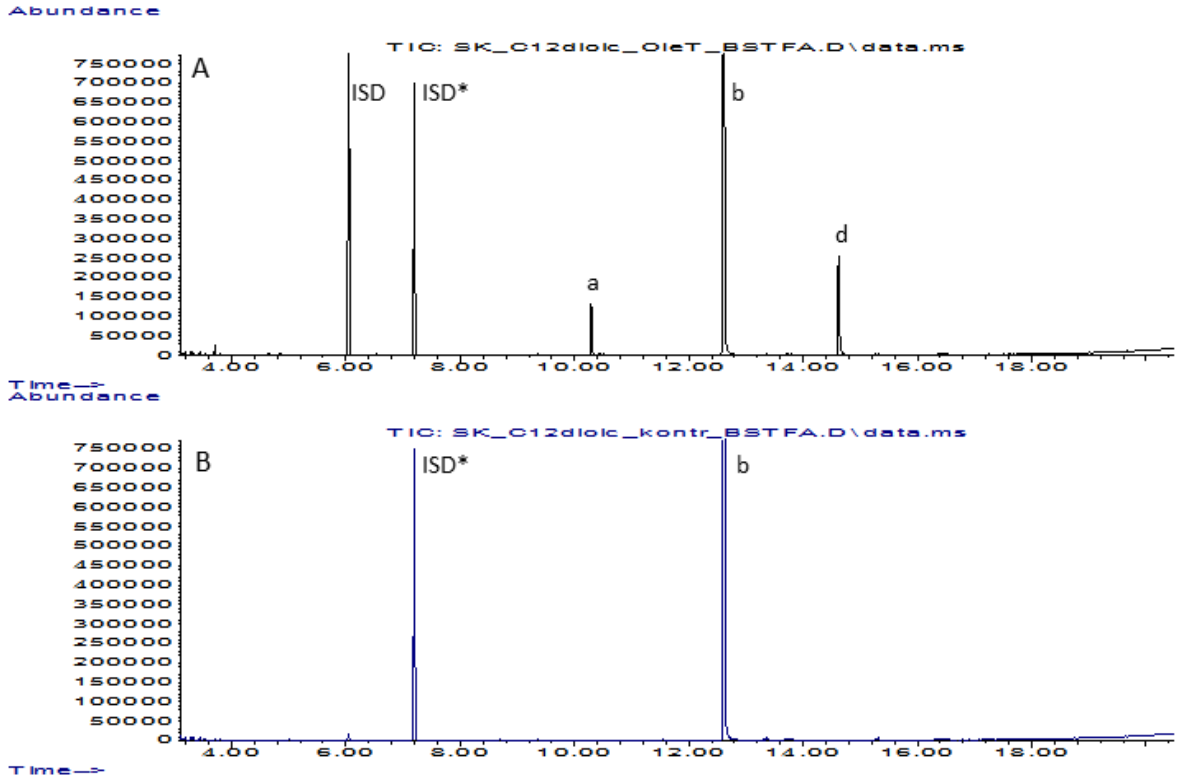

Figure S73. GC-MS chromatograms obtained by conversion of **5a** (10 mM) after derivatization with $TMSCHN_2$ and BSTFA. **A** = Conversion of **5a** with the OleT-CamAB-FDH system. **B** = Conversion of **5a** in the absence of OleT (negative control). **ISD** = internal standard (0.1 % (v/v) 1-decanol); **ISD*** = silylated internal standard; **a** = **5g**-methyl ester; **b** = dimethyl ester of **5a** (substrate); **d** = TMS-**5f**-dimethyl ester.

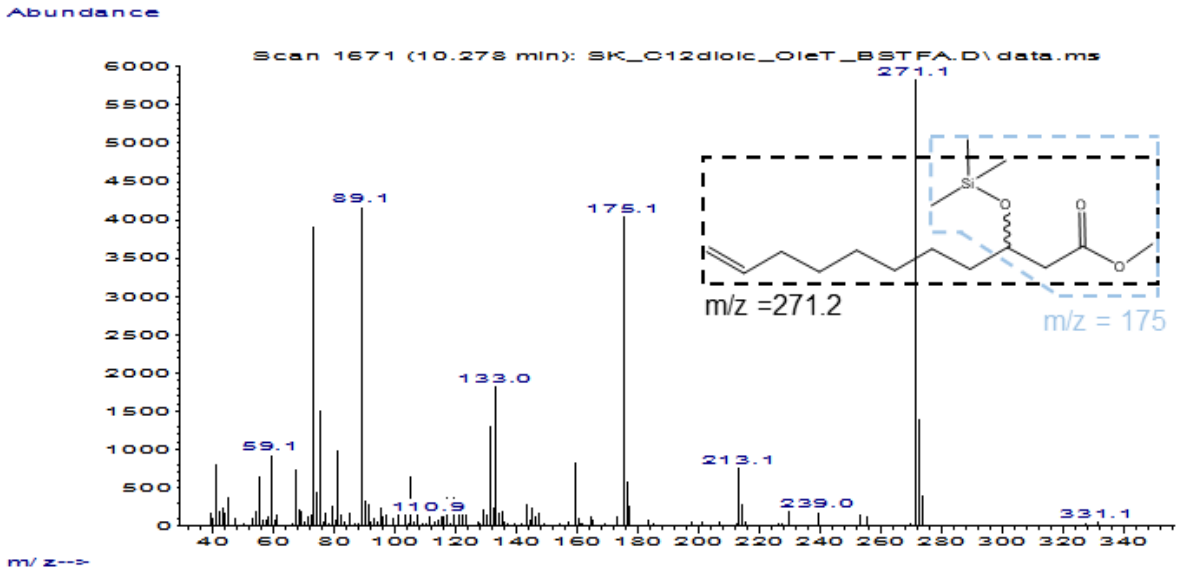

Figure S74. GC-MS spectra of TMS-**5g**-methyl ester obtained by conversion of **5a** (10 mM) with the OleT-CamAB-FDH system (corresponds to peak a in Figure S73 A). The characteristic ions *m*/z = 175 and *m*/z = 271.2 were used to assign product as described elsewhere.[2]

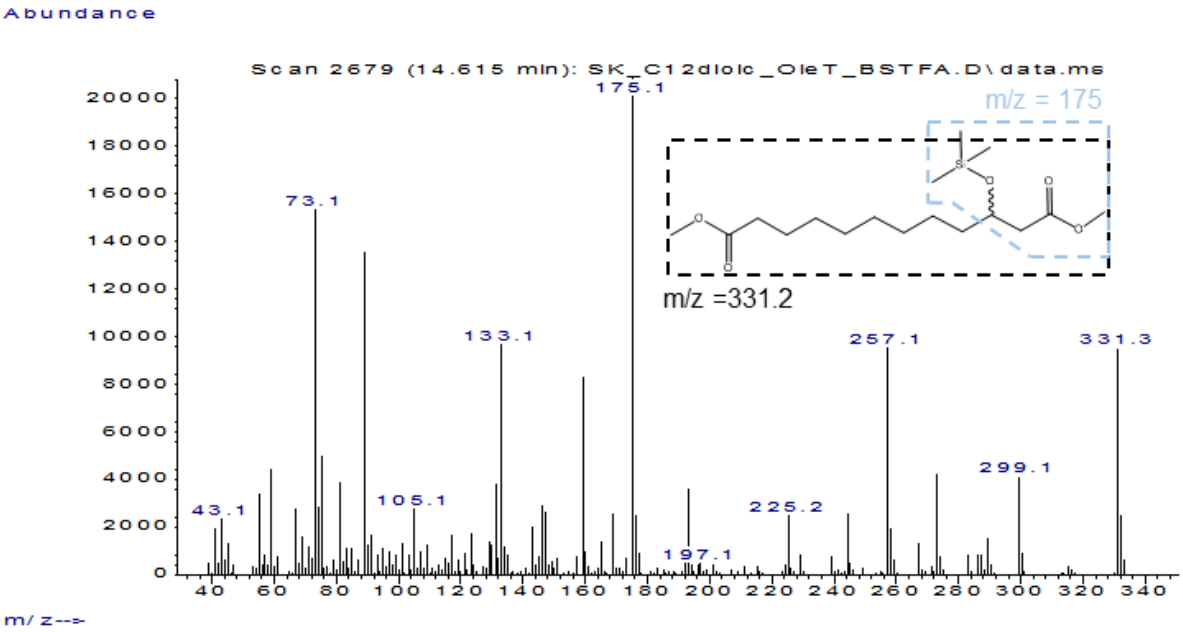

Figure S75. GC-MS spectra of TMS-**5f**-dimethyl ester obtained by conversion of **5a** (10 mM) with the OleT-CamAB-FDH system (corresponds to peak d in Figure S73 A). The characteristic ions *m*/z = 175 and *m*/z = 331.2 were used to assign the product as described elsewhere.[2]

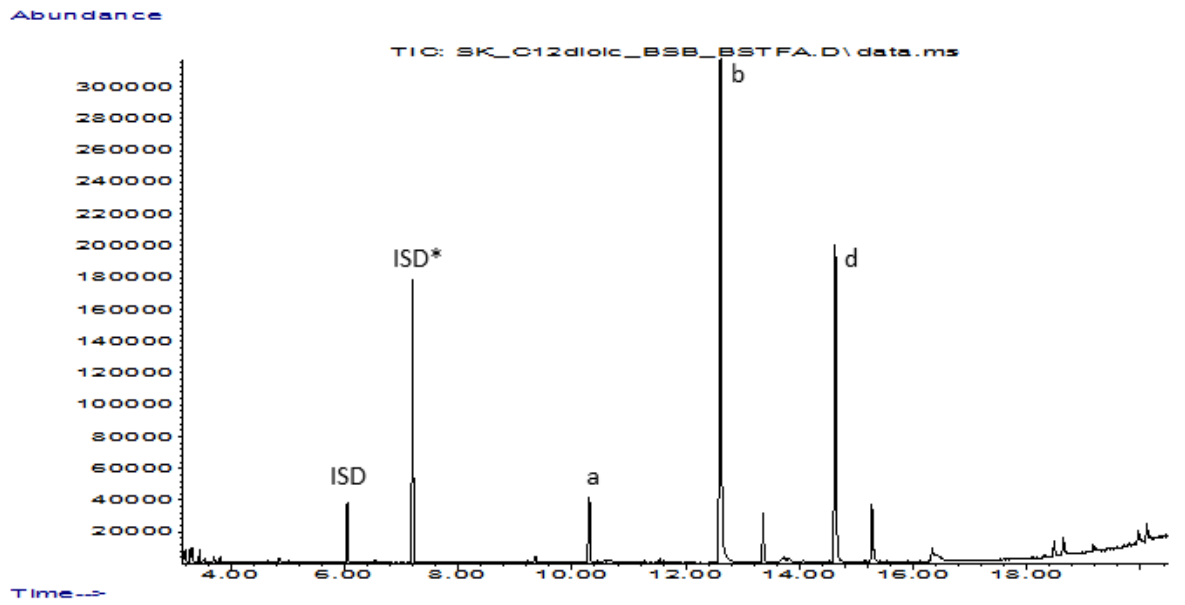

Figure S76. GC-MS chromatograms obtained by conversion of **5a** (10 mM) with $CYP_{BS\beta}$ and H_2O_2 as oxidant after derivatization with $TMSCHN_2$ and BSTFA. **ISD** = internal standard (0.1 % (v/v) 1-decanol); **ISD*** = silylated internal standard (TMS-1-decanol); **a** = TMS-**5g**-methyl ester; **b** = dimethyl ester of **5a** (substrate); **d** = TMS-**5f**-dimethyl ester.

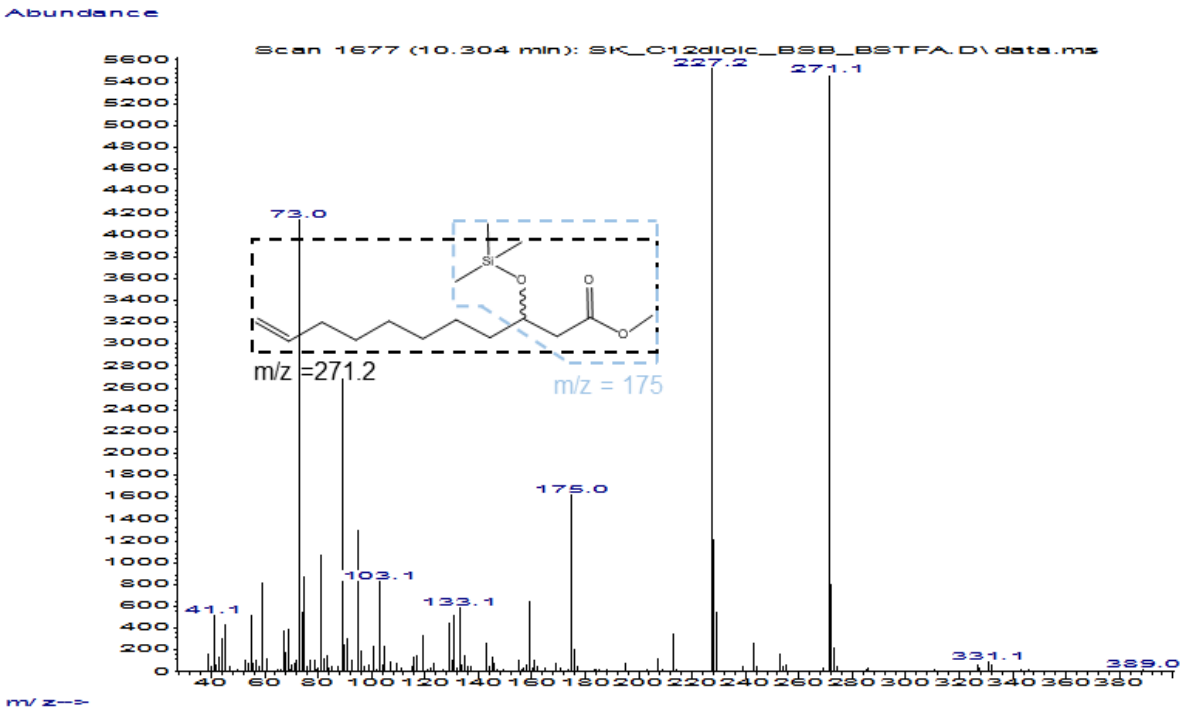

Figure S77. GC-MS spectra of TMS-**5g**-methyl ester obtained by conversion of **5a** (10 mM) with $CYP_{BS\beta}$ and H_2O_2 as oxidant (corresponds to peak a in Figure S76). The characteristic ions *m*/z = 175 and *m*/z = 271.2 were used to assign the product as described elsewhere.[2]

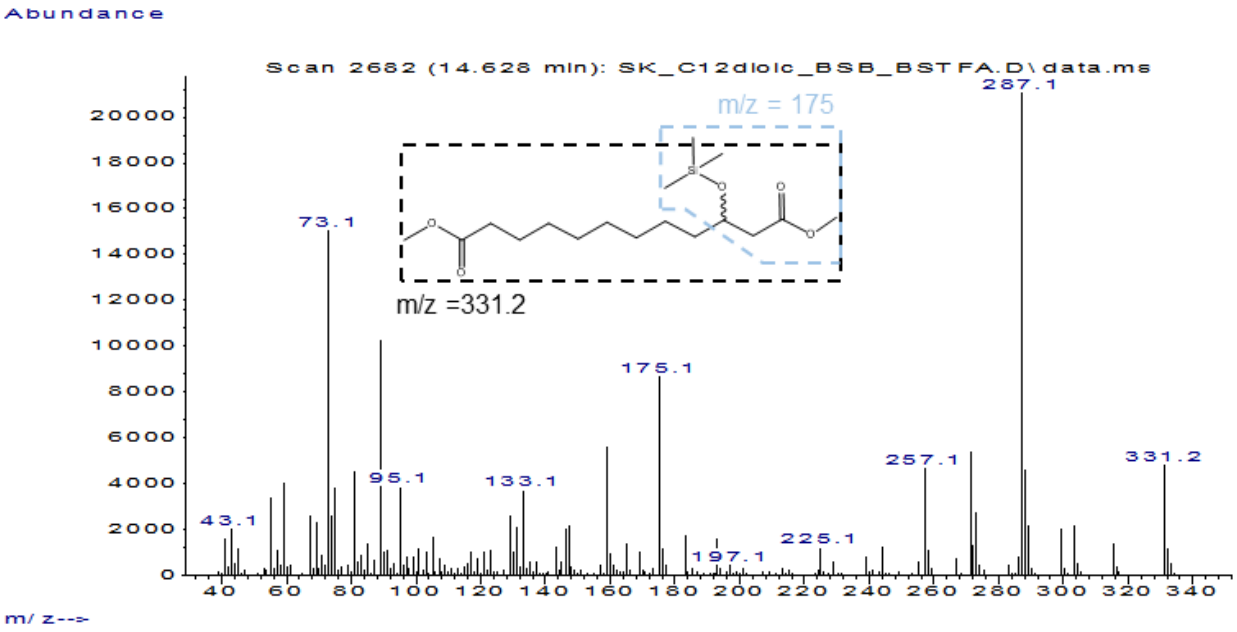

Figure S78. GC-MS spectra of TMS-**5f**-dimethyl ester obtained by conversion of **5a** (10 mM) with $CYP_{BS\beta}$ and H_2O_2 as oxidant (corresponds to peak d in Figure S76). The characteristic ions *m*/z = 175 and *m*/z = 331.2 were used to assign the product as described elsewhere.[2]

7.1.6 **Conversion of 6a**

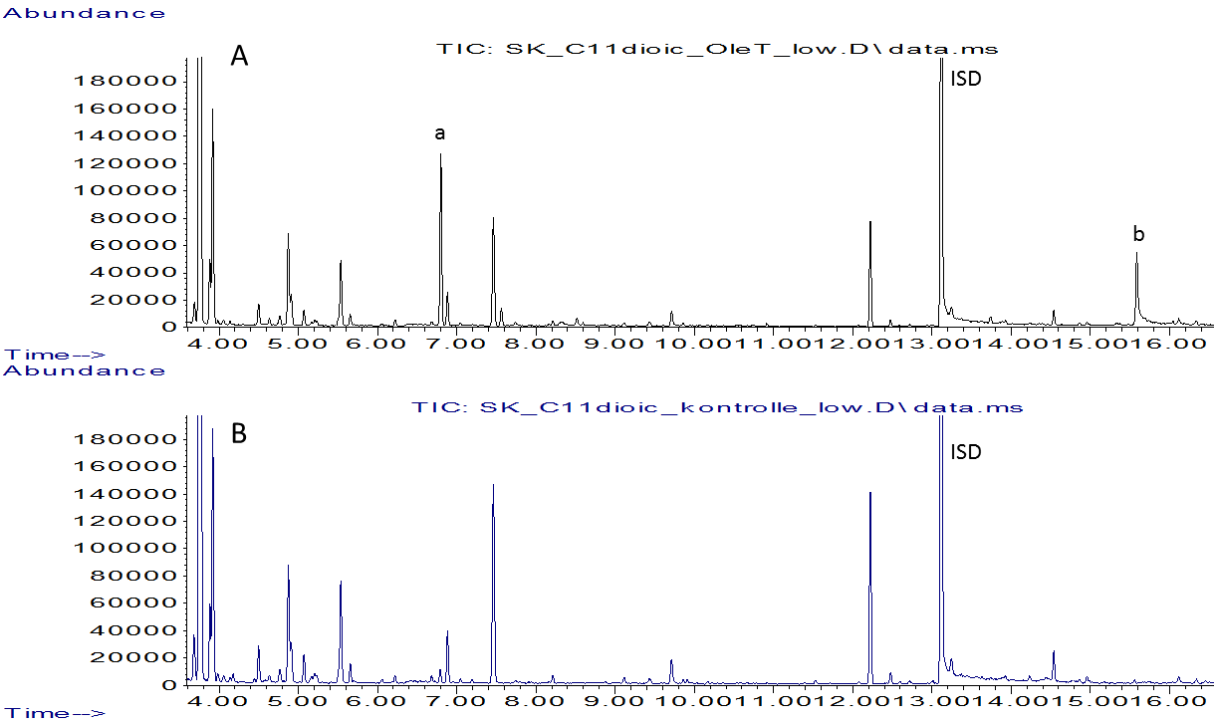

Figure S79. GC-MS chromatograms obtained by conversion of **6a** (10 mM). **A** = Conversion of **6a** with the OleT-CamAB-FDH system. **B** = Conversion of **6a** in the absence of OleT (negative control). **ISD** = internal standard (0.1 % (v/v) 1-decanol); **a** = **6c**; **b** = **6g**-methyl ester; compare also conversion of **6b** with $CYP_{BS\ß}$ (see Figure S133 A and Figure S135).

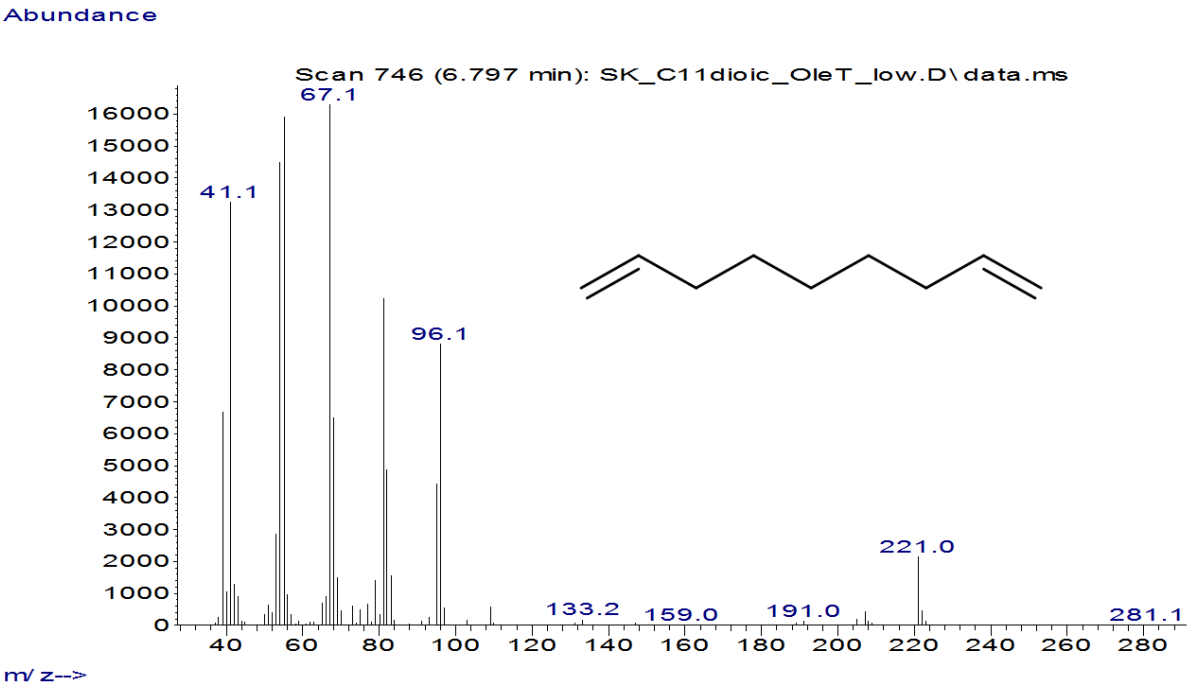

Figure S80. GC-MS spectra of **6c** (124.13 g mol^{-1}) obtained by conversion of **6a** (10 mM) with the OleT-CamAB-FDH system (corresponds to peak a in Figure S79 A).

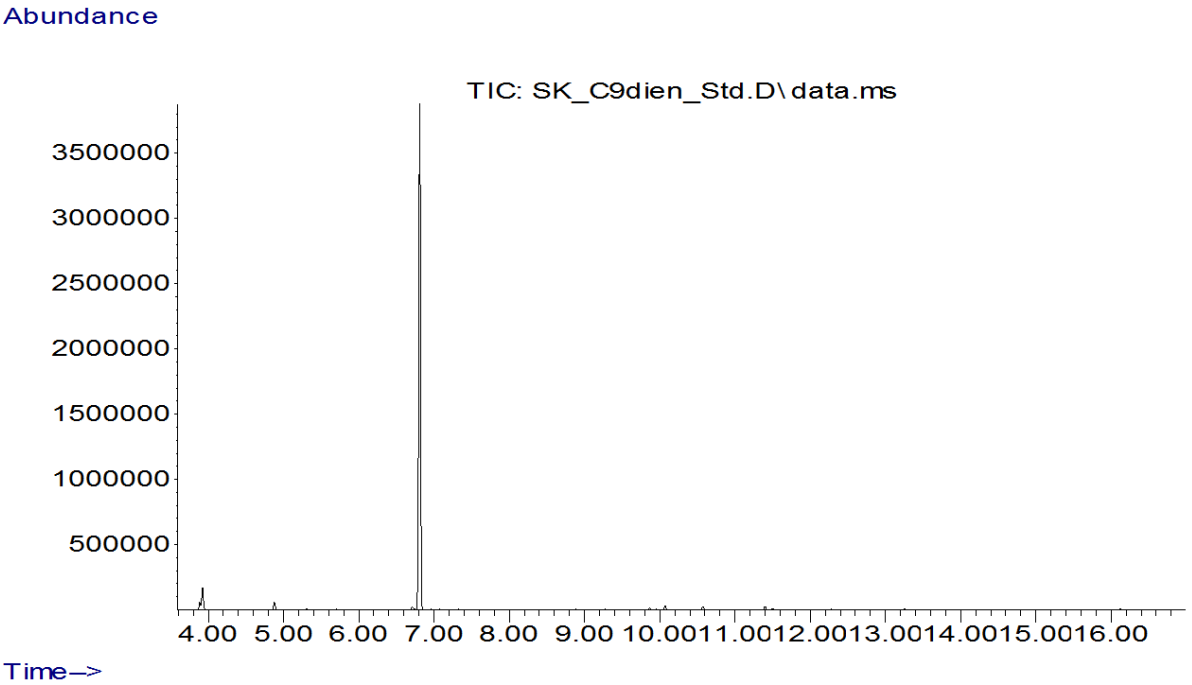

Figure S81. GC-MS chromatogram of a commercial standard of **6c**.

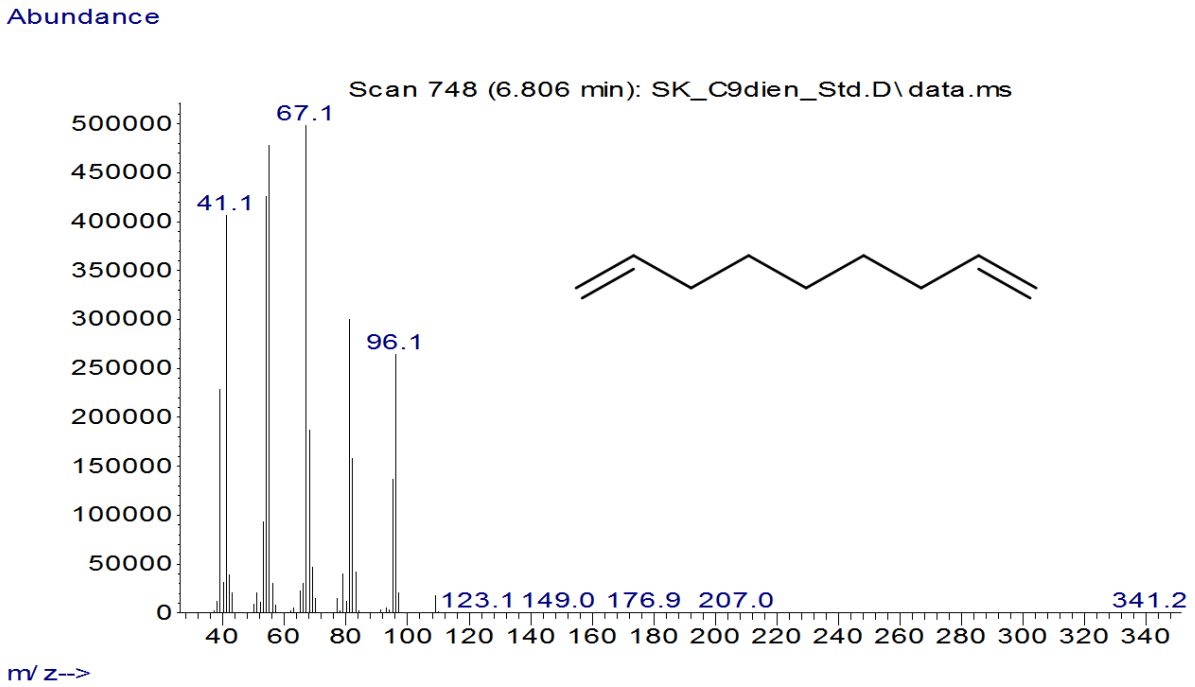

Figure S82. GC-MS spectra of a commercial standard of **6c** (124.13 g mol^{-1}).

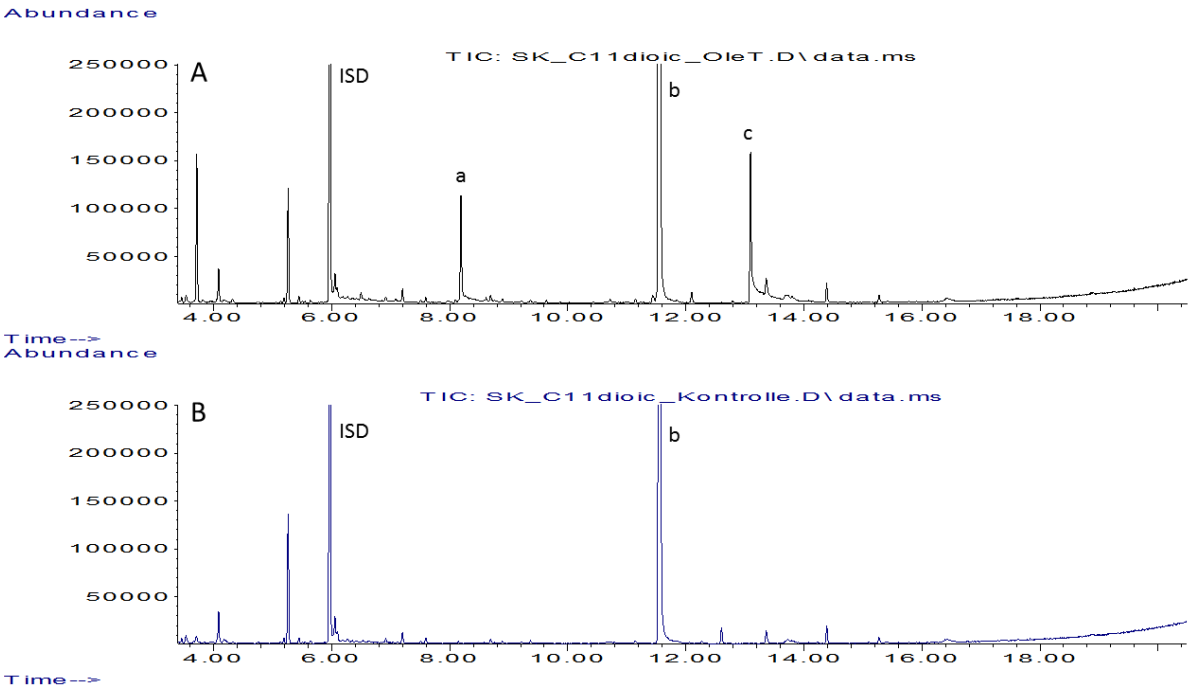

Figure S83. GC-MS chromatograms obtained by conversion of **6a** (10 mM). **A** = Conversion of **6a** with the OleT-CamAB-FDH system. **B** = Conversion of **6a** in the absence of OleT (negative control). **ISD** = internal standard (0.1 % (v/v) 1-decanol); **a** = **6g**-methyl ester (13 % GC area; see also Figure S133 and Figure S135 for comparison) **b** = dimethyl ester of **6a** (substrate); **c** = **6f**-dimethyl ester.

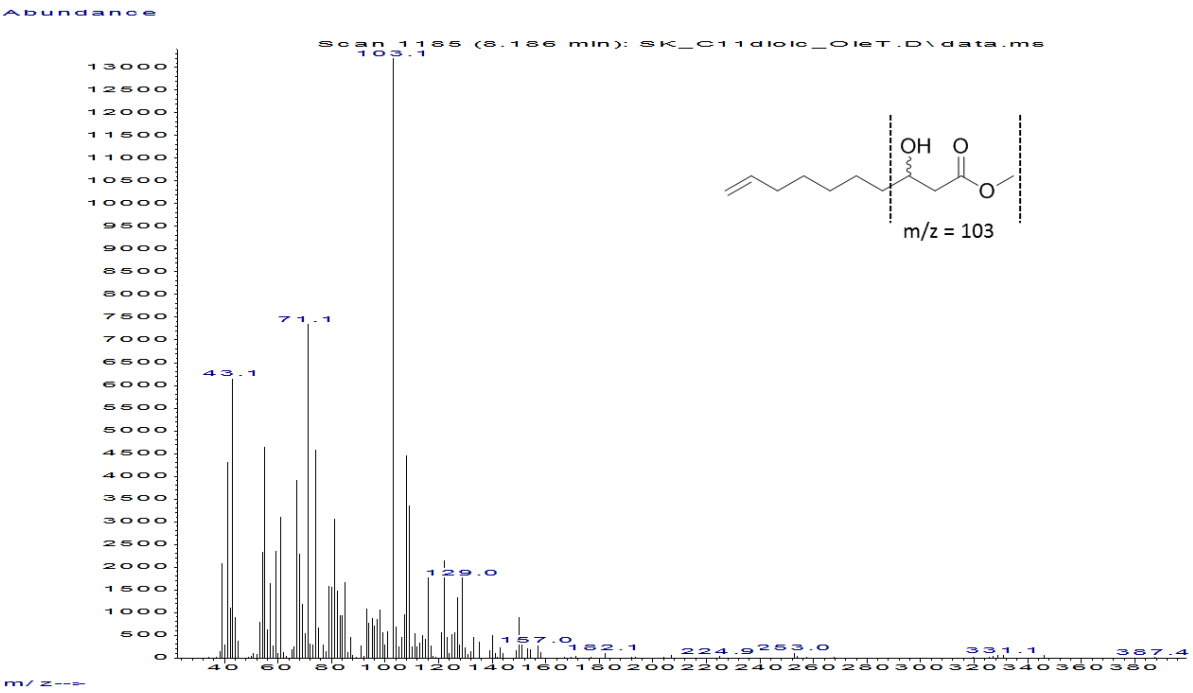

Figure S84. GC-MS spectra of **6g**-methyl ester (200.14 g mol^{-1}) obtained by conversion of **6a** (10 mM) with the OleT-CamAB-FDH system (corresponds to peak a in Figure S83). The characteristic ion *m*/z = 103 was used to assign the product. For further analytics see also peak a in Figure S89 A, Figure S88 andFigure S90.

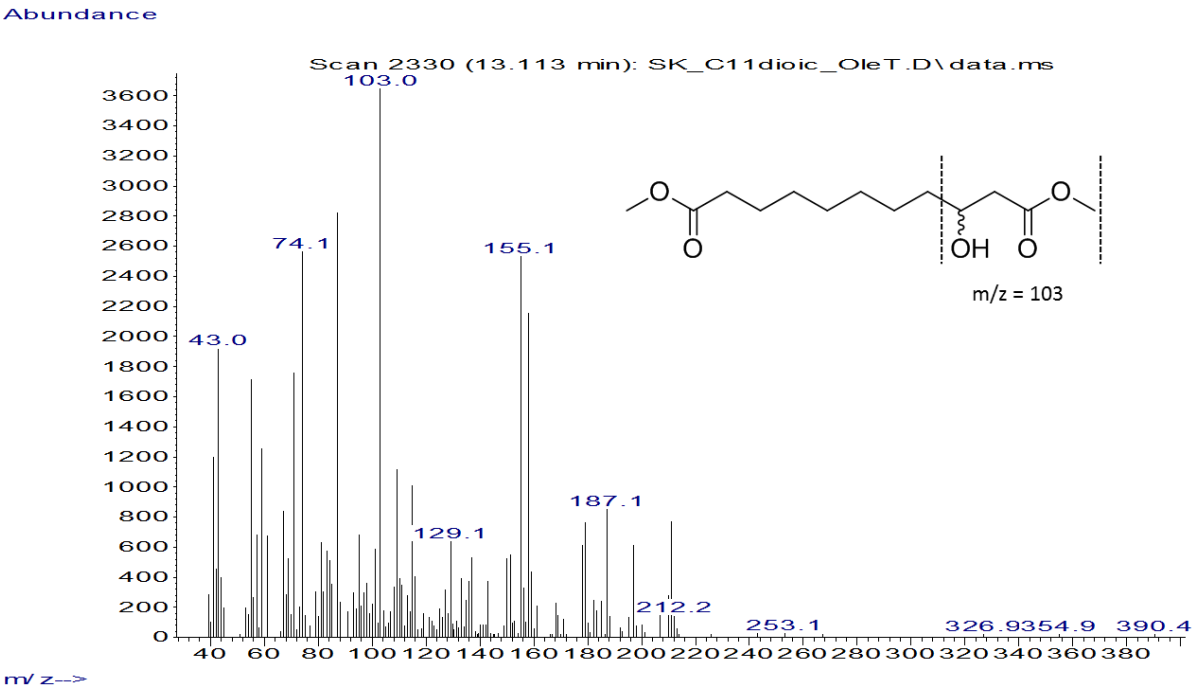

Figure S85. GC-MS spectra of **6f**-dimethyl ester (260.16 g mol^{-1}) obtained by conversion of **6a** (10 mM) with the OleT-CamAB-FDH system (corresponds to peak c in Figure S83 A). The characteristic ion *m*/z = 103 was used to assign the product.

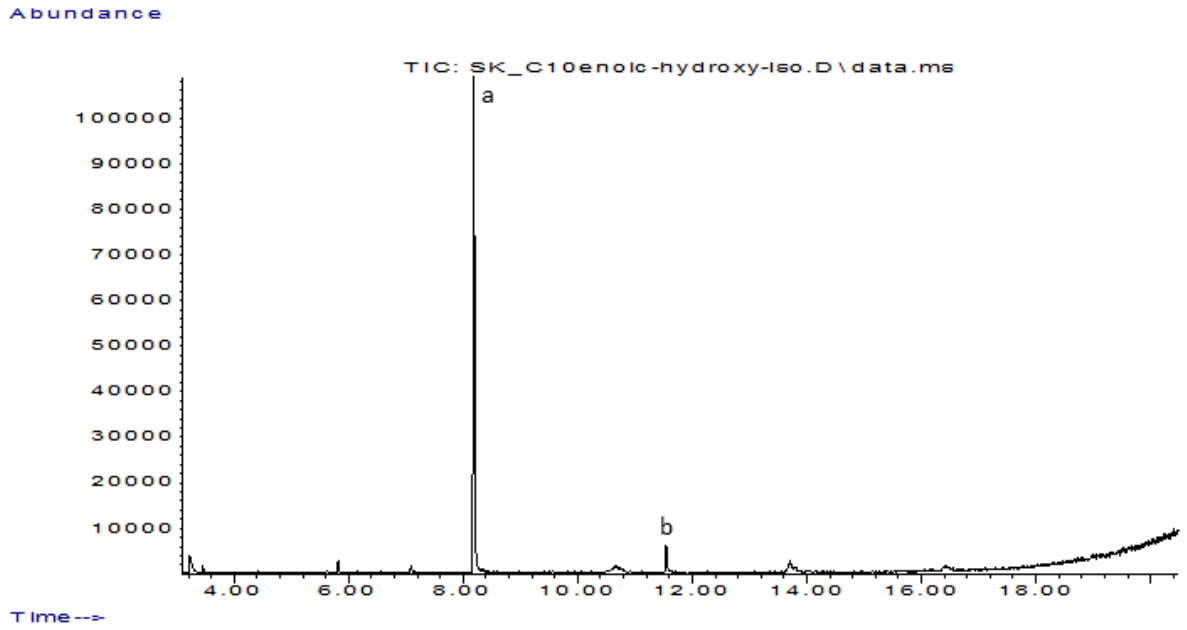

Figure S86. GC-MS chromatogram of isolated and purified **6g**-methyl ester (**a**; purity 72 % GC-area) obtained by conversion of **6a** with the OleT-CamAB-FDH system (10 mM substrate, 20 mL volume). **b** = dimethyl ester of **6a** (substrate).

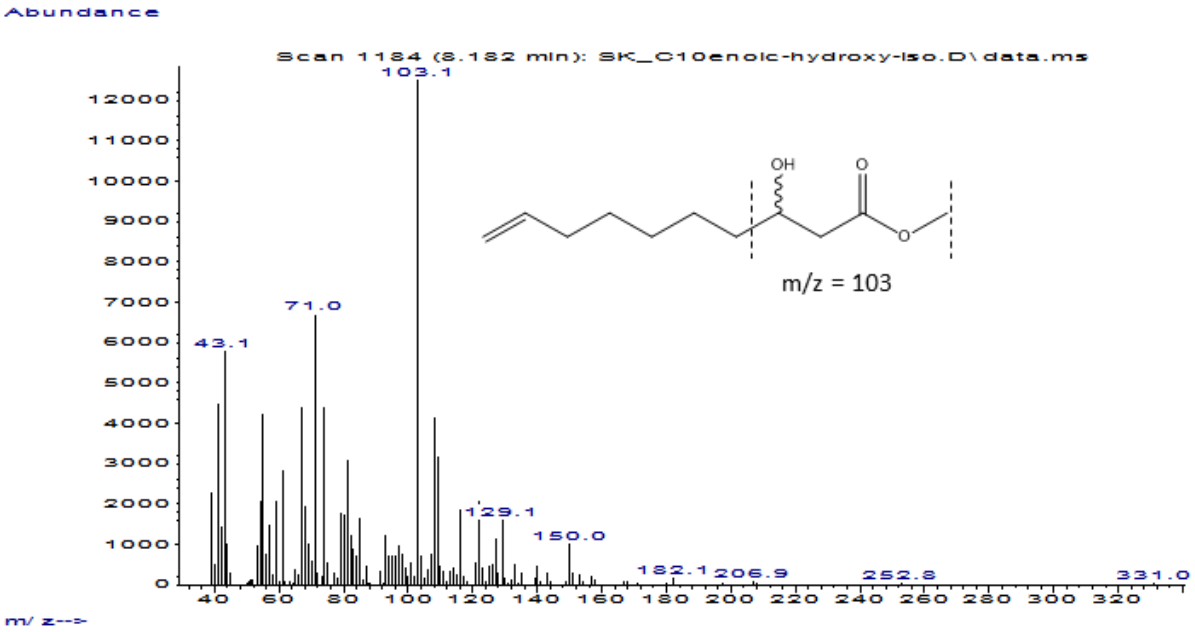

Figure S87. GC-MS spectra of isolated and purified **6g**-methyl ester (200.14 g mol^{-1}) obtained by conversion of **6a** with the OleT-CamAB-FDH system (corresponds to peak a in Figure S86). The characteristic ion *m*/z = 103 was used to assign the product. Compare also to Figure S84 and Figure S90.

Methyl 3-hydroxydec-9-enoate (**6g**-methyl ester) (8 mg, white powder): ^{1}H NMR (300 MHz, $CDCl_3$): δ = 5.89-5.76 (m, 1 H, CH_2=$CHCH_2$), 5.05-4.93 (m, 2 H, CH_2=$CHCH_2$), 4.02 (m, 1

H, $CH_2C\mathbf{H}(OH)CH_2$), 3.74 (s, 3 H, $C\mathbf{H_3}$), 2.88 (s, 1 H, OH), 2.57-2.39 (m, 2 H, $CH(OH)C\mathbf{H_2}C{=}O$), 2.10-2.03 (m, 2 H, $CH_2{=}CHC\mathbf{H_2}$), 1.55-1.27 (m, 8 H, $(C\mathbf{H_2})_4CH(OH)$).

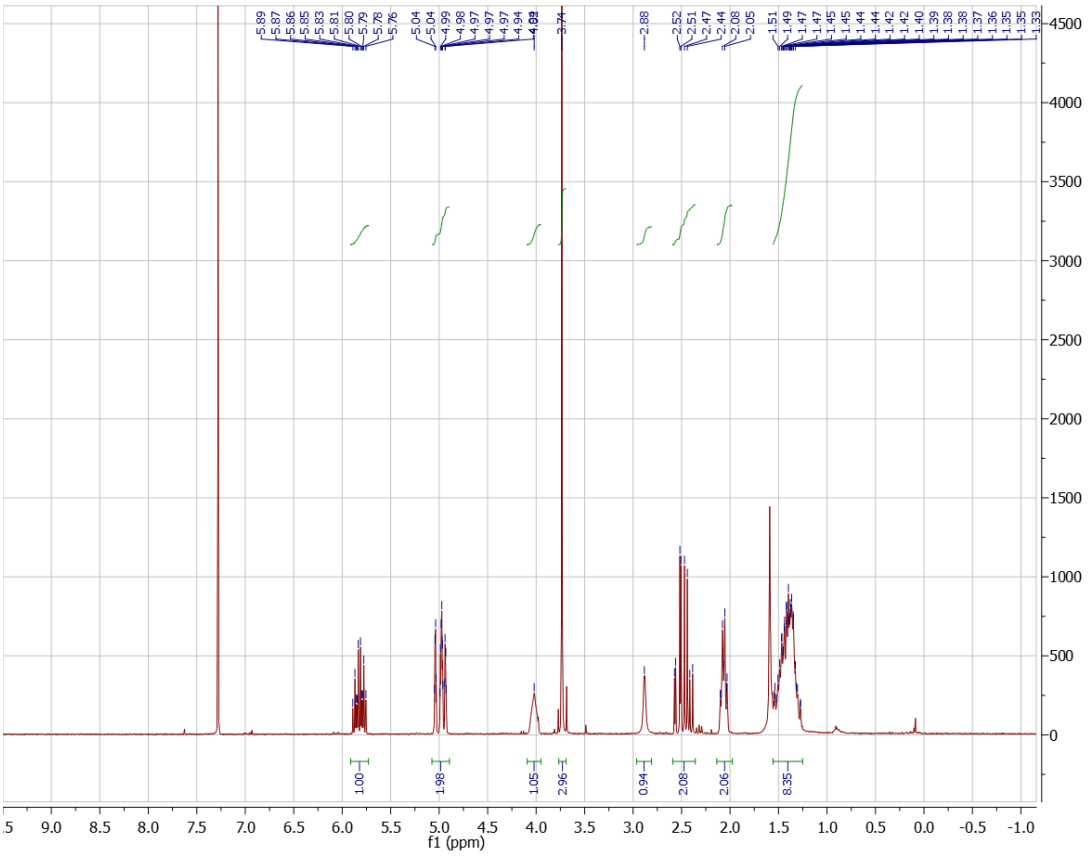

Figure S88. ^{1}H-NMR chromatogram of isolated and purified methyl 3-hydroxydec-9-enoate (**6g**-methyl ester) obtained by conversion of **6a** with the OleT-CamAB-FDH system.

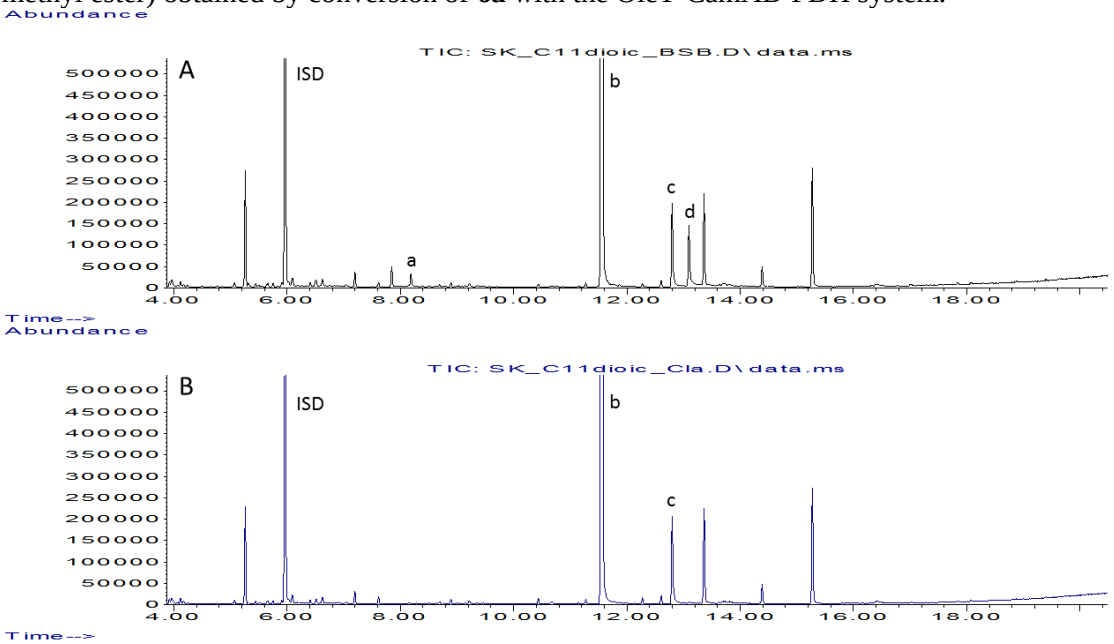

Figure S89. GC-MS chromatograms obtained by conversion of **6a** (10 mM) with $CYP_{BSß}$ (**A**) and $P450_{Cla}$ (**B**) using H_2O_2 as oxidant. **ISD** = internal standard (0.1 % (v/v) 1-decanol); **a** = **6g**-methyl ester; **b** = dimethyl ester of **6a** (substrate); **c** = **6d**-dimethyl ester; **d** = **6f**-dimethyl ester.

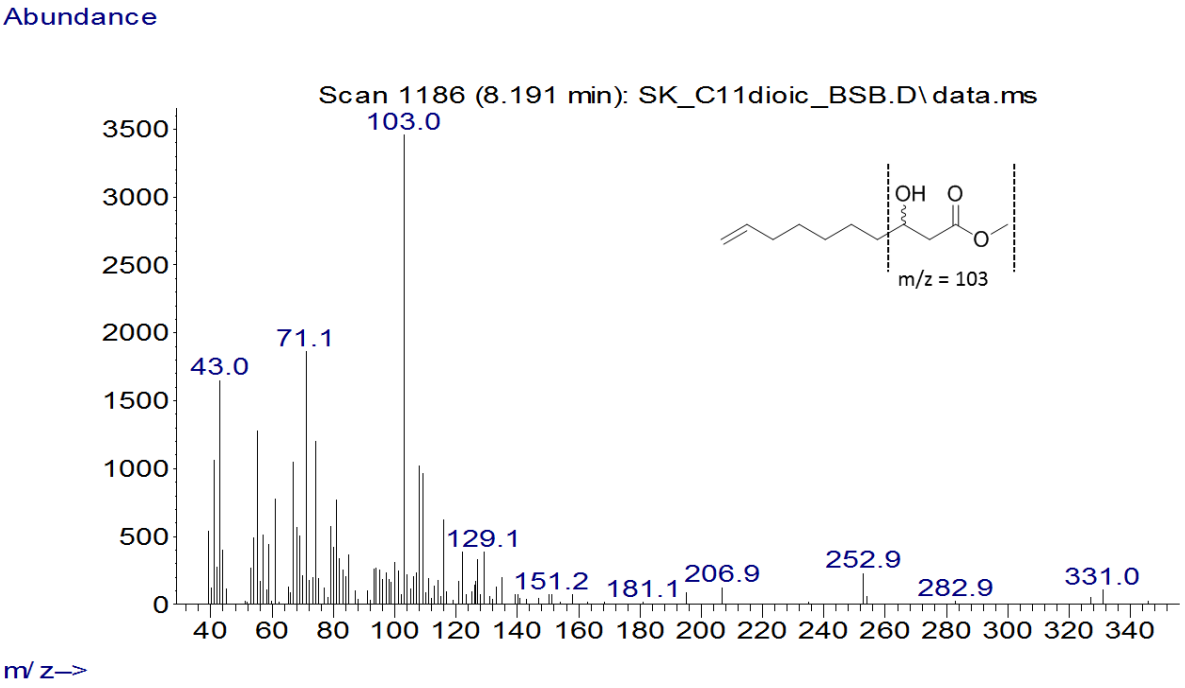

Figure S90. GC-MS spectra of **6g**-methyl ester obtained by conversion of **6a** (10 mM) with $CYP_{BSß}$ and H_2O_2 as oxidant (corresponds to peak a in Figure S89 A). The characteristic ion *m*/z = 103 was used to assign the product (see also Figure S132, Figure S133 and Figure S135 for comparison; conversion of **6b** with OleT and $CYP_{BSß}$).

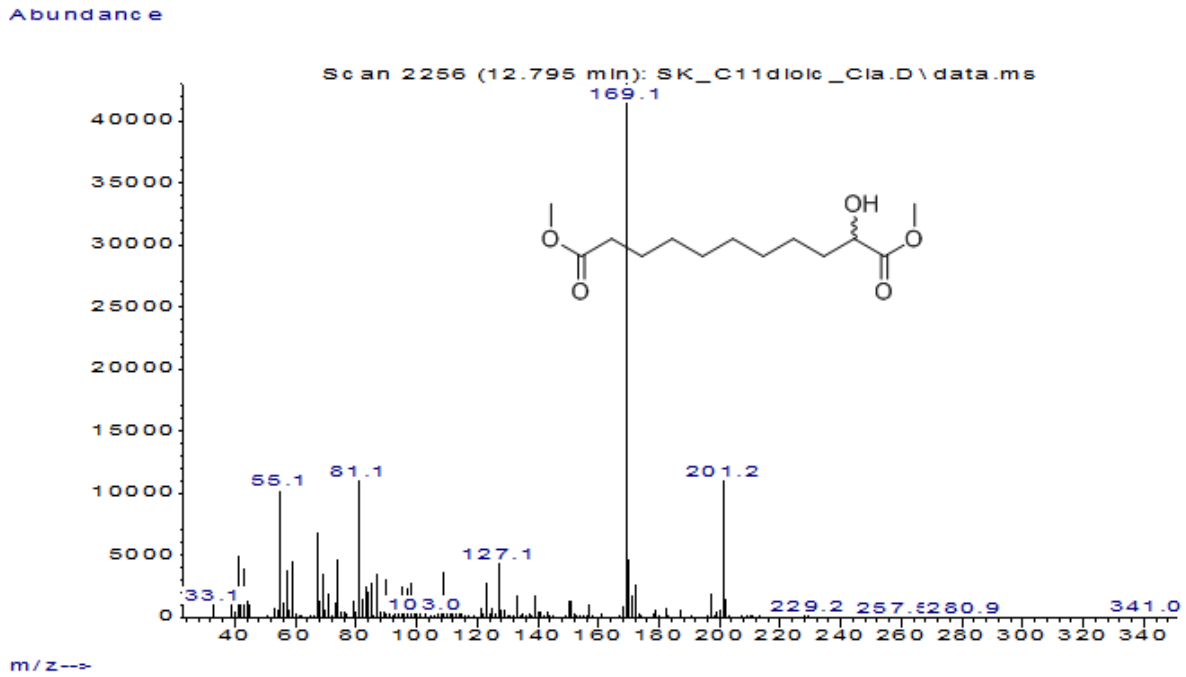

Figure S91. GC-MS spectra of **6d**-dimethyl ester (260.16 g/mol) obtained by conversion of **6a** (10 mM) with $P450_{Cla}$ and H_2O_2 as oxidant (corresponds to peak c in Figure S89 B).

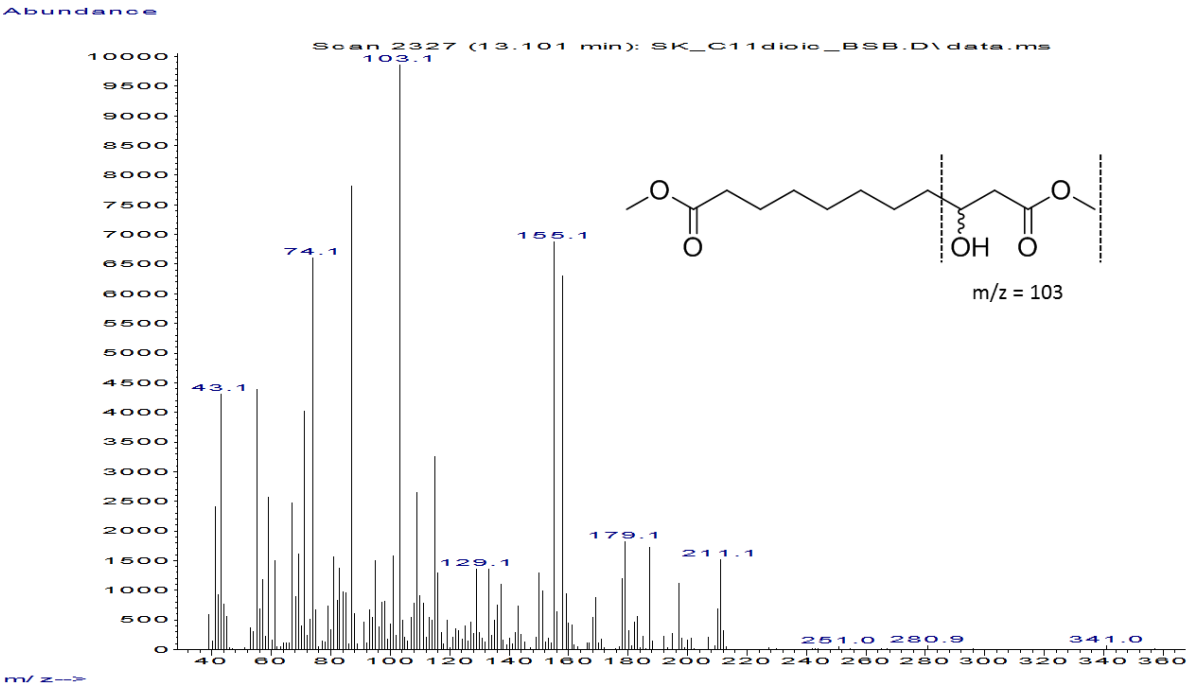

Figure S92. GC-MS spectra of **6f**-dimethyl ester obtained by conversion of **6a** (10 mM) with $CYP_{BSß}$ and H_2O_2 as oxidant (corresponds to peak d in Figure S89 A). The characteristic ion *m*/z = 103 was used to assign the product.

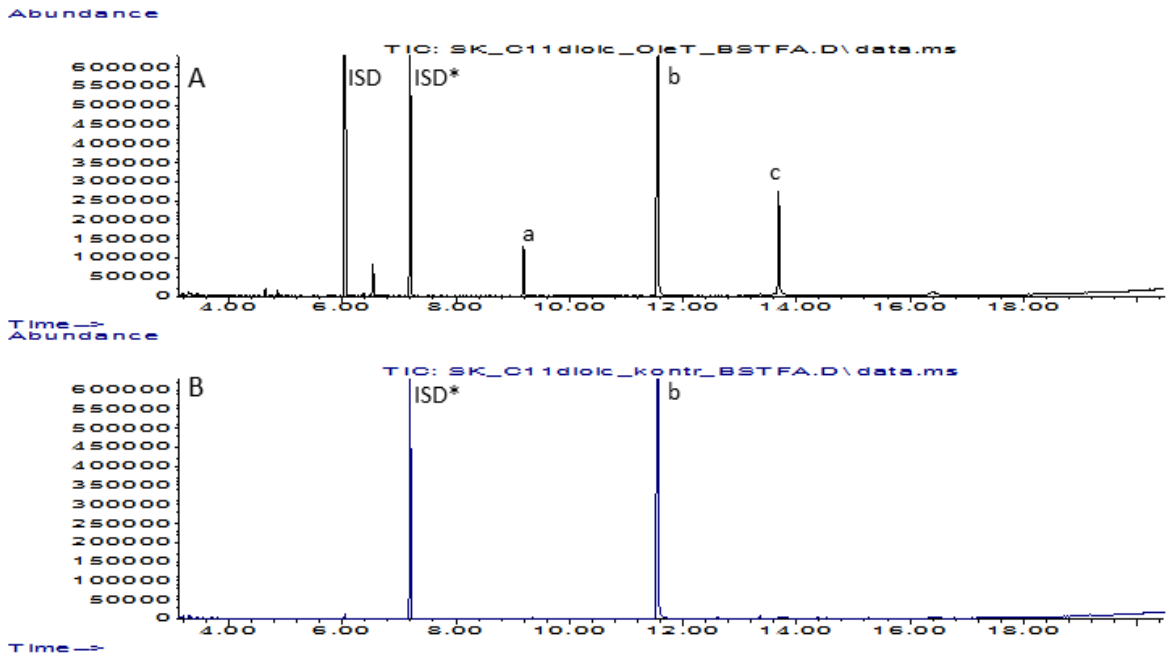

Figure S93. GC-MS chromatograms obtained by conversion of **6a** (10 mM) after derivatization with $TMSCHN_2$ and BSTFA. **A** = Conversion of **6a** with the OleT-CamAB-FDH system. **B** = Conversion of **6a** in the absence of OleT (negative control). **ISD** = internal standard (0.1 % (v/v) 1-decanol); **ISD*** = silylated internal standard (TMS-1-decanol); **a** = TMS-**6g**-methyl ester; **b** = dimethyl ester of **6a** (substrate); **c** = TMS-**6f**-dimethyl ester.

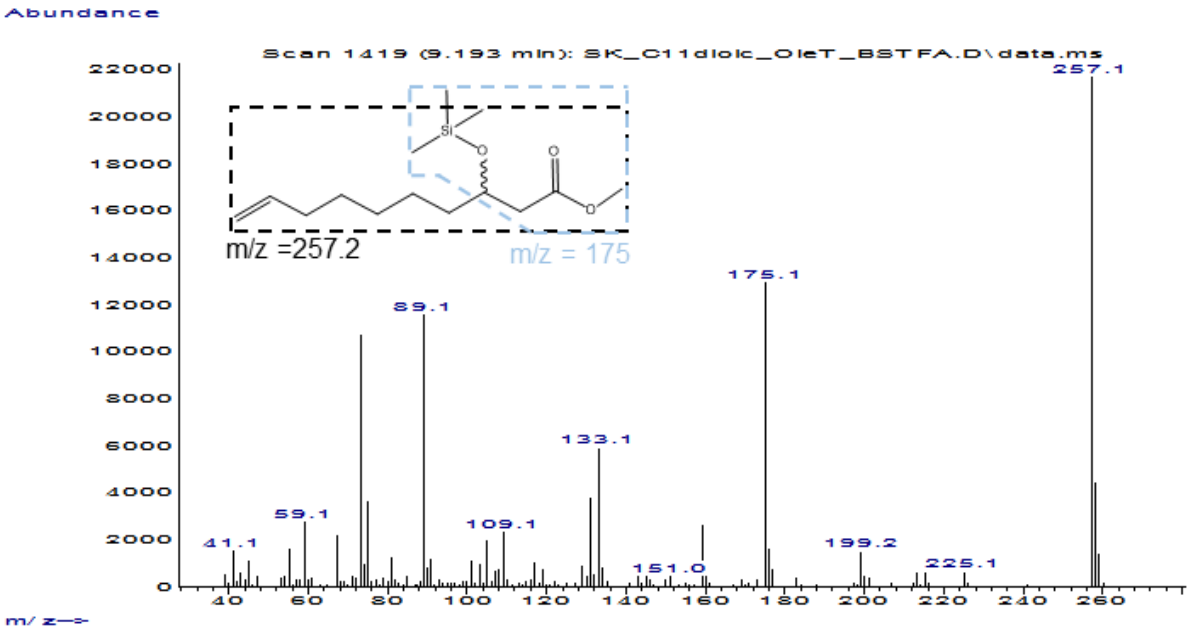

Figure S94. GC-MS spectra of TMS-**6g**-dimethyl ester obtained by conversion of **6a** (10 mM) with the OleT-CamAB-FDH system (corresponds to peak a in Figure S93 A). The characteristic ions *m*/z = 175 and *m*/z = 257.2 were used to assign the product as described elsewhere.[2]

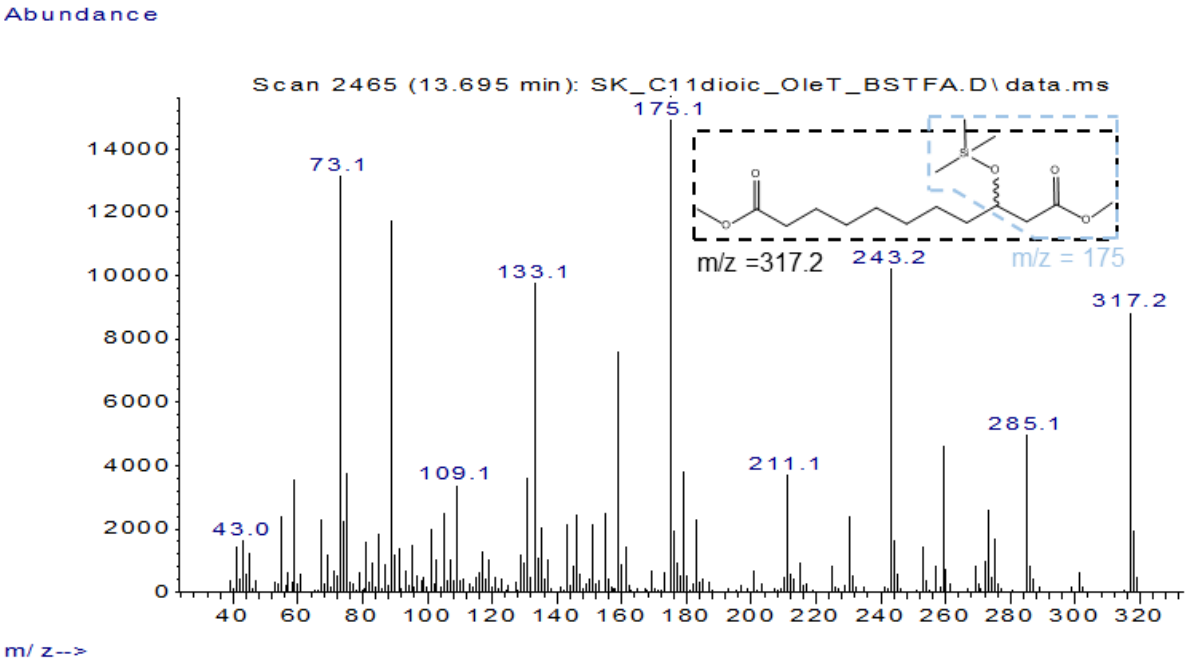

Figure S95. GC-MS spectra of TMS-**6f**-dimethyl ester obtained by conversion of **6a** (10 mM) with the OleT-CamAB-FDH system (corresponds to peak c in Figure S93 A). The characteristic ions *m*/z = 175 and *m*/z = 317.2 were used to assign the product as described elsewhere.[2]

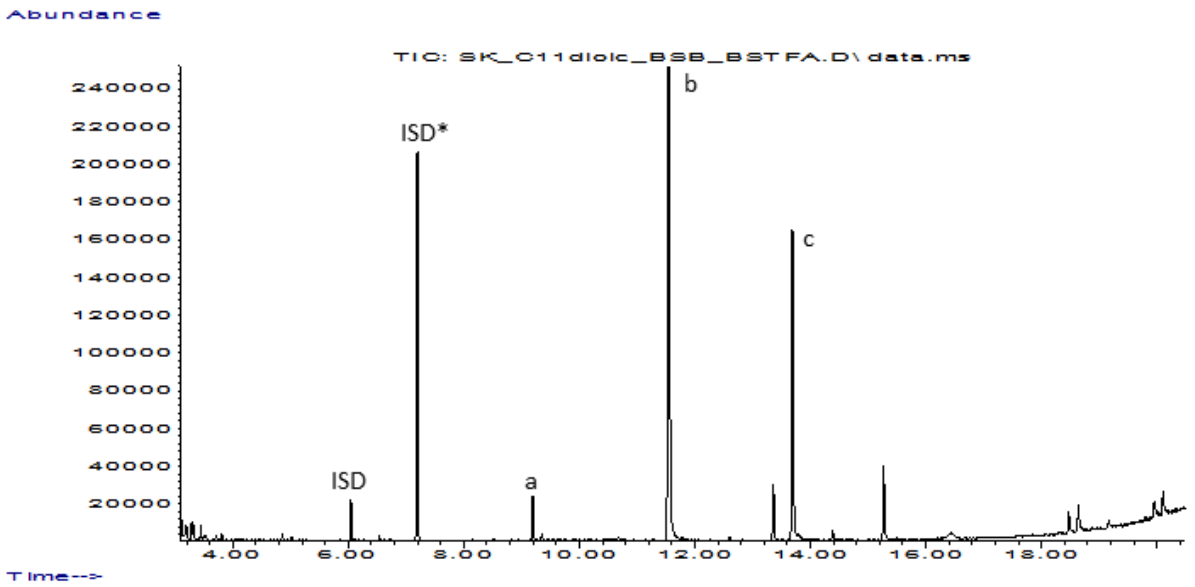

Figure S96. GC-MS chromatograms obtained by conversion of **6a** (10 mM) with $CYP_{BS\beta}$ and H_2O_2 as oxidant after derivatization with $TMSCHN_2$ and BSTFA. **ISD** = internal standard (0.1 % (v/v) 1-decanol); **ISD*** = silylated internal standard (TMS-1-decanol); **a** = TMS-**6g**-methyl ester; **b** = dimethyl ester of **6a** (substrate); **c** = TMS-**6f**-dimethyl ester.

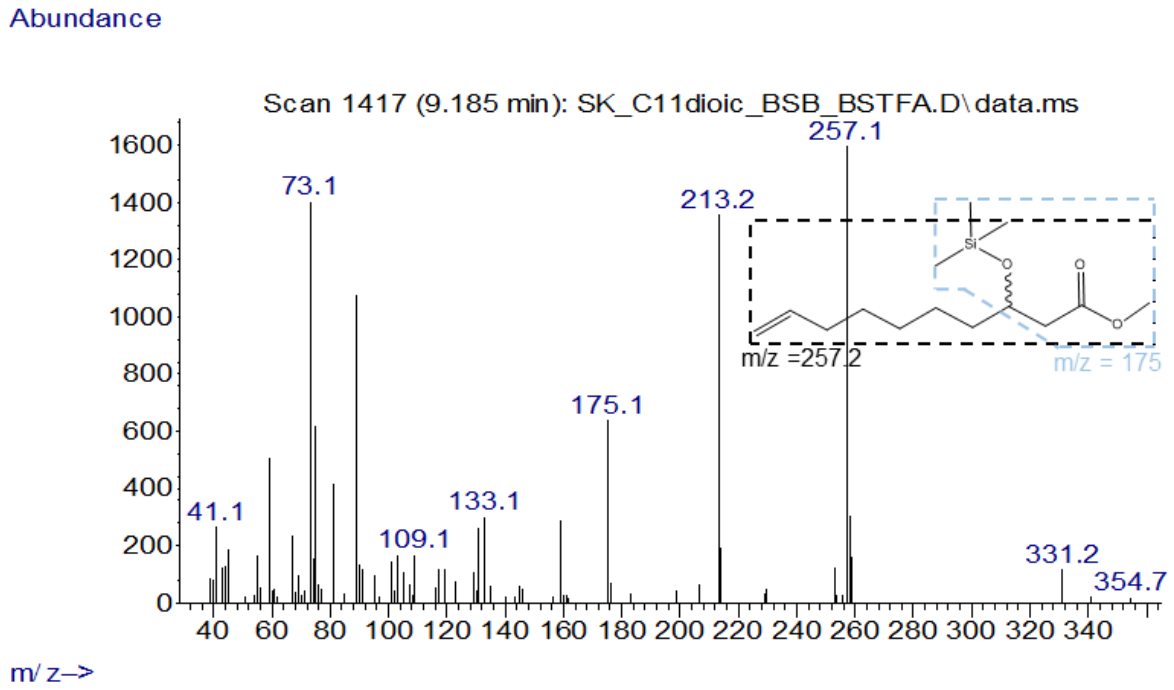

Figure S97. GC-MS spectra of TMS-**6g**-methyl ester obtained by conversion of **6a** (10 mM) with $CYP_{BS\beta}$ and H_2O_2 as oxidant (corresponds to peak a in Figure S96). The characteristic ions *m*/z = 175 and *m*/z = 257.2 were used to assign the minor side product as described elsewhere.[2]

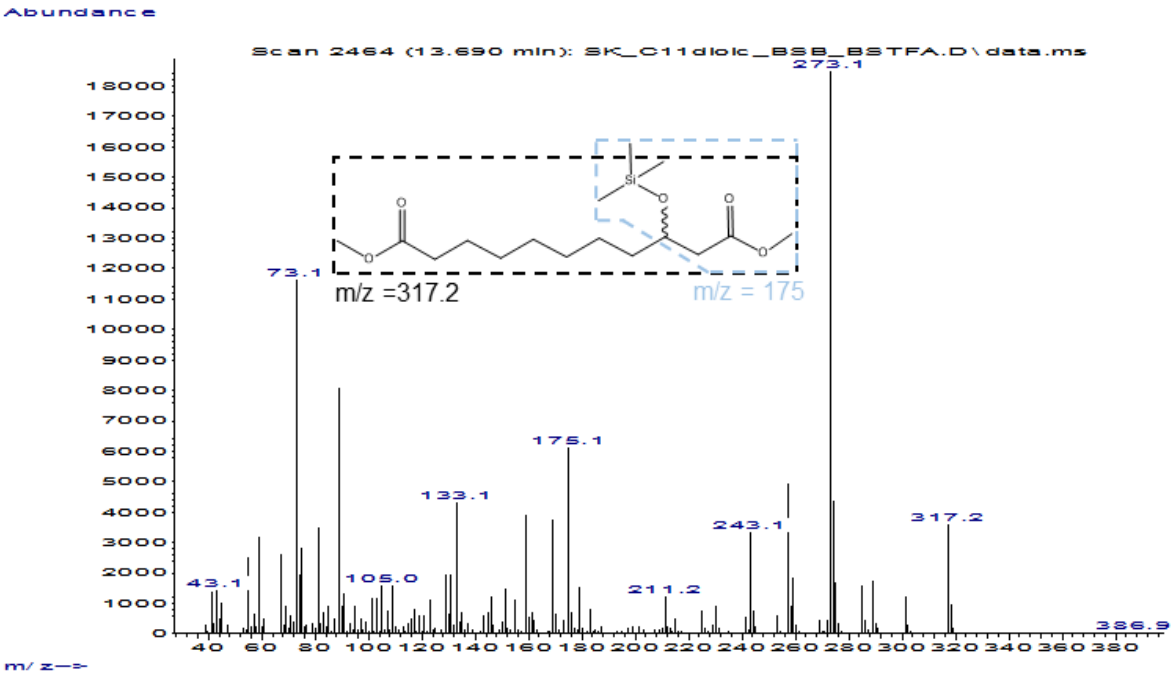

Figure S98. GC-MS spectra of TMS-**6f**-dimethyl ester obtained by conversion of **6a** (10 mM) with $CYP_{BS\beta}$ and H_2O_2 as oxidant (corresponds to peak c in Figure S96). The characteristic ions *m*/z = 175 and *m*/z = 317.2 were used to assign the product as described elsewhere.[2]

7.1.7 **Conversion of 7a**

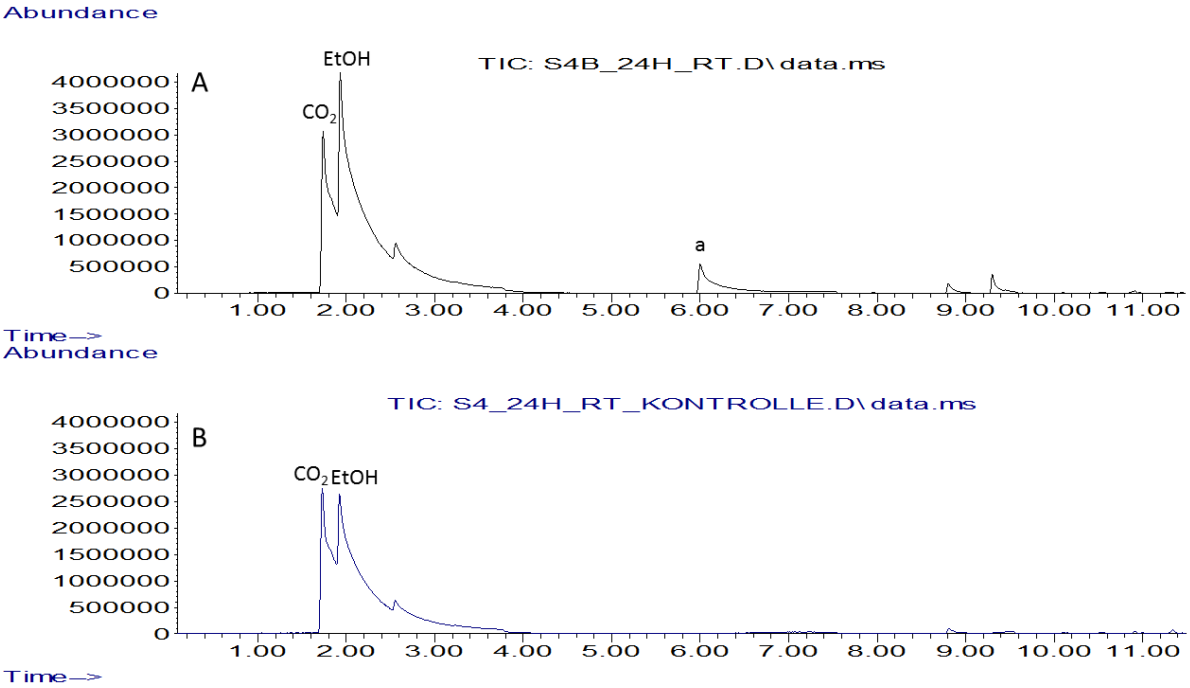

Figure S99. Headspace GC-MS analysis by conversion of **7a** (10 mM). **A** = Conversion of **7a** with the OleT-CamAB-FDH system. **B** = Conversion of **7a** in the absence of OleT (negative control). **a** = **7c**. 5 % (v/v) EtOH was used as co-solvent.

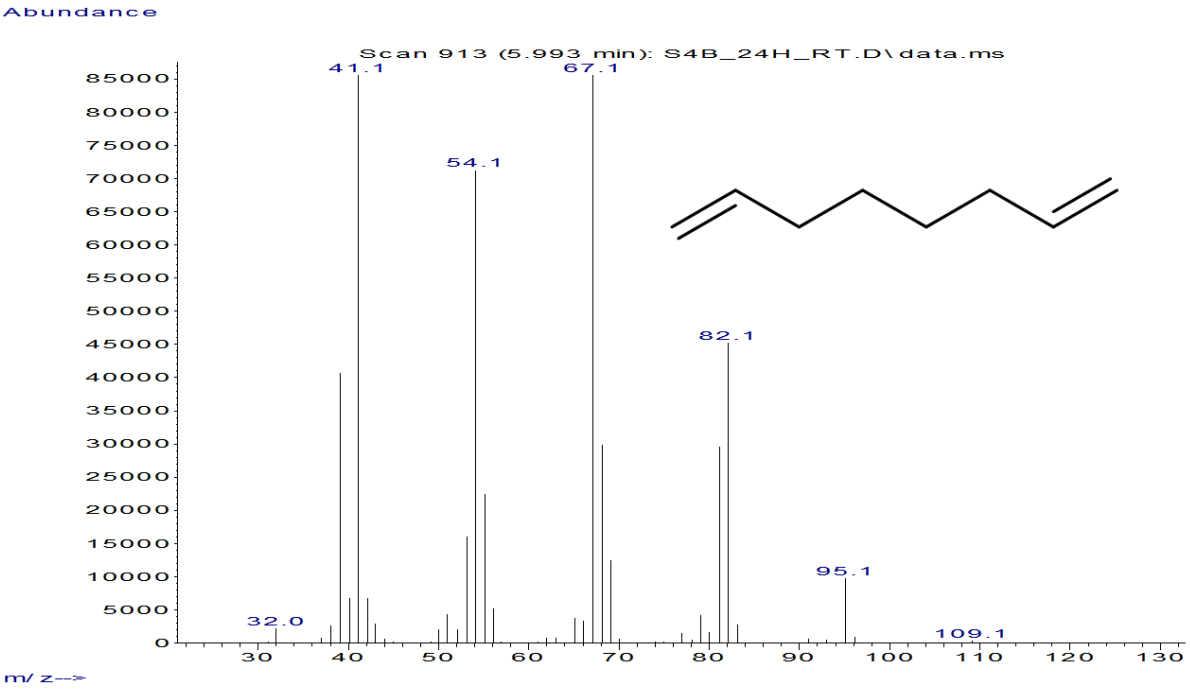

Figure S100. GC-MS spectra of **7c** (110.11 g mol^{-1}) obtained by conversion of **7a** (10 mM) with the OleT-CamAB-FDH system (corresponds to peak a in Figure S99 A).

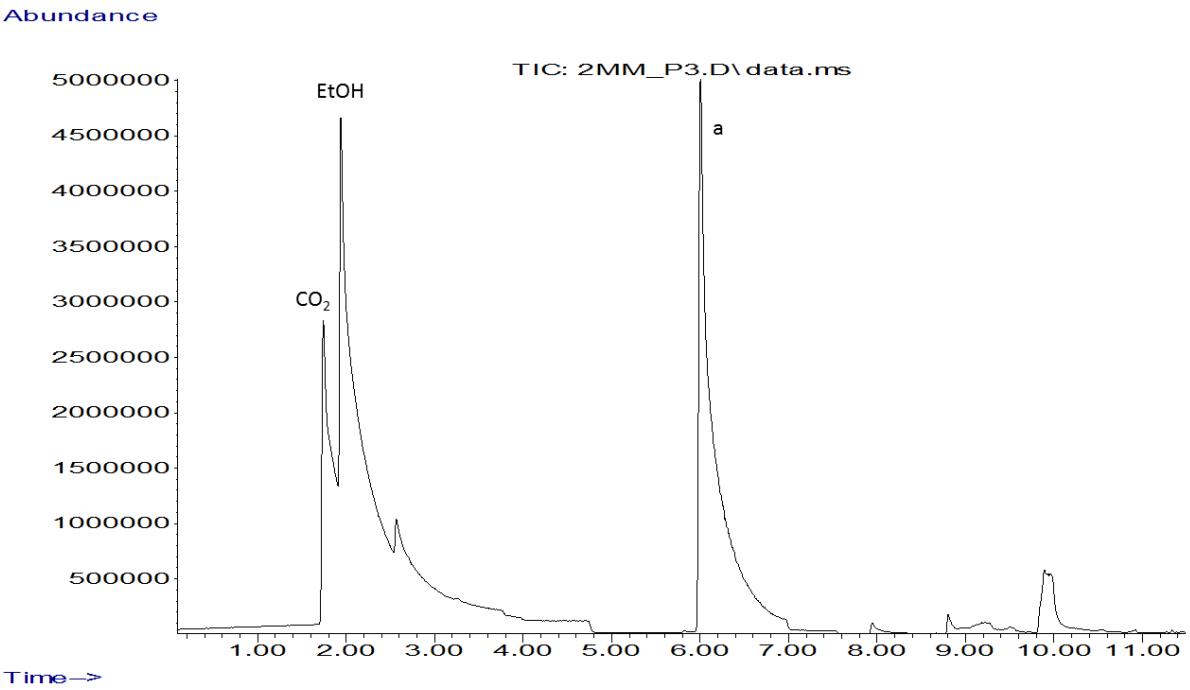

Figure S101. Headspace GC-MS analysis of a commercial standard of **7c** (**a**).

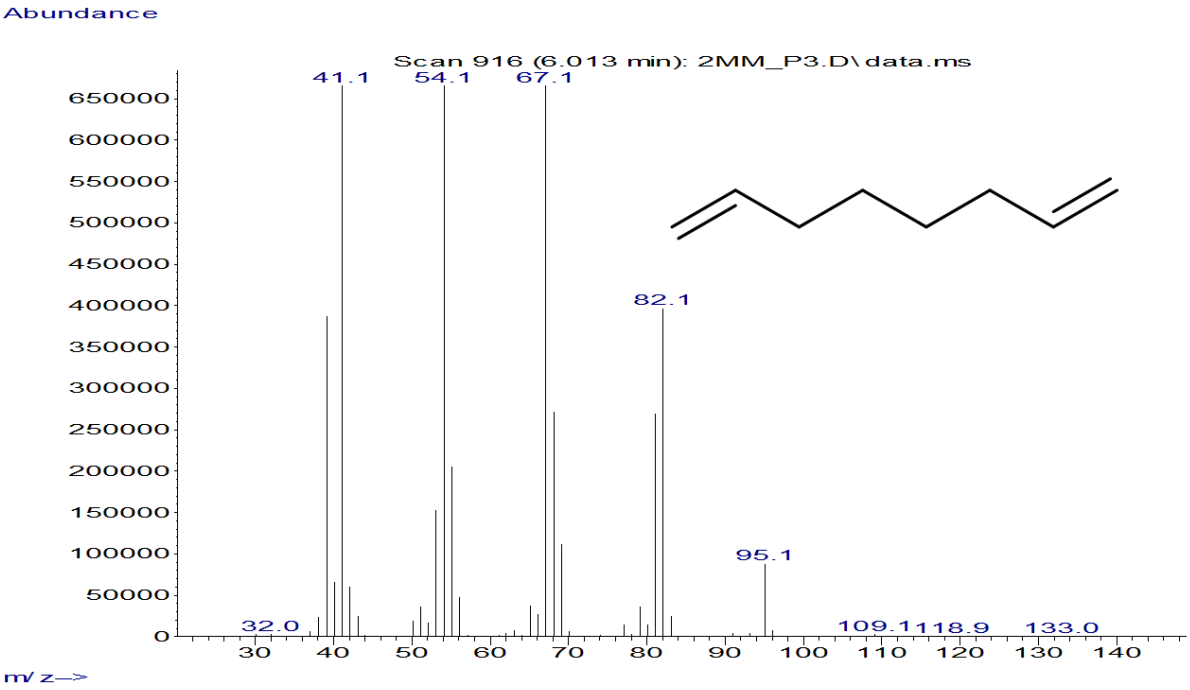

Figure S102. GC-MS spectra of a commercial standard of **7c** (110.11 g mol^{-1}).

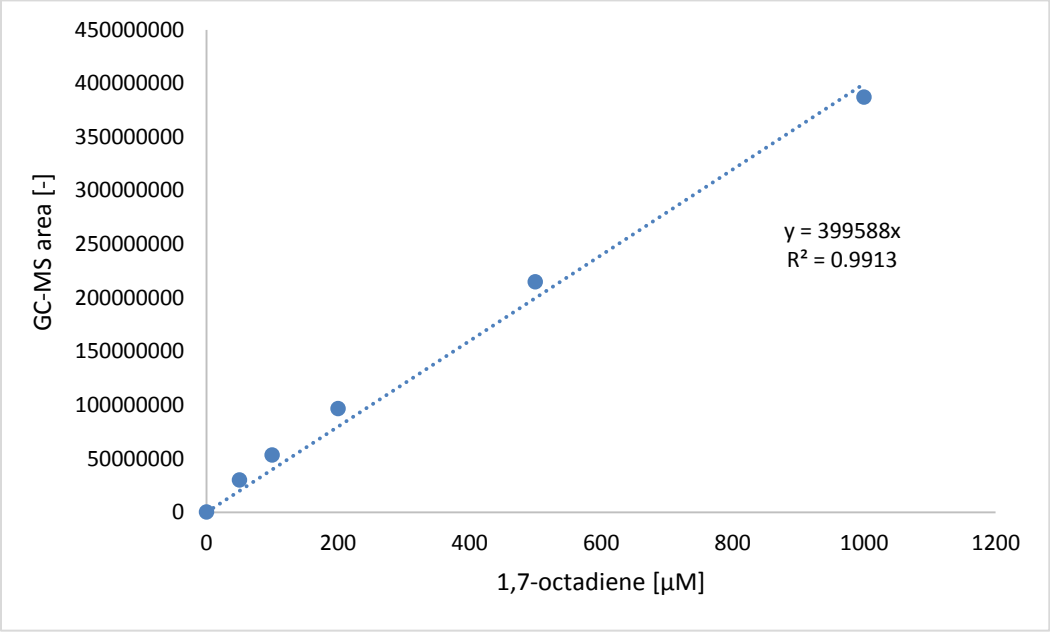

Figure S103. Calibration curve obtained after headspace GC-MS analysis of defined concentrations **7c**.

7.1.8 **Conversion of 8a**

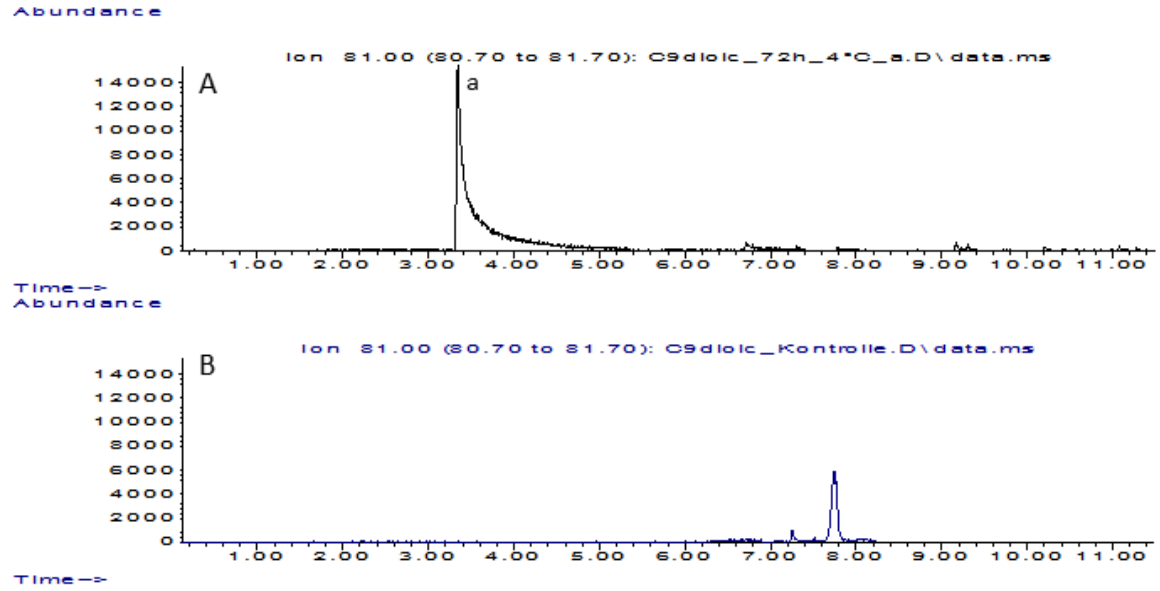

Figure S104. GC-MS chromatograms obtained by conversion of **8a** (10 mM). **A** = Conversion of **8a** with the OleT-CamAB-FDH system. **B** = Conversion of **8a** in the absence of OleT (negative control). Signals of extracted ion *m*/z = 81 are shown. **a** = **8c**.

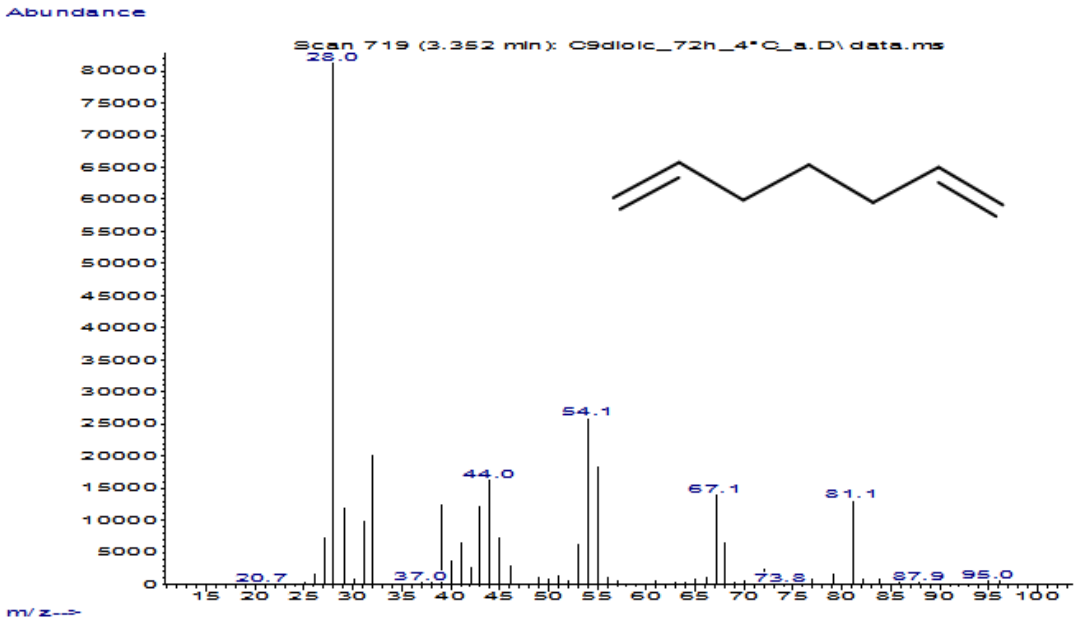

Figure S105. GC-MS spectra of **8c** (96.09 g mol^{-1}) obtained by conversion of **8a** (10 mM) with the OleT-CamAB-FDH system (corresponds to peak a in Figure S104 A).

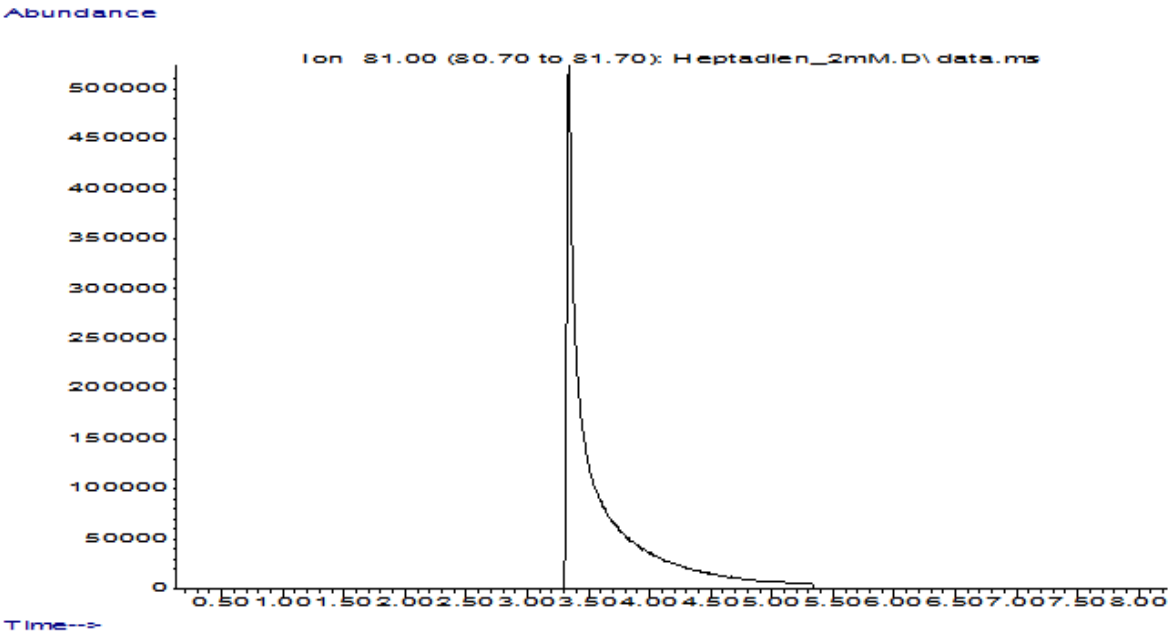

Figure S106. Headspace GC-MS analysis of a commercial standard of **8c** (concentration 2 mM). The signal of extracted ion *m*/z = 81 is shown.

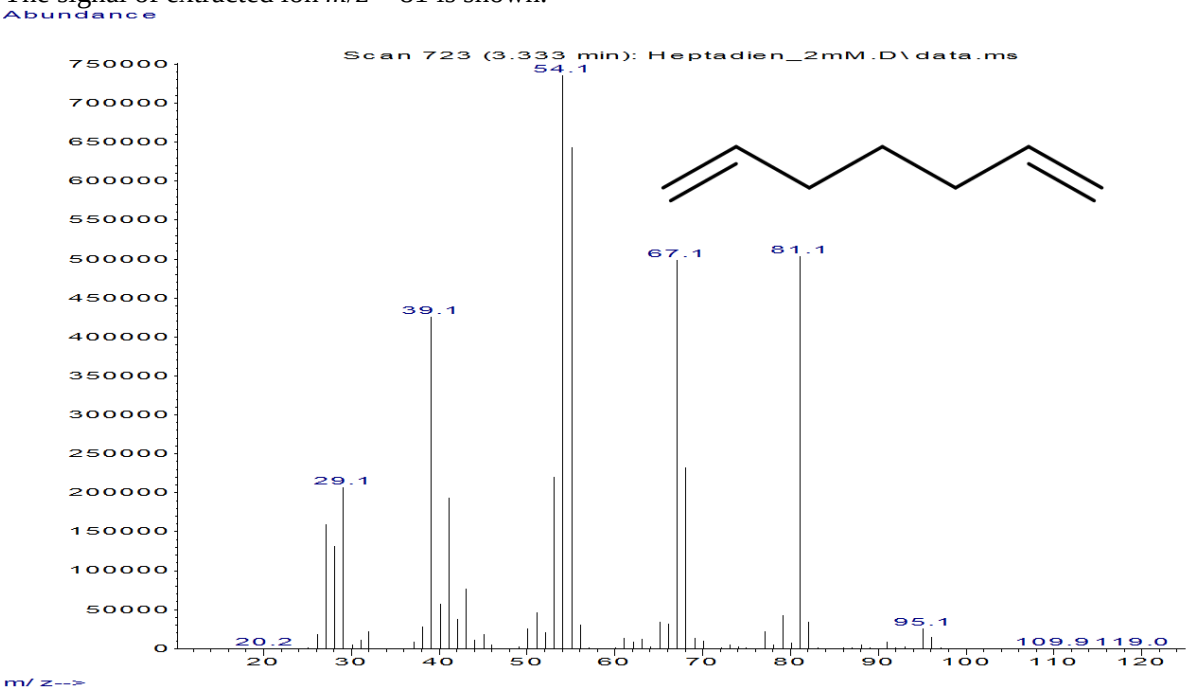

Figure S107. GC-MS spectra of a commercial standard of **8c** (96.09 g mol^{-1}).

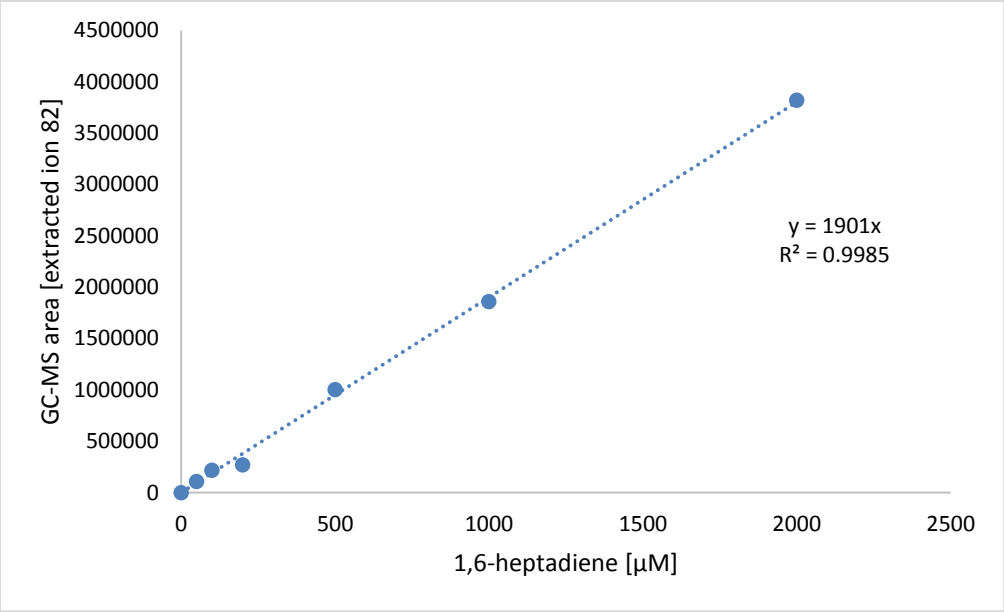

Figure S108. Calibration curve obtained by headspace space GC-MS analysis of defined concentrations of **8c**. The extracted ion *m*/z = 82 was used to generate a calibration curve.

7.1.9 **Conversion of 9a**

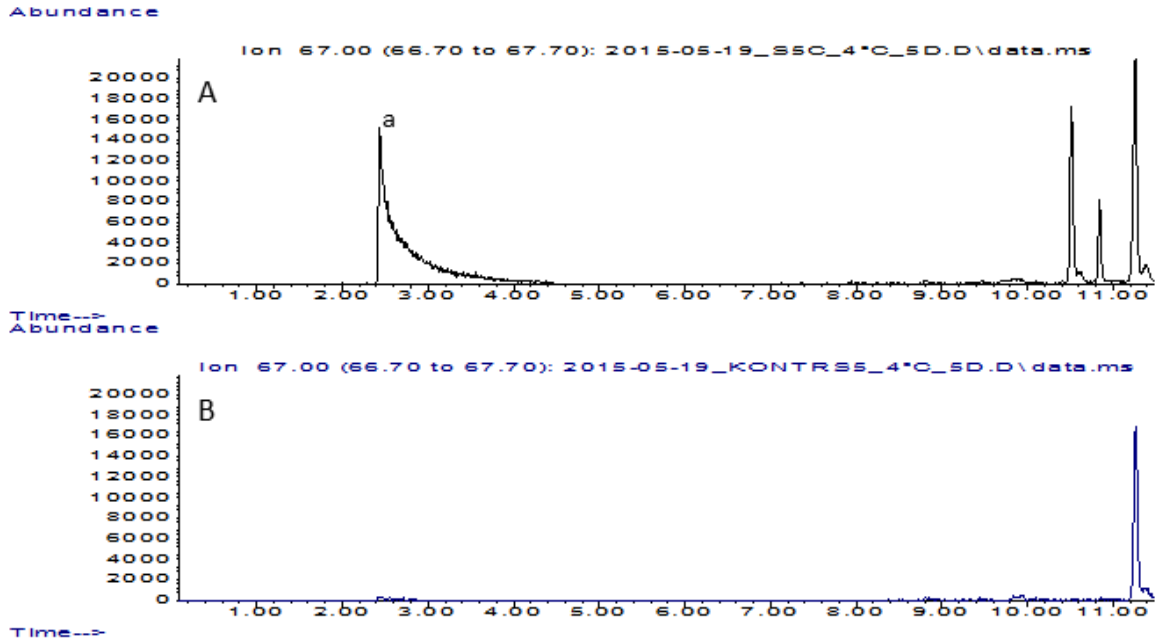

Figure S109. GC-MS chromatograms obtained by conversion of **9a** (10 mM). **A** = Conversion of **9a** with the OleT-CamAB-FDH system. **B** = Conversion of **9a** in the absence of OleT (negative control). The signal of extracted ion *m*/z = 67 is shown. **a** = **9c**.

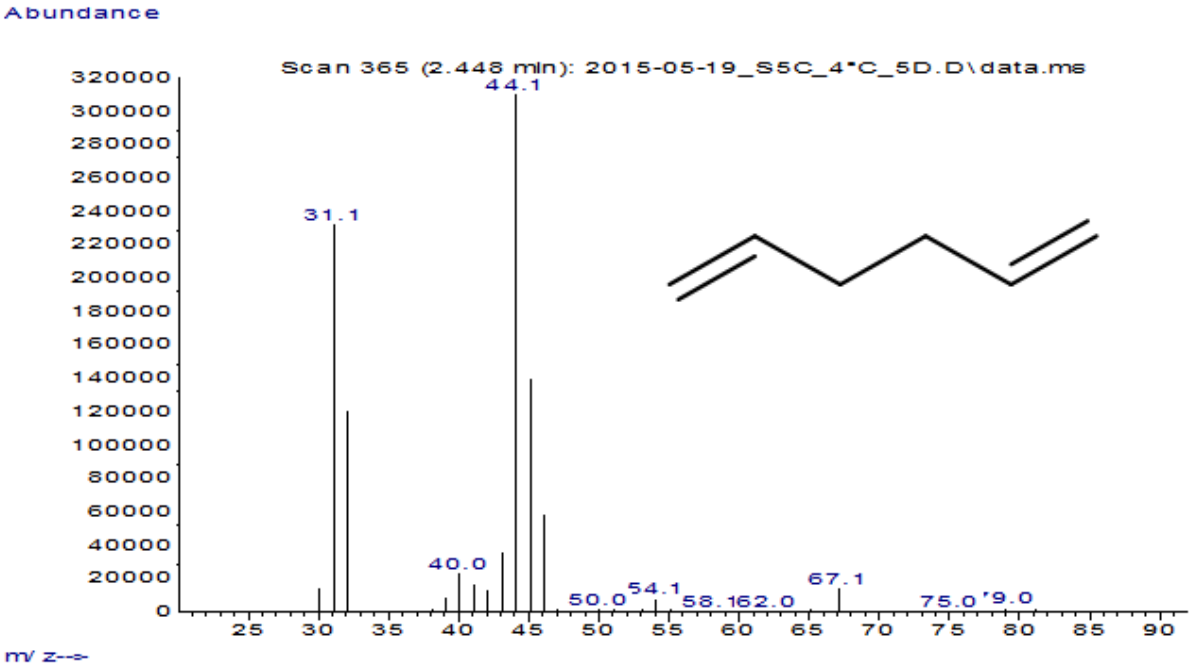

Figure S110. GC-MS spectra of **9c** (82.08 g mol^{-1}) obtained by conversion of **9a** (10 mM) with the OleT-CamAB-FDH system (corresponds to peak a in Figure S109 A).

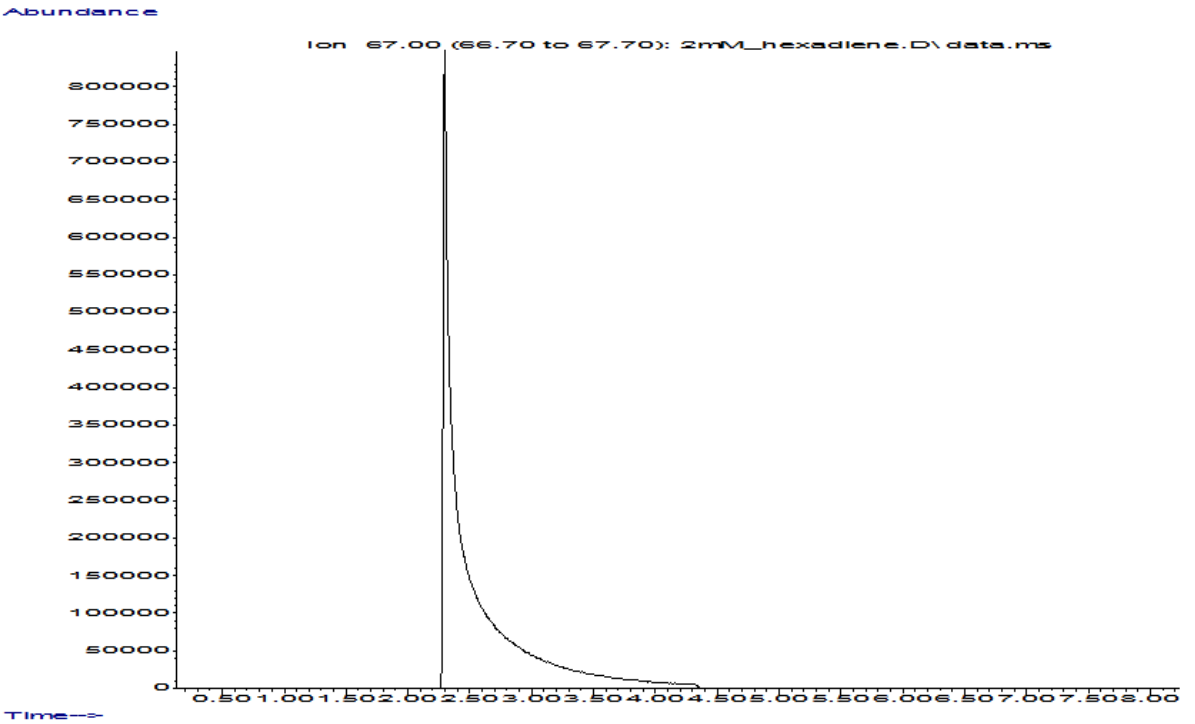

Figure S111. Headspace GC-MS analysis of a commercial standard of **9c**. The signal of extracted ion *m*/z = 67 is shown.

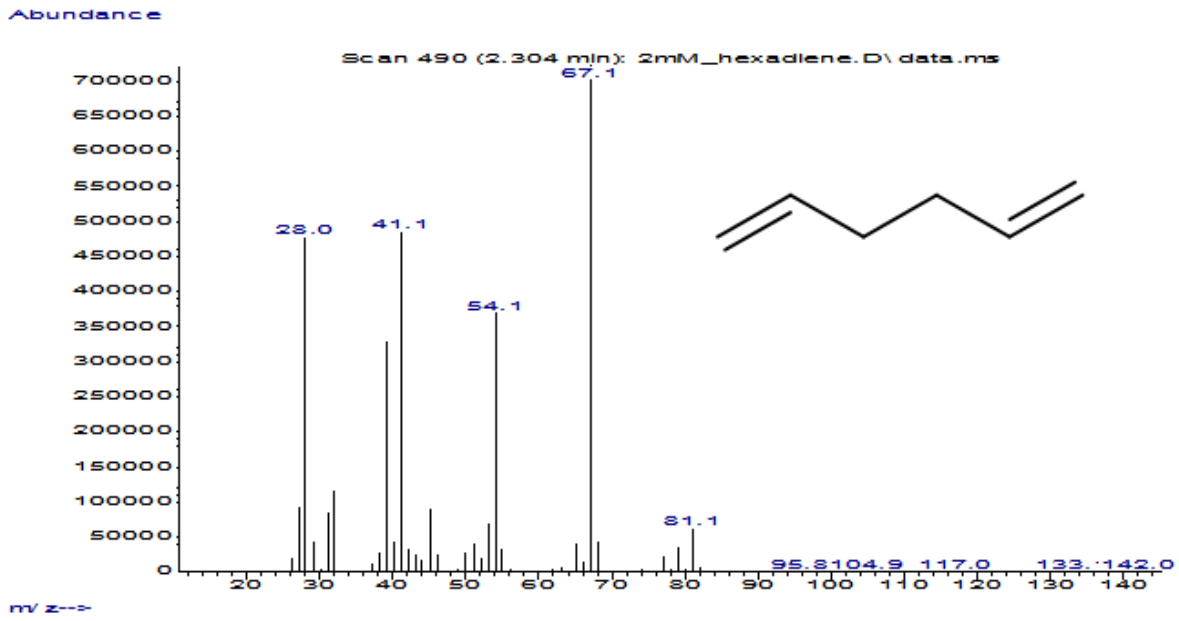

Figure S112. GC-MS spectra of a commercial standard of **9c** (82.08 g mol^{-1}).

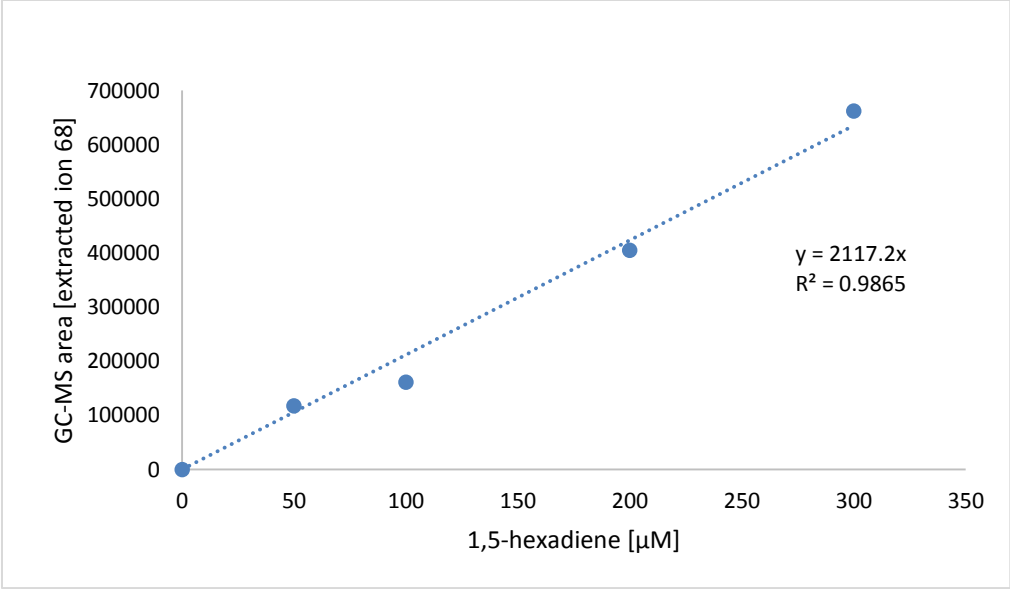

Figure S113. Calibration curve obtained by headspace GC-MS analysis of defined concentrations of **9c**. The extracted ion *m*/z = 68 was used for the generation of a calibration curve.

7.2 Conversion of ω-enoic acids (5b-9b) with the OleT-CamAB-FDH system

7.2.1 Conversion of 5b

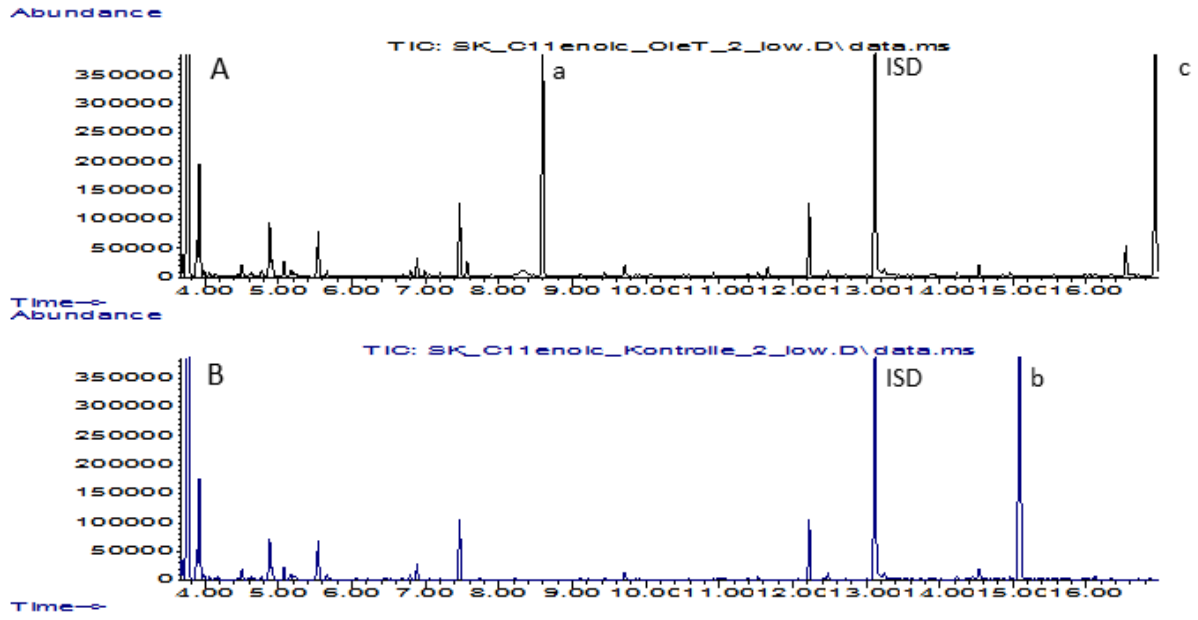

Figure S114. GC-MS chromatograms obtained by conversion of **5b** (4 mM). **A** = Conversion of **5b** with the OleT-CamAB-FDH system. **B** = Conversion of **5b** in the absence of OleT (negative control). **ISD** = internal standard (0.1 % (v/v) 1-decanol); **a** = **5c**; **b** = methyl ester of **5b** (substrate); **c** = **5g**-methyl ester.

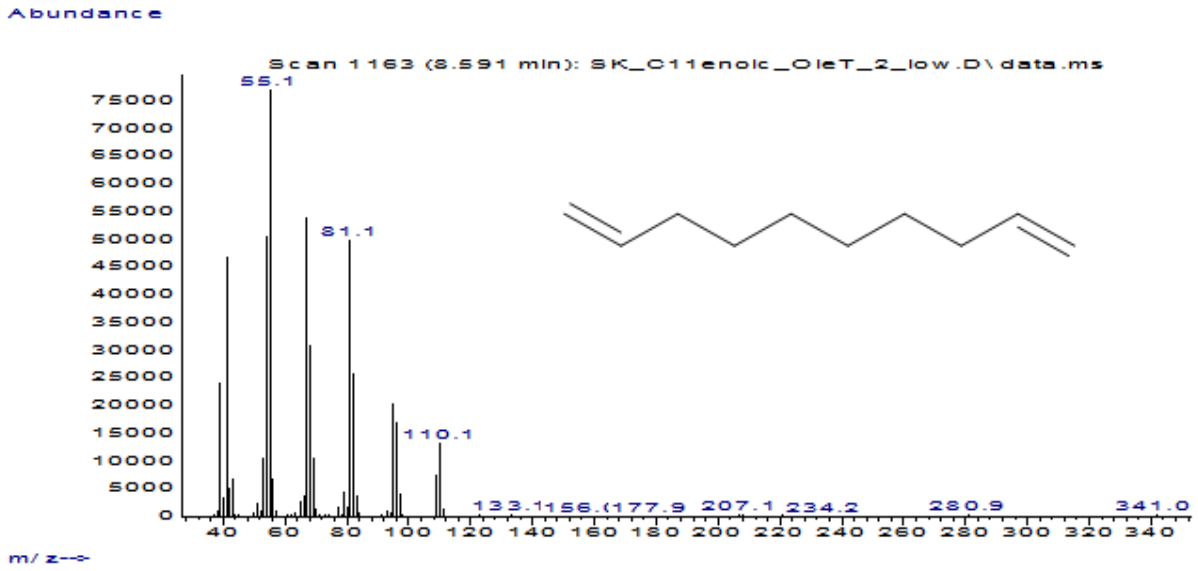

Figure S115. GC-MS spectra of **5c** (138,14 g mol^{-1}) obtained by conversion of **5b** (4 mM) with the OleT-CamAB-FDH system (corresponds to peak a in Figure S114 A).

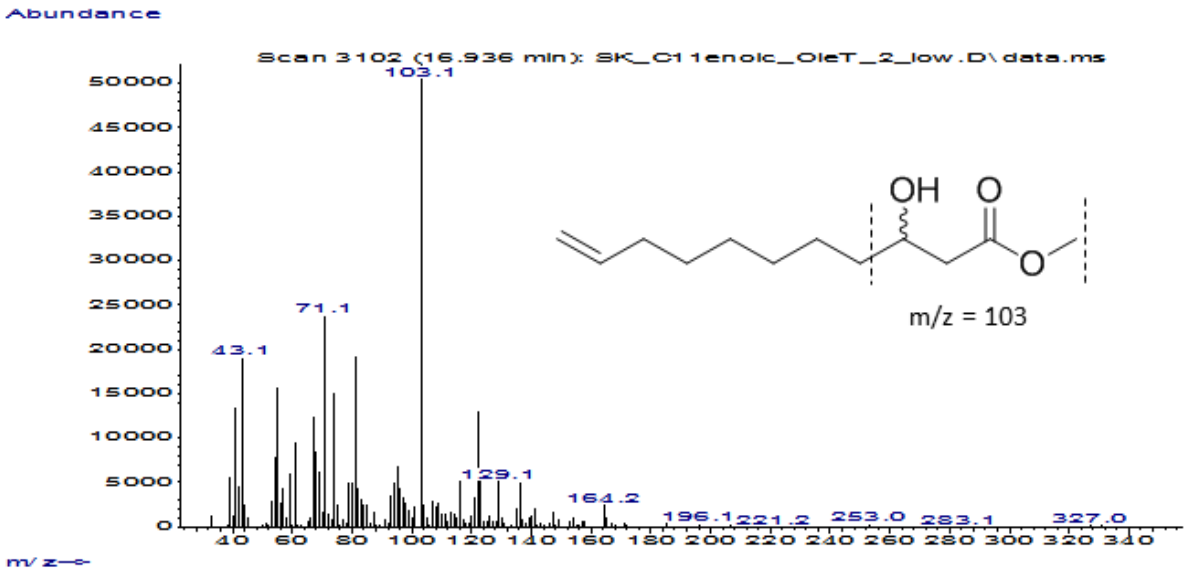

Figure S116. GC-MS spectra of **5g**-methyl ester (214.16 g mol^{-1}) obtained by conversion of **5b** (4 mM) withthe OleT-CamAB-FDH system (corresponds to peak c in Figure S114 A).

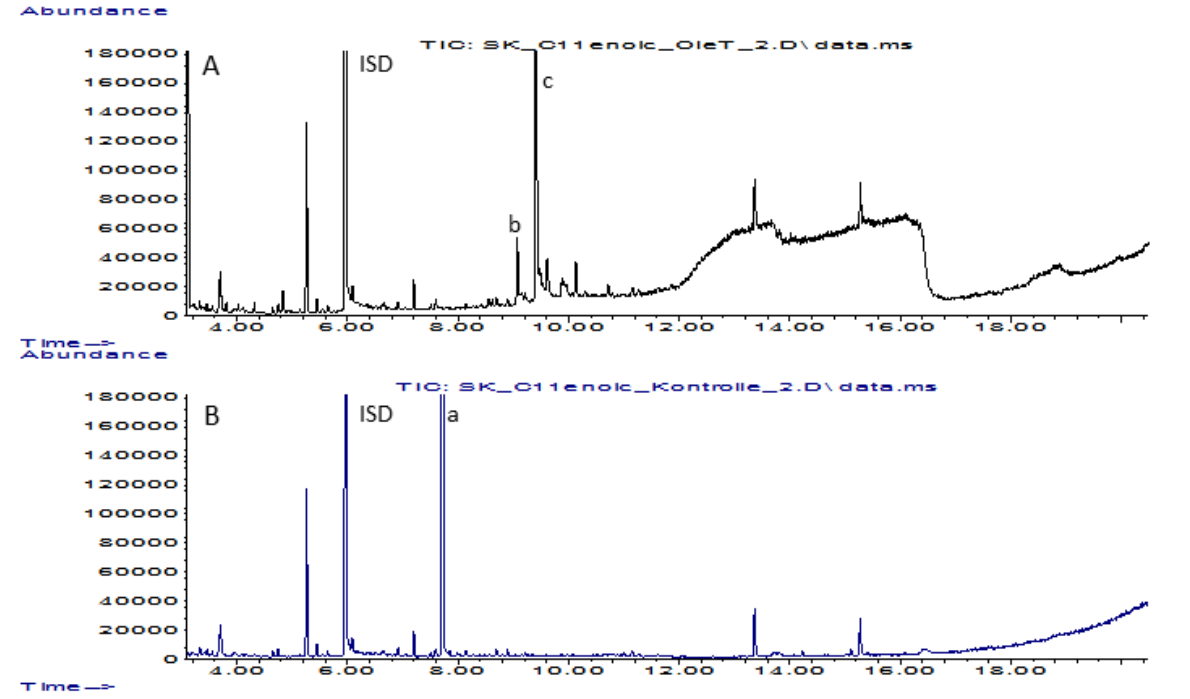

Figure S117. GC-MS chromatograms obtained by conversion of **5b** (4 mM). **A** = Conversion of **5b** with the OleT-CamAB-FDH system. **B** = Conversion of **5b** in the absence of OleT (negative control). **ISD** = internal standard (0.1 % (v/v) 1-decanol); **a** = **5b** methyl ester (substrate); **b** = **5e**-methyl ester; **c** = **5g**-methyl ester.

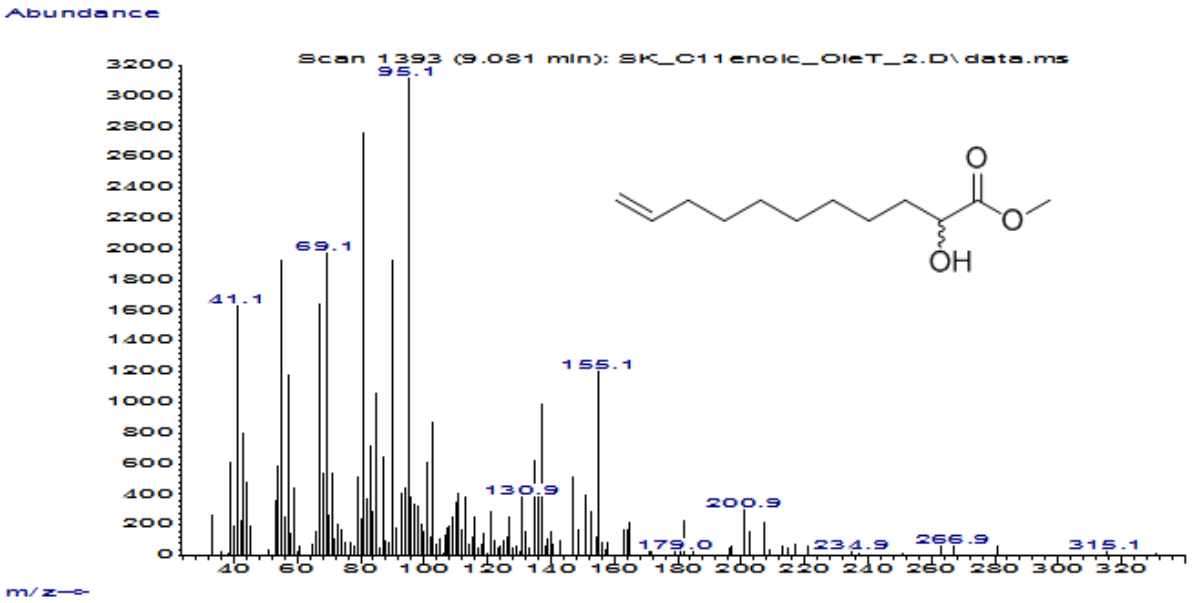

Figure S118. GC-MS spectra of **5e**-methyl ester (214.16 g mol^{-1}) obtained by conversion of **5b** (4 mM) with the OleT-CamAB-FDH system (corresponds to peak b in Figure S117 A). See also Figure S120 B and Figure S121 for comparison.

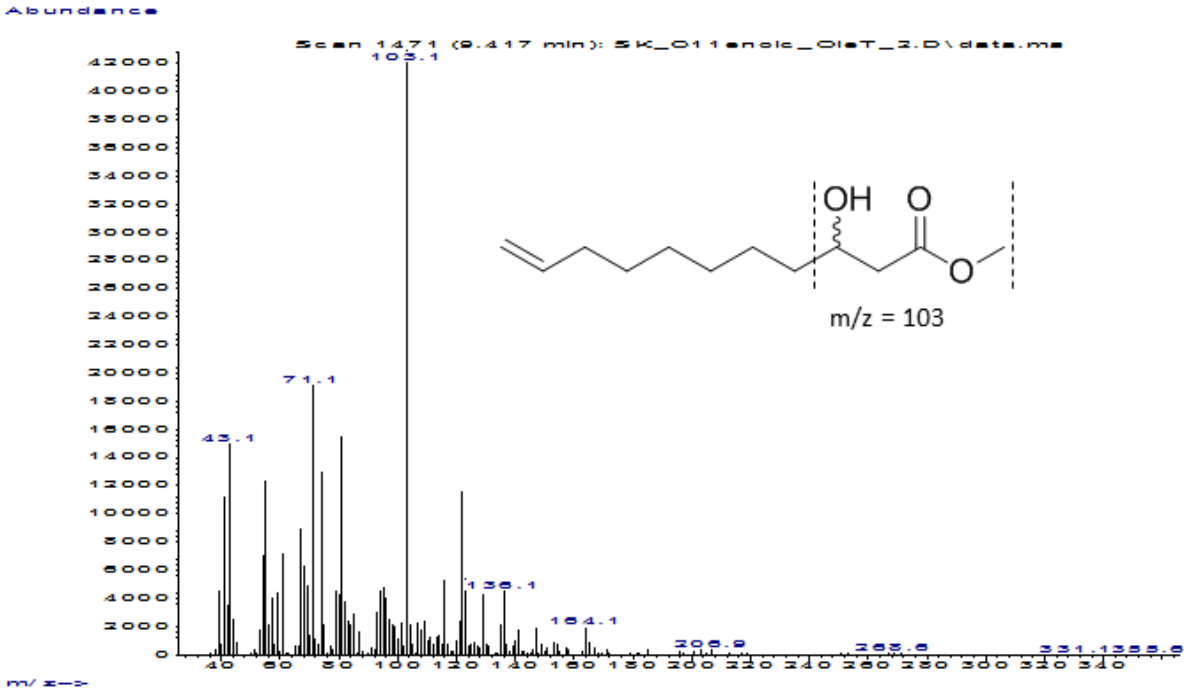

Figure S119. GC-MS spectra of **5g**-methyl ester (214.16 g mol^{-1}) obtained by conversion of **5b** (4 mM) with the OleT-CamAB-FDH system (corresponds to peak c in Figure S117 A). See also Figures Figure S120 A and Figure S122 for comparison.

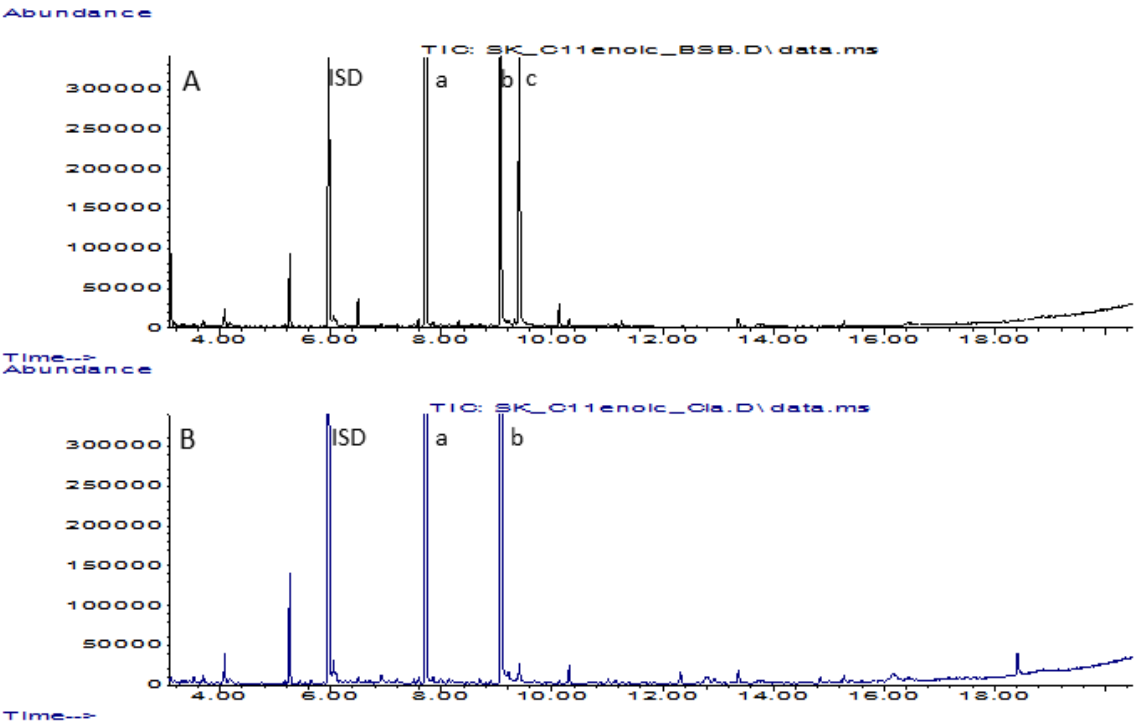

Figure S120. GC-MS chromatograms obtained by conversion of **5b** (10 mM) with $CYP_{BSß}$ (**A**) and $P450_{Cla}$ (**B**) using H_2O_2 as oxidant. **ISD** = internal standard (0.1 % (v/v) 1-decanol); **a** = **5b** methyl ester (substrate); **b** = **5e**-methyl ester; **c** = **5g**-methyl ester.

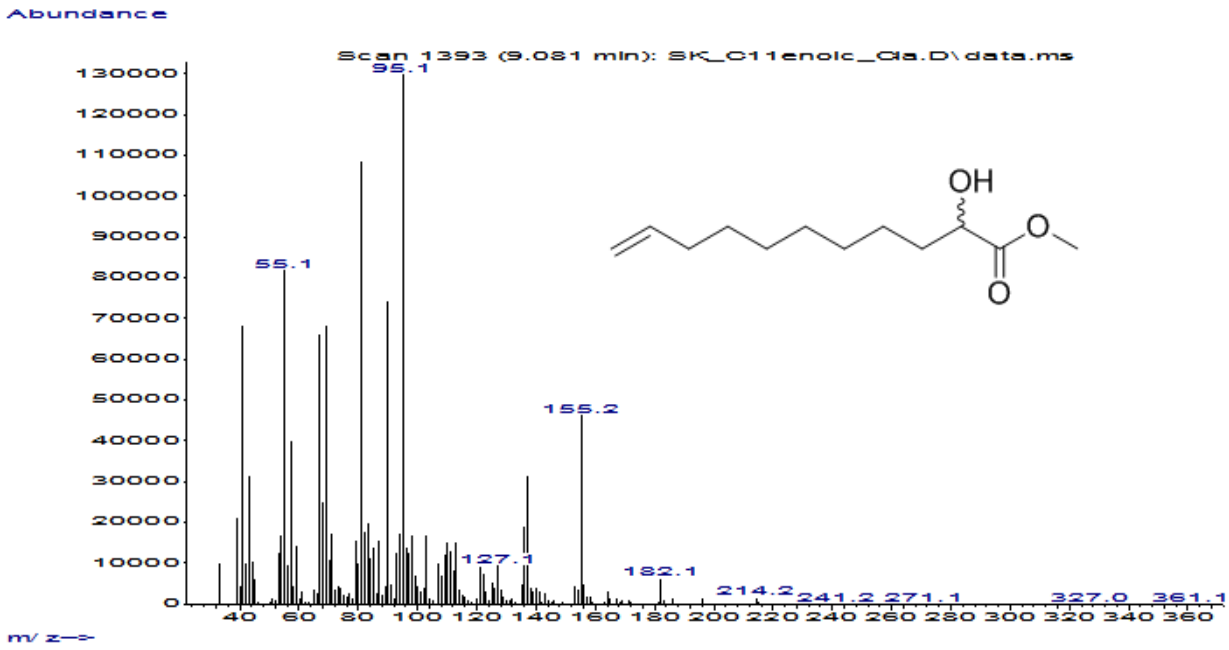

Figure S121. GC-MS spectra of **5e**-methyl ester (214.16 g mol^{-1}) obtained by conversion of **5b** (10 mM) with $P450_{Cla}$ and H_2O_2 as oxidant (corresponds to peak b in Figure S120 B).

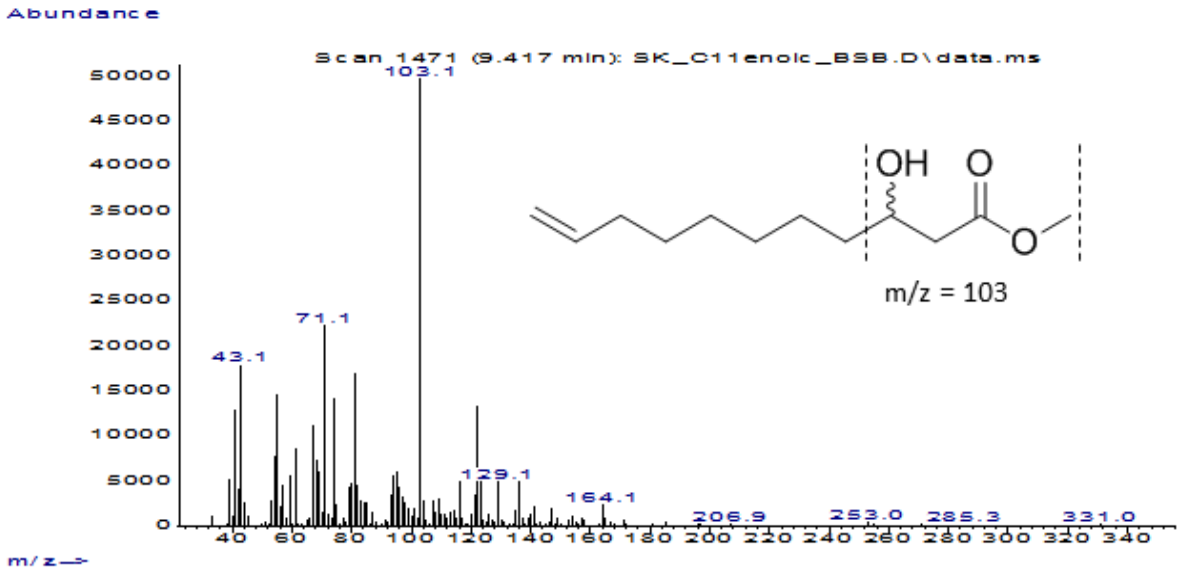

Figure S122. GC-MS spectra of **5g**-methyl ester (214.16 g mol^{-1}) obtained by conversion of **5b** (10 mM) with $CYP_{BSß}$ and H_2O_2 as oxidant (corresponds to peak c in Figure S120 A). The characteristic ion *m*/z = 103 was used to assign the product.

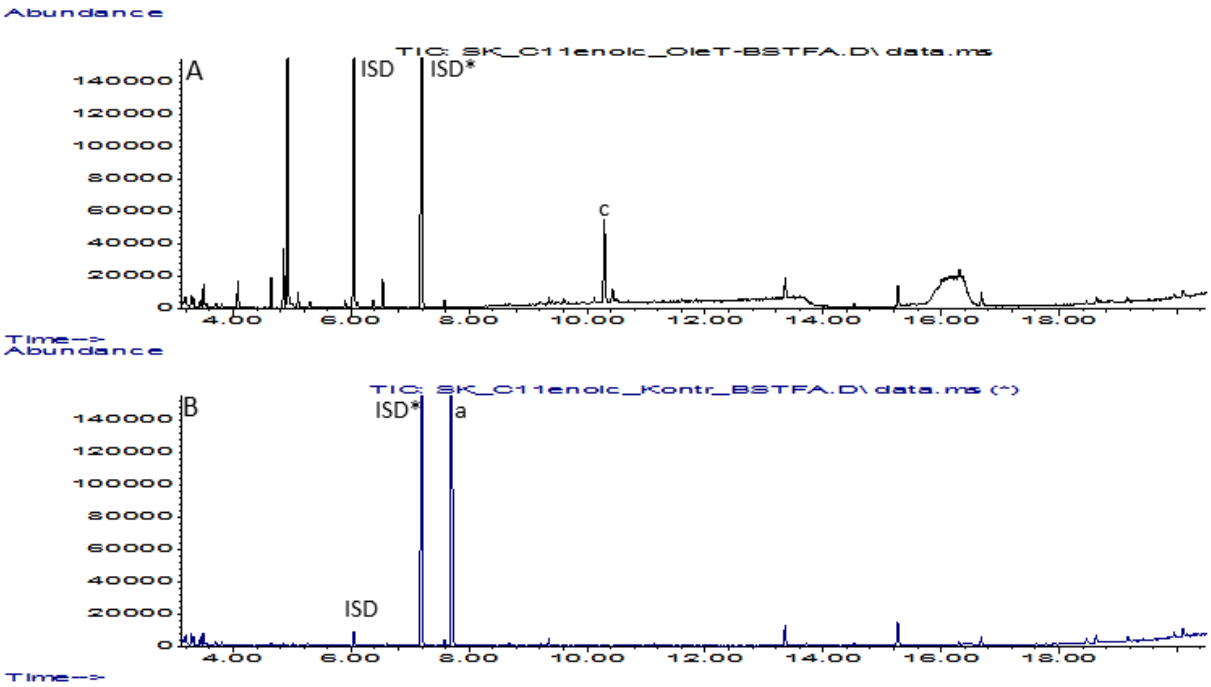

Figure S123. GC-MS chromatograms obtained by conversion of **5b** (4 mM) after derivatization with $TMSCHN_2$ and BSTFA. **A** = Conversion of **5b** with the OleT-CamAB-FDH system. **B** = Conversion of **5b** in the absence of OleT (negative control). **ISD** = internal standard (0.1 % (v/v) 1-decanol); **ISD*** = silylated internal standard (TMS-1-decanol); **a** = **5b**-methyl ester (substrate); **c** = TMS-**5g**-methyl ester.

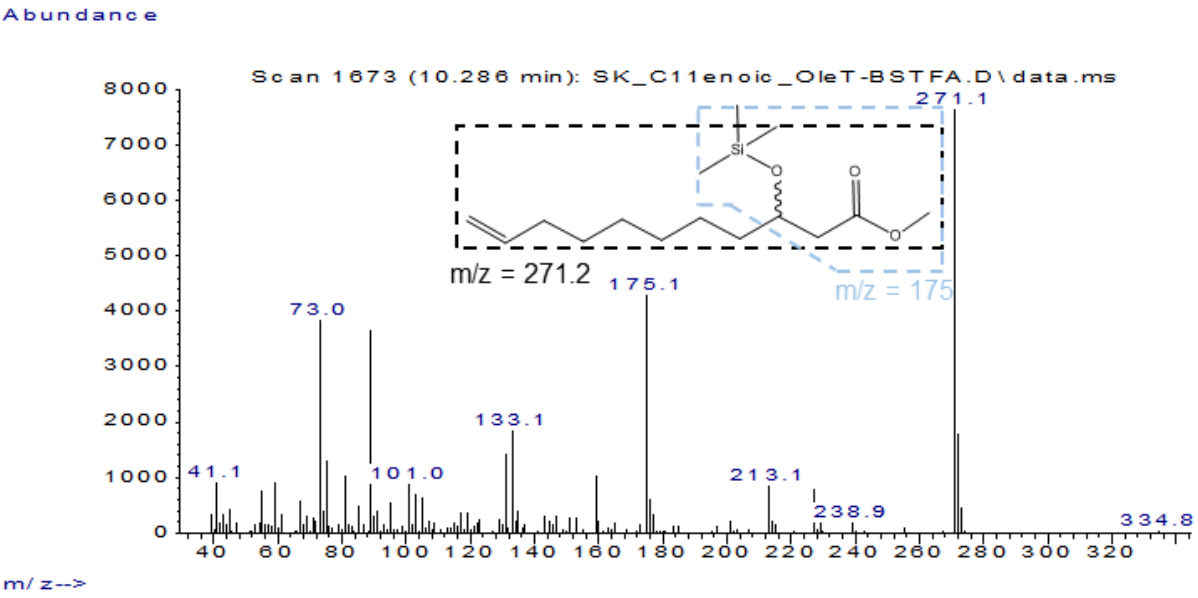

Figure S124. GC-MS spectra of TMS-**5g**-methyl ester obtained by conversion of **5b** (4 mM) with the OleT-CamAB-FDH system (corresponds to peak c in Figure S123 A). The characteristic ions *m*/z = 175 and *m*/z = 271.2 were used to assign product as described elsewhere (see also Figure S125 and Figure S126 for comparison).[2]

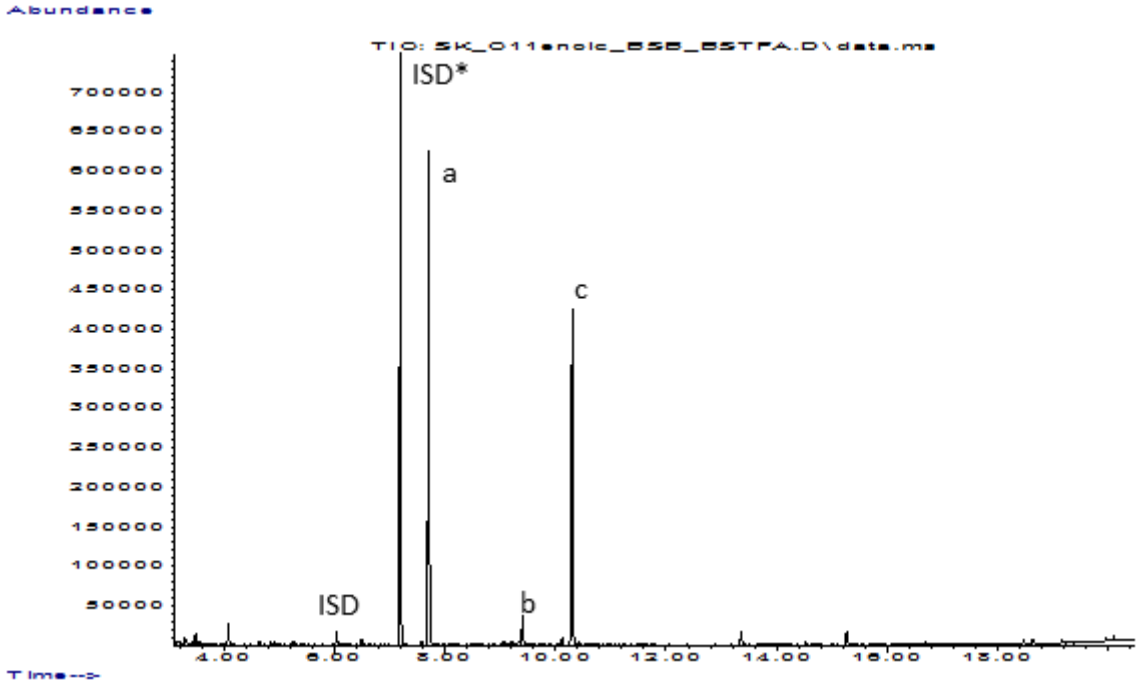

Figure S125. GC-MS chromatograms obtained by conversion of **5b** (10 mM) with $CYP_{BS\beta}$ and H_2O_2 as oxidant after derivatization with $TMSCHN_2$ and BSTFA. **ISD** = internal standard (0.1 % (v/v) 1-decanol); **ISD*** = silylated internal standard (TMS-1-decanol); **a** = **5b**-methyl ester (substrate); **b** = TMS-**5e**-methyl ester; **c** = TMS-**5g**-methyl ester.

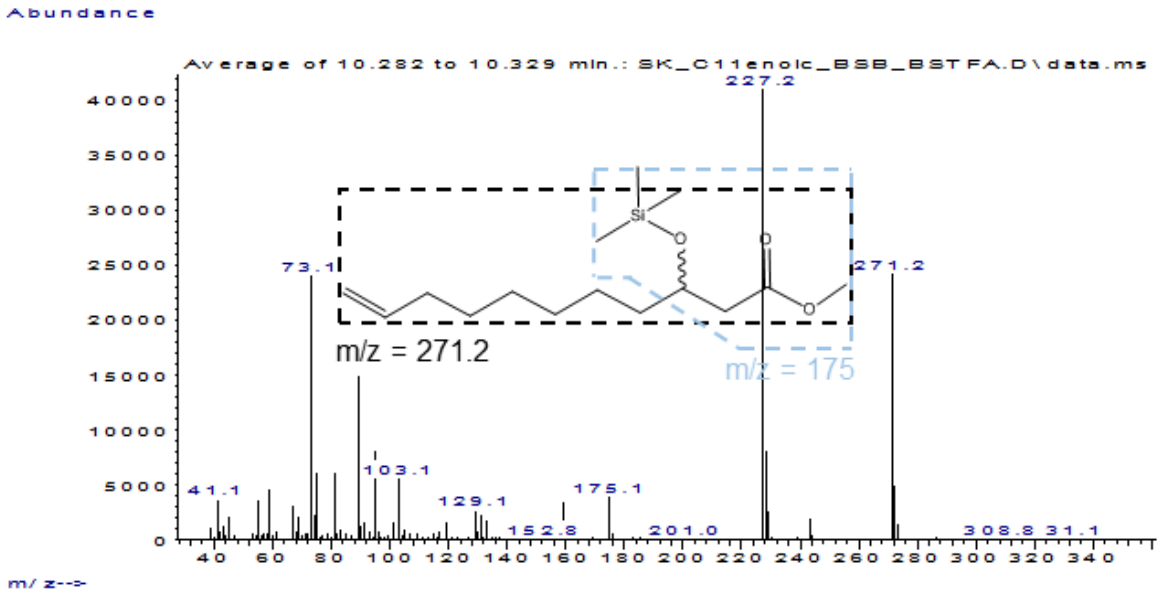

Figure S126. GC-MS spectra of TMS-**5g**-methyl ester obtained by conversion of **5b** (10 mM) with $CYP_{BS\beta}$ and H_2O_2 as oxidant (corresponds to peak c in Figure S125). The characteristic ions *m*/z = 175 and *m*/z = 271.2 were used to assign the minor side product as described elsewhere.[2]

7.2.2 **Conversion of 6b**

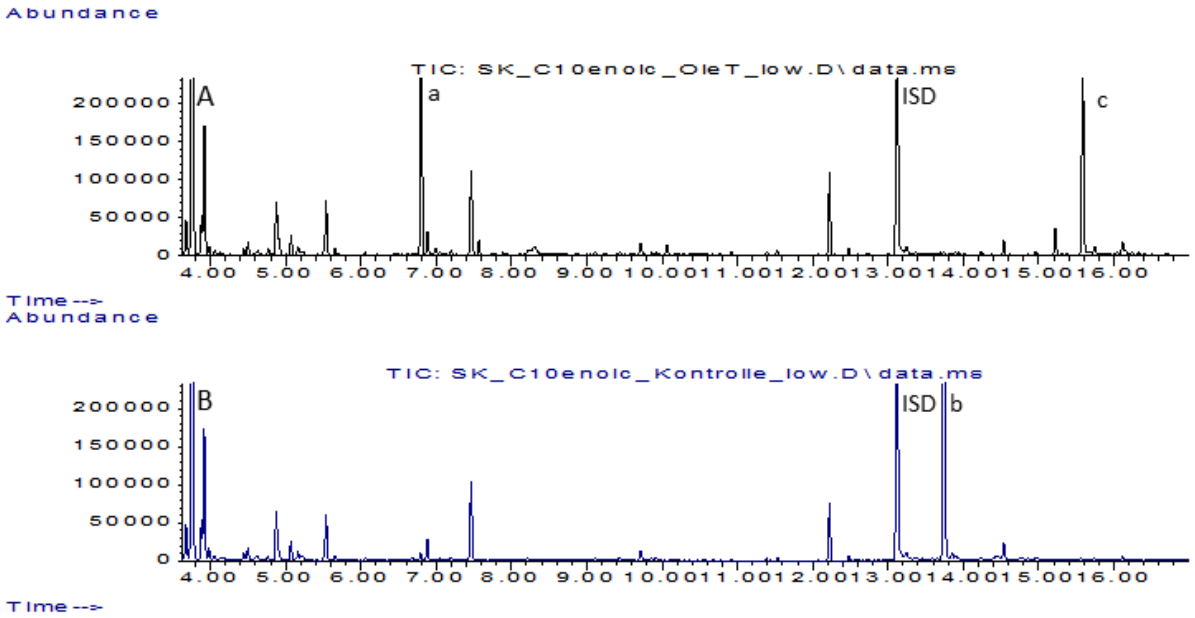

Figure S127. GC-MS chromatograms obtained by conversion of **6b** (4 mM). **A** = Conversion of **6b** with the OleT-CamAB-FDH system. **B** = Conversion of **6b** in the absence of OleT (negative control). **ISD** = internal standard (0.1 % (v/v) 1-decanol); **a** = **6c**; **b** = **6b**-methyl ester (substrate); **c** = **6g**-methyl ester.

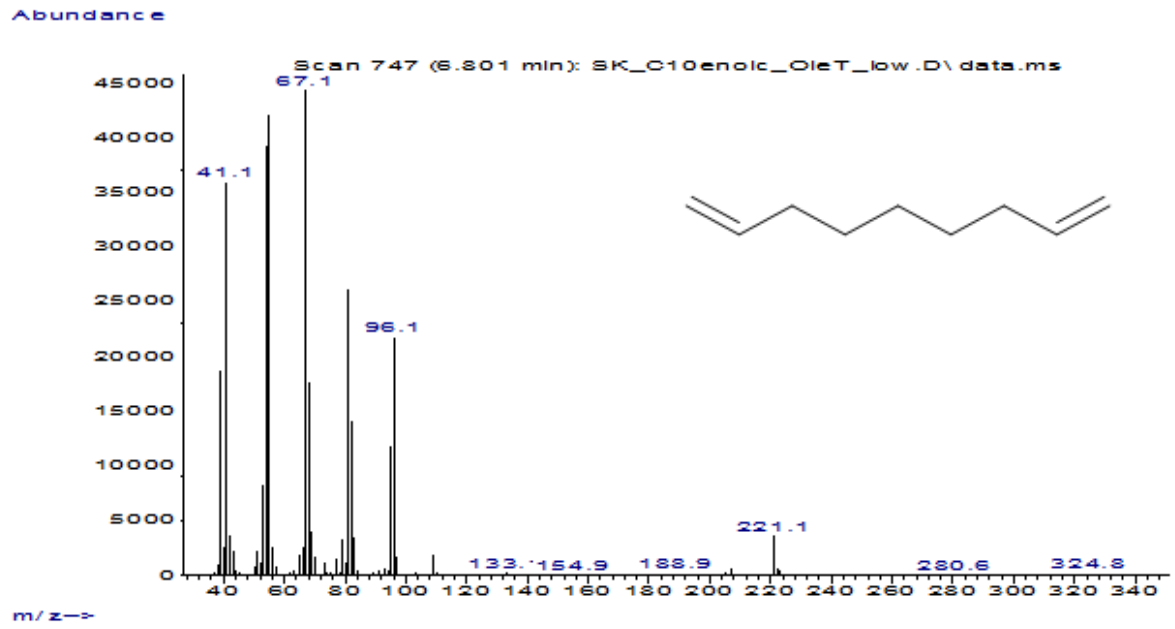

Figure S128. GC-MS spectra of **6c** (124.13 g mol^{-1}) obtained by conversion of **6b** (4 mM) with the OleT-CamAB-FDH system (corresponds to peak a in Figure S127 A).

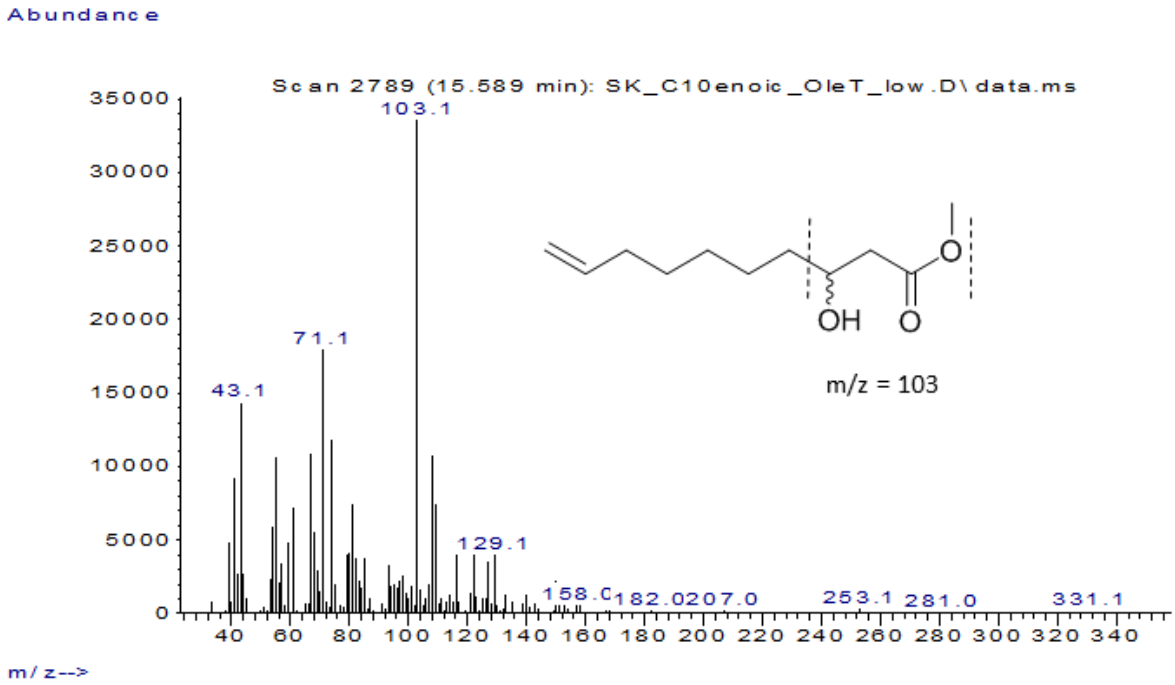

Figure S129. GC-MS spectra of **6g**-methyl ester (200.14 g mol^{-1}) obtained by conversion of **6b** (4 mM) with the OleT-CamAB-FDH system (corresponds to peak c in Figure S127 A).

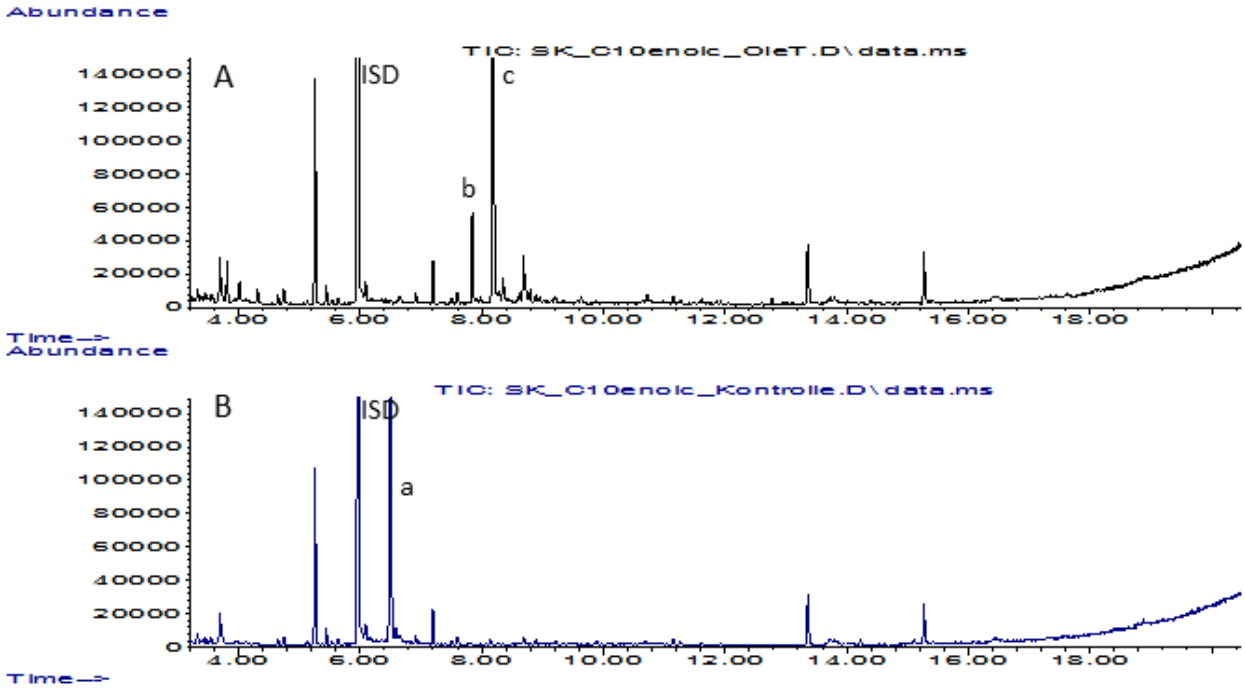

Figure S130. GC-MS chromatograms obtained by conversion of **6b** (4 mM). **A** = Conversion of **6b** with the OleT-CamAB-FDH system. **B** = Conversion of **6b** in the absence of OleT (negative control). **ISD** = internal standard (0.1 % (v/v) 1-decanol); **a** = **6b** methyl ester (substrate); **b** = **6e**-methyl ester; **c** = **6g**-methyl ester.

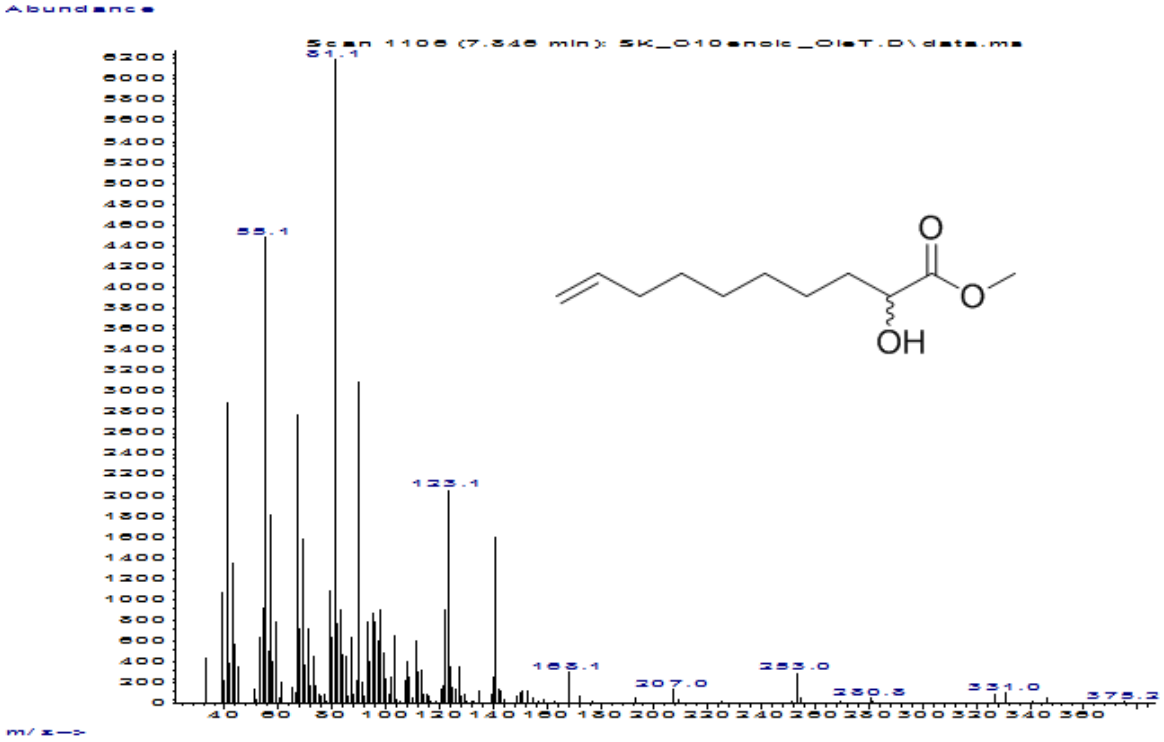

Figure S131. GC-MS spectra of **6e**-methyl ester (200.14 g mol^{-1}) obtained by conversion of **6b** (4 mM) with the OleT-CamAB-FDH system (corresponds to peak b in Figure S130 A). See also Figure S134 for comparison.

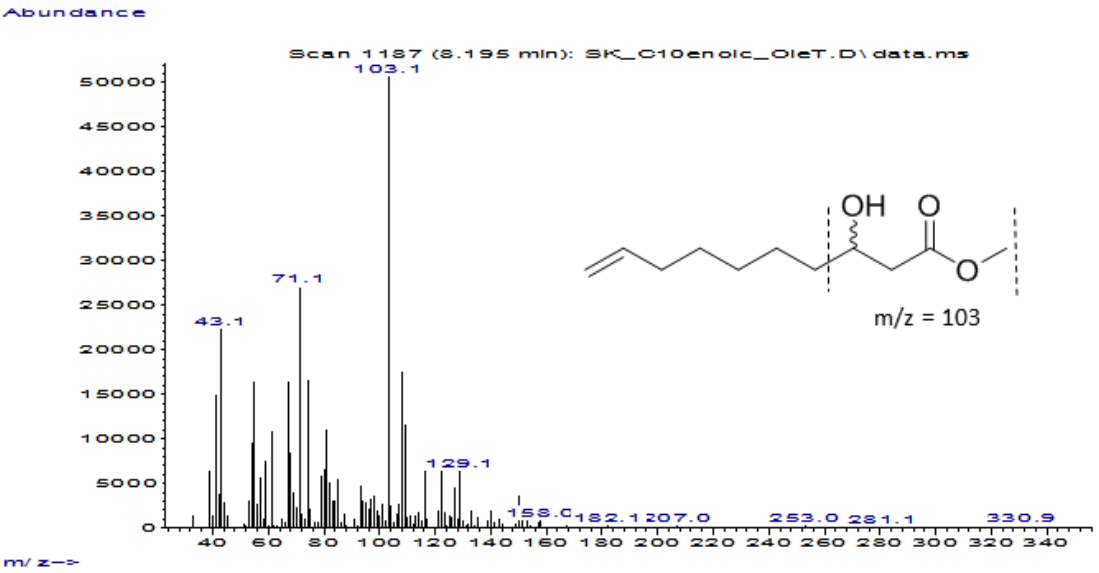

Figure S132. GC-MS spectra of **6g**-acid methyl ester (200.14 g mol^{-1}) obtained by conversion of **6b** (4 mM) with the OleT-CamAB-FDH system (corresponds to peak c in Figure S130 A).

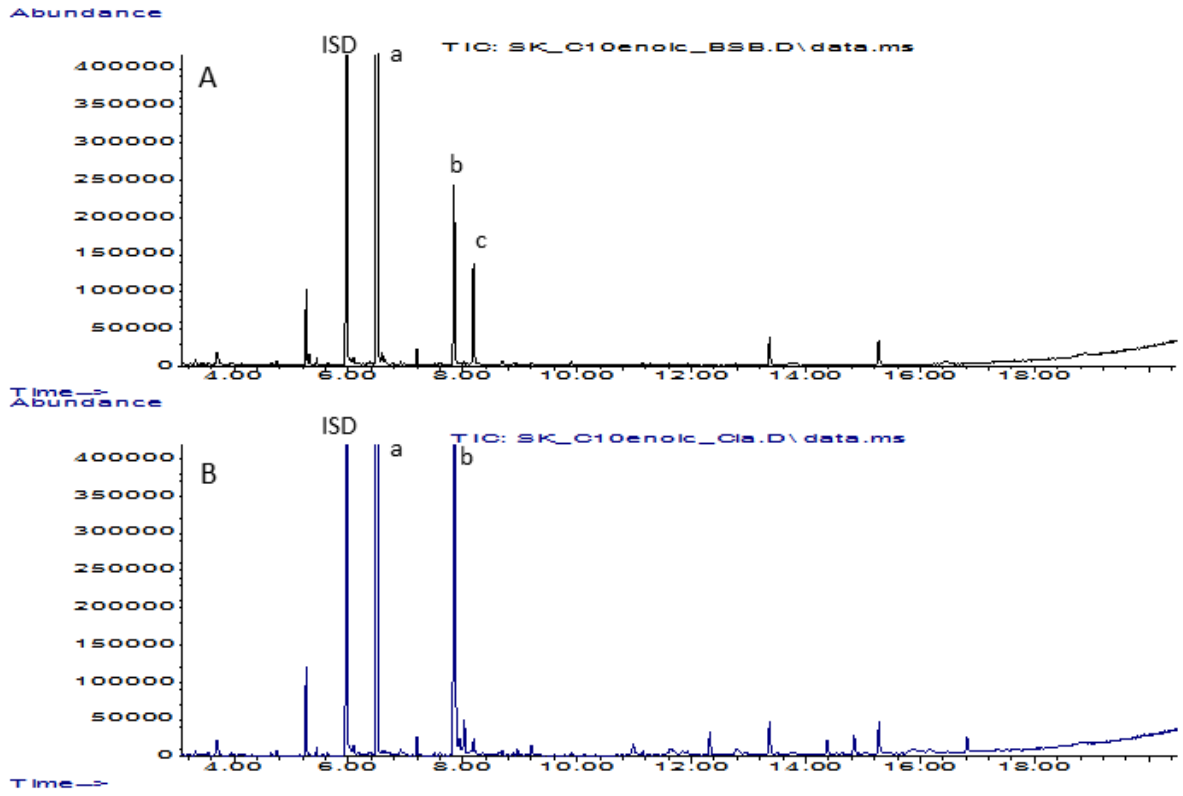

Figure S133. GC-MS chromatograms obtained by conversion of **6b** (10 mM) with $CYP_{BSß}$ (**A**) and $P450_{Cla}$ (**B**) using H_2O_2 as oxidant. **ISD** = internal standard (0.1 % (v/v) 1-decanol); **a** = **6b** methyl ester (substrate); **b** = **6e**-methyl ester; **c** = **6g**-methyl ester.

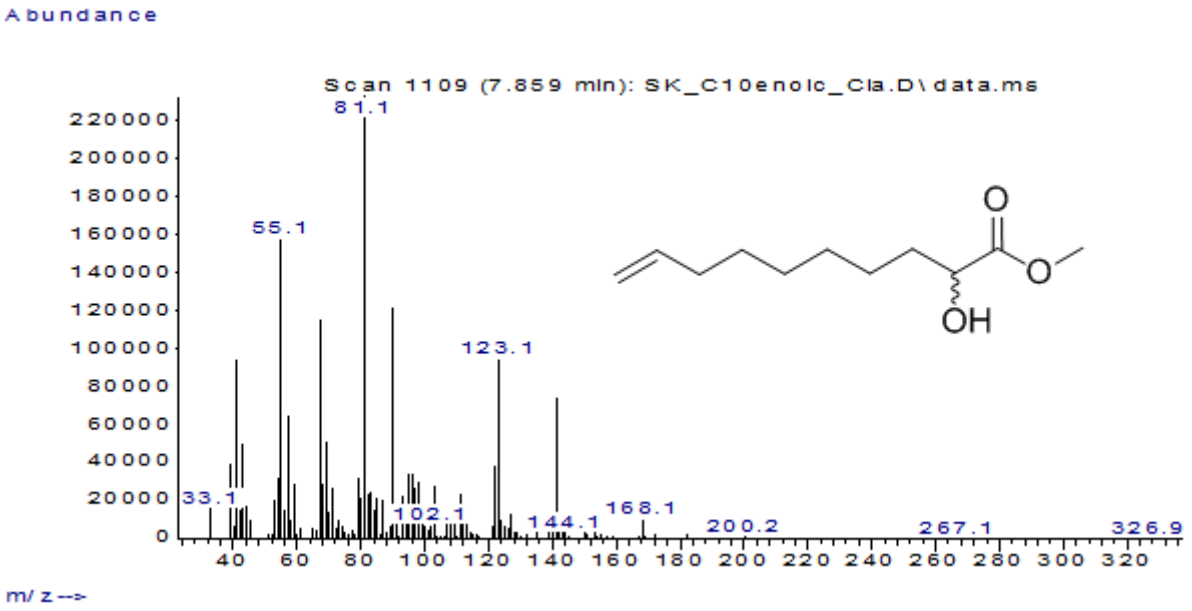

Figure S134. GC-MS spectra of **6e**-methyl ester (200.14 g mol^{-1}) obtained by conversion of **6b** (10 mM) with $P450_{Cla}$ and H_2O_2 as oxidant (corresponds to peak b in Figure S133 B).

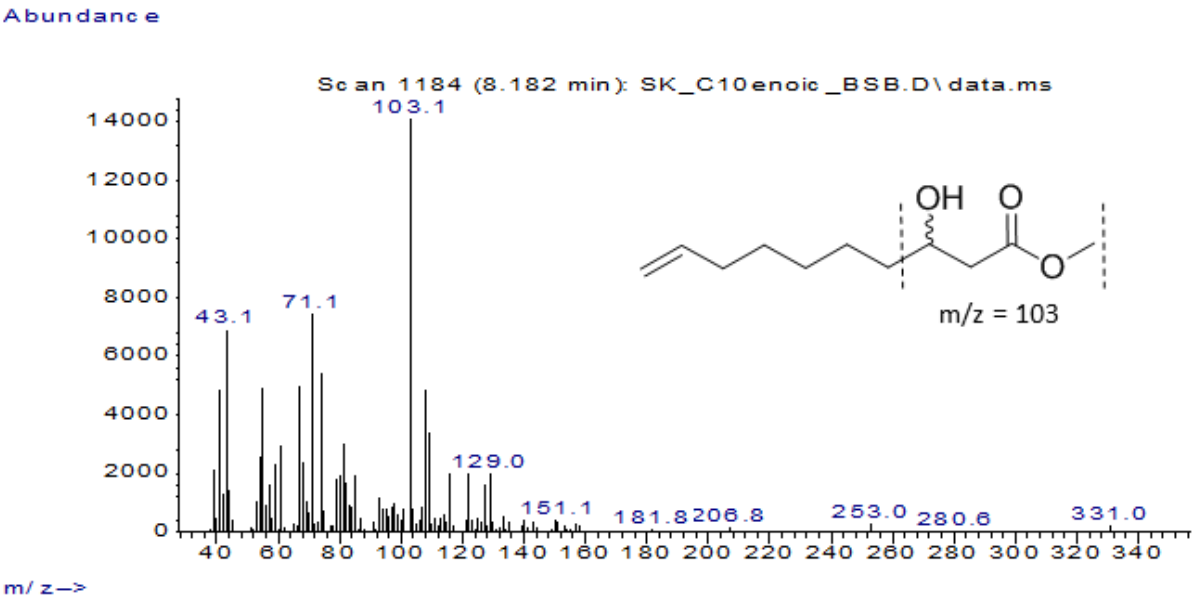

Figure S135. GC-MS spectra of **6g**-methyl ester (200.14 g mol^{-1}) obtained by conversion of **6b** (10 mM) with $CYP_{BSß}$ and H_2O_2 as oxidant (corresponds to peak c in Figure S133 A). The characteristic ion *m*/z = 103 was used to assign the product.

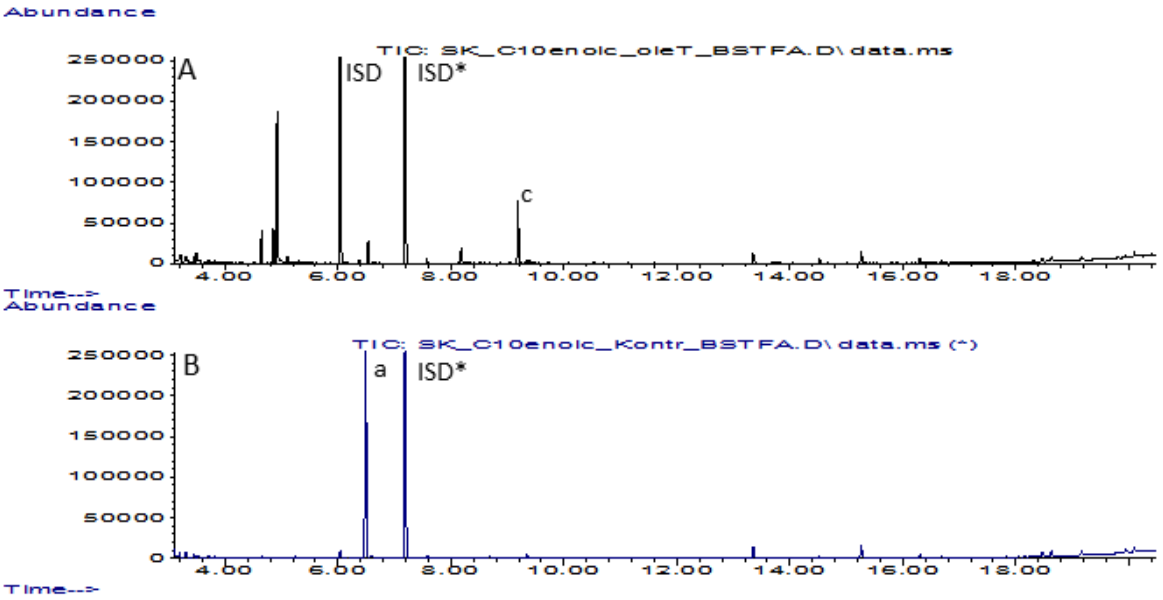

Figure S136. GC-MS chromatograms obtained by conversion of **6b** (4 mM) after derivatization with $TMSCHN_2$ and BSTFA. **A** = Conversion of **6b** with the OleT-CamAB-FDH system. **B** = Conversion of **6b** in the absence of OleT (negative control). **ISD** = internal standard (0.1 % (v/v) 1-decanol); **ISD*** = silylated internal standard (TMS-1-decanol); **a** = **6b**-methyl ester (substrate); **c** = TMS-**6g**-methyl ester.

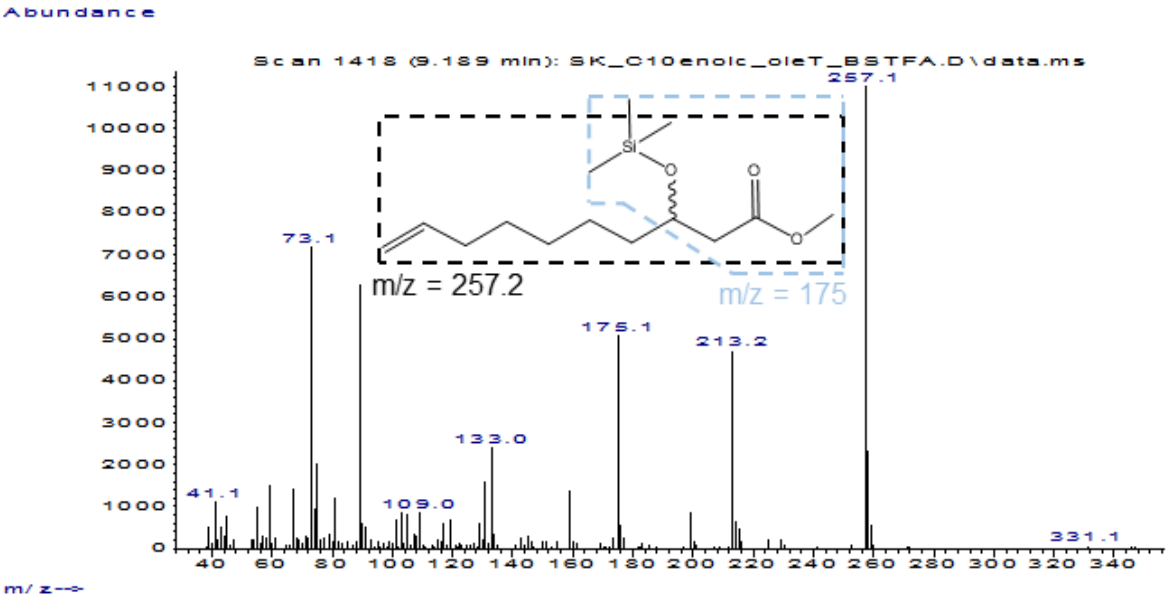

Figure S137. GC-MS spectra of TMS-**6g**-methyl ester obtained by conversion of **6b** (4 mM) with the OleT-CamAB-FDH system (corresponds to peak c in Figure S136 A). The characteristic ions *m*/z = 175 and *m*/z = 257.2 were used to assign the minor side product as described elsewhere.[2]

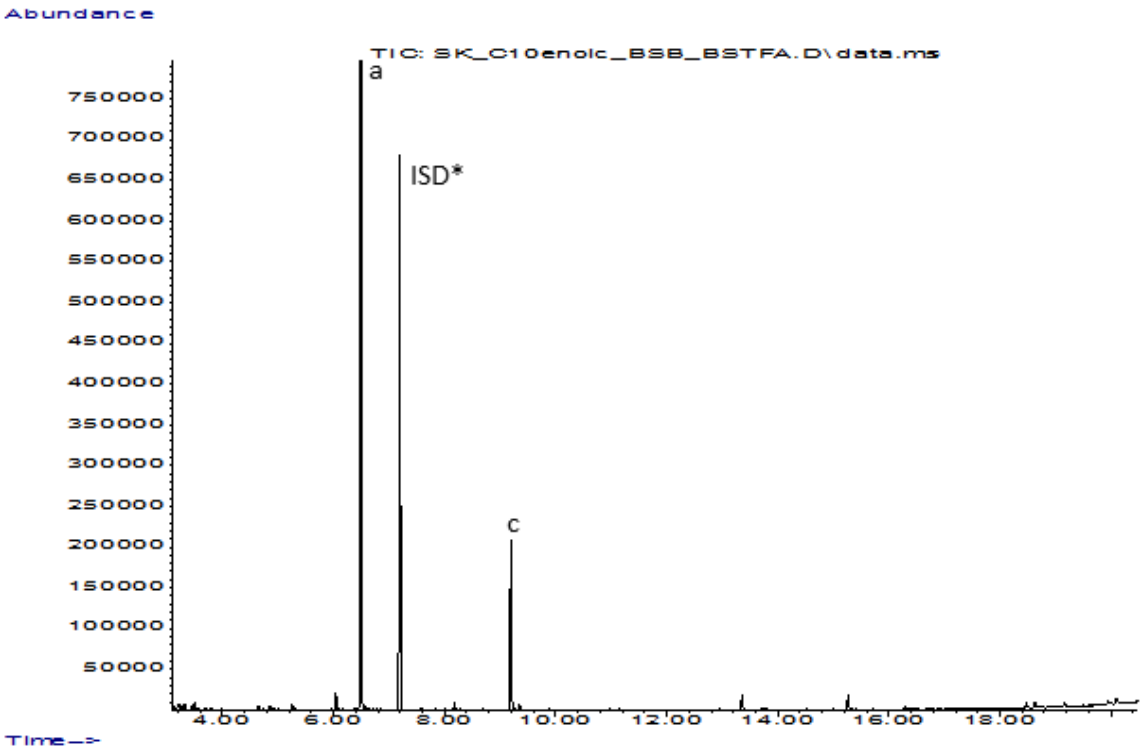

Figure S138. GC-MS chromatograms obtained by conversion of **6b** (10 mM) with $CYP_{BS\beta}$ and H_2O_2 as oxidant after derivatization with $TMSCHN_2$ and BSTFA. **ISD** = internal standard (0.1 % (v/v) 1-decanol); **ISD*** = silylated internal standard (TMS-1-decanol); **a** = **6b**-methyl ester (substrate); **c** = TMS-**6g**-methyl ester.

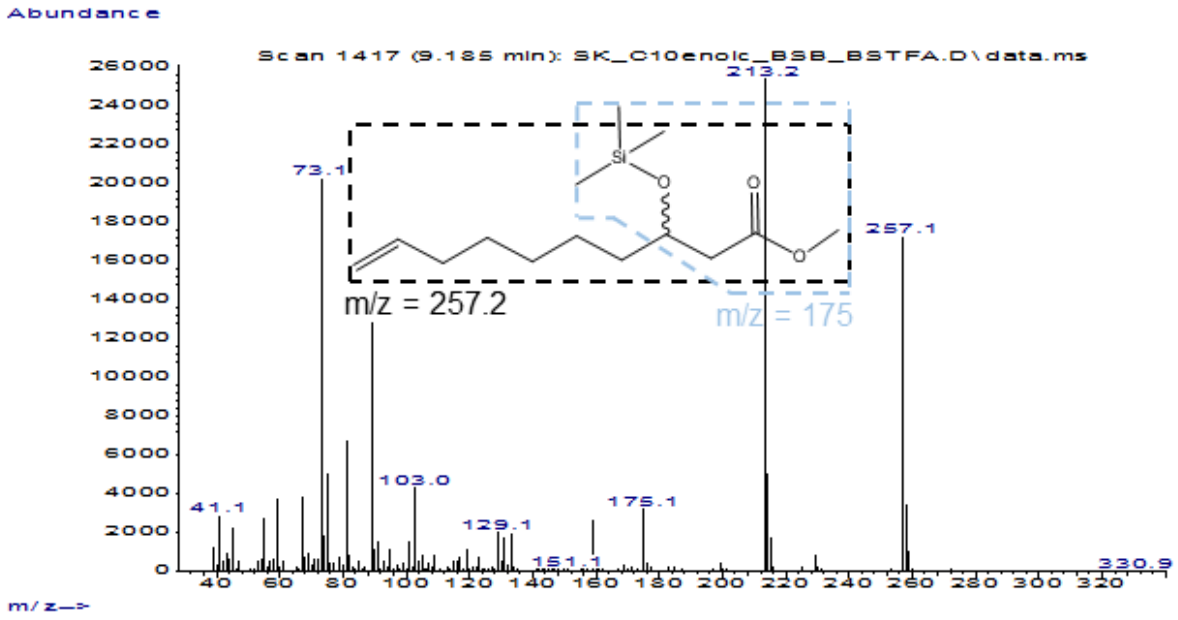

Figure S139. GC-MS spectra of TMS-**6g**-methyl ester obtained by conversion of **6b** (10 mM) with $CYP_{BS\beta}$ and H_2O_2 as oxidant (corresponds to peak c in Figure S138). The characteristic ions *m*/z = 175 and *m*/z = 257.2 were used to assign the minor side product as described elsewhere.[2]

7.2.3 **Conversion of 7b**

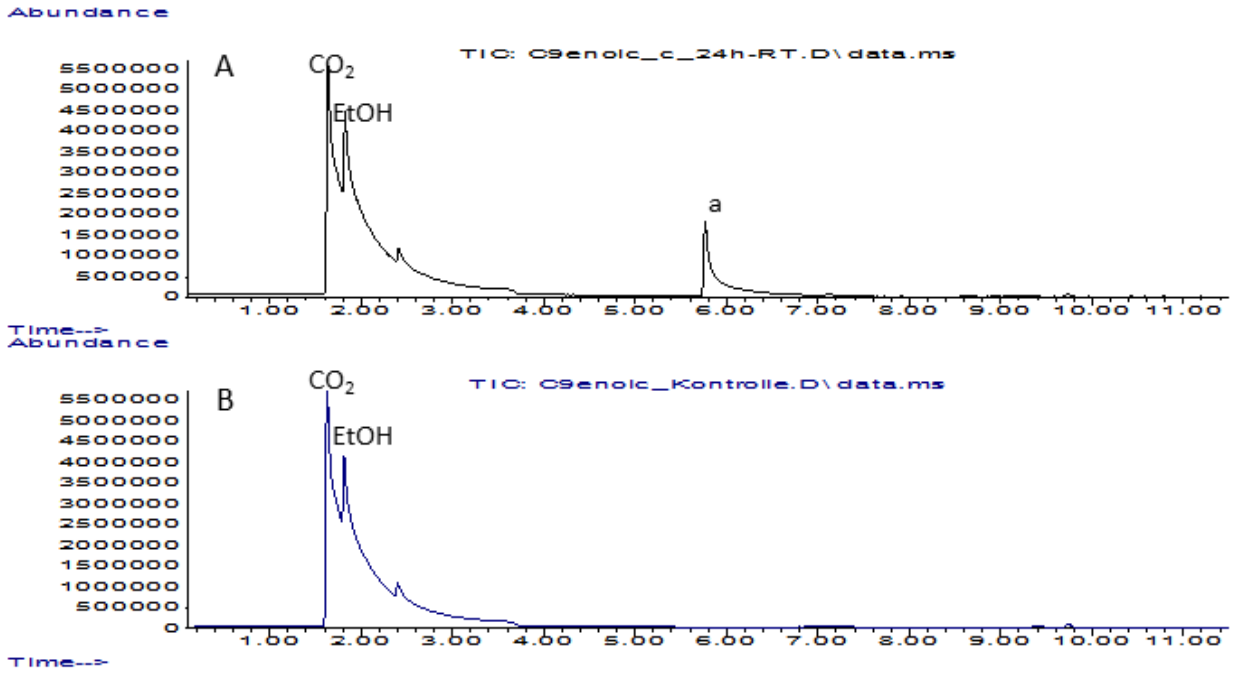

Figure S140. Headspace GC-MS chromatograms obtained by conversion of **7b** (10 mM). **A** = Conversion of **7b** with the OleT-CamAB-FDH system. **B** = Conversion of **7b** in the absence of OleT (negative control). **a** = **7c**. 5 % (v/v) EtOH was used as co-solvent.

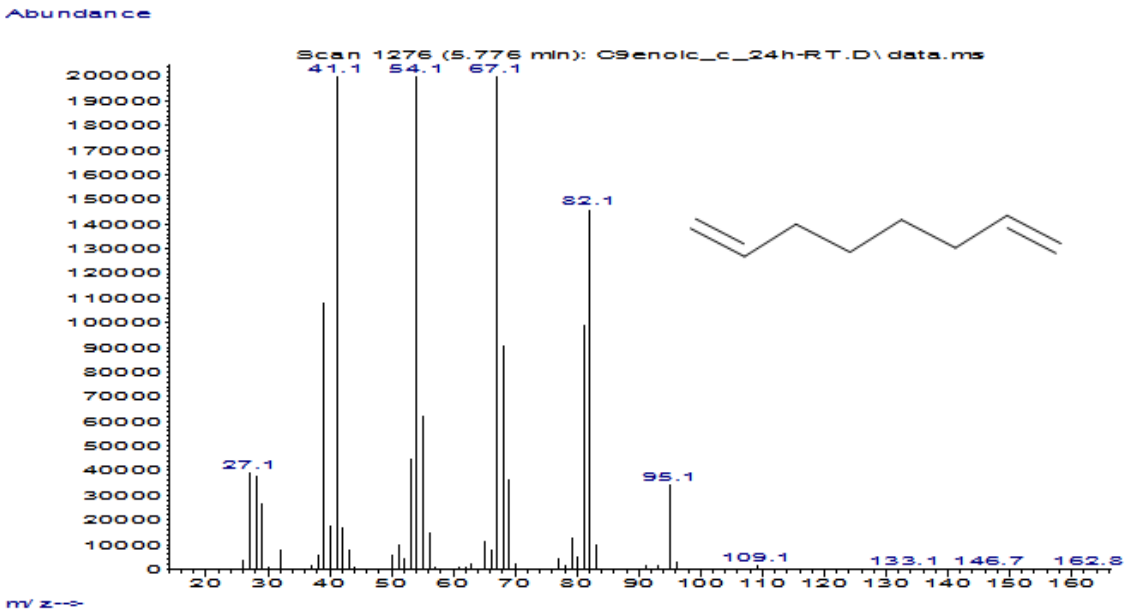

Figure S141. GC-MS spectra of **7c** (110.11 g mol^{-1}) obtained by conversion of **7b** (10 mM) with the OleT-CamAB-FDH system (corresponds to peak a in Figure S140 A).

7.2.4 **Conversion of 8b**

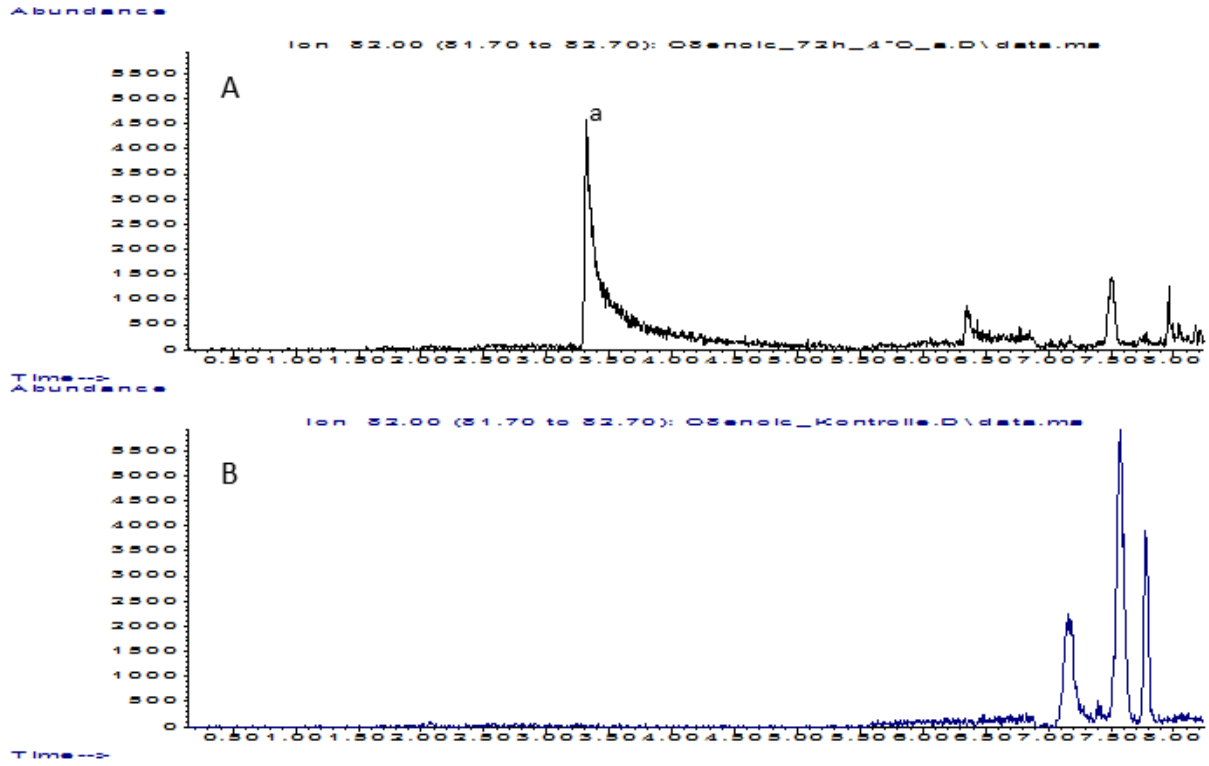

Figure S142. Headspace GC-MS chromatograms obtained by conversion of **8b** (10 mM). **A** = Conversion of **8b** with the OleT-CamAB-FDH system. **B** = Conversion of **8b** in the absence of OleT (negative control). Extracted signals of extracted ion *m*/z = 82 are shown. **a** = **8c**.

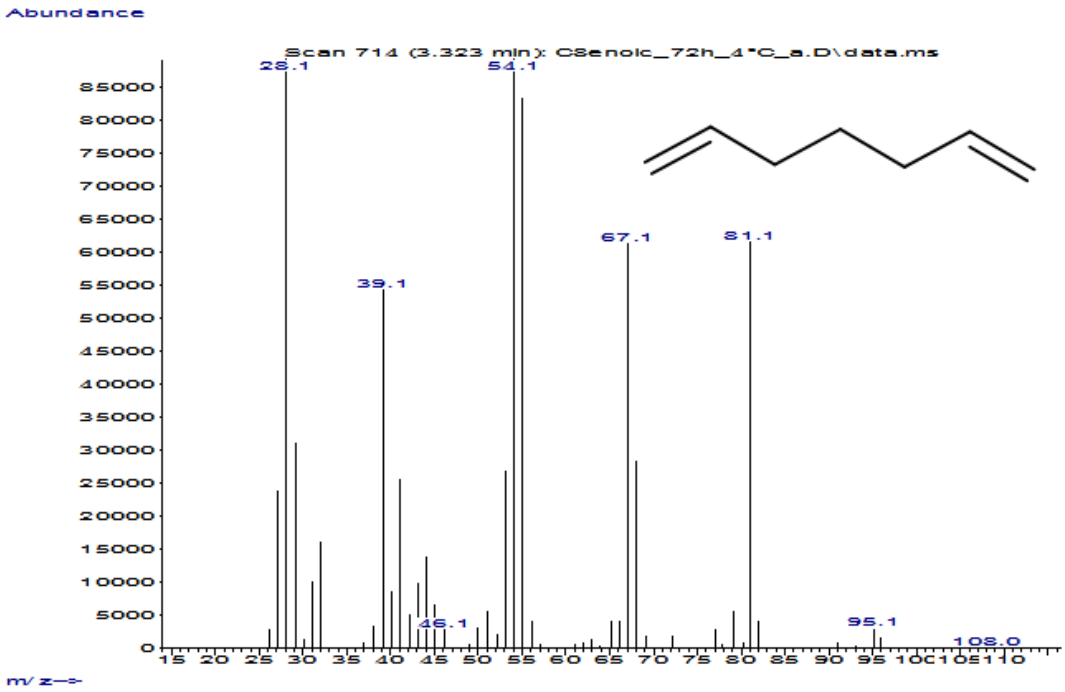

Figure S143. GC-MS spectra of **8c** (96.09 g mol^{-1}) obtained by conversion of **8b** (10 mM) with the OleT-CamAB-FDH system (corresponds to peak a in Figure S142 A).

7.2.5 **Conversion of 9b**

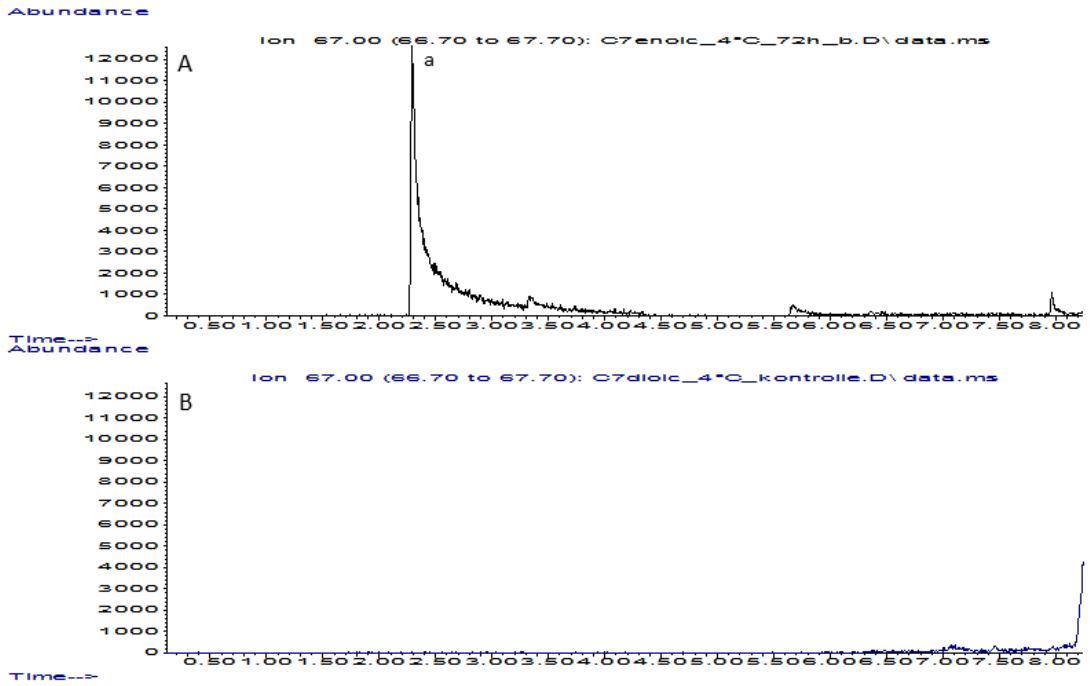

Figure S144. GC-MS chromatograms obtained by conversion of **9b** (10 mM). **A** = Conversion of **9b** with the OleT-CamAB-FDH system. **B** = Conversion of **9b** in the absence of OleT (negative control). Signals of extracted ion *m*/z = 67 are shown. **a** = **9c**.

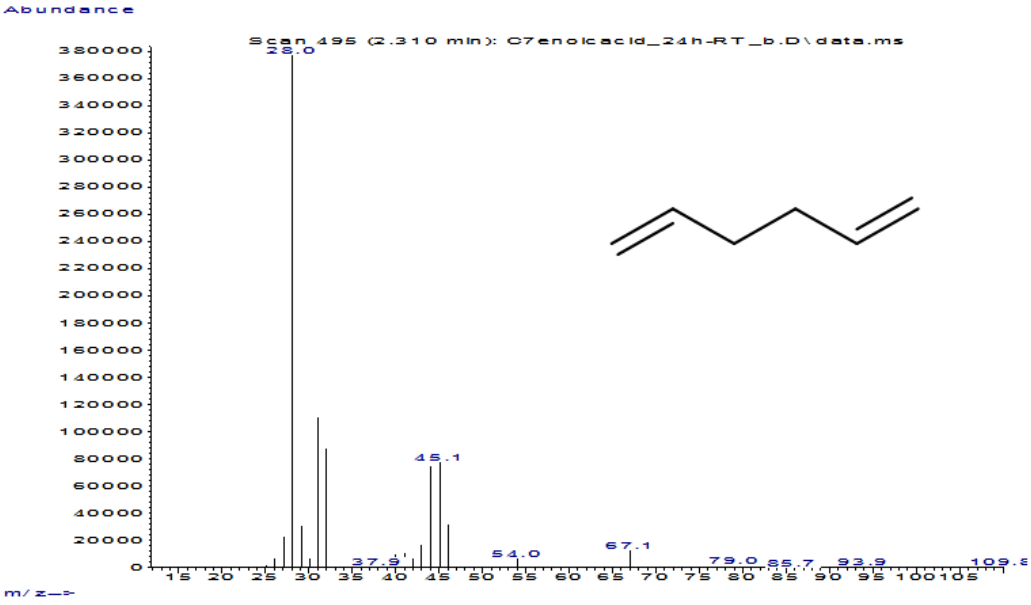

Figure S145. GC-MS spectra of **9c** (82.08 g mol^{-1}) obtained by conversion of **9b** (10 mM) with the OleT-CamAB-FDH system (corresponds to peak a in Figure S144 A).

7.3 Conversion of 10a and 10b with the OleT-CamAB-FDH system

7.3.1 Conversion of 10a

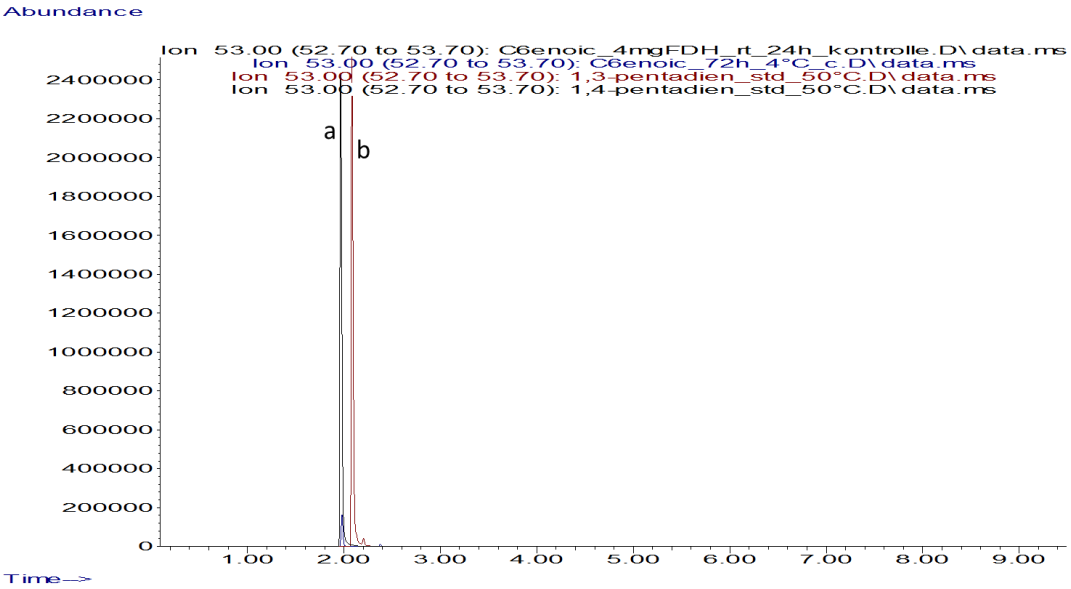

Figure S146. Separation of *trans*-1,3 and 1,4-pentadiene (signals from extracted ion *m*/z = 53 are shown). **Black lane =** injection of analytical standard of **10c** (**a** = 1,4-pentadiene, 1.97 min); **Red lane** = injection of analytical standard of *trans*-1,3-pentadiene (**b**, 2.12 min). **Blue lane** = conversion of **10b** with the OleT-CamAB-FDH system.

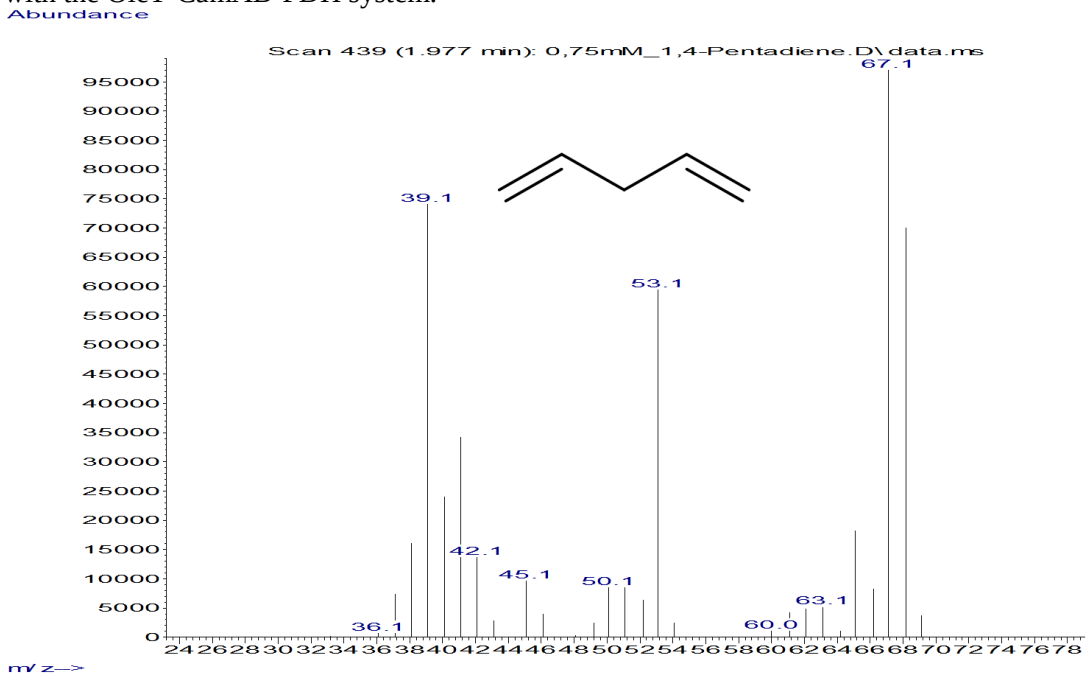

Figure S147. GC-MS spectra of a commercial standard of **10c** (68.06 g mol^{-1}).

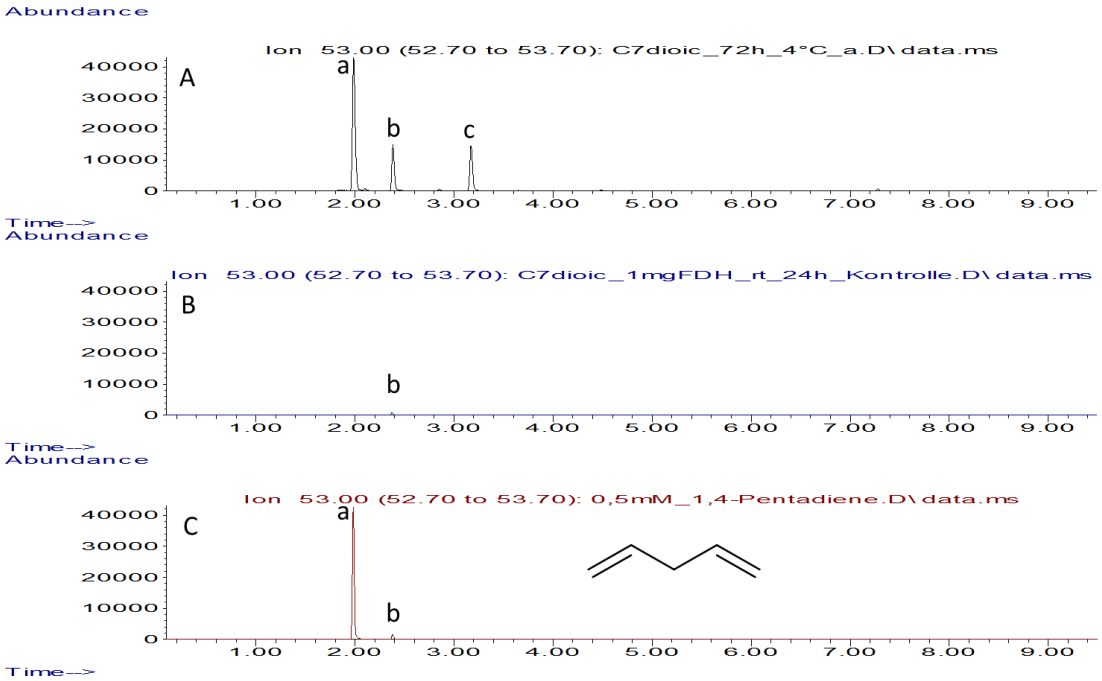

Figure S148. Headspace GC-MS chromatograms obtained by conversion of **10a** (10 mM) (signals from extracted ion *m*/z = 53 are shown). **A** = Conversion of **10a** with the OleT-CamAB-FDH system. **B** = Conversion of **10a** in the absence of OleT (negative control). **C** = Commercial standard of **10c**. **a** = **10c**; **b** = 2-butanone (present in all conversions; industrial supplement for denaturation of EtOH); **c** = 1-heptene. 5 % (v/v) EtOH was used as co-solvent.

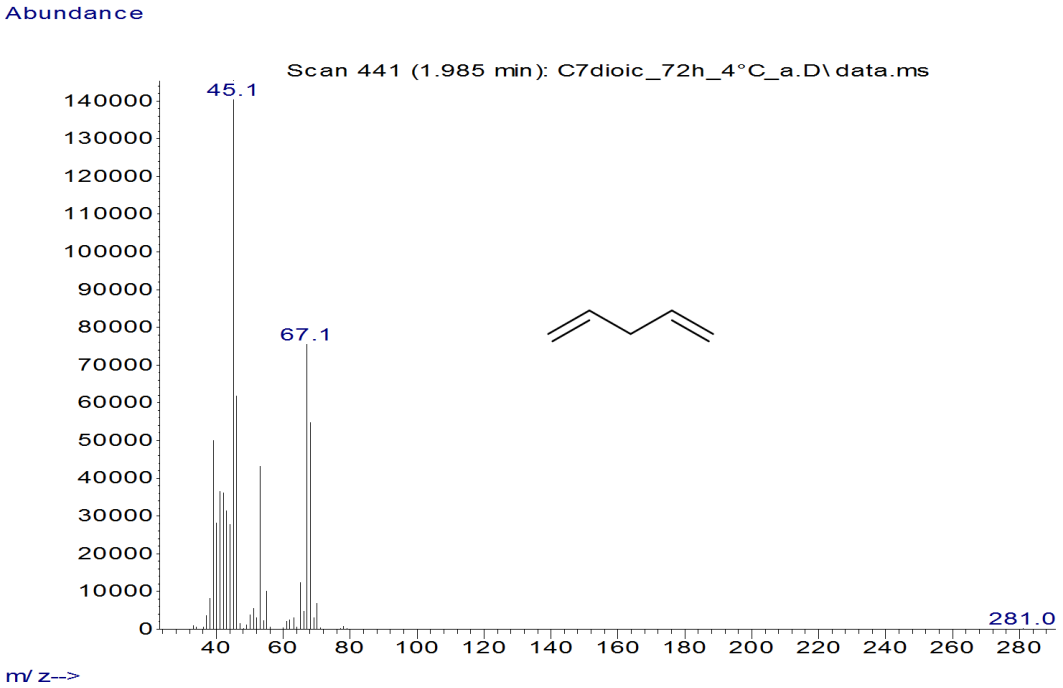

Figure S149. GC-MS spectra of **10c** (110.11 g mol^{-1}) obtained by conversion of **10a** (10 mM) with the OleT-CamAB-FDH system (corresponds to peak a in Figure S149A).

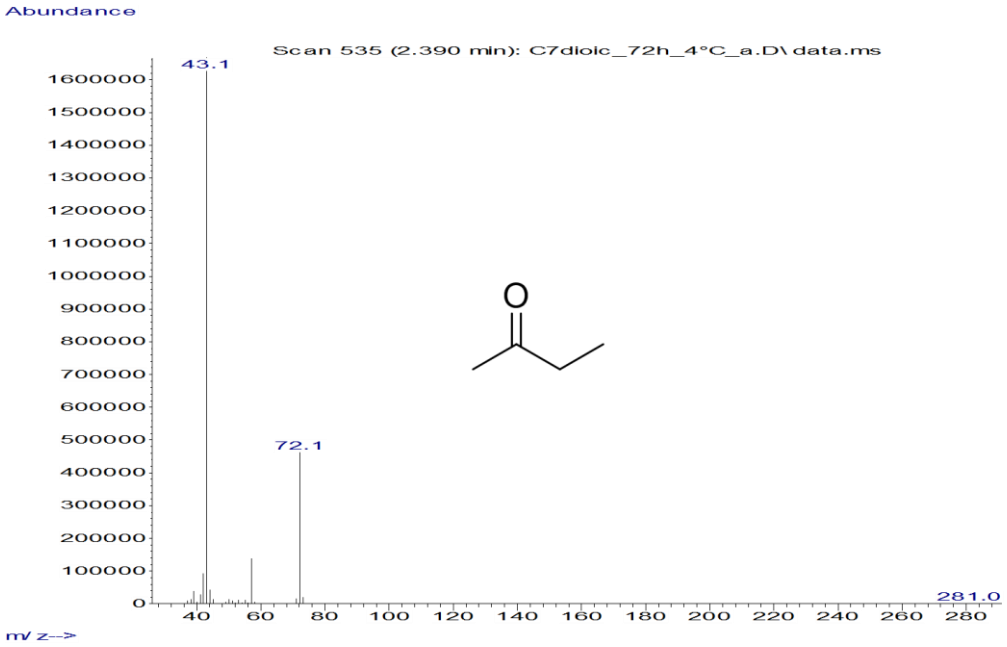

Figure S150. GC-MS spectra of 2-butanone (*m*/z = 72.06). The compound was present in all control reactions (derived from denaturation of EtOH (cosolvent)).

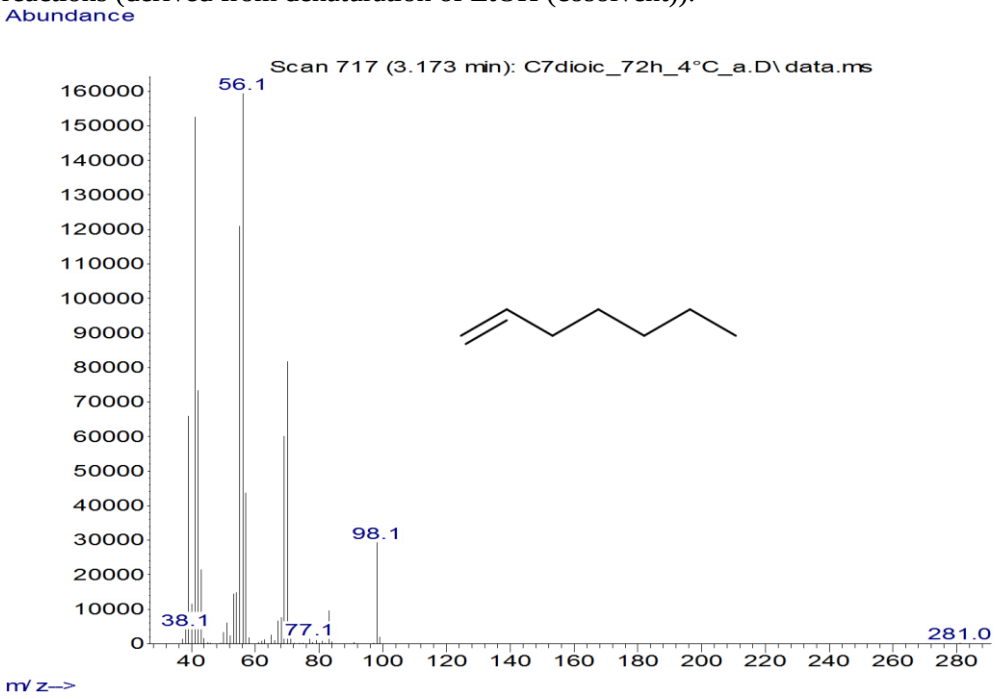

Figure S151. GC-MS spectra of 1-heptene detected after conversion of **10a** (98.11 g mol^{-1}; corresponds to peak c in Figure S149 A; GC-MS score 98 %). The compound was not present in any of the control reactions. Very likely the substrate contains octanoic acid (C8:0) in traces (substrate purity was 98 %).

7.3.2 **Conversion of 10b**

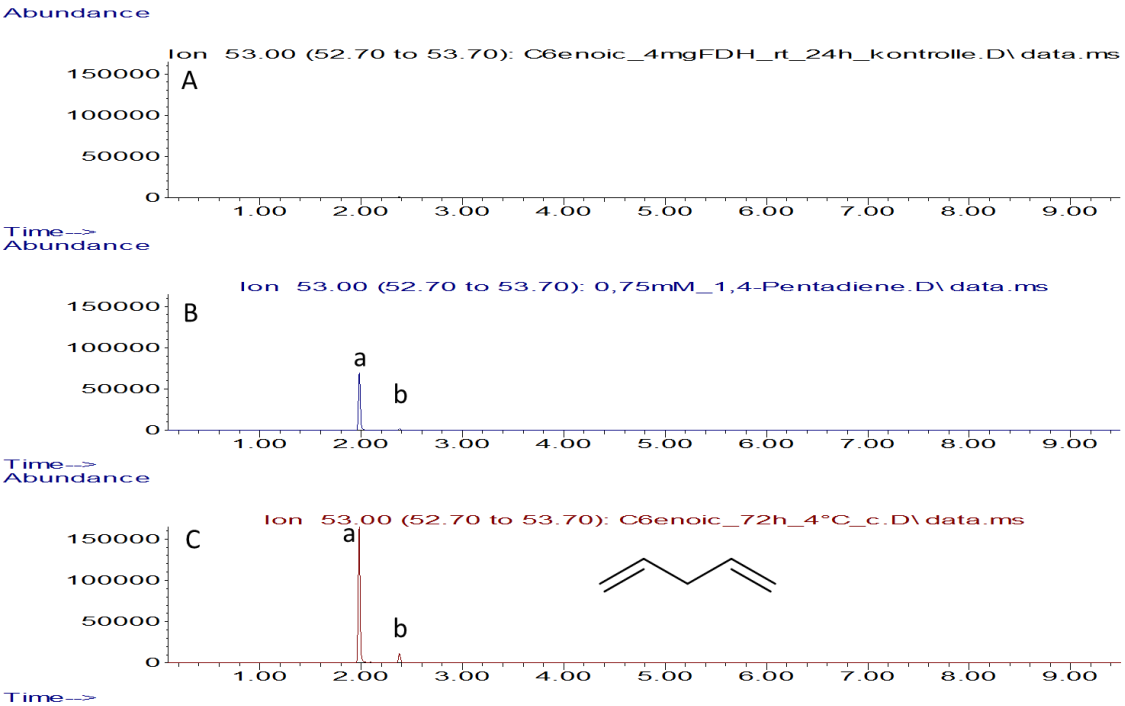

Figure S152. Headspace GC-MS chromatograms obtained by conversion of **10b** (10 mM) (signals from extracted ion *m*/z = 53 are shown). **A** = Conversion of **10b** in the absence of OleT (negative control). **B** = Commercial standard of **10c**. **C** = Conversion of **10b** with the OleT-CamAB-FDH system. **a** = **10c**; b = 2-butanone; 5 % (v/v) EtOH was used as co-solvent.

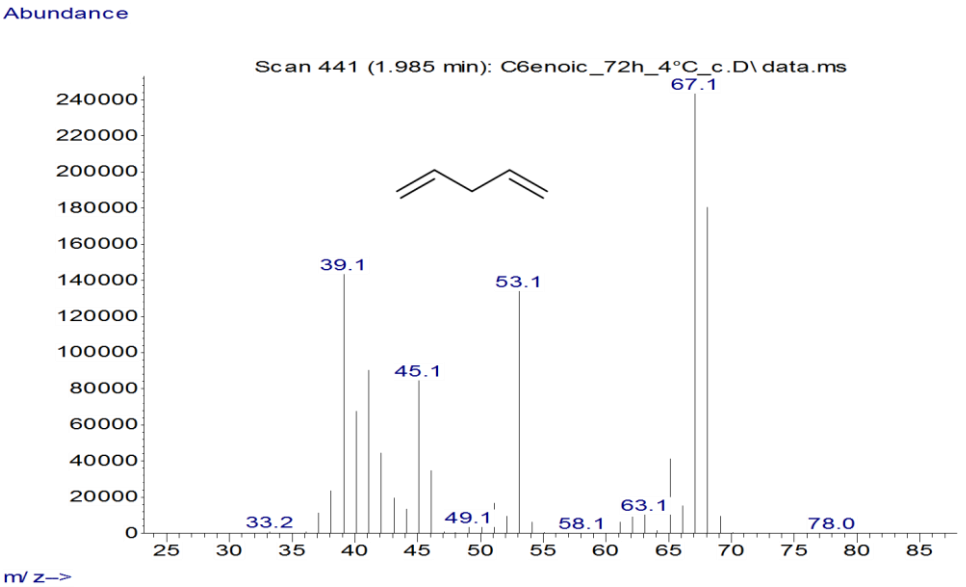

Figure S153. GC-MS spectra of **10c** (68.06 g mol^{-1}) obtained by conversion of **10b** (10 mM) with the OleT-CamAB-FDH system (corresponds to peak a in Figure S153 C).

7.3.3 **Conversion of 11b**

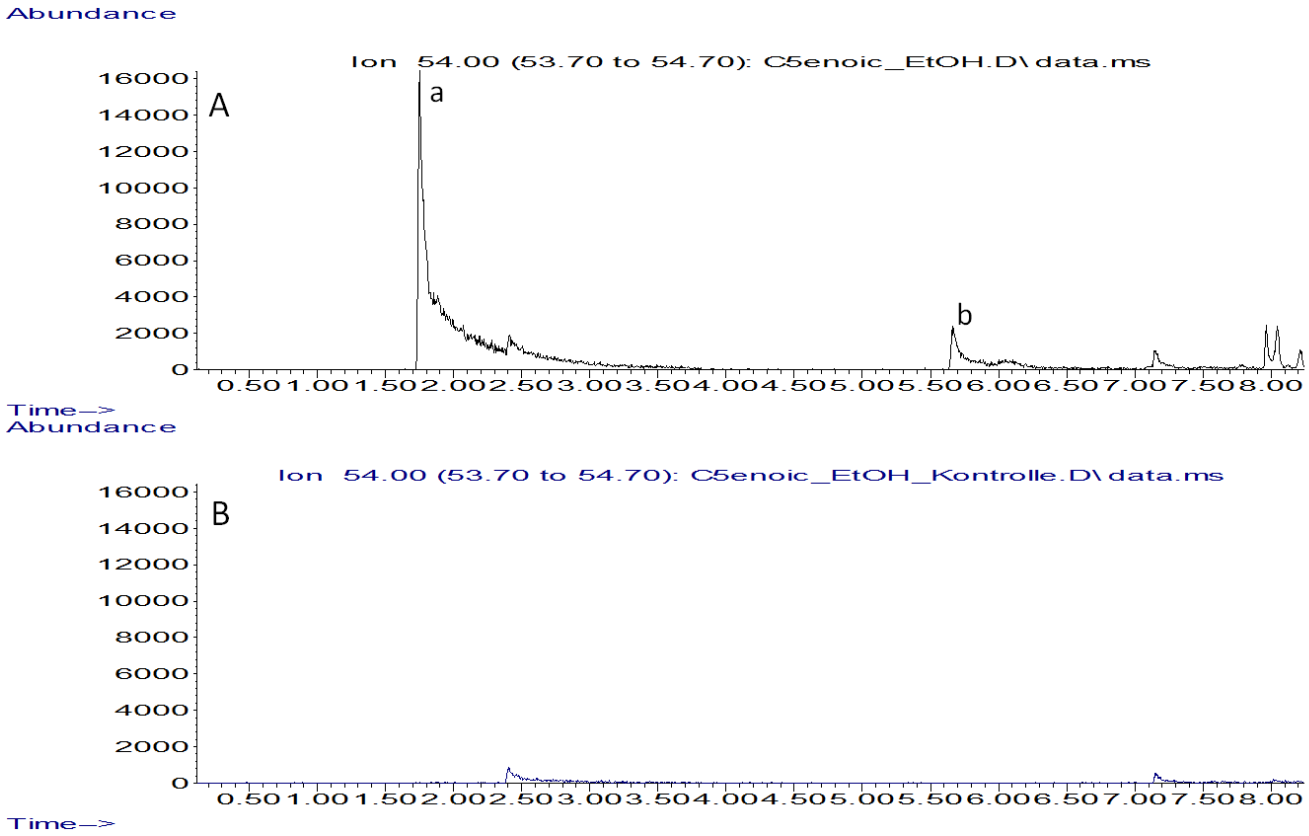

Figure S154. Headspace GC-MS analysis by conversion of **11b** (10 mM). **A** = Conversion of **11b** with the OleT-CamAB-FDH system. **B** = Conversion of **11b** in the absence of OleT (negative control). **a** = **11c**. b = unidentified side product, 5 % (v/v) EtOH was used as co-solvent. The signal of extracted ion *m*/z = 54 is shown.

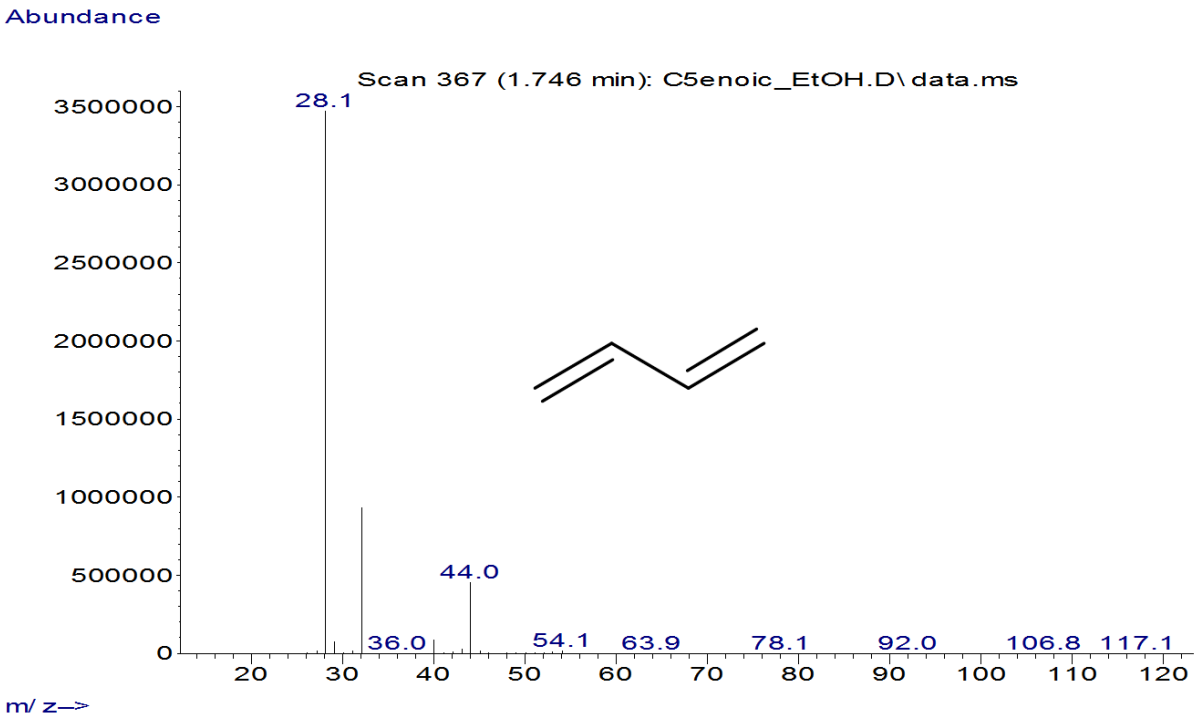

Figure S155. GC-MS spectra of **11c** (54.00 g mol^{-1}) obtained by conversion of **11b** (10 mM) with the OleT-CamAB-FDH system (corresponds to peak a in 0 A).

7.4 Conversion of branched fatty acids (12a -16a) with OleT-CamAB-FDH cascade

7.4.1 Conversion of 12a

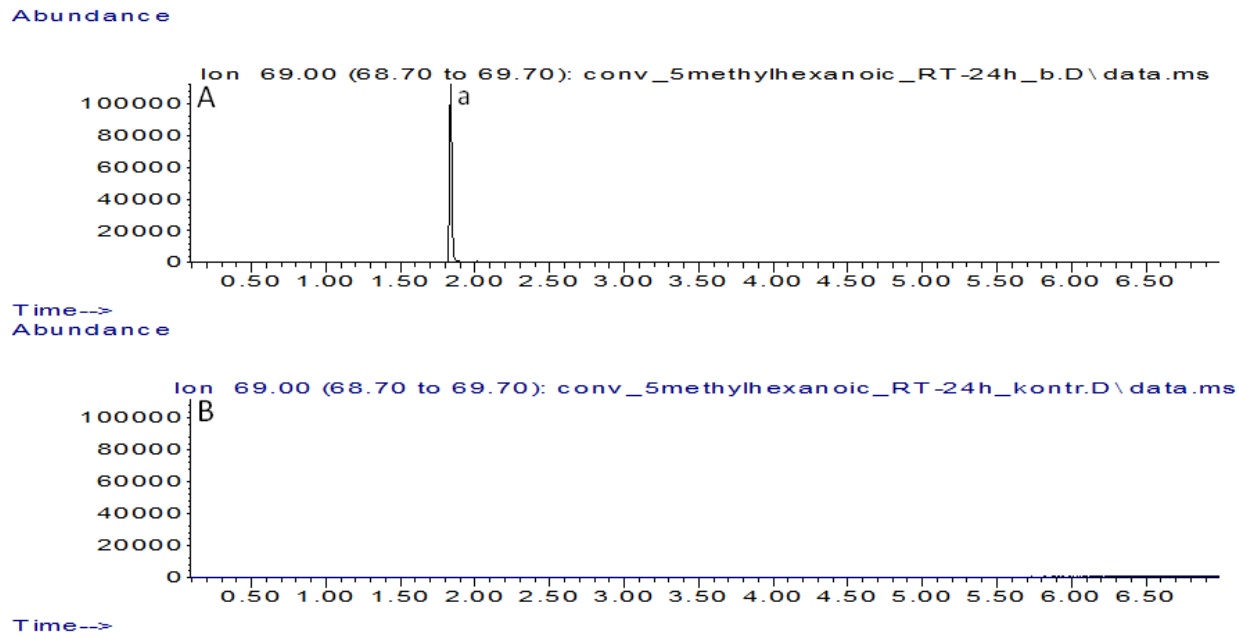

Figure S156. Headspace GC-MS analysis by conversion of **12a** (10 mM). **A** = Conversion of **12a** with the OleT-CamAB-FDH system. **B** = Conversion of **12a** in the absence of OleT (negative control). **a** = **11c**. 5 % (v/v) EtOH was used as co-solvent. The signal of extracted ion *m*/z = 69 is shown.

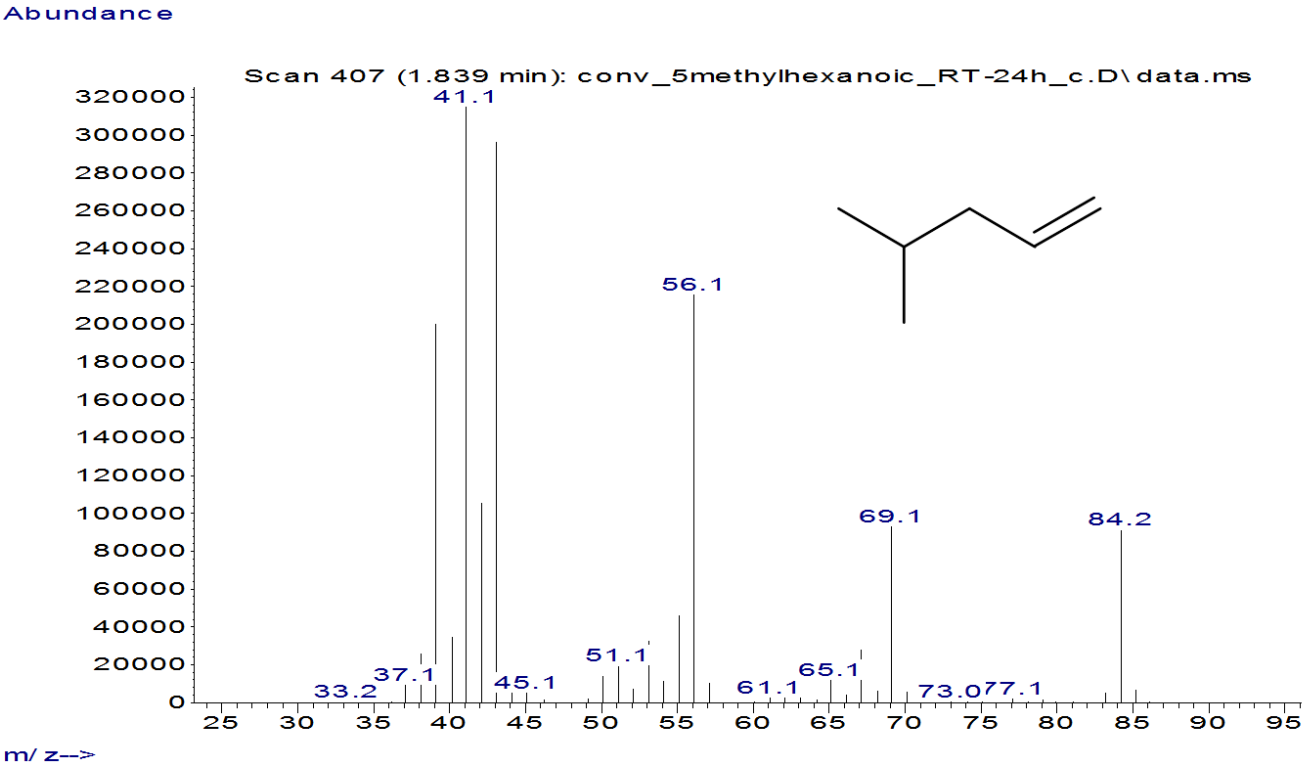

Figure S157. GC-MS spectra of **12c** (84.16 g mol^{-1}) obtained by conversion of **12a** (10 mM) with the OleT-CamAB-FDH system (corresponds to peak a in Figure S156 A).

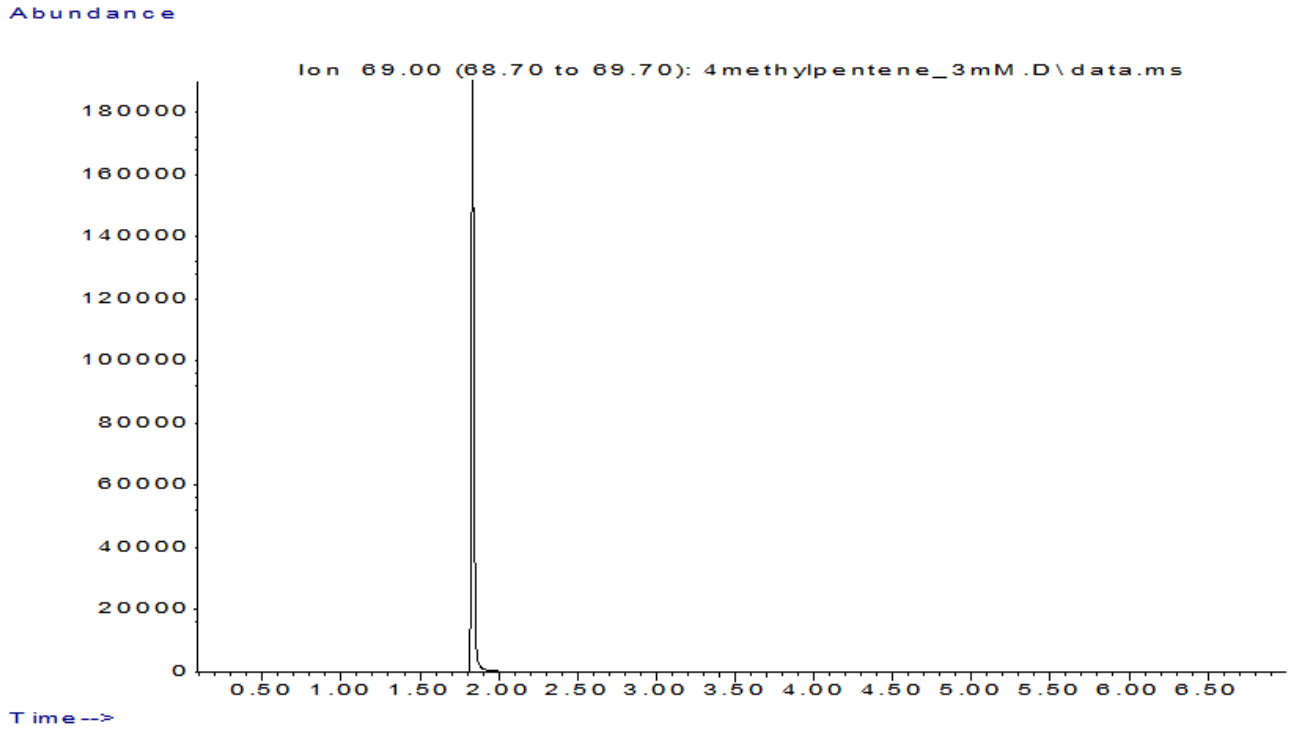

Figure S158. Headspace GC-MS analysis of a commercial standard of **12c**. The signal of extracted ion *m*/z = 69 is shown.

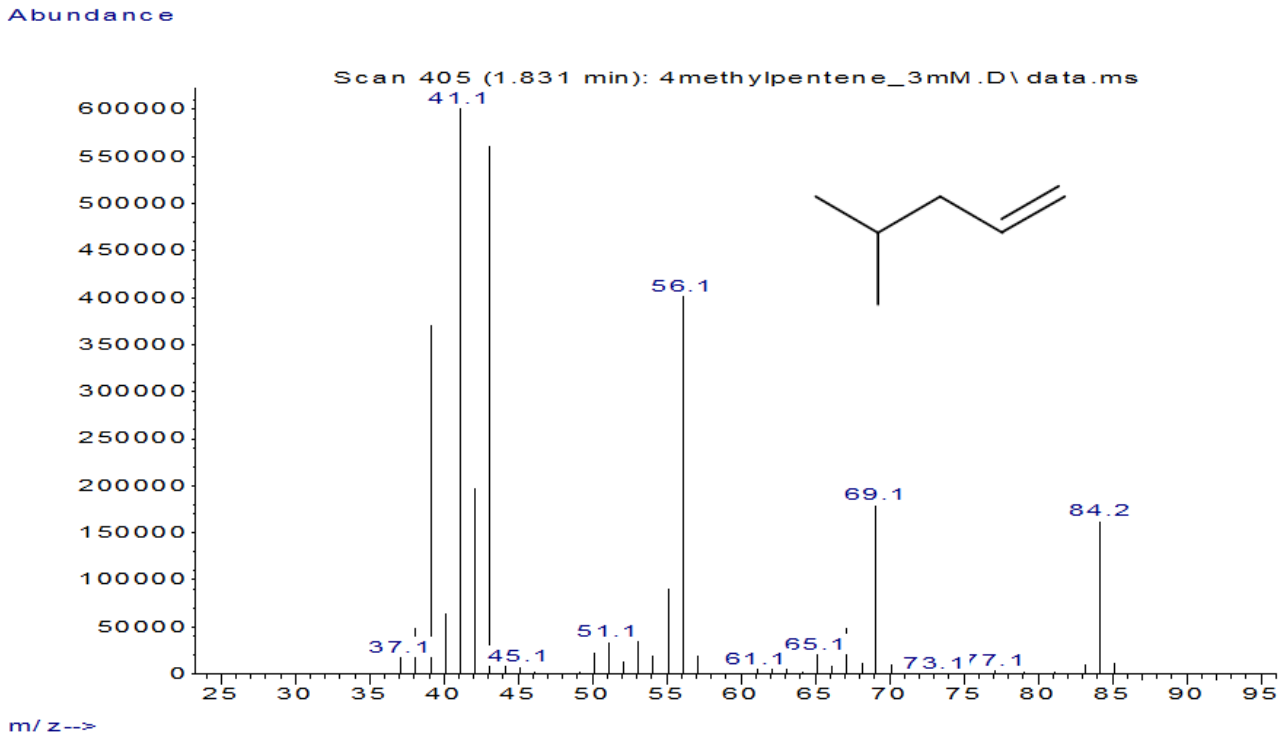

Figure S159. GC-MS spectra of a commercial standard of **12c** (84.16 g mol^{-1}).

7.4.2 **Conversion of 13a**

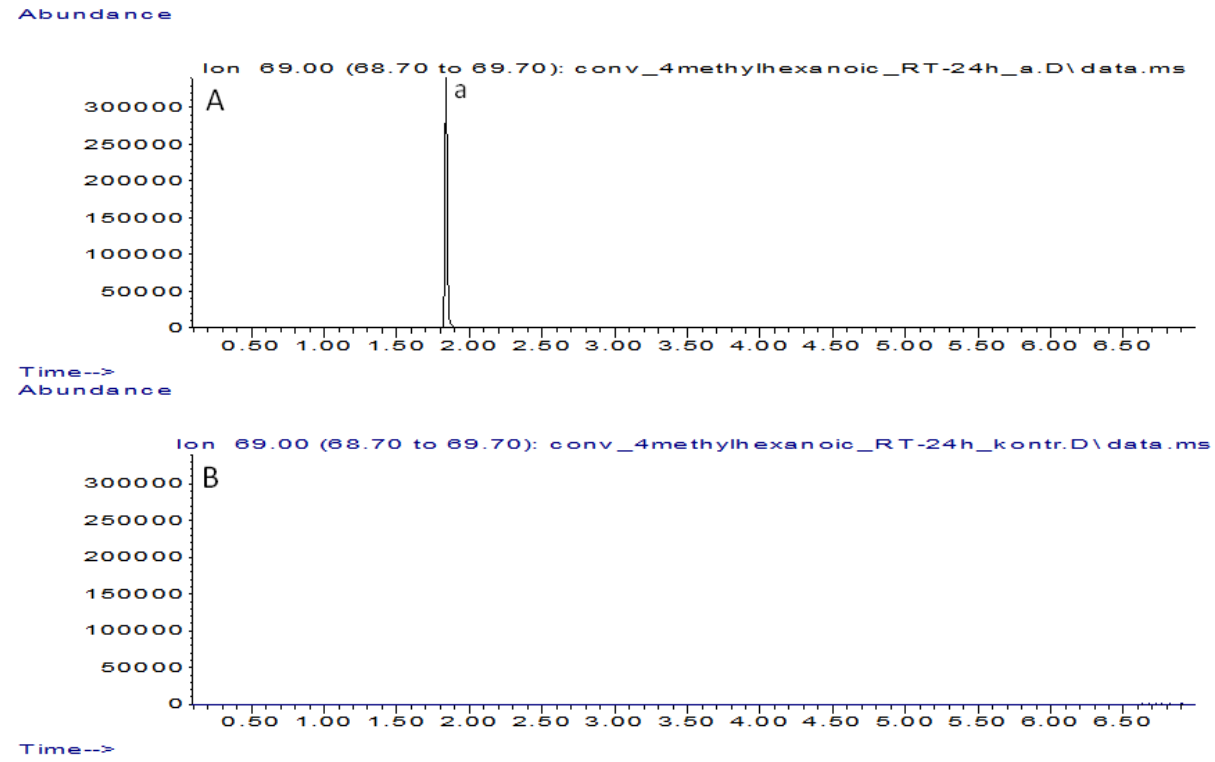

Figure S160. Headspace GC-MS analysis by conversion of **13a** (10 mM). **A** = Conversion of **13a** with the OleT-CamAB-FDH system. **B** = Conversion of **13a** in the absence of OleT (negative control). **a** = **13c**. 5 % (v/v) EtOH was used as co-solvent. The signal of extracted ion *m*/z = 69 is shown.

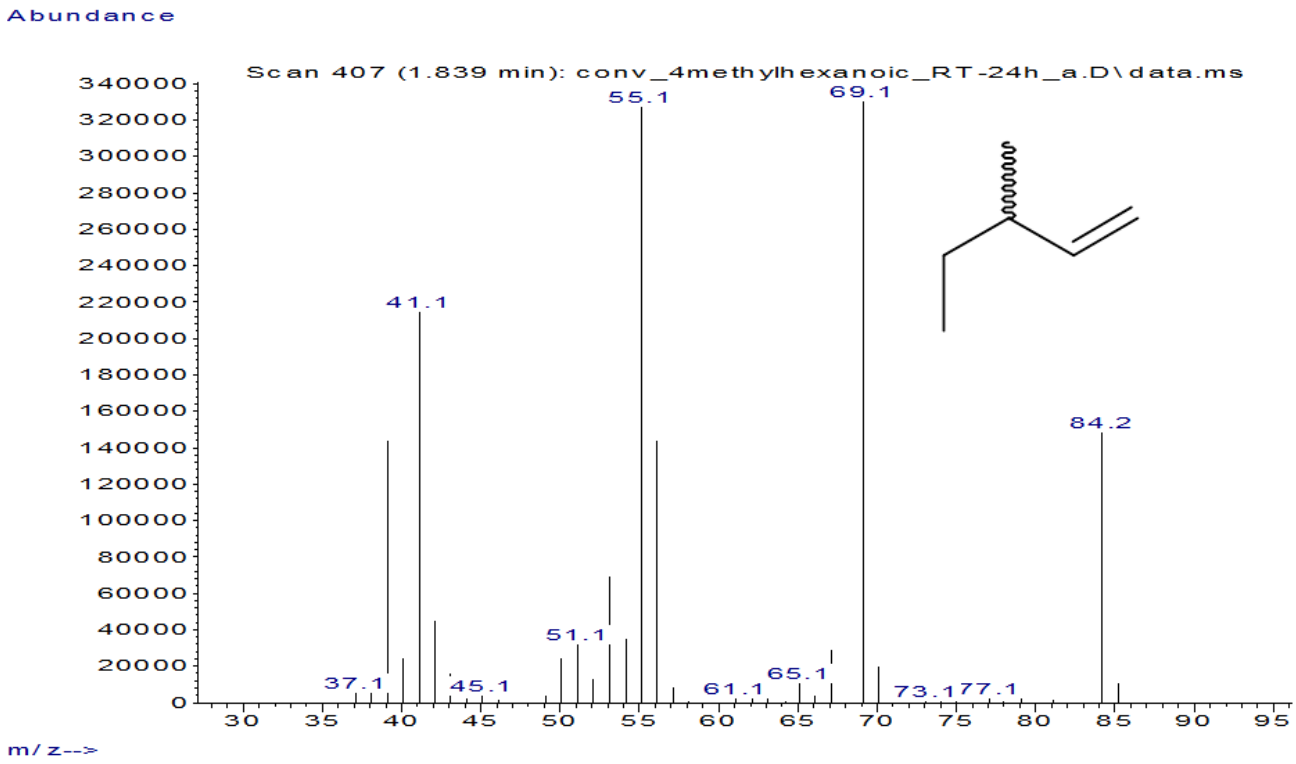

Figure S161. GC-MS spectra of **13c** (84.16 g mol^{-1}) obtained by conversion of **13a** (10 mM) with the OleT-CamAB-FDH system (corresponds to peak a in Figure S160 A).

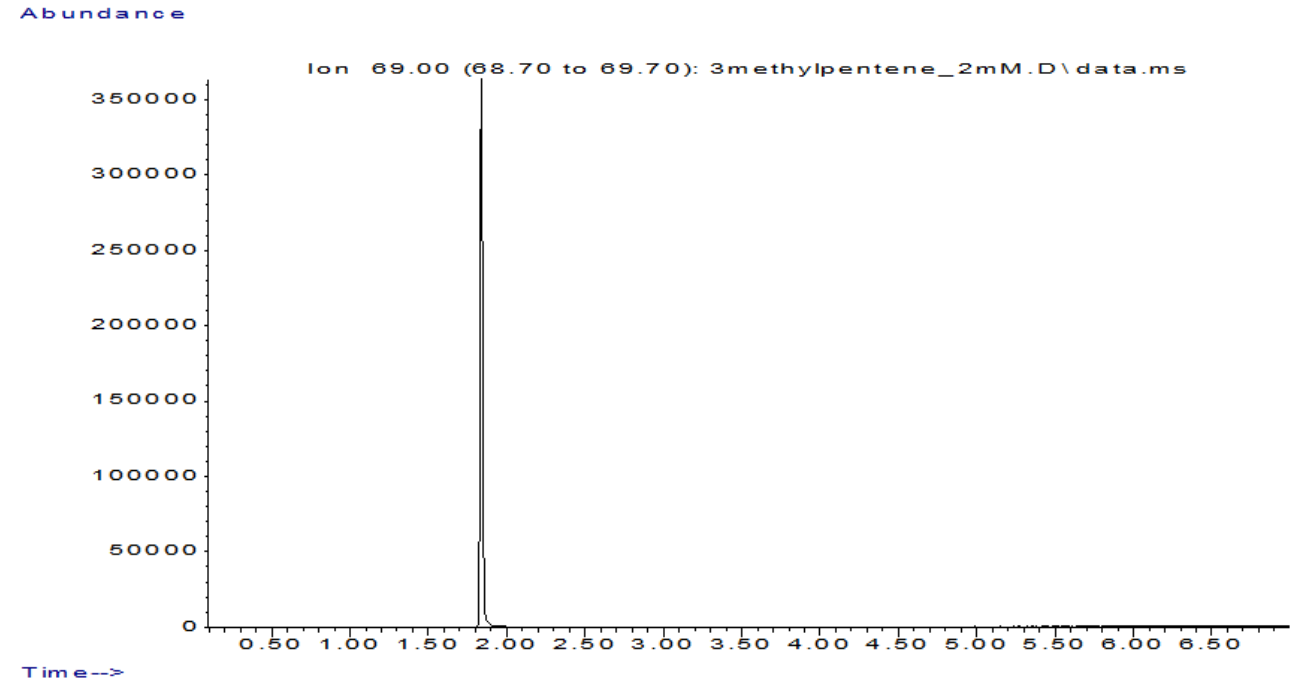

Figure S162. Headspace GC-MS analysis of a commercial standard of **13c**. The signal of extracted ion *m*/z = 69 is shown.

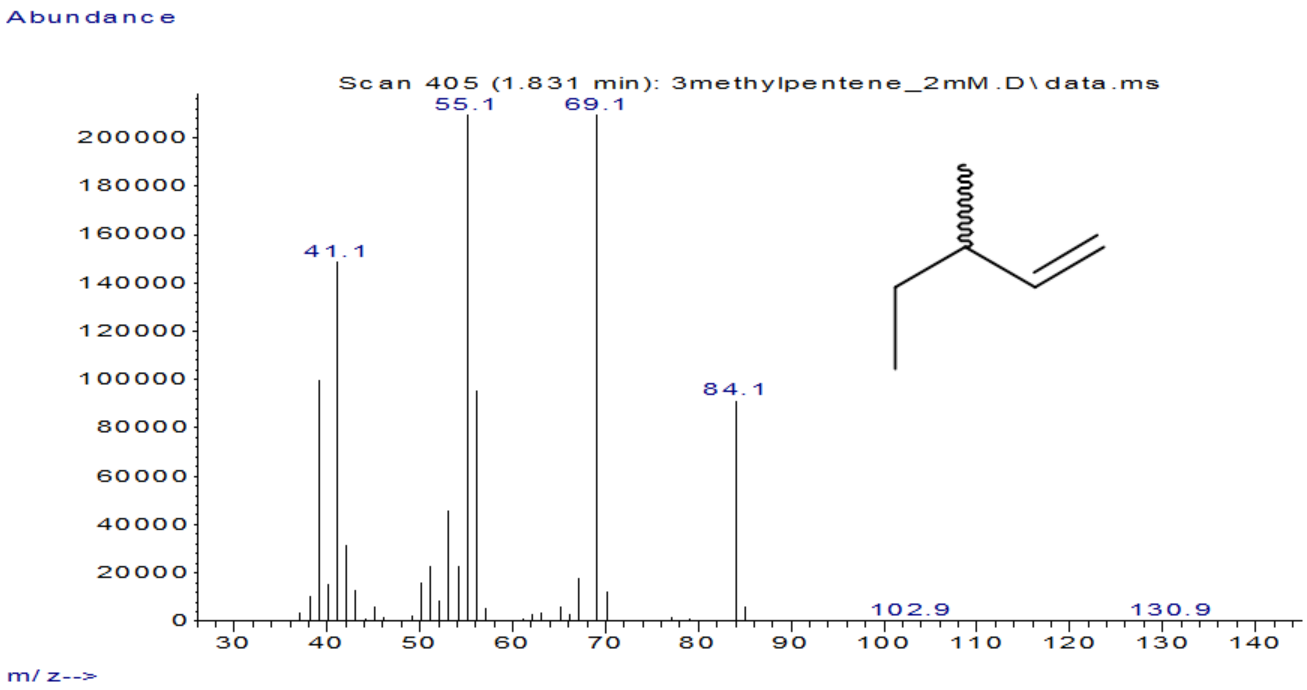

Figure S163. GC-MS spectra of a commercial standard of **13c** (84.16 g mol^{-1}).

7.4.3 **Conversion of 14a**

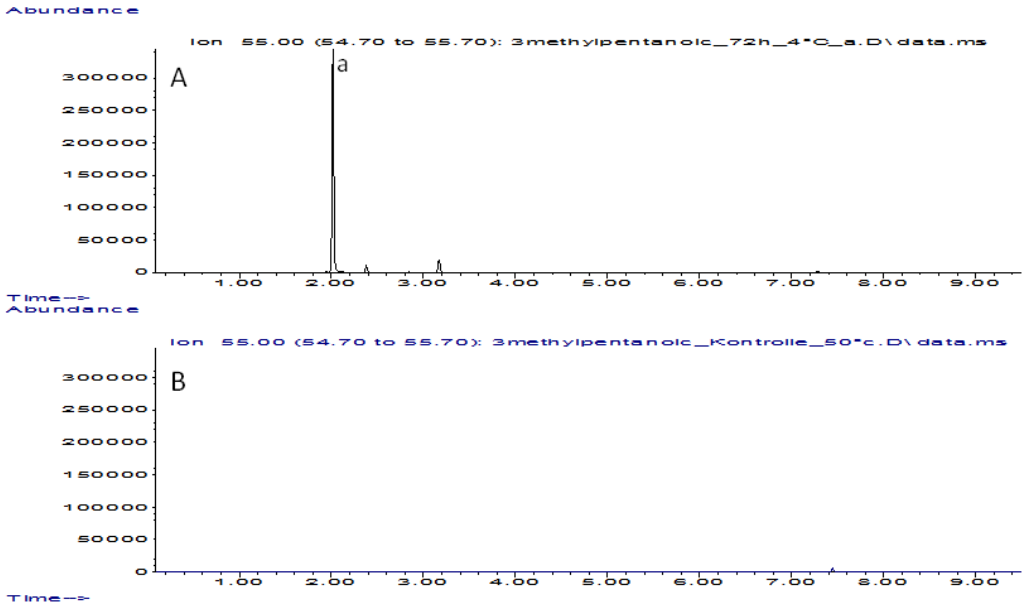

Figure S164. Headspace GC-MS analysis by conversion of **14a** (10 mM). **A** = Conversion of **14a** with the OleT-CamAB-FDH system. **B** = Conversion of **14a** in the absence of OleT (negative control). **a** = **14c**. 5 % (v/v) EtOH was used as co-solvent. The signal of extracted ion *m*/z = 55 is shown.

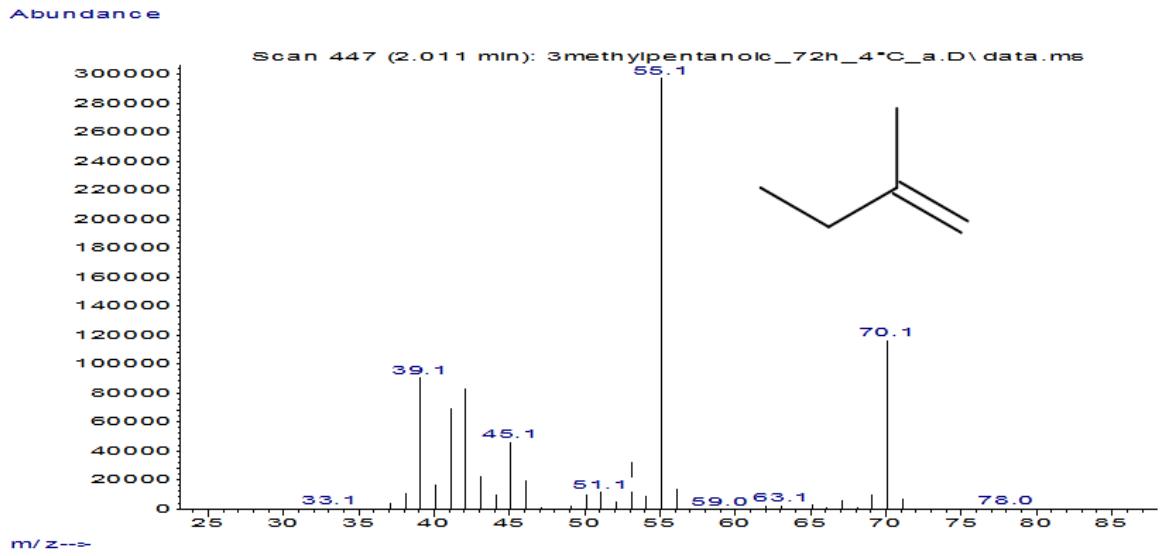

Figure S165. GC-MS spectra of **14c** (70.13 g mol^{-1}) obtained by conversion of **14a** (10 mM) with the OleT-CamAB-FDH system (corresponds to peak a in Figure S164 A).

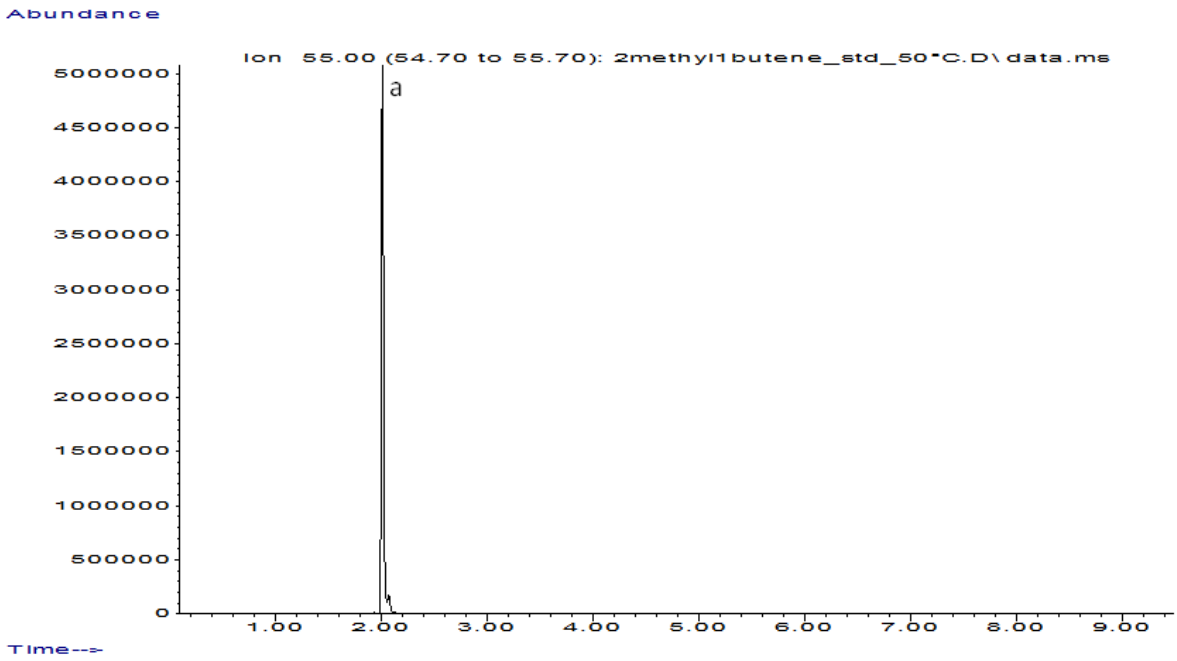

Figure S166. Headspace GC-MS analysis of a commercial standard of **14c**. The signal of extracted ion *m*/z = 55 is shown.

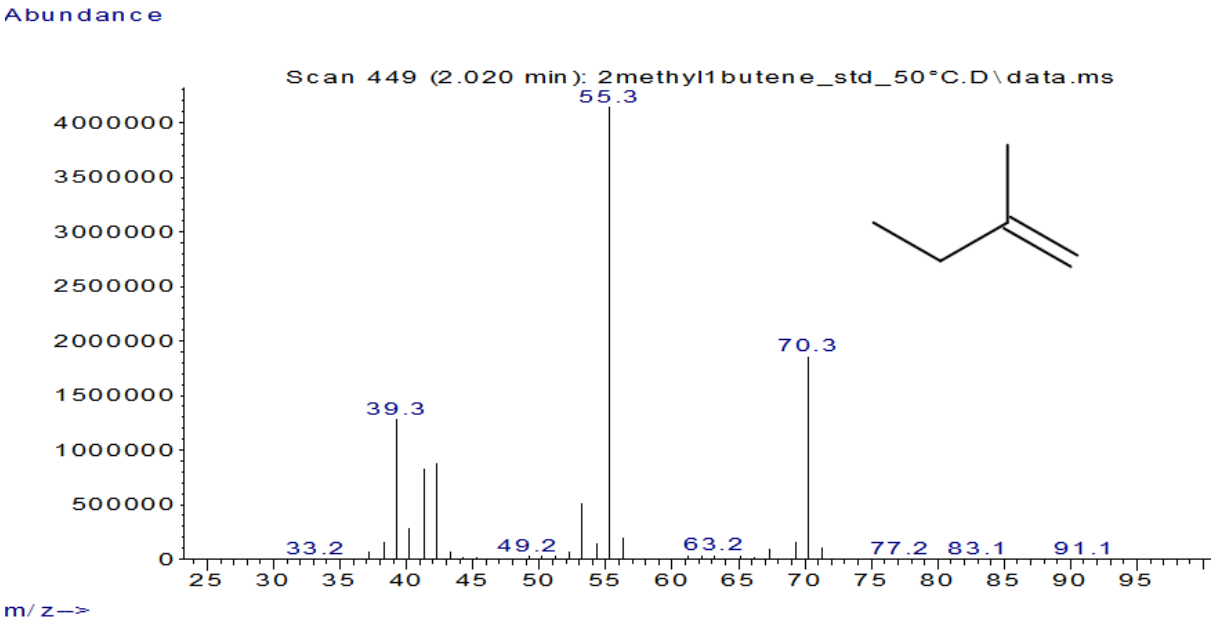

Figure S167. GC-MS spectra of a commercial standard of **14c** (70.13 g mol^{-1}).

7.4.4 Conversion of 15a

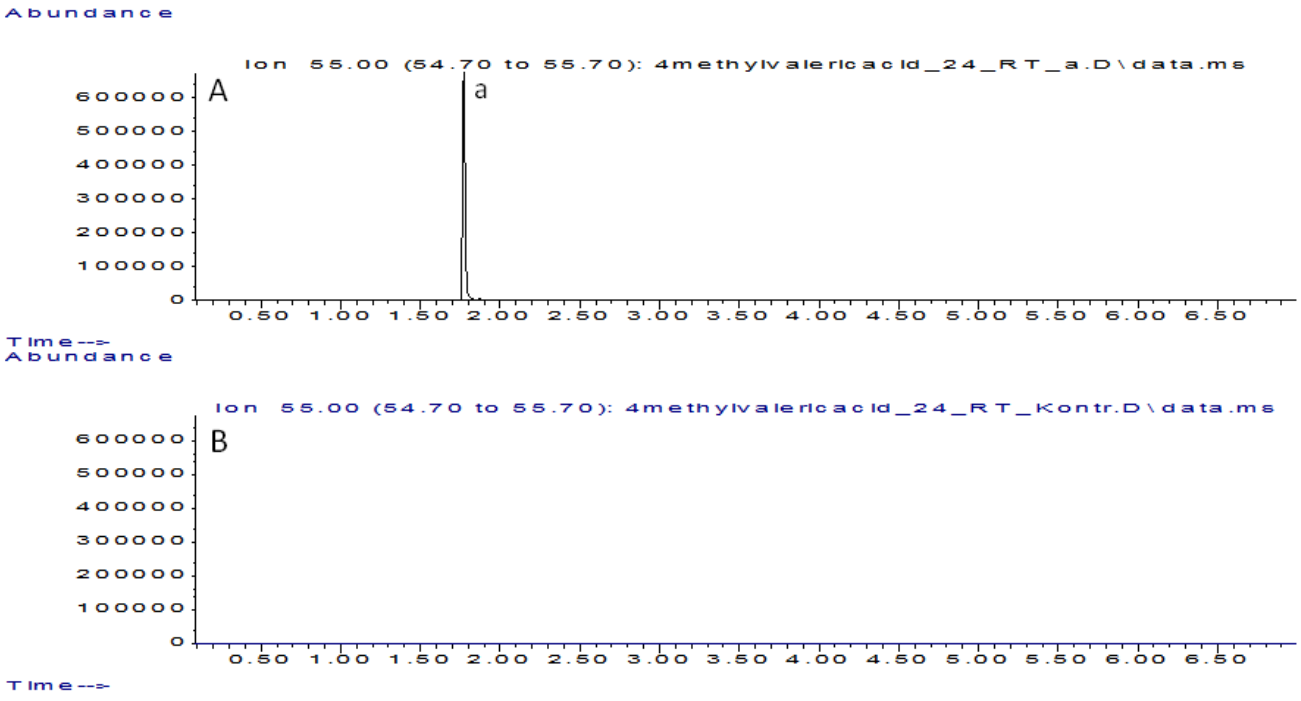

Figure S168. Headspace GC-MS analysis by conversion of **15a** (10 mM). **A** = Conversion of **15a** with the OleT-CamAB-FDH system. **B** = Conversion of **15a** in the absence of OleT (negative control). **a** = **15c**. 5 % (v/v) EtOH was used as co-solvent. The signal of extracted ion *m*/z = 55 is shown.

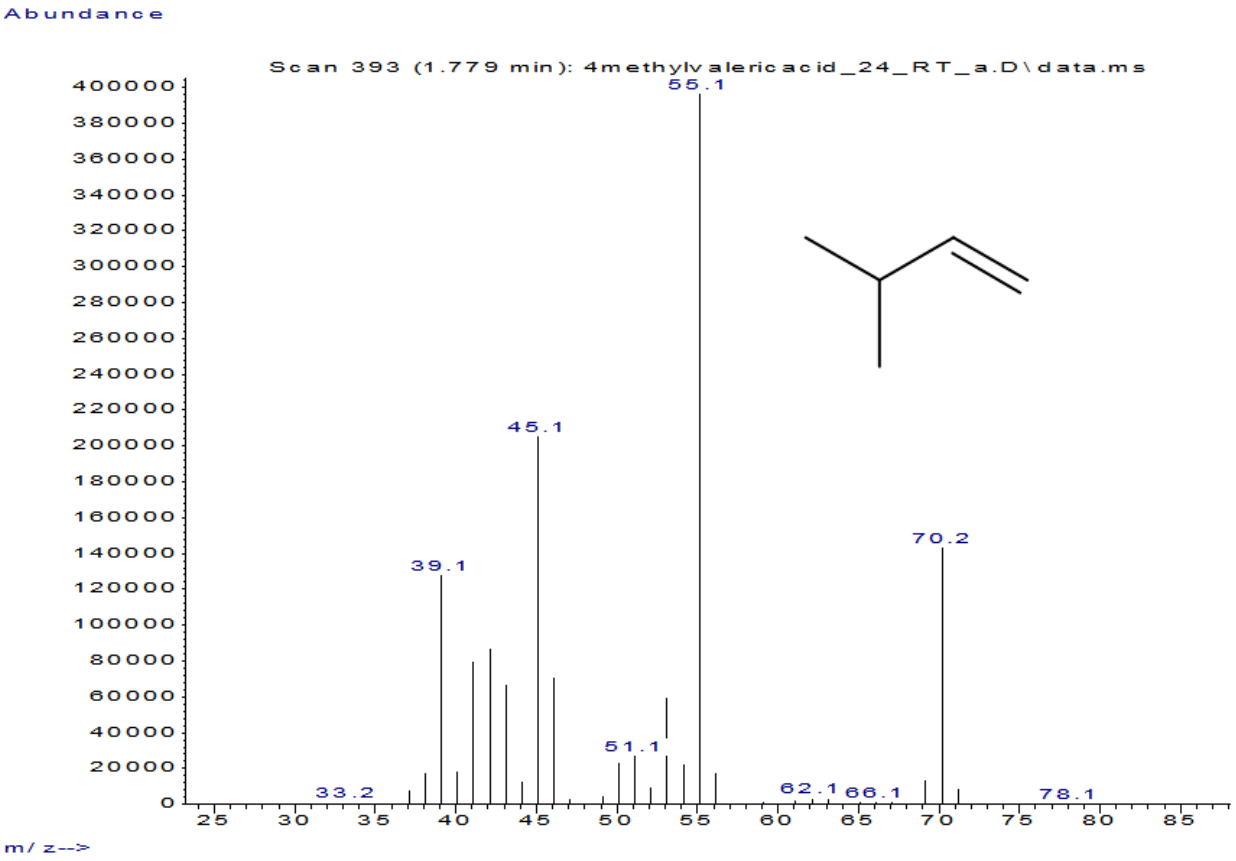

Figure S169. GC-MS spectra of **15c** (70.13 g mol^{-1}) obtained by conversion of **15a** (10 mM) with the OleT-CamAB-FDH system (corresponds to peak a in Figure S168A).

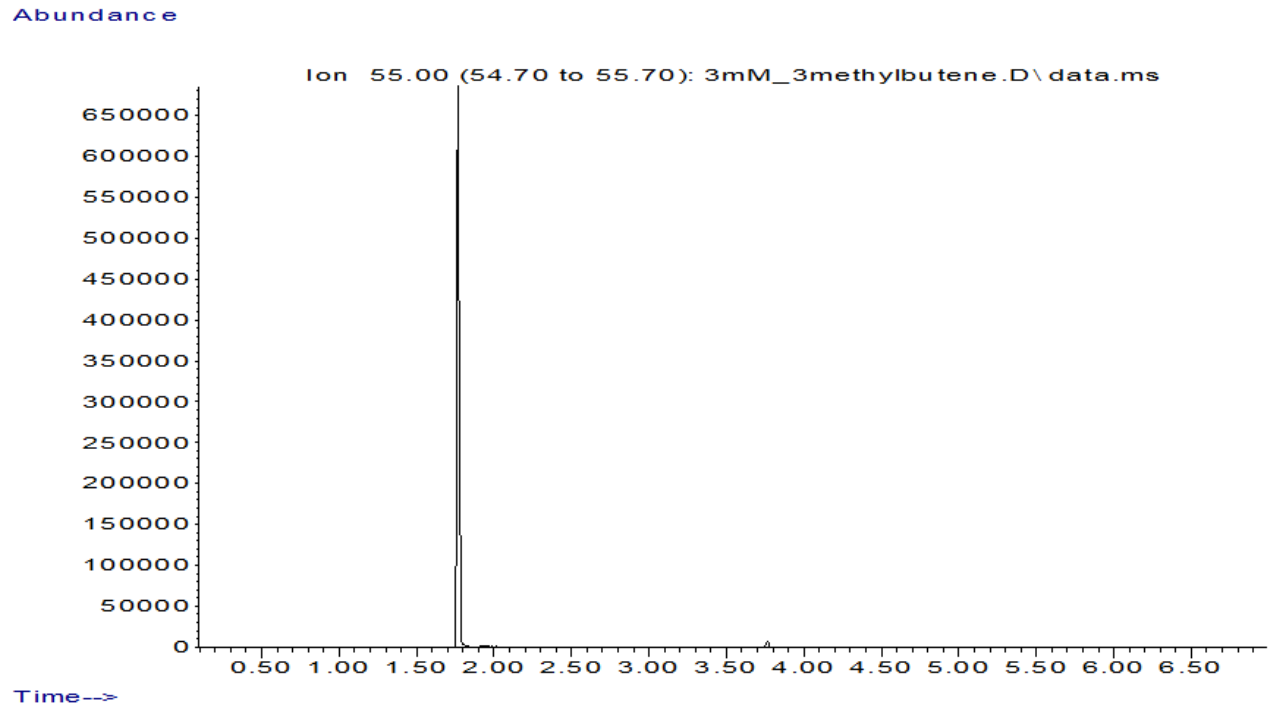

Figure S170. Headspace GC-MS analysis of a commercial standard of **15c**. The signal of extracted ion *m*/z = 55 is shown.

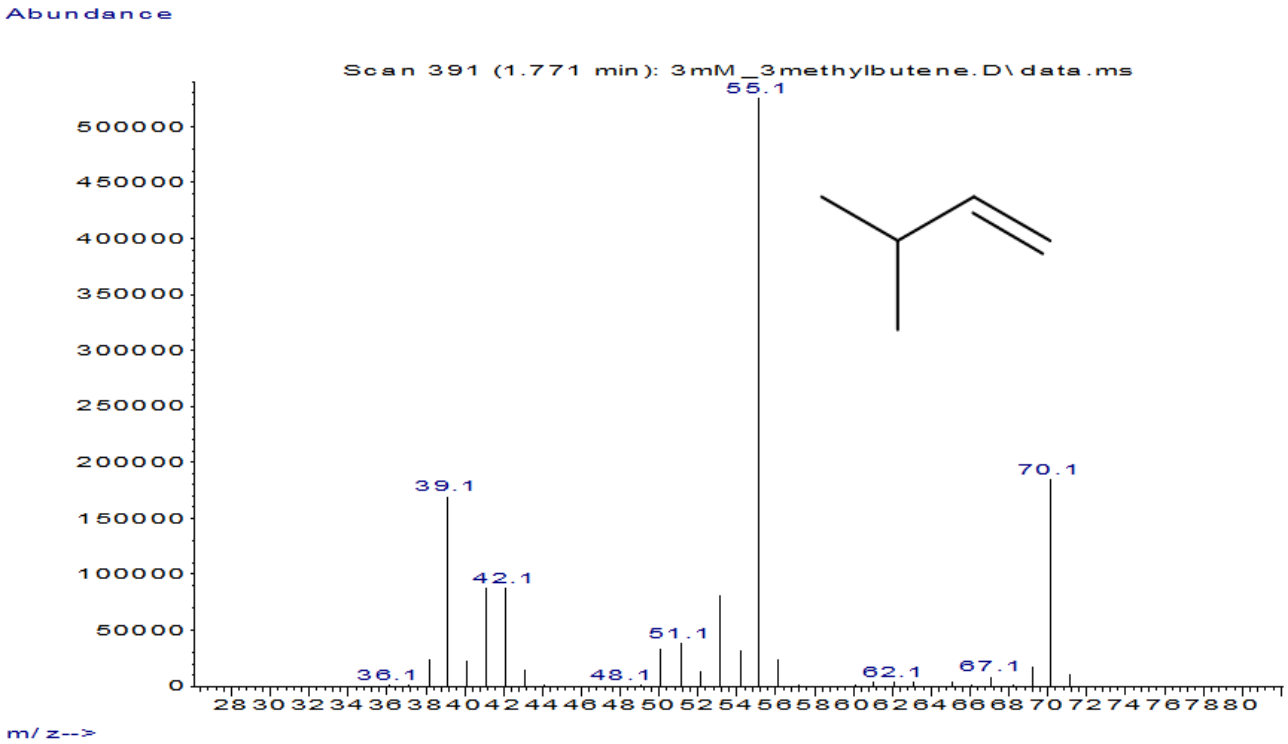

Figure S171. GC-MS spectra of a commercial standard of **14c** (70.13 g mol^{-1}).

7.4.5 **Conversion of isovaleric acid**

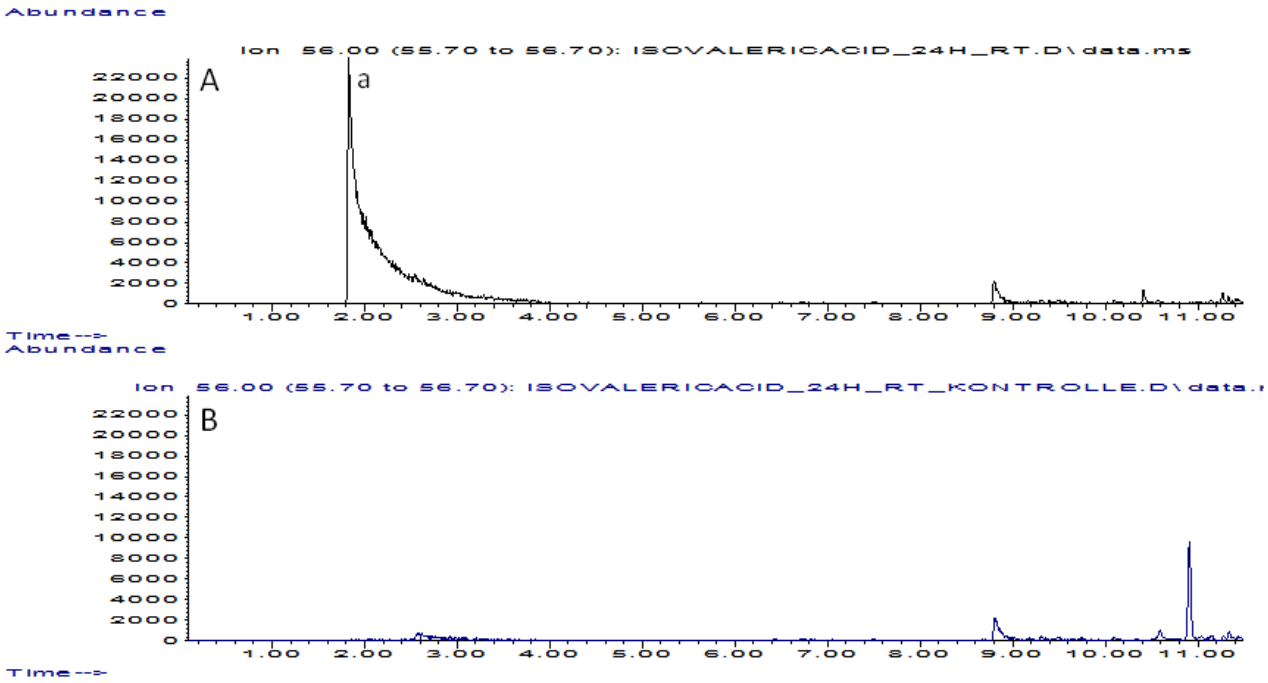

Figure S172. Headspace GC-MS analysis by conversion of isovaleric acid (10 mM). **A** = Conversion of **16a** with the OleT-CamAB-FDH system. **B** = Conversion of isovaleric acid in the absence of OleT (negative control). **a** = isobuten. 5 % (v/v) EtOH was used as co-solvent. The signal of extracted ion *m*/z = 56 is shown.

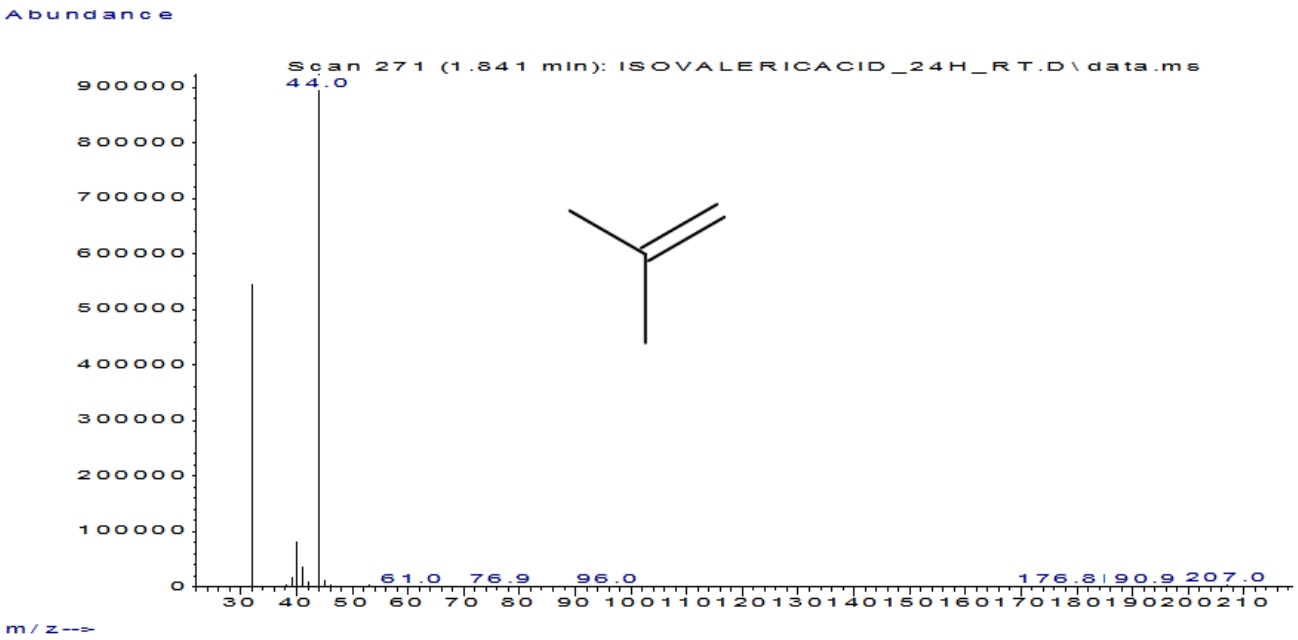

Figure S173. GC-MS spectra of isobutene (56.11 g mol^{-1}) obtained by conversion of isovaleric acid (10 mM) with the OleT-CamAB-FDH system (corresponds to peak a in 0 A)

7.5 In-situ bromination of conversions of branched fatty acids with OleT-CamAB-FDH cascade

7.5.1 Bromination of conversion of 15a

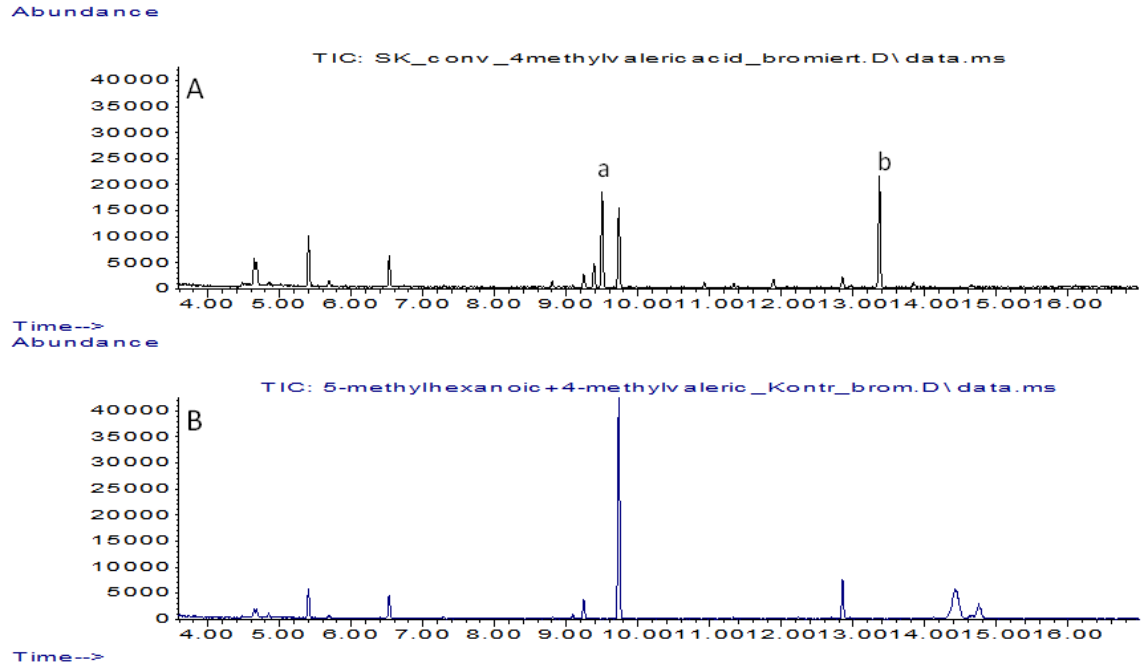

Figure S174. GC-MS chromatograms obtained by conversion of **15a** (10 mM) with in-situ bromination. **A** = Conversion of **15a** with the OleT-CamAB-FDH system. **B** = Conversion of **15a** in the absence of OleT (negative control). **a** = dibrominated derivative of **15c**; **b** = triborminated derivative of **15c**

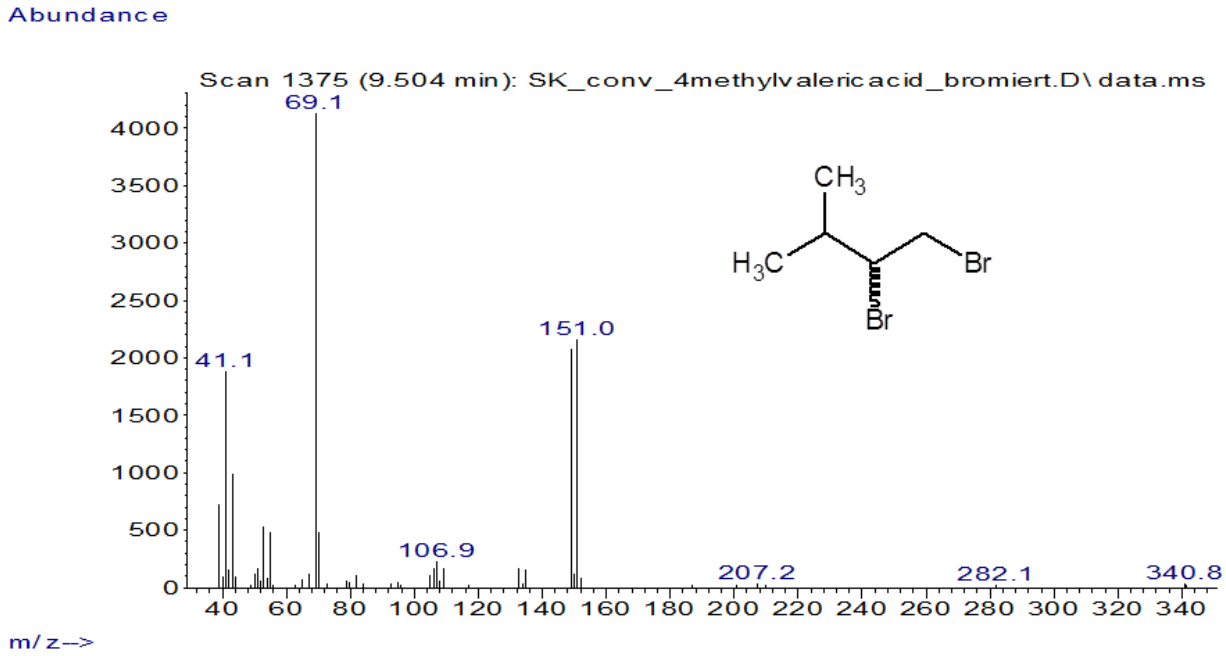

Figure S175. GC-MS spectra of a dibrominated derivative of **15c** (exact position of Br not defined) (229.94 g mol^{-1}) obtained by conversion of **15a** with the OleT-CamAB-FDH system with in-situ bromination (corresponds to peak a in Figure S174 A).

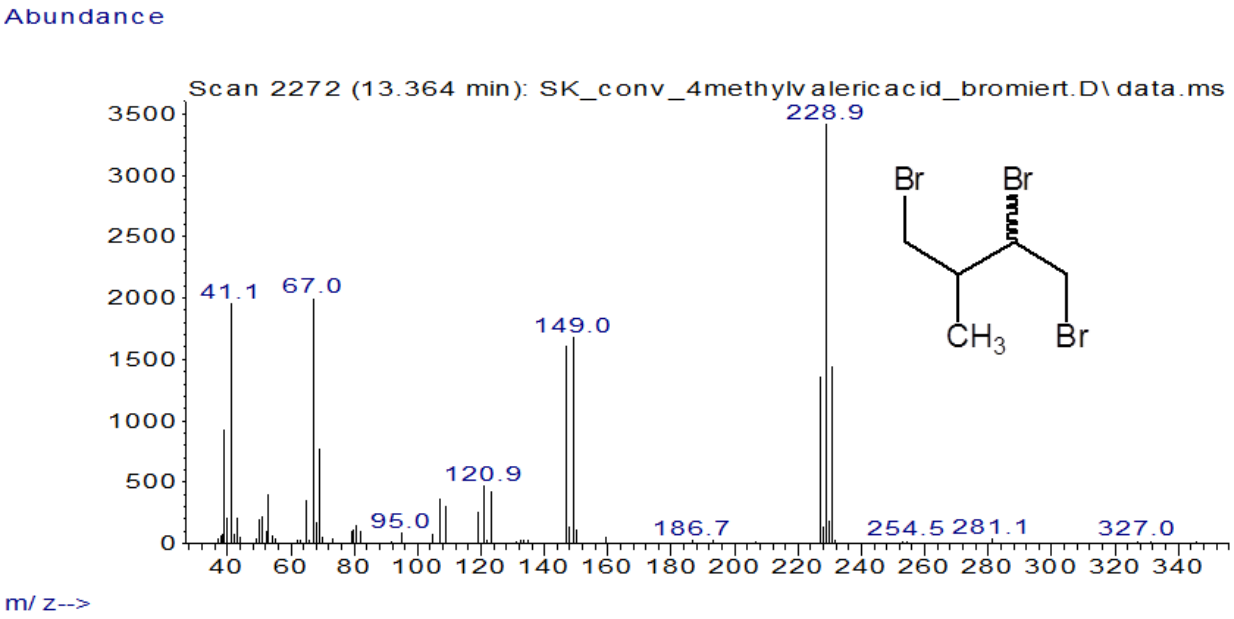

Figure S176. GC-MS spectra of a tribrominated derivative of **15c** (exact position of Br not defined) (308.94 g mol^{-1}) obtained by conversion of **15a** with the OleT-CamAB-FDH system with in-situ bromination (corresponds to peak b in Figure S174 A).

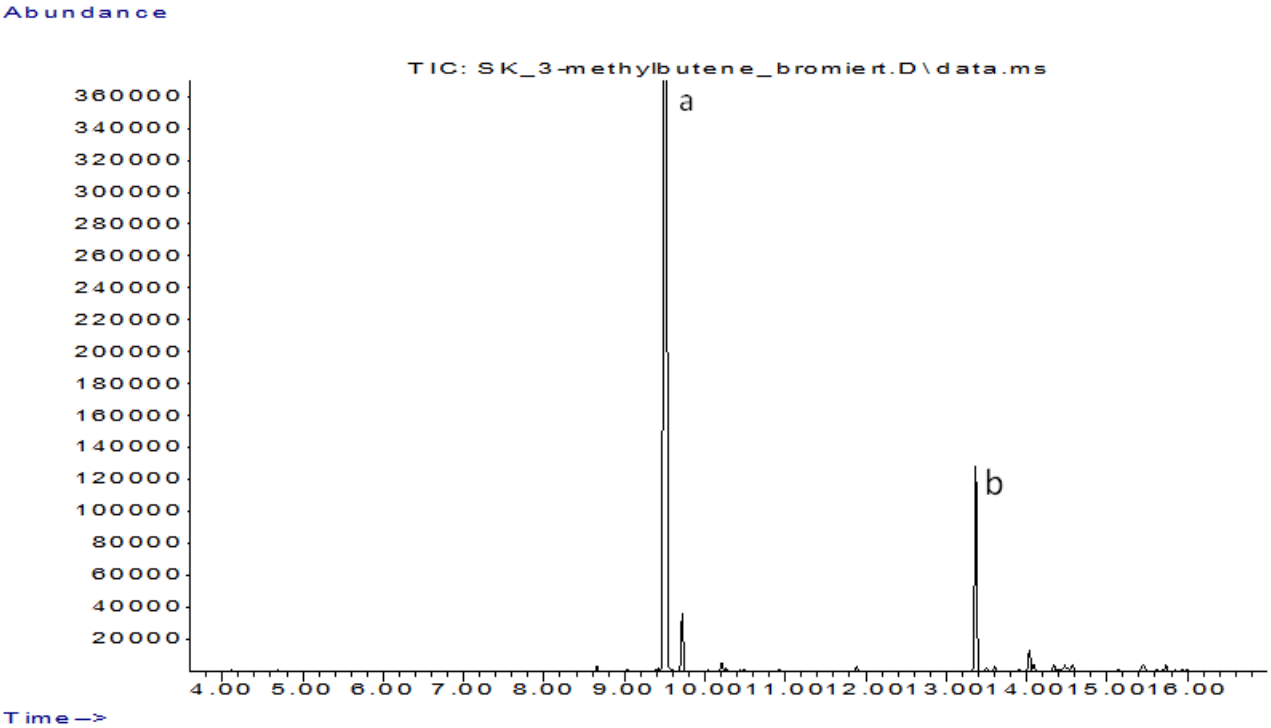

Figure S177. GC-MS chromatogram obtained by bromination of commercial **15c**. **a** = dibrominated derivative of **15c**; **b** = triborminated derivative of **15c**

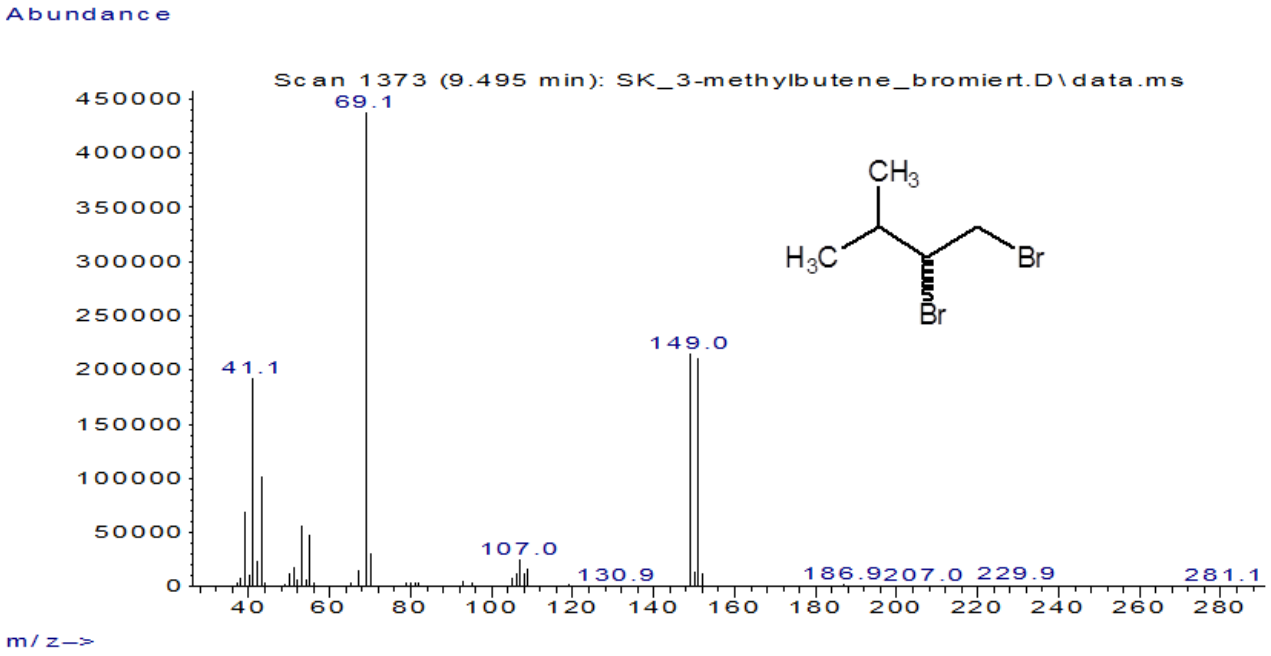

Figure S178. GC-MS spectra of a dibrominated derivative of **15c** (exact position of Br not defined) (229.94 g mol^{-1}) obtained by bromination of commercial **15c** (corresponds to peak a in Figure S177).

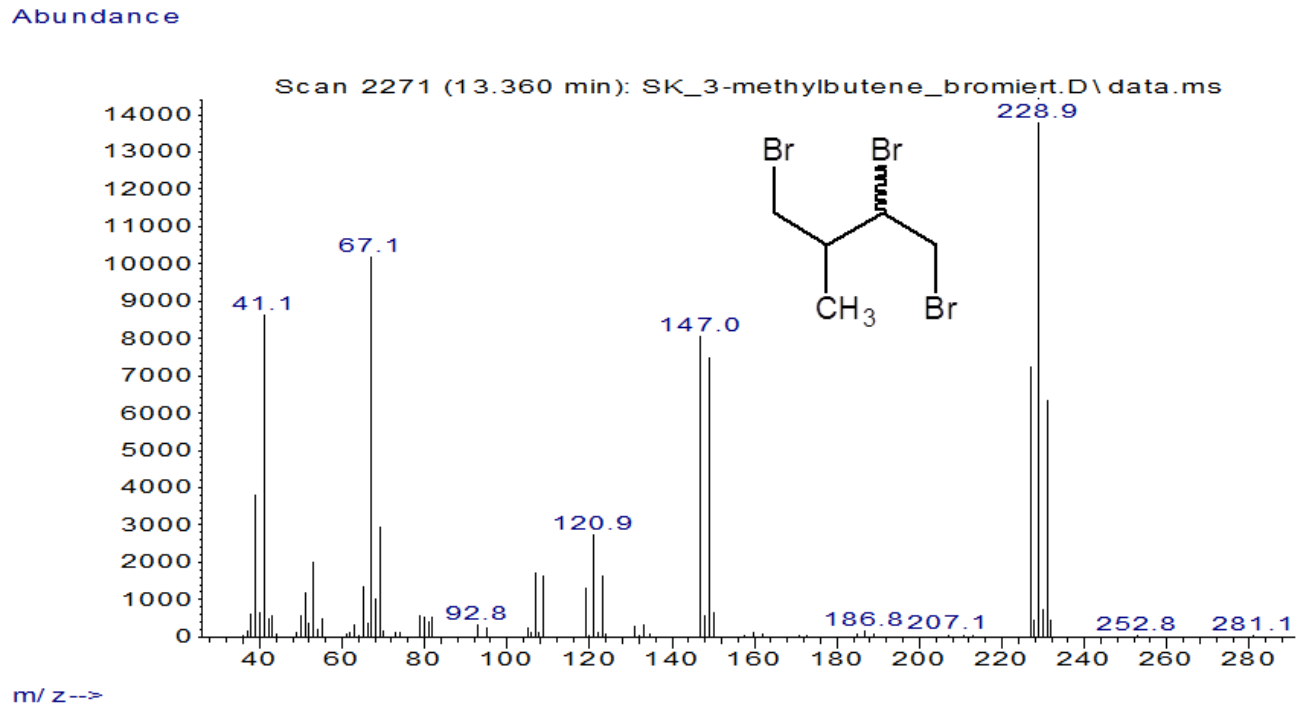

Figure S179. GC-MS spectra of a tribrominated derivative of **15c** (exact position of Br not defined) (308.94 g mol^{-1}) obtained by bromination of commercial **15c** (corresponds to peak b in Figure S177).

7.5.2 **Bromination of conversion of 12a**

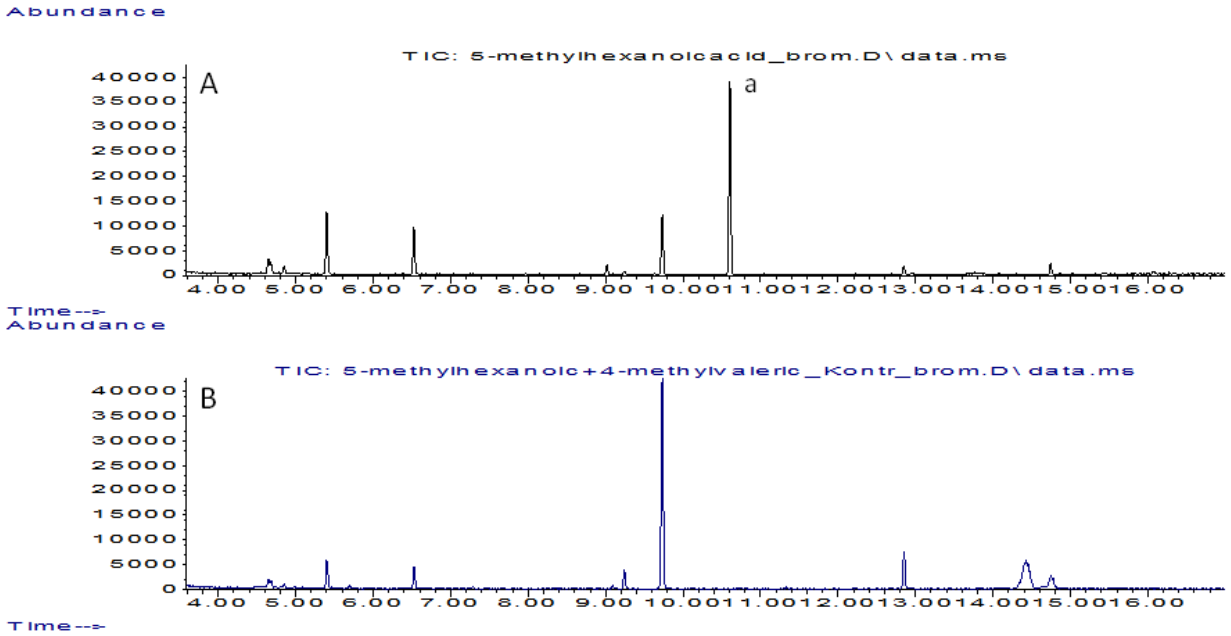

Figure S180. GC-MS chromatograms obtained by conversion of **12a** (10 mM) with in-situ bromination. **A** = Conversion of **12a** with the OleT-CamAB-FDH system. **B** = Conversion of **12a** in the absence of OleT (negative control). **a** = dibrominated derivative of **12c**

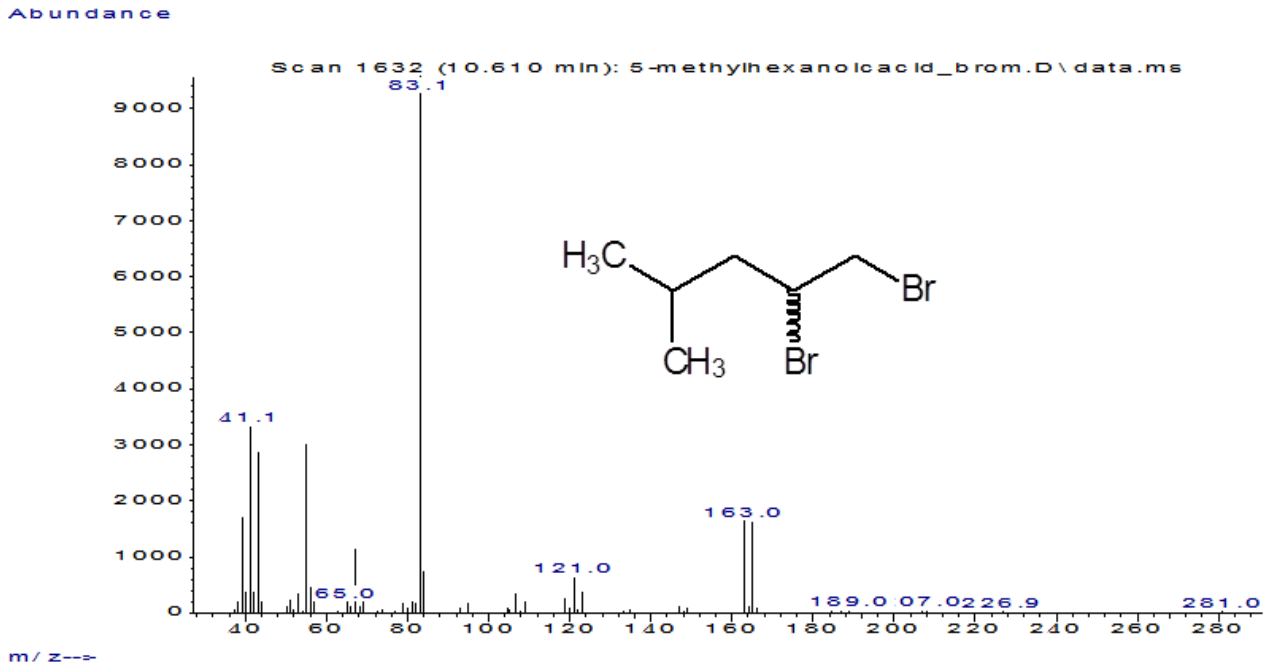

Figure S181. GC-MS spectra of a dibrominated derivative of **12c** (exact position of Br not defined) (243.97 g mol^{-1}) obtained by conversion of **12a** with the OleT-CamAB-FDH system with in-situ bromination (corresponds to peak a in Figure S180 A).

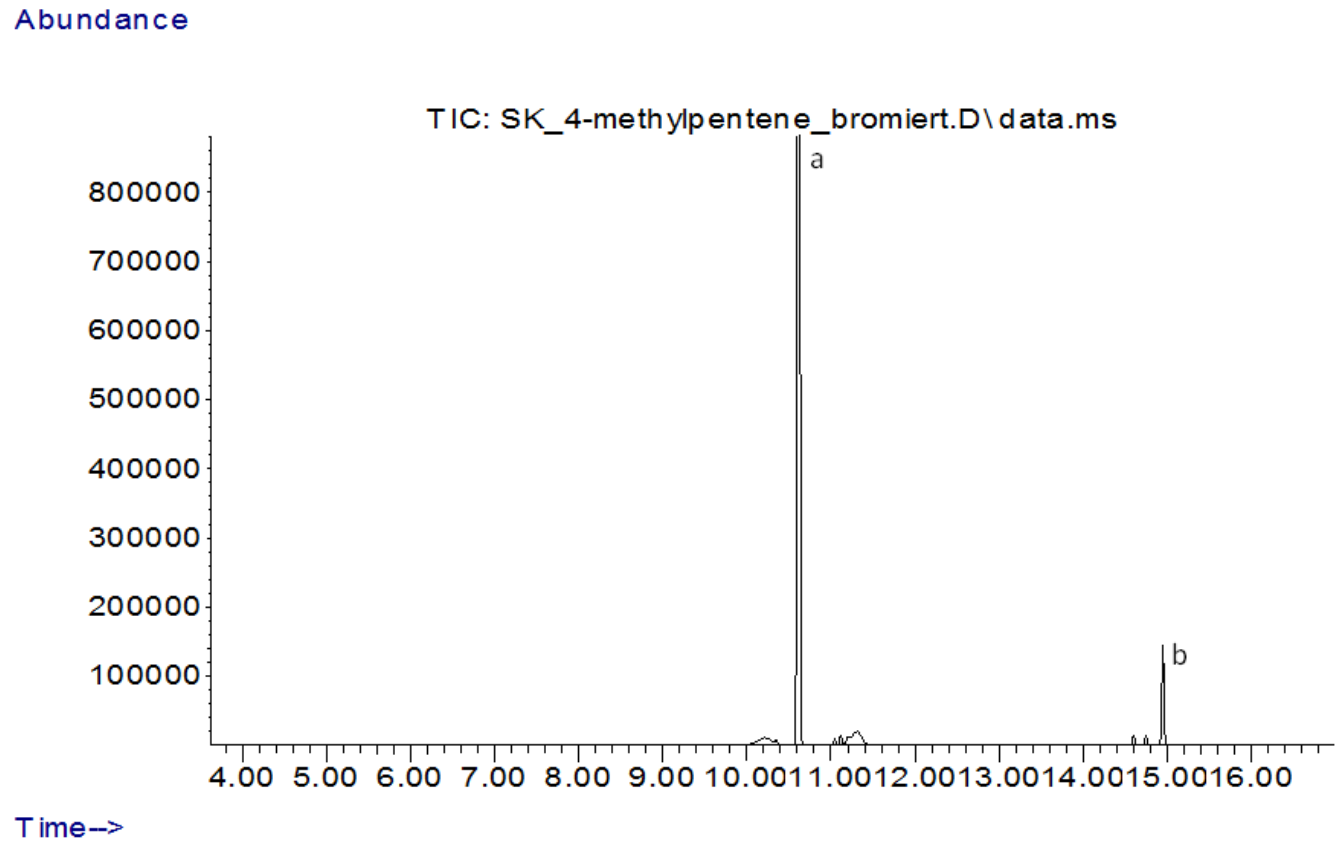

Figure S182. GC-MS chromatogram obtained by bromination of commercial **12c**. **a** = dibrominated derivative of **12c**; **b** = triborminated derivative of **12c**

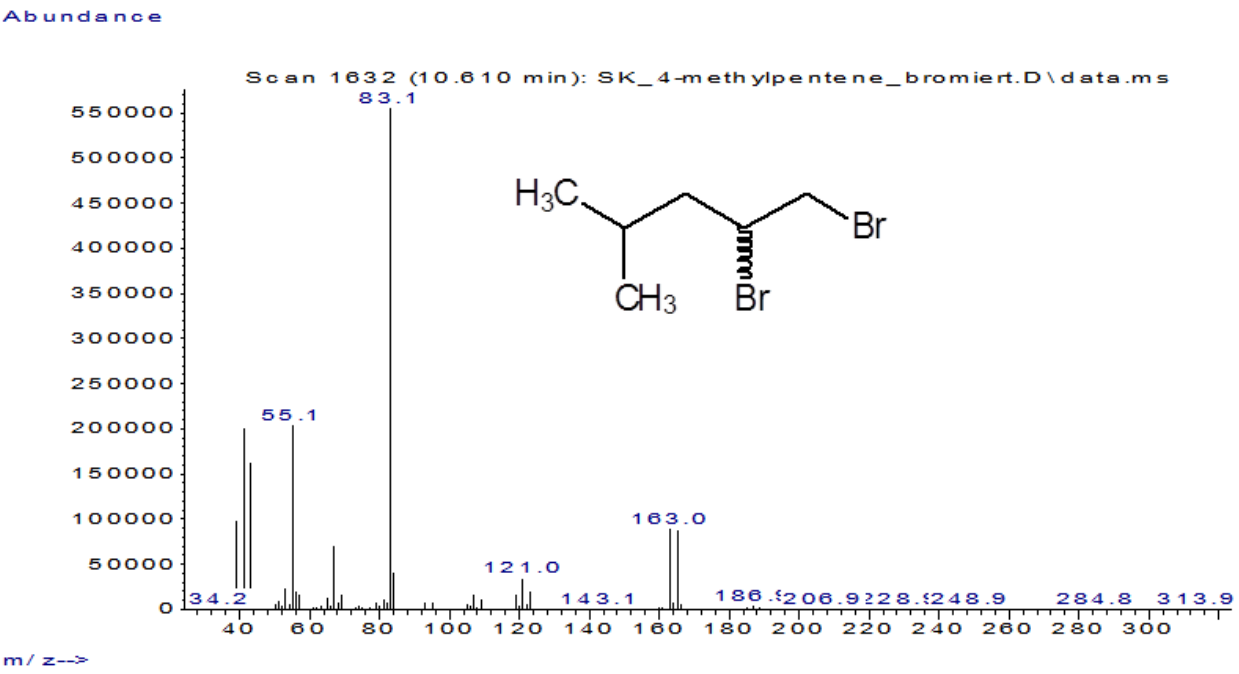

Figure S183. GC-MS spectra of a dibrominated derivative of **12c** (exact position of Br not defined) (243.97 g mol^{-1}) obtained by bromination of commercial **12c** (corresponds to peak a in Figure S182).

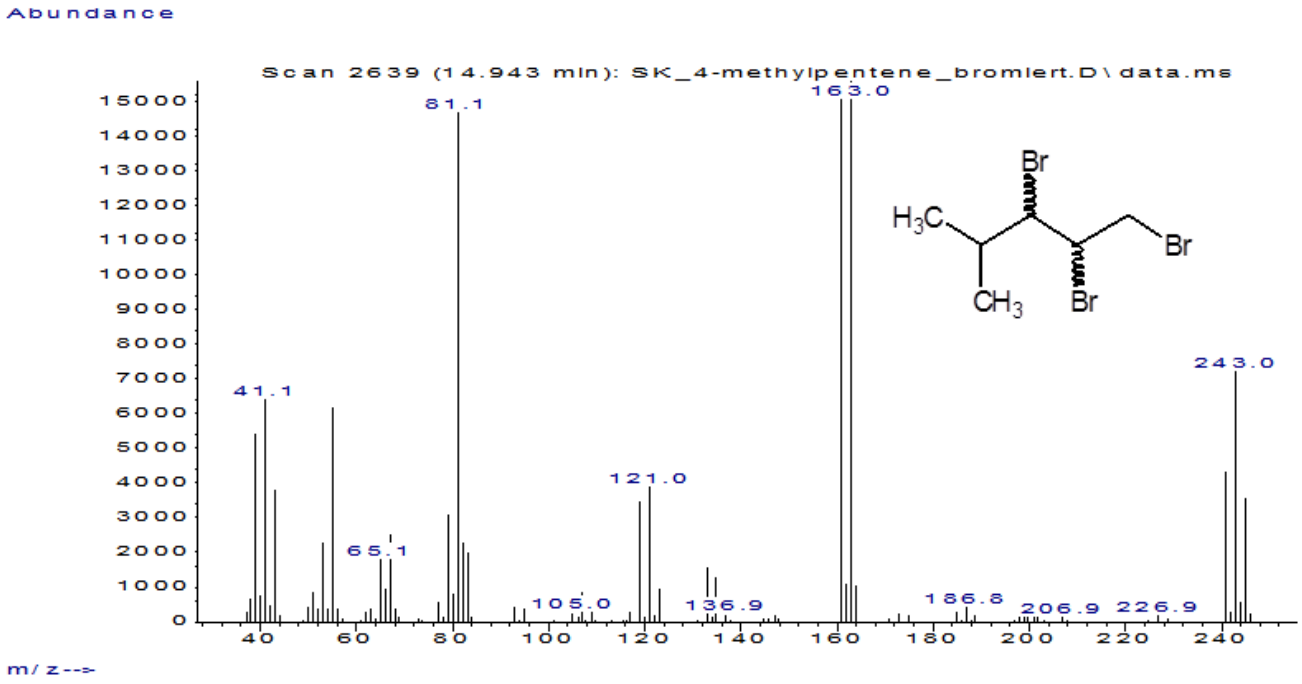

Figure S184. GC-MS spectra of a tribrominated derivative of **12c** (exact position of Br not defined) (322.97 g mol^{-1}) obtained by bromination of commercial **12c** (corresponds to peak b in Figure S182).

7.5.3 **Bromination of conversion of 13a**

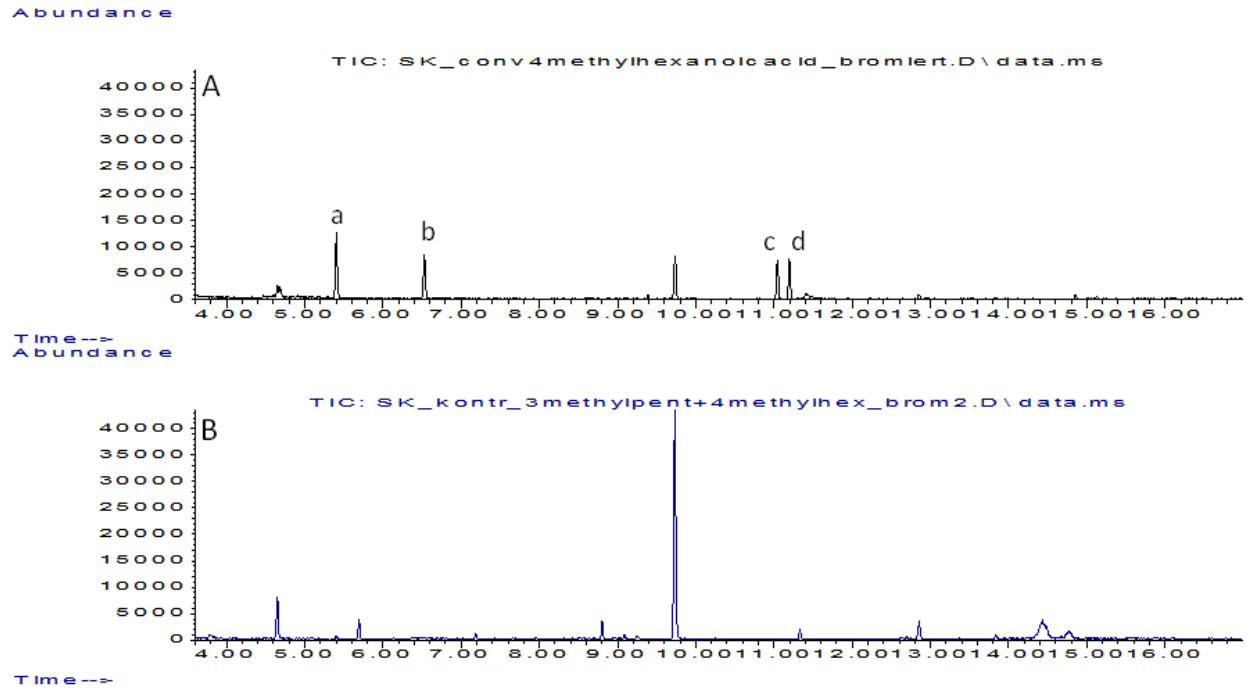

Figure S185. GC-MS chromatograms obtained by conversion of **13a** (10 mM) with in-situ bromination. **A** = Conversion of **13a** with the OleT-CamAB-FDH system. **B** = Conversion of **13a** in the absence of OleT (negative control). **a** = 3-bromo-2-butanone (score MS = 59 %); **b** = 1-bromo-2-butanone (score MS = 90 %); **c** = dibrominated derivative of **12c**; **d** = dibrominated derivative of **12c.**

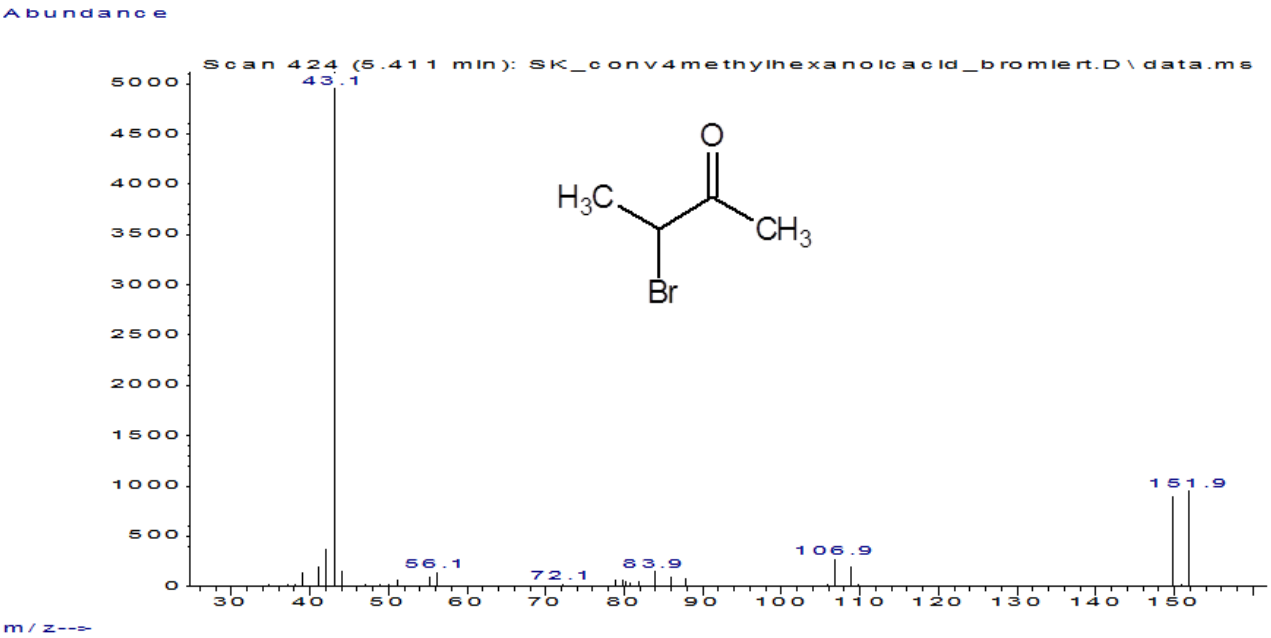

Figure S186. GC-MS spectra of 3-bromo-2-butanone (151.00 g mol^{-1}) obtained by conversion of **13a** with the OleT-CamAB-FDH system with in-situ bromination (corresponds to peak a in Figure S185 A).

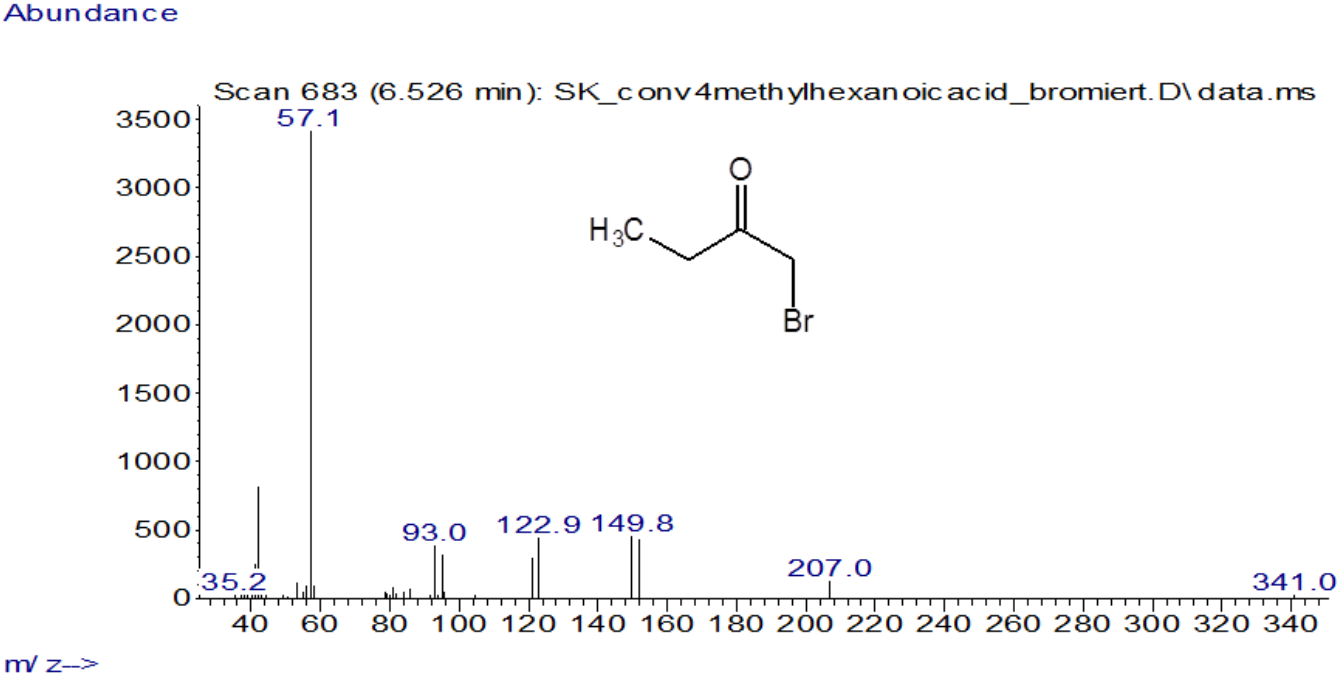

Figure S187. GC-MS spectra of 1-bromo-2-butanone (151.00 g mol^{-1}) obtained by conversion of **13a** with the OleT-CamAB-FDH system with in-situ bromination (corresponds to peak b in Figure S185 A).

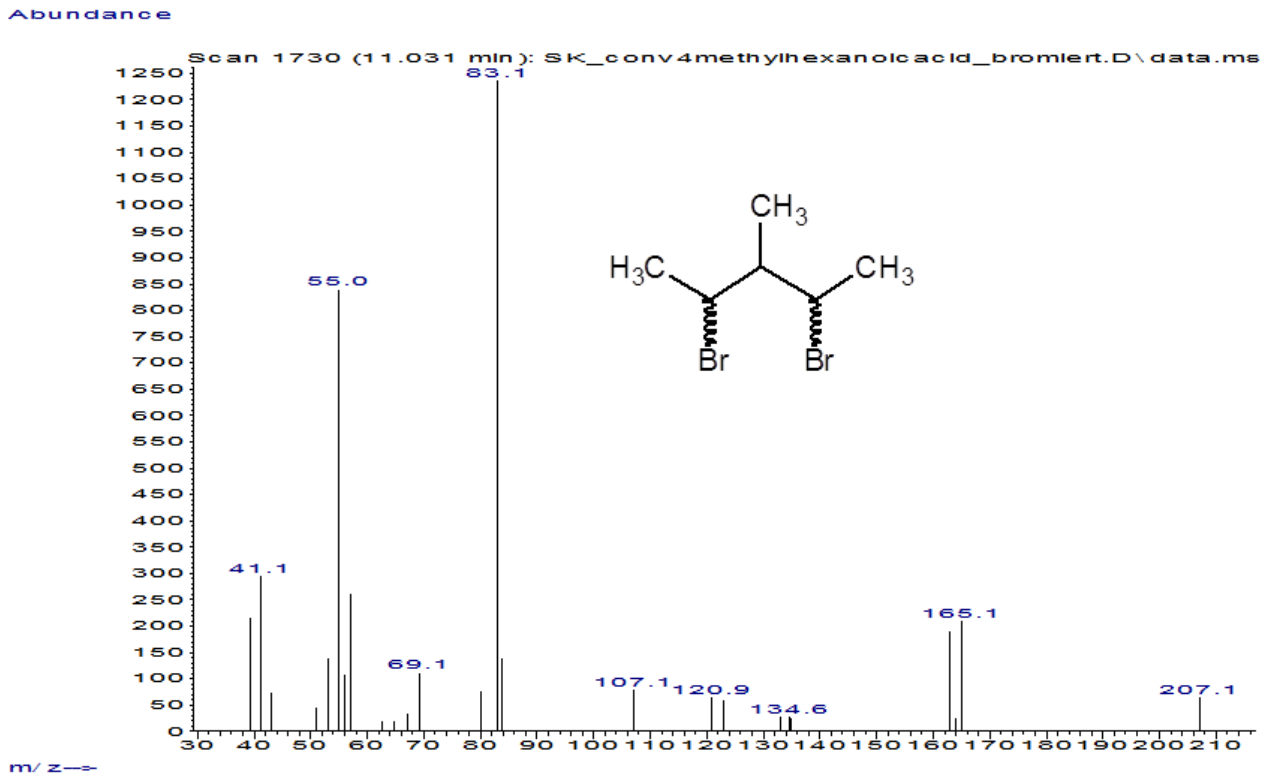

Figure S188. GC-MS spectra of a dibrominated derivative of **13c** (exact position of Br not defined) (243.97 g mol^{-1}) obtained by conversion of **13a** with the OleT-CamAB-FDH system with in-situ bromination (corresponds to peak c in Figure S185 A).

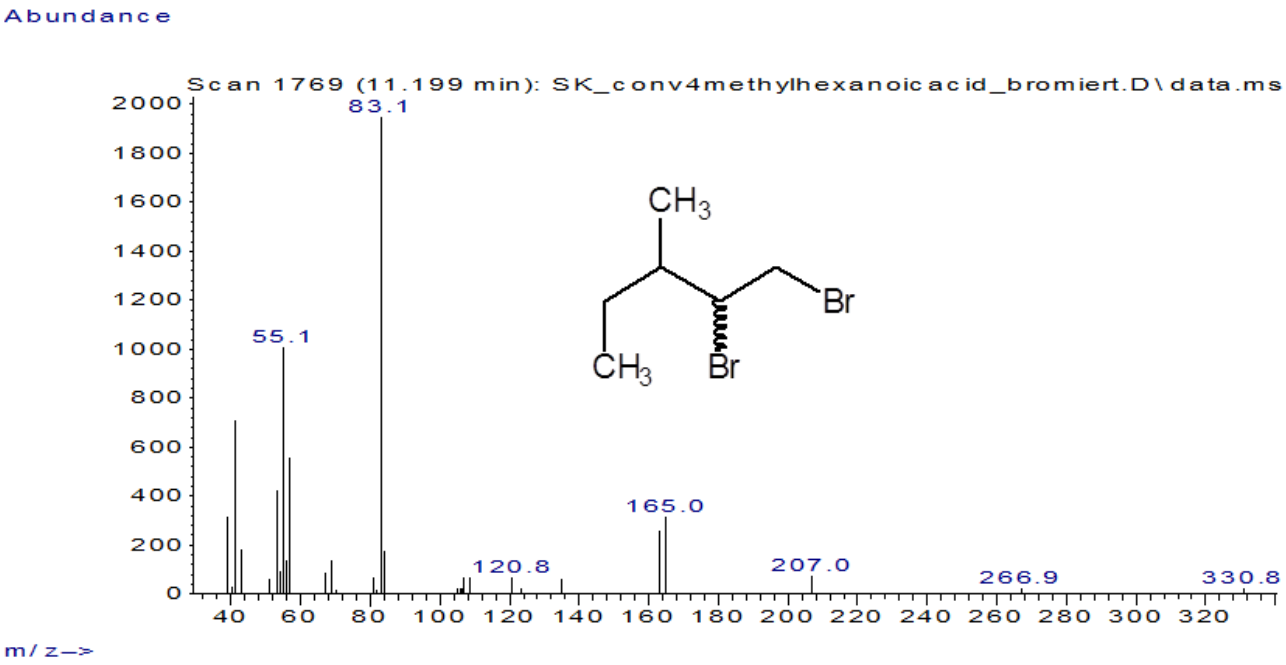

Figure S189. GC-MS spectra of a dibrominated derivative of **13c** (exact position of Br not defined) (243.97 g mol^{-1}) obtained by conversion of **13a** with the OleT-CamAB-FDH system with in-situ bromination (corresponds to peak d in Figure S185 A).

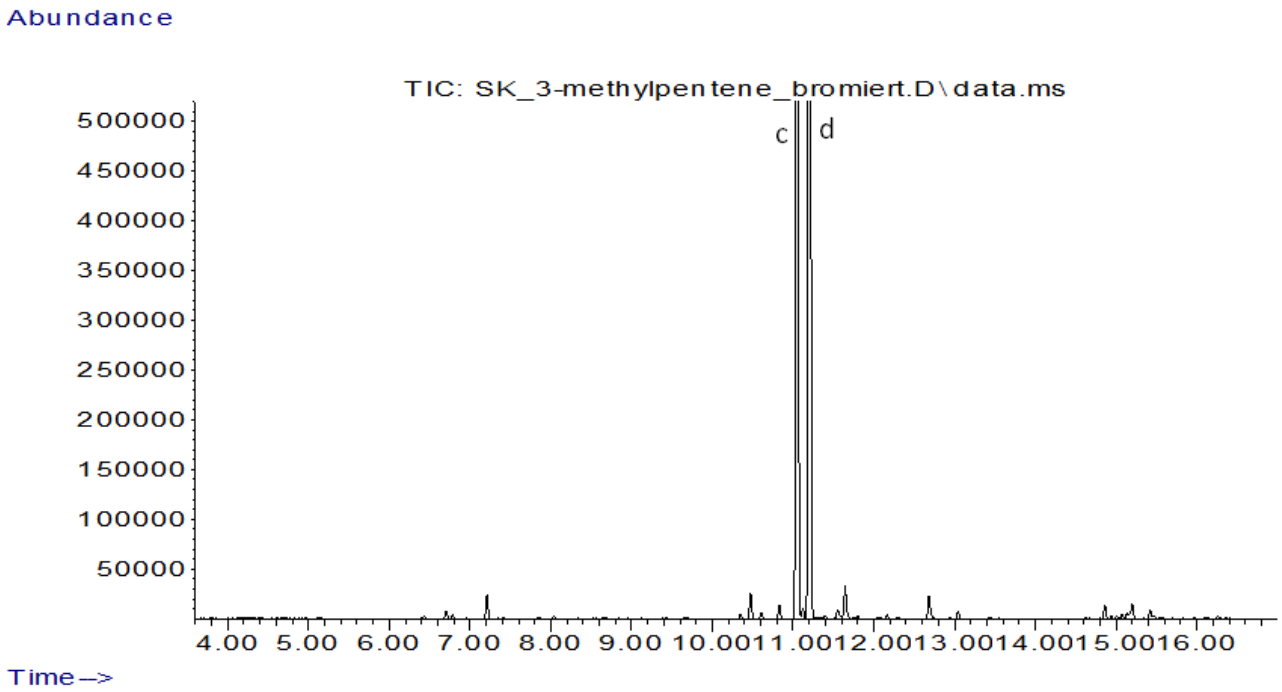

Figure S190. GC-MS chromatogram obtained by bromination of commercial **13c**. **c** = dibrominated derivative of **13c**; **d** = dibrominated derivative of **13c.**

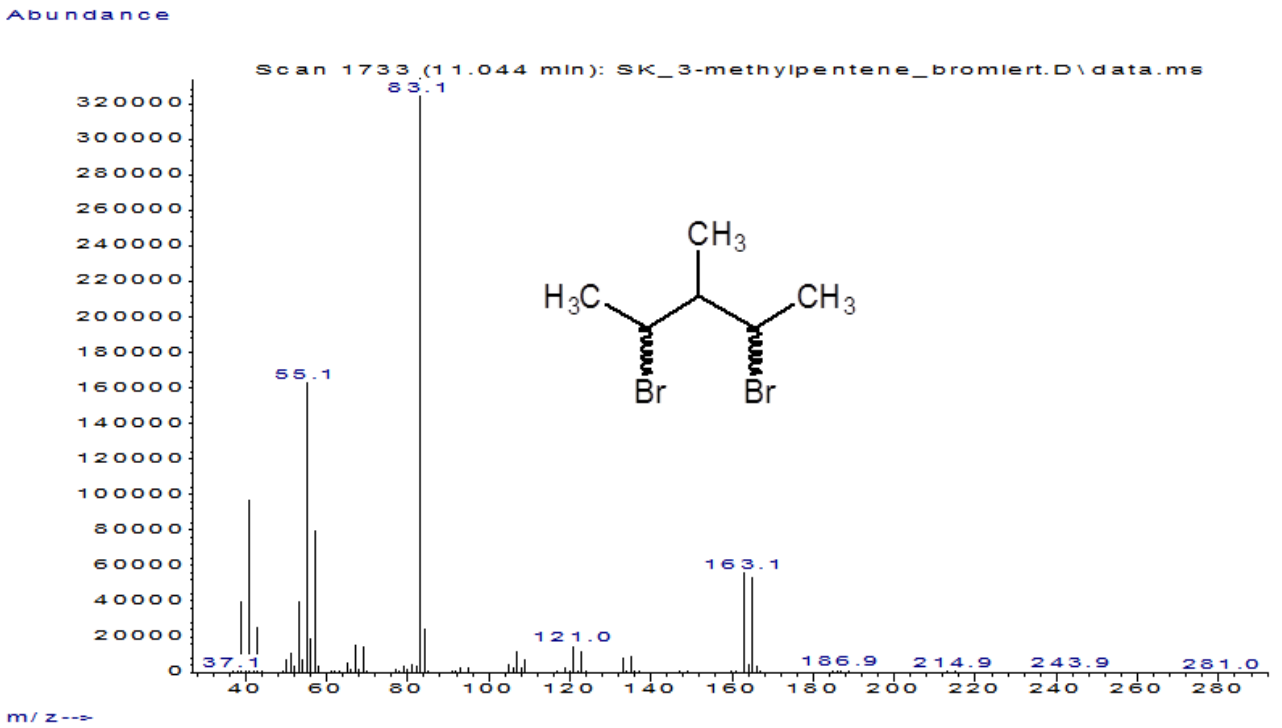

Figure S191. GC-MS spectra of a dibrominated derivative of **13c** (exact position of Br not defined) (243.97 g mol^{-1}) obtained by bromination of commercial **13c** (corresponds to peak c in Figure S190).

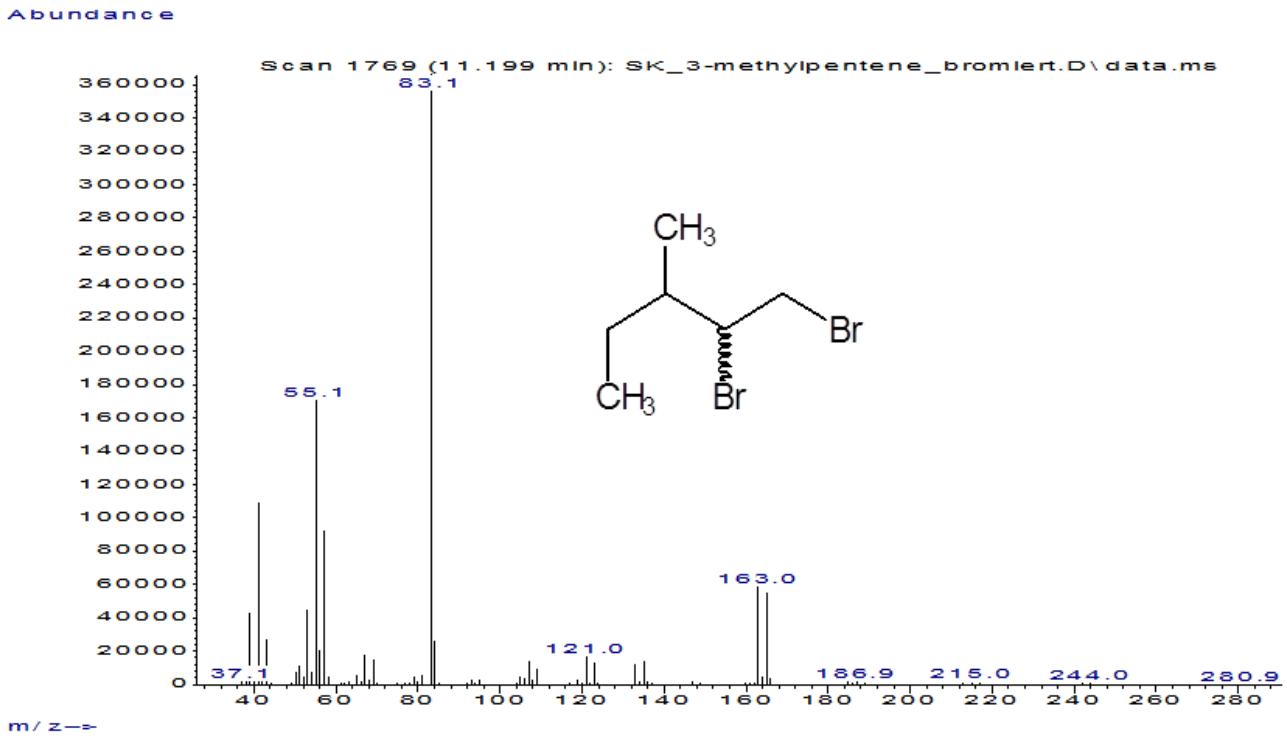

Figure S192. GC-MS spectra of a dibrominated derivative of **13c** (exact position of Br not defined) (243.97 g mol^{-1}) obtained by bromination of commercial **13c** (corresponds to peak d in Figure S190).

7.6 Conversion of 3a with alternative reaction systems

7.6.1 Conversion of 3a with OleT-Fdr/FldA-FDH cascade

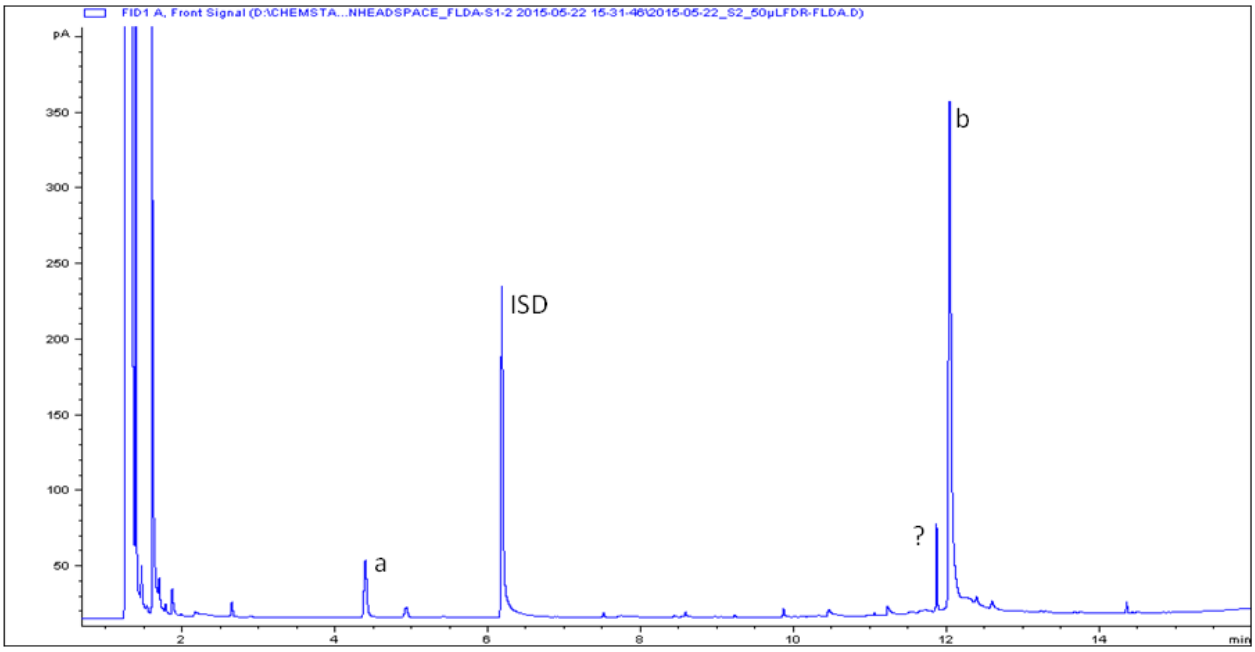

Figure S193. GC-FID chromatogramm obtained by conversion of **3a** (10 mM) with OleT-Fdr/FldA-FDH cascade. **ISD** = internal standard internal standard (0.1 % (v/v) 1-decanol); **a** = **3c**; **b** = substrate (**3a**); **?** = undefined compound – probably derived from incomplete derivatization.

7.6.2 **Conversion of 3a with OleT and H_2O_2**

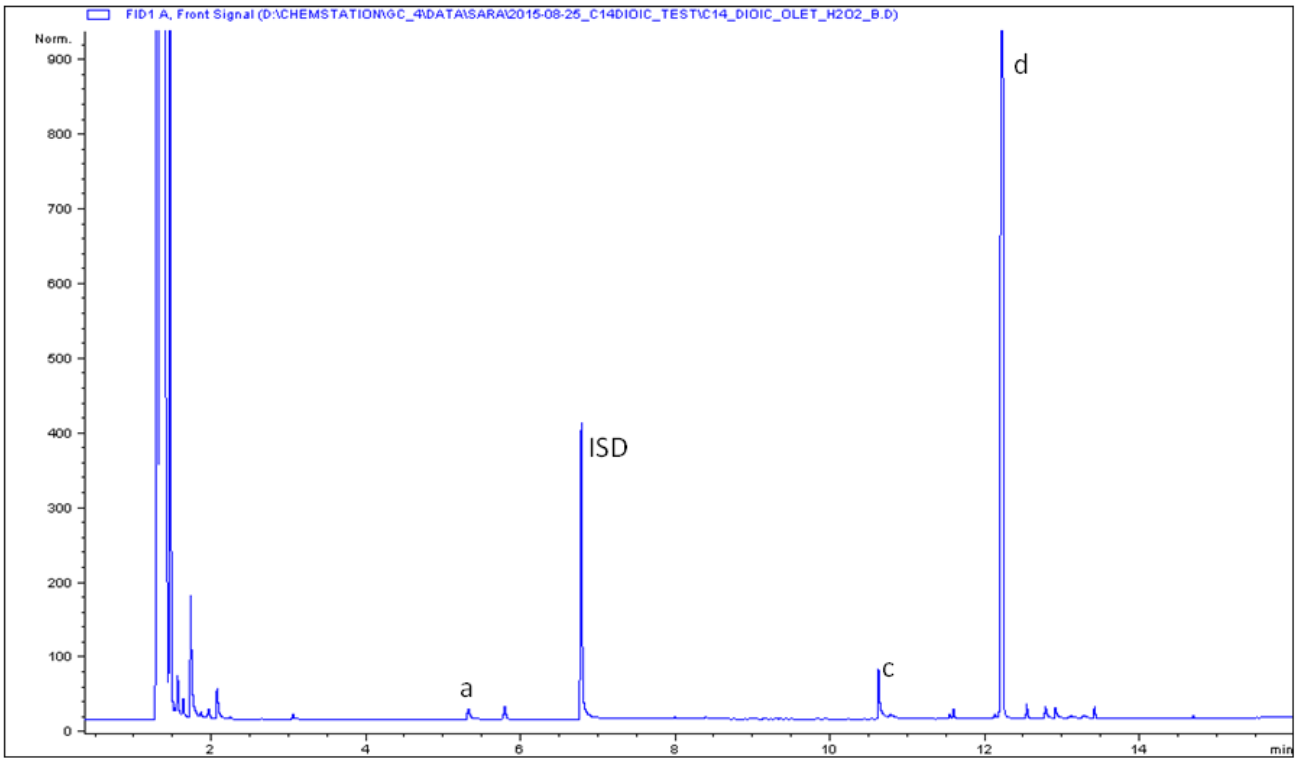

Figure S194. GC-FID chromatogramm obtained by conversion of **3a** (10 mM) with OleT and H_2O_2 as oxidant. **ISD** = internal standard internal standard (0.1 % (v/v) 1-decanol); **a** = **3c**; **c** = **3g; d** = substrate (**3a**).

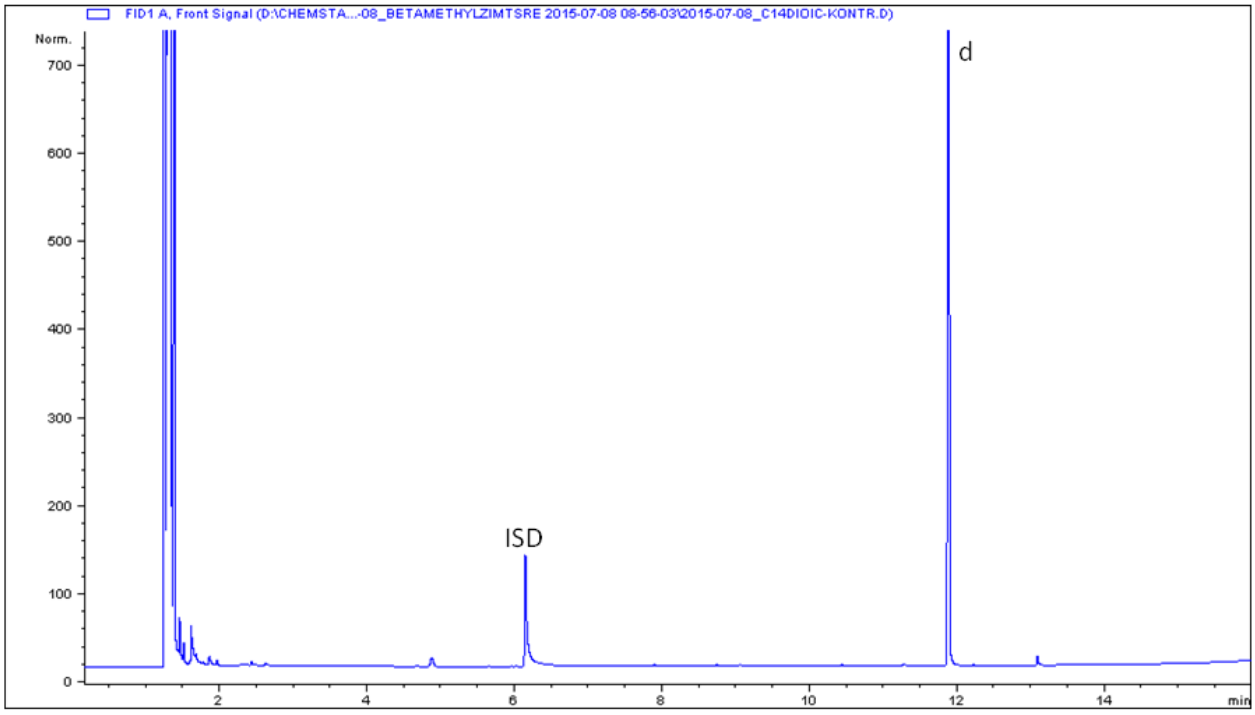

Figure S195. GC-FID chromatogramm obtained by conversion of **3a** (10 mM) without OleT (negative control). **ISD** = internal standard internal standard (0.1 % (v/v) 1-decanol); **d** = substrate (**3a**).

References

1 A. Dennig, M. Kuhn, S. Tassoti, A. Thiessenhusen, S. Gilch, T. Bulter, T. Haas, M. Hall and K. Faber, *Angew. Chem. Int. Ed.*, 2015, **54**, 8819-8822.

2 I. Matsunaga, A. Ueda, N. Fujiwara, T. Sumimoto and K. Ichihara, *Lipids*, 1999, **34**, 841-846.

ChemPubSoc Europe

DOI: 10.1002/ejoc.201600358

EurJOC European Journal of Organic Chemistry

Communication

Dienes from Diacids

Enzymatic Oxidative Tandem Decarboxylation of Dioic Acids to Terminal Dienes

Alexander Dennig,[a] Sara Kurakin,[b] Miriam Kuhn,[b] Andela Dordic,[a] Mélanie Hall,[b] and Kurt Faber*[b]

Abstract: The biocatalytic oxidative tandem decarboxylation of C_7–C_{18} dicarboxylic acids to terminal C_5–C_{16} dienes was catalyzed by the P450 monooxygenase OleT with conversions up to 29 % for 1,11-dodecadiene (0.49 g L^{-1}). The sequential nature of the cascade was proven by the fact that decarboxylation of intermediate C_6–C_{11} ω-alkenoic acids and heptanedioic acid exclusively gave nonconjugated 1,4-pentadiene; scale-up allowed the isolation of 1,15-hexadecadiene and 1,11-dodecadiene; the system represents a short and green route to terminal dienes from renewable dicarboxylic acids.

Introduction

To reposition the chemical economy, novel metal-free synthetic routes to chemical building blocks from renewable C sources are demanded.[1,2] Among the primary platform chemicals, short- and medium-chain 1-alkenes (obtained by steam cracking of crude oil at >800 °C)[3] are of outstanding economic importance.[4] In contrast, terminal dienes (>C_4) cannot be obtained from steam cracking, the Shell higher olefin process (SHOP) process,[4b] or the chemical decarboxylation of fatty acids (FAs),[3,5] but they are synthesized by cross-metathesis cleavage of cycloalkenes or polyenes with lower alkenes, such as ethylene (ethenolysis).[6] As dienes represent essential building blocks for synthetic rubbers, co-crosslinkers, and starting materials for macrocycle synthesis, alternative routes are highly desired.[1b,2d] A sustainable synthetic route to terminal dienes from dicarboxylic acids has so far not been reported. In 2011, Rude et al. reported the first direct enzymatic oxidative decarboxylation of FAs by the P450 monooxygenase OleT to yield long-chain 1-alkenes[7] through a not-yet-elucidated mechanism.[8] By employing whole cells, cell-free extracts, or purified enzyme preparations,[7–9] the reaction proceeds either with H_2O_2 or O_2 as the oxidant. By using purified OleT in combination with the putidaredoxin electron-transfer system CamAB,[10] efficient NADH (NAD = nicotinamide adenine dinucleotide) regeneration and atmospheric O_2 as the oxidant allowed the synthesis of 1-alkenes ranging from C_3 to C_{21}[9c] with product titers close to 1 g L^{-1}. In contrast, in vivo production by using whole cells (e.g., *E. coli* and electron-transfer proteins Fdr/FldA) led to mixtures of 1-alkenes (4–48 mg L^{-1} d^{-1}),[9a,9e] and dienes were only detected in their terminal/internal forms (e.g., 1,10-heptadecadiene).[7,9e] Other promising 1-alkene-forming enzymes are the non-heme di-iron monooxygenase UndA,[11] which is limited by a narrow substrate scope and low total turnover numbers (TTNs), and ferulic acid decarboxylases,[12] which require α,β-unsaturated acids as substrates. On the other hand, aliphatic diacids are widely distributed in various metabolic pathways[13] and hence represent a renewable basis for the synthesis of terminal dienes. Alternatively, enzymatic ω-oxidation of FAs yields C_6–C_{22} diacids in industrially relevant quantities (>100 g L^{-1}).[14] Further sources of diacids (e.g., adipic acid) are polyester waste materials.[2c]

Results and Discussion

To explore the synthetic potential and substrate scope of the P450 monooxygenase OleT, we investigated the direct tandem decarboxylation of dicarboxylic acids to terminal dienes (Scheme 1). As saturated FAs are initially regarded as the natural substrates of OleT, it was unclear to what extent terminal modification of the substrate would influence the overall catalytic performance. Initial experiments with the use of **5a** (10 mM) and the OleT-CamAB-FDH reaction system[9c] and O_2 as the oxidant revealed the formation of **5c** with 12.4 % conversion. After product extraction and derivatization of the remaining acid(s) in the reaction medium, α- and β-hydroxy diacids were found as side products (in total 38 %, Table 1), whereas intermediate **5b** was not found (see the Supporting Information). However, α- and β-hydroxy derivatives of **5b** were detected. To explore the substrate scope, 10 dicarboxylic acids (i.e., compounds **1a**–**10a**, 10 mM) were subjected to the OleT-CamAB-FDH reaction system (Scheme 1, Route 1; Table 1).

Terminal dienes **1c**–**10c** were detected with up to 29 % conversion at a 0.06 mol-% catalyst loading. The highest conversion was obtained with **3a**, which yielded up to 29 % of **3c**; this

[a] *Austrian Centre of Industrial Biotechnology (ACIB), c/o Department of Chemistry, Organic & Bioorganic Chemistry, University of Graz, Heinrichstrasse 28, 8010 Graz, Austria*

[b] *Department of Chemistry, Organic & Bioorganic Chemistry, University of Graz, Heinrichstrasse 28, 8010 Graz, Austria*
E-mail: Kurt.Faber@Uni-Graz.at
http://biocatalysis.uni-graz.at

Supporting information for this article is available on the WWW under http://dx.doi.org/10.1002/ejoc.201600358.

© 2016 Wiley-VCH Verlag GmbH & Co. KGaA, Weinheim

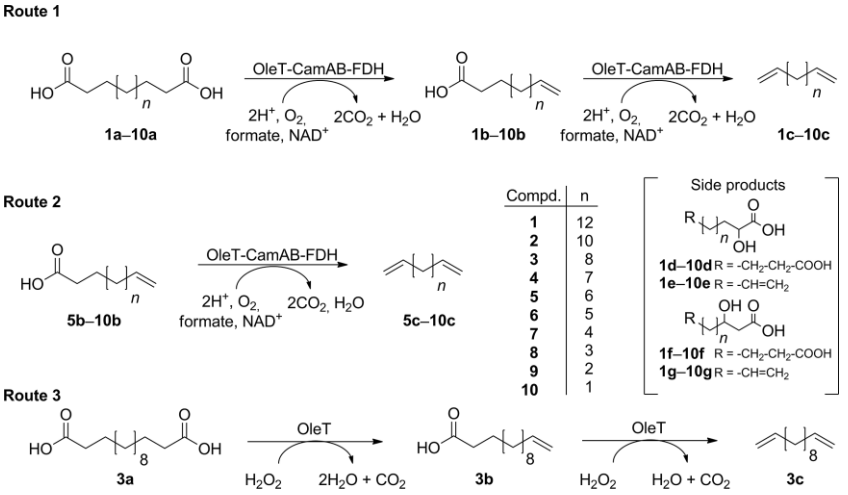

Scheme 1. Biocatalytic routes to terminal dienes through oxidative decarboxylation of (di)carboxylic acids by using P450 monooxygenase OleT. Route 1: Tandem decarboxylation of dicarboxylic acids (C_{18}–C_7) to dienes with the OleT-CamAB-FDH cascade[9c] and O_2 as oxidant. Route 2: Decarboxylation of ω-alkenoic acids (C_{11}–C_6) with the OleT-CamAB-FDH cascade and O_2 as oxidant. Route 3: Tandem decarboxylation of C_{14} dioic acid with OleT and H_2O_2 as oxidant; 2- and 3-hydroxy diacid/ω-alkenoic acid side products are shown in brackets.

Table 1. Decarboxylation of dicarboxylic acids with the OleT-CamAB-FDH cascade at room temperature and at 4 °C.[a]

Entry	Substrate	Diene [mM] r.t./4 °C	TOF [h^{-1}][b]	TTN r.t./4 °C	Diene [%] r.t./4 °C	α-OH + β-OH diacids [%][c] r.t./4 °C	α-OH + β-OH ω-enoic acids [%][c] r.t./4 °C
1	**1a**	n.d./n.d.	n.d.	n.d./n.d.	66/70	9/9[d]	25/21[d]
2	**2a**	1.12/0.74	18 ± 1	373/245	54/69	46/31[d]	0/0[d]
3	**3a**	2.93/1.63	73 ± 2	978/542	48/51	41/43	11/6
4	**4a**	0.31/0.95	36 ± 2	104/317	24/44	51/37	25/19
5	**5a**	1.24/1.22	91 ± 9	413/406	44/43	38/37	18/20
6	**6a**	0/2.05	n.d.	n.d./684	0/48	74[e]/39	26[e]/13
7	**7a**	0.06/<0.05[f]	n.d.	20/13	≥99[g]/≥99[g]	n.d./n.d.	n.d./n.d.
8	**8a**	<0.05[f]/0.09	n.d.	4/29	≥99[g]/≥99	n.d./0	n.d./0
9	**9a**	0.12/0.1	n.d.	38/34	≥99[g]/≥99[g]	n.d./n.d.	n.d./n.d.
10	**10a**	<0.05/0.4	n.d.	4/146	≥99[g,h]/≥99[g,h]	n.d./n.d.	n.d./n.d.

[a] General reaction conditions: Unless stated otherwise, all reactions were performed in 4 mL glass vials closed with a polytetrafluoroethylene (PTFE) septum by using potassium phosphate buffer (KPi, pH 7.5, 0.1 M) containing 6 μM purified OleT, 0.05 U CamAB, 2 U FDH, 1200 U catalase (for H_2O_2 removal), 100 mM ammonium formate, 0.4 mM NAD^+, 10 mM substrate, and 5 % EtOH (v/v) in a final volume of 1 mL at r.t. (24 h and 170 rpm shaking) or at 4 °C (72 h and 100 rpm stirring). Reference data for the assignment of side products can be found in the Supporting Information; n.d.: not determined. [b] Turnover frequency (TOF) calculated from the product amount after 1 h reaction time. [c] % GC area of products (α,ω-diene + α-/β-hydroxy acids = 100 % GC area). [d] Additional minor side products were detected during conversion of diacids **1a** and **2a**; 5 % DMSO (v/v) was used as co-solvent. [e] No diene was formed; therefore, the ratio between hydroxy diacid/hydroxy enoic acid peak areas is given. [f] Detection limit 50 μM. [g] Volatile fraction analyzed. [h] 1-Heptene was detected in the volatile fraction; TOF (product extraction and quantification after 1 h reaction time) and TTN (product extraction and quantification after 24 or 72 h reaction time) were calculated on the basis of quantified diene products. Volatile dienes **6c**–**10c** were quantified by headspace GC–MS analysis by using commercial standards for calibration (see the Supporting Information).

corresponds to a product titer of 0.49 mg mL^{-1} (or 0.49 g L^{-1}) and a TTN of 978. Remarkably, the corresponding saturated FA with identical chain length (C_{14}:0) gave only 5.5 % conversion under similar reaction conditions.[9c] Lowering the concentration of **3a** to 5 and 2 mM decreased the TTN of OleT by 3.1- and 8.9-fold, respectively (5 mM: 18 % conversion; TTN 312; 2 mM: 19 % conversion, TTN 110), which indicated a strong dependence of OleT activity/productivity on the concentration of the diacid substrate. To address the low solubility of long-chain fatty acid/diacid substrates (>C_{14}), we performed a co-solvent study by using 10 mM stearic acid as the model substrate and six water-miscible organic solvents (Figure 1). OleT displayed the highest TTN (1028 to 1817) in the presence of EtOH, DMF, and dioxane with an optimal concentration of 5 % (v/v). In contrast, THF and propan-2-ol led to a significant decrease in productivity at very low concentrations (>2.5 %). Interestingly, DMSO was tolerated from 0 to 20 % (v/v), albeit at significantly decreased productivities (TTN max. 445) relative to the other co-solvents. The selectivity for the formation of dienes (defined as the amount of diene formed relative to that of all reaction products) ranged between 0 and 99 %: >99 % of **7c**–**10c** was identified in the volatile fraction starting from **7a**–**10a**. Besides α- and β-hydroxy diacids (7–74 % of total products), minor amounts of α- and β-hydroxy ω-alkenoic acids, presumably arising from hydroxylation of the ω-alkenoic acids, were detected (6–26 % of total products; Tables 1 and 2, also see the Supporting Information). In the case of **6a**, only hydroxy acid products were detected in a ratio of 74:26 [(α/β-hydroxy diacid)/(α/β-hydroxy ω-alkenoic acid); Table 1, entry 6; r.t. value],[15] which indicated that mono-decarboxylation had occurred.

© 2016 Wiley-VCH Verlag GmbH & Co. KGaA, Weinheim

Table 2. Decarboxylation of intermediate ω-alkenoic acids to terminal dienes at room temperature and at 4 °C.

Substrate	Concentration [mM]	Diene [μM] r.t./4 °C	TTN r.t./4 °C	Diene [%] r.t./4 °C	α-OH + β-OH ω-enoic acids[c] [%] r.t./4 °C
5b	4	141/n.d.	24/n.d.	70/n.d.	30/n.d.
5b	10	0/0	0/0	0/0	0/13*
6b	10	21/0	4/0	45/0	55/3*
6b	2	267/n.d.	53/n.d.	47/n.d.	53/n.d.
7b	10	345/669	57/111	≥99[a]/≥99[a]	n.d./10*
8b	10	77/192	13/32	≥99[a]/≥99[a]	n.d./0
9b	10	71/34	12/7	≥99[a]/≥99[a]	n.d./0
10b	10	59/1776[b]	10/296	≥99[a]/≥99[a]	n.d./n.d.

[a] Volatile fraction analyzed. [b] Trace amounts of 1-heptene (derived from trace amounts of octanoic acid in the starting material). [c] % GC area of products (α,ω-diene + α-/β-hydroxy acids = 100 % GC area). *GC area compared to GC area of internal standard (0.1 % v/v 1-decanol); n.d.: not determined.

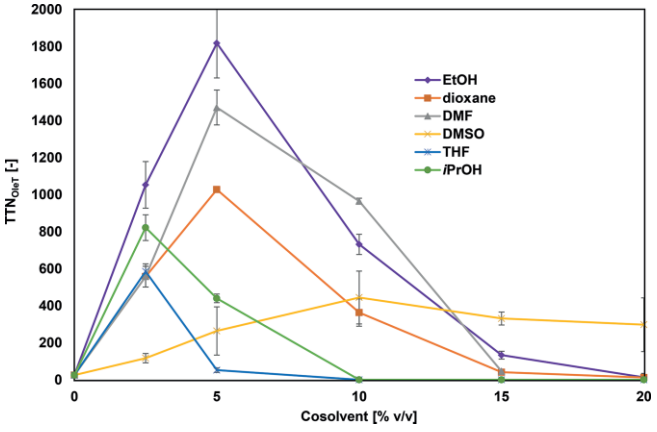

Figure 1. Influence of co-solvents on the catalytic activity of OleT for the conversion of 10 mM stearic acid. TTN values were calculated on the basis of the formation of 1-heptadecene by using 6 μM of OleT. Experiments were performed as described in the general reaction setup for decarboxylation with the OleT-CamAB-FDH system (see the Supporting Information). Reaction buffer volume was replaced by a given amount of co-solvent.

Identification of α/β-hydroxy ω-enoic acid side products during conversion of **1a**–**6a** indicate that dicarboxylic acids undergo tandem decarboxylation via ω-alkenoic acid intermediates to yield the corresponding terminal dienes (Scheme 1, Route 1). To prove the practical applicability of the method, reactions were scaled up to 20 mL to isolate dienes **1c** (4.9 mg, 5 % isolated yield) and **3c** (6 mg, 7.2 % isolated yield).[16]

In addition to the CamAB electron-transfer system, the decarboxylation of **3a** was tested with a crude cell-free lysate of Fdr/FldA from *E. coli*[9e,17] (not optimized), which resulted in a fivefold lower conversion to **3c** (0.56 mM; TTN 185). This indicates that the class I/ferredoxin-based electron-transfer system CamAB is more compatible with OleT.[9c,18] With H_2O_2 as the oxidant under reaction conditions (supplementation of 1.6 mM h^{-1}) identical to those used for the P450 peroxygenases $P450_{Cla}$ and $CYP_{BS\beta}$[15] at elevated catalyst loading (6 μM OleT), only trace amounts of **3c** (1.4 %, 140 μM; TTN 32) were detected; the amount was 31-fold lower than that obtained with the CamAB system (Table 1), which supports the redefinition of OleT as a monooxygenase rather than a peroxygenase.[8,9,9c,9e] As the catalytic performance (TTN and conversion) of OleT depended not only on the substrate chain length, type of oxidant, and source of electrons but also, in particular, on the reaction temperature,[9c] **1a**–**10a** were also converted at 4 °C. Overall, a lower temperature did not influence the product distribution, except for **4a**. Whereas the conversion of **6a** did not show any diene formation at room temperature (Table 1, entry 6), at 4 °C it turned out to be the best accepted substrate, which led to a remarkable conversion of 20.5 % (TTN 684; 0.25 g L^{-1} of **6c**; Table 1). The shortest diacids converted by OleT were **9a** and **10a** to yield **9c** and **10c** (Table 1). Although the conversion remained low (≈1 %; TTN 34 to 38 for **9a**), the selectivity for diene formation was very high (>99 %). Owing to a radical enzyme mechanism, we initially assumed that the C_5 diene formed from heptanedioic acid (**10a**) and 5-hexenenoic acid (**10b**) would be the more stable conjugated 1,3-pentadiene rather than the nonconjugated 1,4-analogue (see the Supporting Information). Much to our surprise, only nonconjugated 1,4-pentadiene was obtained as the major product. This indicates that OleT exerts strict control over β-radical formation followed by specific α/β-carbon bond cleavage. The TTN values for **4a**, **6a**, **8a**, and **10a** converted at 4 °C were, on average, higher than those at room temperature (Table 1), which indicates increased stability of OleT with certain substrates at 4 °C.[9c] The stability and productivity of P450 monooxygenases are strongly related to electron-transfer efficiency and O_2 activation during formation of the reactive oxygenating species (compound I),[19] which determines substrate turnover and catalyst lifetime.[20] Lowering the reaction temperature can significantly alter the productivity and selectivity of OleT, which was the most prominent for the conversions of **4a** and **6a** (Table 1). One explanation could be that a change in the temperature impacts the redox potential of the mediator CamB (5 °C = –0.195 V; 25 °C = –0.242 V),[21] which thereby affects the productivity of OleT.[18–20] Given that attempts to decarboxylate medium- and short-chain diacids (i.e., compounds **7a**–**10a**) generated only small amounts of dienes (max. ≤4 % conversion, 0.4 mM, TTN 146), the decarboxylation of ω-enoic acids was investigated as an alternative route to terminal dienes. The conversion of six ω-enoic acids (i.e., compounds **5b**–**10b**; Scheme 1, Route 2) allowed the synthesis of **5c**–**10c** (Table 2), which confirmed that ω-alkenoic acids are intermediates during the tandem decarboxylation of diacids (Route 1). In addition, the conversions and TTNs for **7b**, **8b**, and **10b** at 4 °C were higher (up to 17 %, TTN 296) than the conver-

© 2016 Wiley-VCH Verlag GmbH & Co. KGaA, Weinheim

sions of shorter diacids (i.e., compounds **7a**–**10a**; Table 1 vs. 2), which can be explained by the similarity of the lipophilic ω-olefinic terminus with that of the saturated FAs. The highest conversion and TTN values were achieved for **10b** (17 %; TTN 296 at 4 °C), which yielded **10c** with >99 % selectivity in the nonconjugated form. Again, lowering the reaction temperature allowed an improved conversion and a higher TTN, in particular for **10b** and **7b** (6.7 % conversion, TTN 111; Table 2, entry 5). Nonetheless, the conversion of **7b** was still 2 to 2.7-fold lower than that for the decarboxylation of nonanoic acid at 10 mM (18 % 1-octene),[9c] which is indicative of a strong influence of the ω terminus on substrate conversion by OleT. Decarboxylation was the main reaction with **5b** (70 % diene; 30 % hydroxylated product); however, in the case of **6b** (one carbon less), the selectivity shifted towards hydroxylation (45 % diene, 55 % hydroxylated products: Table 2). One explanation for this unpredictable change in chemoselectivity (depending on substrate chain length) is variations in the hydrogen-bonding interactions in the active site of OleT, which can alter energy barriers for decarboxylation/hydroxylation pathways.[8b] Under the standard reaction conditions, various diacids were converted into terminal dienes without any detectable formation of ω-enoic acid intermediates (Table 1), whereas decarboxylation of **6a** and **5b** to the respective dienes failed at room temperature (Tables 1 and 2). The ω-enoic acid intermediate either undergoes secondary decarboxylation to yield the terminal diene or is subject to hydroxylation to yield the corresponding hydroxy ω-enoic acid (Table 1, entry 6; Scheme 1, Route 1).

The failed decarboxylation of **5b** (Table 2, entry 2) prompted us to investigate the effect of substrate concentration on the decarboxylation of ω-enoic acids by OleT, which is important for process design. Conversions were repeated at varying concentrations of **5b** and **6b** (0.1 to 10 mM) at room temperature. Interestingly, the decarboxylation of **5b** to **5c** became feasible if the substrate concentration was decreased to 6 mM (≤1 % conversion, Figure 2). The optimum productivity was reached at 4 mM **5b**, which yielded 0.14 mM of **5c** (3.5 % conversion; Figure 2 and Table 2). Similarly, for **6b** a higher conversion was obtained at a 2 mM substrate concentration (13.3 %, Figure 2; Table 2, entry 4), whereas no substrate was recovered (Figure 2) and α/β-hydroxy ω-decenoic acids were identified as major products (55 %). This indicates a dramatic switch from decarboxylation to hydroxylation activity by modification of the ω terminus of the substrate. The results indicate that the conversion of dioic acids into terminal dienes by OleT proceeds in a stepwise fashion (Scheme 1, Route 1). For this, the ω-enoic acid intermediate formed during the first step leaves the substrate channel and rebinds in an inverted (u-turn) orientation. Substrate concentration, co-solvents, and reaction temperature all had a significant influence on catalyst productivity and conversions. Inhibition of OleT by unsaturated FAs[9d] has been suggested but has not been investigated in detail. This constitutes a key for future strategies with the use of whole-cell terminal alkene production, which is complicated by the hosts own FA metabolism.[22] So far, free enzyme (purified or cell-free lysates) proved to be the most productive reaching up to 1 g L^{-1} for 1-alkenes[9c] and 0.49 g L^{-1} for terminal dienes (Table 1, entry 3), which is (at least) one order of magnitude higher than the 1-alkene titers reported for whole-cell systems: Detailed studies on reaction/expression optimization and metabolic engineering to improve whole-cell conversions with OleT have (so far) not exceeded 48 mg L^{-1} d^{-1} in *E. coli* and have reached only 4 mg L^{-1} d^{-1} in *S. cerevisiae*.[9a,9e] A product titer of up 0.49 g L^{-1} for **3c** can be regarded as a good value for a P450-catalyzed reaction,[19,22] in particular considering that the ω-carboxylic acid functionality of a diacid substrate is likely to impair with the hydrophobic nature of the substrate channel of OleT.[9b]

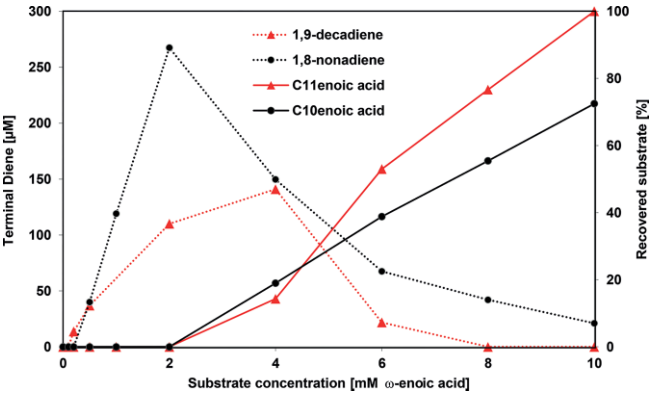

Figure 2. Substrate-concentration-dependent productivity of OleT for the conversions of **5b** and **6b**. Experiments were performed in triplicate according to the standard reaction protocol at room temperature and 1 mL scale (see legend of Table 1). Reactions went to completion at ≤2 mM of **5b** and **6b** (no substrate recovered). For both substrates, control reactions without OleT were performed as reference to calculate the recovery of the unconverted substrate; α-OH and β-OH ω-enoic acids were detected as side products.

Conclusions

For the first time, the production of terminal dienes with chain lengths of C_{16} to C_5 was achieved by sequential oxidative decarboxylation of dicarboxylic acids or ω-enoic acids by using O_2 as the sole oxidant catalyzed by the P450 monooxygenase OleT. The highest productivity of OleT was obtained for tetradecanedioic acid (**3a**), which yielded 1,11-dodecadiene (**3c**) after optimization of the substrate concentration, type of oxidant, and reaction temperature (TTN 978, 29 % conversion, 0.49 g L^{-1}). OleT showed the best performance as a cell-free catalyst with O_2 as the oxidant, and the highly selective formation of nonconjugated 1,4-pentadiene (rather than the more stable 1,3-isomer) underlines the advantages of the mild reaction conditions.

Supporting Information (see footnote on the first page of this article): Experimental details, including catalyst preparation and analytical data (GC-FID/GC–MS traces and ^{1}H NMR spectra) for isolated and purified compounds.

Acknowledgments

Funding by the Austrian Ministry of Science, Research and Economy (BMWFW), the Ministry for Transport, Innovation and Tech-

© 2016 Wiley-VCH Verlag GmbH & Co. KGaA, Weinheim

nology (BMVIT), the Steirische Wirtschaftsförderungsgesellschaft (SFG), the Standortagentur Tirol, Austria, the Government of Lower Austria, and the Technologieagentur der Stadt Wien (ZIT) through the Austrian FFG-COMET-Funding Program is gratefully acknowledged. Bernhard Hauer and co-workers (University of Stuttgart, Germany) are acknowledged for providing the plasmids containing the genes of Fdr/FldA.

Keywords: Biocatalysis · Enzyme catalysis · Carboxylic acids · Decarboxylation · Dienes

[1] a) J. Murray, D. King, *Nature* **2012**, *481*, 433–435; b) J. C. Philp, R. J. Ritchie, J. E. Allan, *Trends Biotechnol.* **2013**, *31*, 219–222.
[2] a) T. Netscher, *Angew. Chem. Int. Ed.* **2014**, *53*, 14313–14315; *Angew. Chem.* **2014**, *126*, 14539–14541; b) U. Biermann, U. Bornscheuer, M. A. Meier, J. O. Metzger, H. J. Schafer, *Angew. Chem. Int. Ed.* **2011**, *50*, 3854–3871; *Angew. Chem.* **2011**, *123*, 3938–3956; c) A. J. J. Straathof, *Chem. Rev.* **2014**, *114*, 1871–1908; d) R. Cernansky, *Nature* **2015**, *519*, 379–380.
[3] S. P. Pyl, T. Dijkmans, J. M. Antonykutty, M. F. Reyniers, A. Harlin, K. M. Van Geem, G. B. Marin, *Bioresour. Technol.* **2012**, *126*, 48–55.
[4] a) R. Kourist, *Angew. Chem. Int. Ed.* **2015**, *54*, 4156–4158; *Angew. Chem.* **2015**, *127*, 4228–4230; b) W. Keim, *Angew. Chem. Int. Ed.* **2013**, *52*, 12492–12496; *Angew. Chem.* **2013**, *125*, 12722–12726.
[5] Y. Liu, K. E. Kim, M. B. Herbert, A. Fedorov, R. H. Grubbs, B. M. Stoltz, *Adv. Synth. Catal.* **2014**, *356*, 130–136.
[6] C. Bruneau, C. Fischmeister, in: *Science of Synthesis: C-1 Building Blocks in Organic Synthesis* (Ed.: P. W. N. M. van Leeuwen), Thieme, Stuttgart, Germany, **2014**, vol. 2, p. 349–353.
[7] M. A. Rude, T. S. Baron, S. Brubaker, M. Alibhai, S. B. Del Cardayre, A. Schirmer, *Appl. Environ. Microbiol.* **2011**, *77*, 1718–1727.
[8] a) J. L. Grant, C. H. Hsieh, T. M. Makris, *J. Am. Chem. Soc.* **2015**, *137*, 4940–4943; b) A. S. Faponle, M. G. Quesne, S. P. de Visser, *Chem. Eur. J.* **2016**, *22*, 5478–5483.
[9] a) B. Chen, D.-Y. Lee, M. W. Chang, *Metab. Eng.* **2015**, *31*, 53–61; b) J. Belcher, K. J. McLean, S. Matthews, L. S. Woodward, K. Fisher, S. E. J. Rigby, D. R. Nelson, D. Potts, M. T. Baynham, D. A. Parker, D. Leys, A. W. Munro, *J. Biol. Chem.* **2014**, *289*, 6535–6550; c) A. Dennig, M. Kuhn, S. Tassoti, A. Thiessenhusen, S. Gilch, T. Bulter, T. Haas, M. Hall, K. Faber, *Angew. Chem. Int. Ed.* **2015**, *54*, 8819–8822; *Angew. Chem.* **2015**, *127*, 8943–8946; d) I. Zachos, S. K. Gassmeyer, D. Bauer, V. Sieber, F. Hollmann, R. Kourist, *Chem. Commun.* **2015**, *51*, 1918–1921; e) Y. Liu, C. Wang, J. Yan, W. Zhang, W. Guan, X. Lu, S. Li, *Biotechnol. Biofuels* **2014**, *7*, 28.
[10] a) P. W. Roome, J. C. Philley, J. A. Peterson, *J. Biol. Chem.* **1983**, *258*, 2593–2598; b) A. Schallmey, G. den Besten, I. G. Teune, R. F. Kembaren, D. B. Janssen, *Appl. Microbiol. Biotechnol.* **2011**, *89*, 1475–1485.
[11] a) Z. Rui, X. Li, X. Zhu, J. Liu, B. Domigan, I. Barr, J. H. Cate, W. Zhang, *Proc. Natl. Acad. Sci. USA* **2014**, *111*, 18237–18242; b) Z. Rui, N. C. Harris, X. Zhu, W. Huang, W. Zhang, *ACS Catal.* **2015**, *5*, 7091–7094.
[12] K. A. Payne, M. D. White, K. Fisher, B. Khara, S. S. Bailey, D. Parker, N. J. Rattray, D. K. Trivedi, R. Goodacre, R. Beveridge, P. Barran, S. E. Rigby, N. S. Scrutton, S. Hay, D. Leys, *Nature* **2015**, *522*, 497–501.
[13] a) M. Pollard, F. Beisson, Y. Li, J. B. Ohlrogge, *Trends Plant Sci.* **2008**, *13*, 236–246; b) Z. Cong, K. Kawamura, S. Kang, P. Fu, *Sci. Rep.* **2015**, *5*, 9580; c) G. Mingrone, M. Castagneto, *Nutr. Rev.* **2006**, *64*, 449–456; d) N. M. Carballeira, M. Reyes, A. Sostre, H. Huang, M. F. Verhagen, M. W. Adams, *J. Bacteriol.* **1997**, *179*, 2766–2768; e) H. Song, S. Y. Lee, *Enzyme Microb. Technol.* **2005**, *39*, 352–361; f) T. Polen, M. Spelberg, M. Bott, *J. Biotechnol.* **2013**, *167*, 75–84.
[14] S. Picataggio, T. Rohrer, K. Deanda, D. Lanning, R. Reynolds, J. Mielenz, L. D. Eirich, *Nat. Biotechnol.* **1992**, *10*, 894–898.
[15] a) M. Girhard, S. Schuster, M. Dietrich, P. Durre, V. B. Urlacher, *Biochem. Biophys. Res. Commun.* **2007**, *362*, 114–119; b) I. Matsunaga, A. Ueda, N. Fujiwara, T. Sumimoto, K. Ichihara, *Lipids* **1999**, *34*, 841–846; c) for identification of hydroxylated side products, P450 peroxygenases $P450_{Cla}$ (selective for α-hydroxylation) (a) and $CYP_{BS\beta}$ (α- and/or β-hydroxylation) (b) were employed to obtain reference materials; (c) selective hydroxylation of dioic/ω-alkenoic acids (see compounds **1a**–**9a** and **5b**–**9b**; 10 mM) was performed with H_2O_2 as the oxidant and products were identified after derivatization by GC–MS fragmentation pattern analysis and comparison with literature data (see the Supporting Information).
[16] 3-Hydroxytetradecanedioic acid (7 mg, 11.6 % yield of isolated material) and 3-hydroxydec-9-enoic acid (8 mg, 20 % yield of isolated material) were isolated after derivatization to the corresponding esters, as no commercial references were available.
[17] C. M. Jenkins, M. R. Waterman, *J. Biol. Chem.* **1994**, *269*, 27401–27408.
[18] F. Hannemann, A. Bichet, K. M. Ewen, R. Bernhardt, *Biochim. Biophys. Acta Gen. Subj. Biochim. Biophys. Acta* **2007**, *1770*, 330–344.
[19] R. Bernhardt, V. B. Urlacher, *Appl. Microbiol. Biotechnol.* **2014**, *98*, 6185–6203.
[20] a) B. Meunier, S. P. de Visser, S. Shaik, *Chem. Rev.* **2004**, *104*, 3947–3980; b) S. Kadkhodayan, E. D. Coulter, D. M. Maryniak, T. A. Bryson, J. H. Dawson, *J. Biol. Chem.* **1995**, *270*, 28042–28048.
[21] V. Reipa, M. J. Holden, M. P. Mayhew, V. L. Vilker, *Biochim. Biophys. Acta Bioenerg. Biochim. Biophys. Acta* **2000**, *1459*, 1–9.
[22] a) M. Schrewe, M. K. Julsing, B. Bühler, A. Schmid, *Chem. Soc. Rev.* **2013**, *42*, 6346–6377; b) M. T. Lundemo, J. M. Woodley, *Appl. Microbiol. Biotechnol.* **2015**, *99*, 2465–2483.

Received: March 22, 2016
Published Online: June 27, 2016

© 2016 Wiley-VCH Verlag GmbH & Co. KGaA, Weinheim